APPLICATIONS OF ISOTHIOUREAS IN SURFACE CHEMISTRY:
MODIFICATION OF SELF-ASSEMBLED MONOLAYERS AND IMMOBILISATION ON POLYMER SUPPORTS

Ross Chisholm

A Thesis Submitted for the Degree of PhD
at the
University of St Andrews

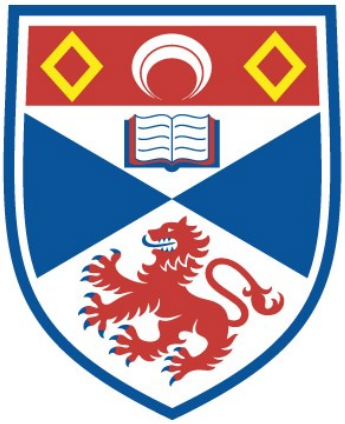

2017

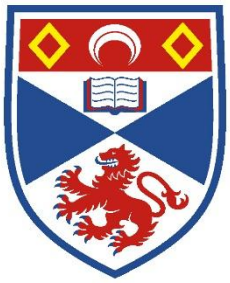

University of
St Andrews

Applications of Isothioureas in Surface Chemistry:

Modification of Self-Assembled Monolayers and Immobilisation on Polymer Supports

Ross Chisholm

2016

This thesis is submitted in partial fulfilment for the degree of PhD at the University of St Andrews

Always look on the bright side of life.

Monty Python

1. Candidate's declarations:

I, Ross Chisholm, hereby certify that this thesis, which is approximately 58,000 words in length, has been written by me, and that it is the record of work carried out by me, or principally by myself in collaboration with others as acknowledged, and that it has not been submitted in any previous application for a higher degree.

I was admitted as a research student in September 2012 and as a candidate for the degree of Doctor of Philosophy in September 2013; the higher study for which this is a record was carried out in the University of St Andrews between 2012 and 2016.

Date…….signature of candidate……..

2. Supervisor's declaration:

I hereby certify that the candidate has fulfilled the conditions of the Resolution and Regulations appropriate for the degree of Doctor of Philosophy in the University of St Andrews and that the candidate is qualified to submit this thesis in application for that degree.

Date…….signature of supervisors…….

3. Permission for publication:

In submitting this thesis to the University of St Andrews I understand that I am giving permission for it to be made available for use in accordance with the regulations of the University Library for the time being in force, subject to any copyright vested in the work not being affected thereby. I also understand that the title and the abstract will be published, and that a copy of the work may be made and supplied to any bona fide library or research worker, that my thesis will be electronically accessible for personal or research use unless exempt by award of an embargo as requested below, and that the library has the right to migrate my thesis into new electronic forms as required to ensure continued access to the thesis. I have obtained any third-party copyright permissions that may be required in order to allow such access and migration, or have requested the appropriate embargo below.

The following is an agreed request by candidate and supervisor regarding the publication of this thesis: Embargo on all or part of print or electronic copy for a period of 2 years on the following ground(s):

Publication would preclude future publication

Date……signature of candidate……..signature of supervisors…….

Acknowledgements

I would like to start by thanking Professor Andrew Smith for giving me the opportunity to work within his highly talented research group, and for seeing the potential in me at an early stage, hopefully he benefitted from me as much as I have from him over the last 4 years. I would also like to thank Dr Georg Hähner whose expert knowledge of surface chemistry helped me pick up some of the trickier concepts, and who has helped drive the project and PhD over the years. Thanks must go to Dr John Parkin who was in this with me from the start contributed greatly to my understanding of surface science. Thanks go to the other members of the Hähner group, Dr Richard Bailey and David Jones who were able to lend a hand towards the end.

As I have found out over the last 4 years, a PhD is not just about science but about the people you meet and share experiences with along the way, making my time in St Andrews some of the best years of my life.

Firstly, I would like to thank Angeliki who has helped me immensely over the last 2 years with her support and encouragement and reminded me that life isn't just about chemistry. Next, I will thank the other members of "The Ranch" lab bay; Tom West for being a good friend and housemate over the past years, his questionable chat and chemistry knowledge making him a tolerable lab mate! Don Diego Javier Barrios Antunez who's extremely loose…..chat kept the bay entertaining during my time there (breakfast of champions!); Danger K for being, well, the most German man I think I've ever met, except when it comes to safety. Next thanks go to the office bay; Claire Young for sharing the same level of enthusiasm for a good mug of scald, "there's always time for tea"; Dr Dan Stark for being the first of our cohort to get through the pearly gates and showing us how it's done; Stéphanie Spoehrle for putting up with my antics in the office and in general! Notable mentions go to Ryan "Cougs" Kerr for his emphatic love of HP; Sam Smith for his love of all things sporty (Sky Sports watch out!) and his computer monitor turned 95 °; Dr James Taylor for his constant and sometimes infectious love for chemistry, all ready (and willing) to proof read regardless of how full his plate might be and his keenness for a chat/chop and Rifa for taking on my project after I leave. Previous group members such as Ed "The Boss" Richmond who willingness to show me the ropes when I started have contributed to the chemist I am today; Dr Eoin Gould whom I had the good fortune to spend 6 months in the same fume hood with and the rest of the ADS group who have contribute to my learning experiences during my time here.

Praise must go to the great post-docs we've had in the ADS in my time; Dr David Daniels, who was never afraid to voice his opinion and to Dr Mark Greenhalgh and Dr Aileen Frost for helping out with proof reading this thesis. Outside the lab there are many people who deserve thanks for hepsling me through the difficult times, most notably my parents Glenda and Martin who have

helped me immensely both emotionally (and financially!) and my grandparents Veronica and Tommy (1941-2013), all of whom I would like to dedicate this PhD thesis to.

I'd like to also thank all the technical services that have contributed to this work; Dr Tomas Lebl and Mrs Melanja Smith at the NMR service, University of St Andrews, Dr Steve Francis at the St Andrews XPS facility; EPSRC UK National Mass Spectrometry Facility at Swansea University and the National EPSRC XPS Users Service, Newcastle University.

Abstract

The research outlined in this thesis describes the development of organocatalytic methodology for the modification of self-assembled monolayers on silicon dioxide surfaces and its extension towards an asymmetric protocol and immobilisation of isothiourea organocatalysts to polystyrene supports.

Chapter 1 aims to describe the fundamental aspects of self-assembled monolayers and their place within the wider area of surface chemistry. A recent overview of catalytic surface functionalisation is discussed as well as the historical context of this project, with respect to research within the Smith group, is also presented. A statement of the initial aims and objectives of the research is presented.

Chapter 2 describes the proof-of-concept study undertaken to develop methodology towards the functionalisation of silicon oxide surfaces using an isothiourea-catalysed organocatalytic Michael addition-lactonisation process. Subsequent characterisation of the resulting surfaces and a reaction scope is also carried out in this system.

Chapter 3 describes an extension of the methodology carried out in the previous chapter to allow for an asymmetric protocol. The sense of enantioenduction of the resulting surfaces was then examined using chemical force microscopy using a novel AFM probe with the results show that chiral discrimination can be achieved using this methodology. Control experiments were also undertaken by depositing enantiopure starting materials on a surface and measuring the adhesion forces confirming the presence of a chiral surface.

Chapter 4 describes the immobilisation (*R*)-BTM and (2*R*,3*S*)-HyperBTM analogues onto polystyrene supports and their evaluation in several different reaction classes previously investigated within the Smith group. Results show that the polymer-supported catalyst (2*R*,3*S*)-HyperBTM can be recycled up to 8 times without any major loss in yield or selectivity.

Chapter 5 offers a brief summary of the work undertaken in this PhD and some of the conclusions that can be drawn from it as well as an insight into the potential future developments of this research and areas where it could possibly expand and develop.

Publications

The work described in this thesis has formed the basis of the following peer reviewed publications:

1) "Isothiourea-Mediated Organocatalytic Michael Addition-Lactonization on a Surface: Modification of SAMs on Silicon Oxide Substrates"

Ross Chisholm, John D. Parkin, Andrew D. Smith and Georg Hähner.

Langmuir, **2016**, *32*, 3130-3138.

2) "Synthesis and chiral discrimination of enantioenriched *C*(6)-trifluoromethyldihydropyranones by chemical force microscopy"

John D. Parkin, Ross Chisholm, Andrew D. Smith and Georg Hähner.

Manuscript in preparation, 2016.

Abbreviations

Ac	Acetyl
APCI	Atmospheric pressure chemical ionisation
app.	Apparent
aq.	Aqueous
Ar	Aromatic
AFM	Atomic force microscopy
atm	Atmosphere
ATR	Attenuated total reflectance
BEMP	2-*tert*-Butylimino-2-diethylamino-1,3-dimethylperhydro-1,3,2-diazaphosphorine
BINAP	2,2'-Bis(diphenylphosphino)-1,1'-binaphthyl
BINOL	1,1’-Bi-2-naphthol
Bn	Benzyl
Boc	*N*-*tert*-Butoxycarbonyl
br	Broad
BTM	Benzotetramisole
Bu	Butyl
Bz	Benzoyl
c	Concentration
C	Celsius
CA	Contact angle
CFM	Chemical force microscopy
CI	Chemical ionisation
Cy	Cyclohexyl
cm	Centimeter
d	Doublet
DBU	1,8-Diazabicyclo[5.4.0]undec-7-ene
DFT	Density functional theory
DHPB	3,4-Dihydro-2*H*-pyrimido[2,1-*b*]benzothiazole
DMAP	4-Dimethylaminopyridine

DMF	Dimethylformamide
DMSO	Dimethyl sulfoxide
dr	Diasteroisomeric ratio
EDG	Electron donating group
ee	Enantiomeric excess
eq	Equivalent molar quantity
ESI	Electrospray ionisation
Et	Ethyl
EWG	Electron withdrawing group
g	Gram(s)
GC	Gas chromatography
h	Hour(s)
HPLC	High performance liquid chromatography
HRMS	High resolution mass spectrometry
Hz	Hertz
*i*PrOH	Isopropanol
IR	Infrared
i	Iso
ITU	Isothiourea
J	Coupling constant
LDA	Lithium di-*iso*-propylamide
M	Molar (*i.e.* mol dm^{-3})
mmol	millimole
m	Multiplet
m	*Meta*
Me	Methyl
Mes	Mesityl
MHz	Megahertz
mg	Milligram(s)
mL	Millilitre(s)

mol	Mole(s)
mp	Melting point
M.S.	Molecular sieves
MW	Microwave-assisted reaction
NBS	*N*-Bromosuccinimide
NMR	Nuclear magnetic resonance
Np	Naphthyl
Nu	Nucleophile
o	*ortho*
p	*para*
PG	Protecting group
Ph	Phenyl
PMP	*para*-Methoxyphenyl
ppm	Parts per million
Pr	Propyl
PS	Polymer-supported
q	Quartet
quant.	Quantitative
quint	Quintuplet
RMS	root mean squared
S	selectivity factor
UV	Ultraviolet
rt	Ambient (room) temperature
s	Singlet
sat.	Saturated
t	Triplet/time
t	*Tert*
T	Temperature
TBD	1,5,7-Triazabicyclo[4.4.0]dec-5-ene
Tf	Triflate

TFA	Trifluoroacetic acid
THF	Tetrahydrofuran
TLC	Thin layer chromatography
TMS	Trimethylsilyl
Ts	Tosyl
XPS	X-Ray photoelectron spectroscopy

Table of Contents

Chapter 1 :Introduction

1.1 Molecular self-assembly

For billions of years Nature has used molecular self-assembly to construct a dazzling array of well-defined supramolecular structures, such as proteins and bio-macromolecules, from smaller and more available building blocks.[1] By studying the intricate chemical strategies and cooperative molecular processes by which supramolecular architectures are assembled in Nature, we can begin to exploit self-assembly processes for the synthesis of entirely new materials.[1] The term self-assembly encompasses a diverse range of processes 'where a disordered system of components spontaneously form an organised structure or pattern as a consequence of local interactions, importantly, without external direction' (Figure 1).[2] The concept of self-assembly is being used in an increasingly large number of disciplines with a different emphasis in each one. Self-assembly has several beneficial attributes such as cost-effectiveness, versatility, and a facile nature owing to the fact that the process occurs towards the systems' thermodynamic minima. Self-assembly is also one of the few practical strategies for making ensembles from nanostructures.[3] There are two main types of self-assembly: static and dynamic. Static self-assembly is the most well studied to date and includes processes such as the assembly of ionic and molecular crystals,[4] liquid crystals,[5] as well as self-assembled monolayers.[6] Dynamic self-assembly includes more complicated processes such as the formation of bacterial colonies,[7] swarms,[8] and weather patterns.[4] To build a molecular scale device, a purpose many self-assembled systems are originally designed for, requires a means of modifying a surface with molecular level control. The main route to achieving this level of control is the use of self-assembled monolayers.[9]

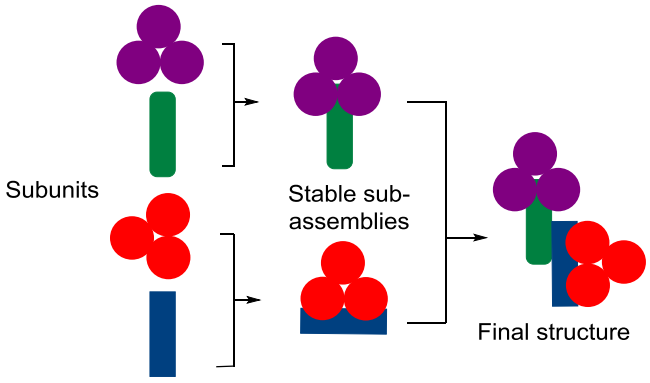

Figure 1: Modular and convergent example of self-assembly. Figure modified from reference 4.

1.2 Self-assembled monolayers on Si/SiO_2

While there exists a myriad of sub-divisions within the realm of molecular self-assembly, the focus of this thesis is on the modification of silicon oxide surfaces using self-assembled monolayers (SAMs) and their subsequent functionalisation using Lewis base organocatalysis. "Self-assembled monolayers are ordered molecular assemblies formed by the adsorption of an active surfactant on a solid surface" (Figure 2).[10]

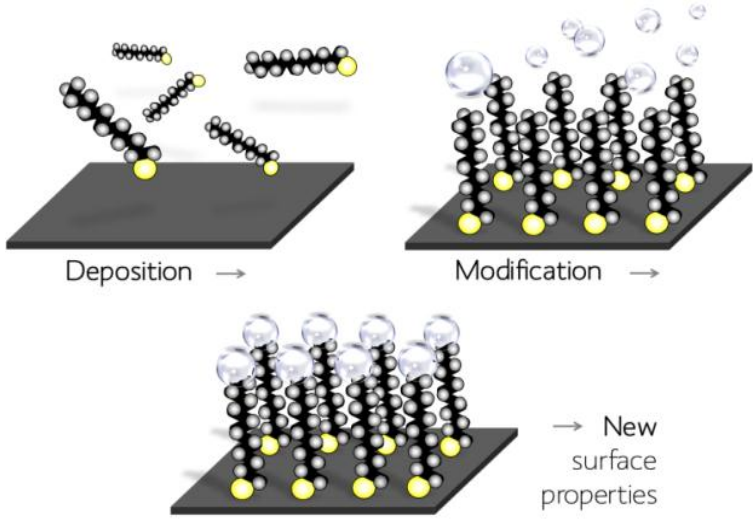

Figure 2: Schematic representation of the deposition and sequent modification of self-assembled monolayers. Figure modified from reference 111.

SAMs were first reported by Zisman and co-workers in a 1946 publication titled "Oleophobic Monolayers I. Films Adsorbed From Solution In Non-Polar Liquids".[11] The authors discovered that upon immersion of a suitable surface (Pt) into a solution of eicosyl alcohol ($C_{20}H_{41}OH$), an oleophobic monolayer formed that was thought to be monomolecular in nature. Subsequent analysis of the resulting SAMs gave strong support for this hypothesis. Surprisingly though, barring a few sporadic reports, [12-15] the field lay dormant for over three decades and it wasn't until 1980 when Sagiv reported the use of octadecyltrichlorosilanes (OTS) **2** as amphipathic precursors for the formation of a well-ordered SAM on glass from dilute solutions (Figure 3).[16] This report inspired a new wave of academic interest in the field of self-assembled monolayers on a variety of solid surfaces.[10, 17-18]

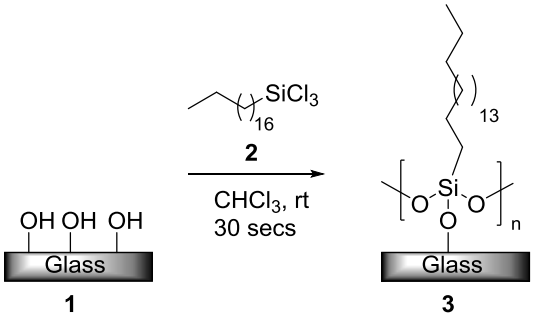

Figure 3: Use of OTS on glass to fabricate a SAM reported by Sagiv.

1.2.1 Deposition mechanism of alkylsilanes on SiO_2

While many, if not all, suitable oxide surfaces can facilitate the formation of an alkylsilane based SAM to some degree, certain surfaces are better than others.[19] The properties of these films, that is; thickness, orientation, chemical composition and order of the alkyl chains, has been studied in detail with a general trend in terms of effectiveness evident (Figure 4).[16, 20-24] Some of the advantages of using alkylsilanes on Si/SiO_2 to form SAMs are their physical,[25-27] thermal [28-29] and chemical stability[10, 18] over their alkanethiol on Au counterparts.

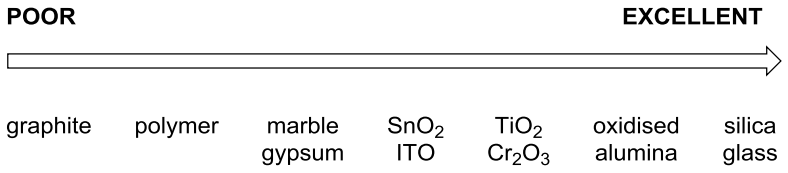

Figure 4: Effectiveness of silane deposition on a variety of oxide surfaces.

The most common protocol for the preparation of alkylsilane based SAMs is the immersion of a hydrophilic Si/SiO_2 surface into a dilute (0.25-2.5 mM) solution of the desired silane for a suitable time (~16 h) at room temperature. Removal and subsequent cleaning usually affords a densely packed SAM. Commonly, the oxide surface in question is activated prior to self-assembly in order to expose the maximum amount of hydroxyl groups.[30] Several methods have been developed to achieve this but usually strong acids and/or oxygen plasma are used.[31-32] This cleaning procedure renders the surface extremely hydrophilic, which makes it prone to the formation of a thin water layer. There is a general consensus that trace amounts of water on the oxide surface is needed to form a well-packed monolayer. In the original report by Sagiv[16] he recognised that water adsorbed onto a surface was necessary to hydrolyse the chlorosilane, and assumed that the hydrolysed silanes underwent condensation reactions with the surface hydroxyl groups as well as adjacent OTS molecules to form a polymerised chain where each OTS molecule is individually anchored to the surface. However, this view was adjusted when Finklea and co-workers showed that a well-packed monolayer of OTS could be formed on an Au surface - a surface devoid of any

hydroxyl groups.[33] The authors concluded that self-assembly must occur on the adsorbed water layer on the Au surface and that the silane groups are incorporated into a 2D cross-linked network of Si-O-Si bonds. In the case of alkylsilanes on Si/SiO_2 the overall deposition picture is similar but with some modifications. It is proposed that only 10-20% of the alkylsilanes need to form a covalent bond to the surface, which suggests that SAM formation is driven primarily by interactions between hydrocarbon chains and Si-O linkages between adjacent silanols (Figure 5). X-ray reflectivity experiments by Silberzan and co-workers[34] also indicated that not all of the molecules are covalently linked to the surface but rather exist in a cross-linked network similar to that proposed by Finklea *et al*.[33] This also explains the observation that alkylsilane SAMs on Si/SiO_2 are mechanically and chemically more robust than the alkylsilane SAMs on Au counterpart.

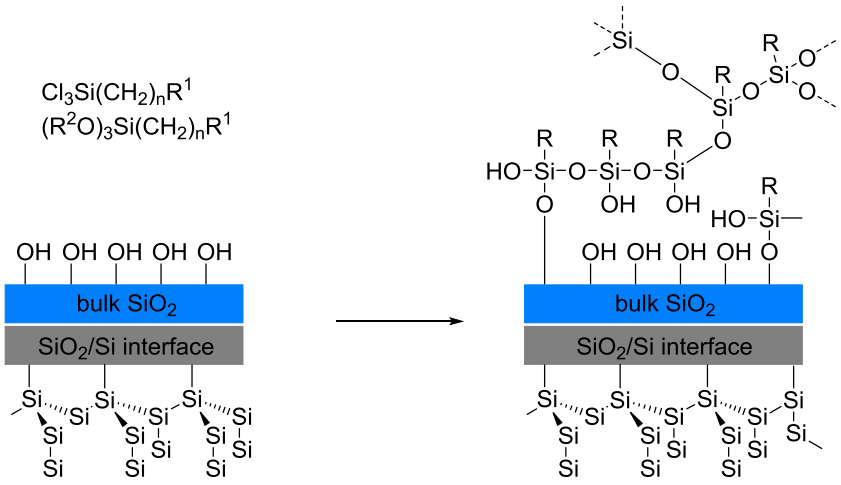

Figure 5: Self-assembly process of alkylsilanes on Si/SiO_2 surfaces. †

The ease of preparation of SAMs on Si/SiO_2 is a major advantage towards their use in nanoscale device fabrication. However, despite their ease of preparation it is exceedingly difficult to reproduce a well-defined SAM as their formation is strongly dependant on a range of parameters including solution age,[35] solvent,[36] water content,[35, 37] deposition time,[38] and temperature.[39-40] One of the major issues with the preparation of alkylsilanes with a headgroup consisting of trichlorosilane ($R\text{-}SiCl_3$), trimethoxysilane ($R\text{-}Si(OMe)_3$) or triethoxysilane ($R\text{-}Si(OEt)_3$) is adventitious formation of polysiloxanes that can physisorb onto the SiO_2 surface.[9, 34] However, it is very difficult to distinguish physically adsorbed silanes from chemically adsorbed ones, which in turn impacts on the performance of the SAM in subsequent applications. An ill-defined

† 2D Si-O-Si network has been greatly simplified (2D vs 3D) in Figure 5 for clarity purposes.

SAM can present a major concern when the monolayer is to be used as the base layer for truly molecular devices.[41]

1.2.2 Applications of SAMs on Si/SiO_2

Alkylsilane based SAMs have varying applications in the field of microelectromechanical systems (MEMS) and their smaller equivalents nanoelectromechanical systems (NEMS). MEMS and NEMS are often made from silicon because of its desirable mechanical properties.[42] The field of MEMS has grown rapidly over the last few years due to the expanded market for micromachined mechanical transducers.[43] Specific applications of MEMS and NEMS include the fabrication of DNA chips and protein microarrays[44-45] as well as microelectrical devices[46] and electrochemical sensors.[47]

Yoshioka *et al*. demonstrated one of the first examples of immobilisation of a monoclonal antibody to a silicon surface (Figure 6).[48] The aim was to immobilise monoclonal antibody **7** on a surface of a glass tube as a model to confirm the stability of ultra-thin SAMs by enzyme immunoassay. The authors deposited an initial amine terminated SAM **4** from 3-aminotriethoxysilane (APTES), which was modified with glutaraldehyde **5** to generate aldehyde terminated SAM **6**. Reductive amination of amine functionalised normal mouse monoclonal Ab **7** afforded surface **8**. The amount of antibody immobilised on the surface was measured using an enzyme immunoassay by reaction with anti-mouse IgG and *p*-nitrophenylphosphate in alkaline phosphatase buffer. The amount of *p*-nitrophenol was monitored by fluorescence to quantify the amount of antibody immobilised.

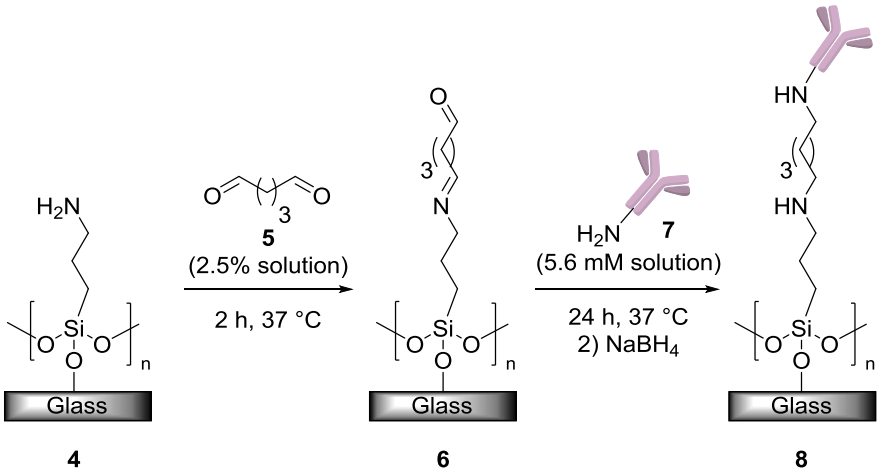

Figure 6: Immobilisation of anti-mouse immunoglobulin G on a glass tube.

1.3 Self-assembled monolayers on Au

Thiolates on Au surfaces are the most studied within the scientific literature,[18] as there are several advantages to using them over other solid surfaces. Au is easy to obtain and is straightforward to prepare as a thin film on a suitable surface. Au is a reasonably inert metal and does not form oxides at ambient temperatures as it does not react with atmospheric O_2. Au can also bind thiols with high affinity and readily forms Au-S bonds on a surface,[49] which is a highly desirable property as they readily displace adventitious materials from the surface during the deposition process. A detailed structure of a thiolate based SAM on Au showing the various impurities and structural defects possible is shown in Figure. 7.

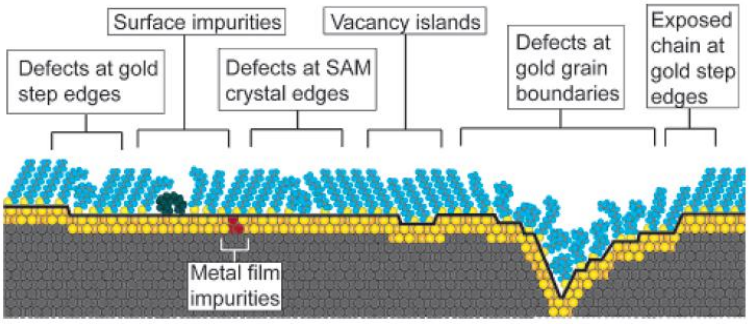

Figure 7: Schematic illustration of some of the intrinsic and extrinsic features of SAMs on Au surfaces. Figure taken from ref 18.

Not long after the seminal work by Sagiv using alkylsilanes on Si/SiO_2, Allara *et al*. published the first report of forming a thiol based SAM on a Au surface.[49] The authors deposited a series of disulfides on Au^0 surfaces and measured the resulting film thickness, contact angle and IR spectra, all of which indicated a densely packed SAM was being formed on the Au surface (Figure 8).

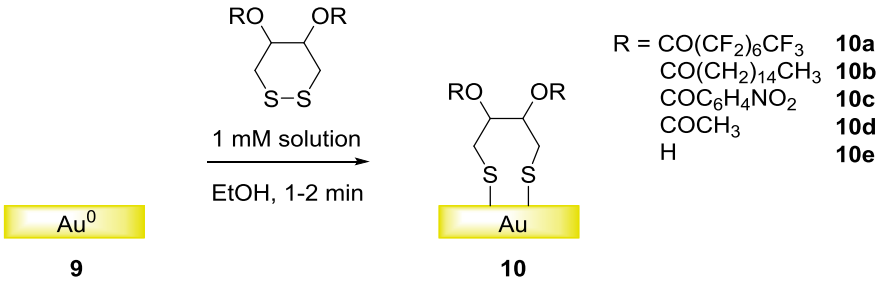

Figure 8: Deposition of series of disufides by Allara *et al*.[49]

1.3.1 Deposition mechanism

The chemistry involved for the absorption of thiols on Au is, in principle, the most straightforward but in many ways remains the most perplexing. As Au does not form stable oxides in ambient

conditions, the formation of SAMs from thiols is not complicated by chemistries that may be required to reduce or displace surface oxides. Surprisingly, the nature of the gold-thiol bond is still a subject of controversy even though many characterisation techniques have been used to study it.[50] While the exact details still remain elusive, a qualitative picture may be presented for certain classes. The formation of a thiolate requires the activation of the S-H bond of the thiol or the S-S bond of a disulfide. The reaction may be considered as a formal oxidative addition of the S-H bond to the Au surface followed by reductive elimination of the hydrogen.[10] The thiol-gold bond is sometimes described as a surface bound thiolate with a bond energy of 170 kJ mol^{-1} due to the polar nature of the bond, and is regarded as a pseudo-covalent bond (Equation 1)[9-10] with van der Waals forces between neighbouring molecules stabilising the structure.[51]

$$R{-}S{-}H \; + \; Au^0 \rightarrow \; R{-}S^{\ominus}\,Au^{\oplus} \cdot Au^0 + 1/2\ H_2$$

Equation 1: Reaction of an alkanethiol with a Au^0 surface to form a Au-S bond.

The initial stage of thiolate chemisorption on Au involves the formation of 'lying down' phases where alkanethiol molecules are parallel to the surface (Figure 9). When the surface coverage increases, a transition from parallel to 'standing-up' configuration takes place and the resulting monolayer formed has the alkyl chains in the all *trans*-conformation, that is, tilted 20-30 ° from the normal to the Au surface.

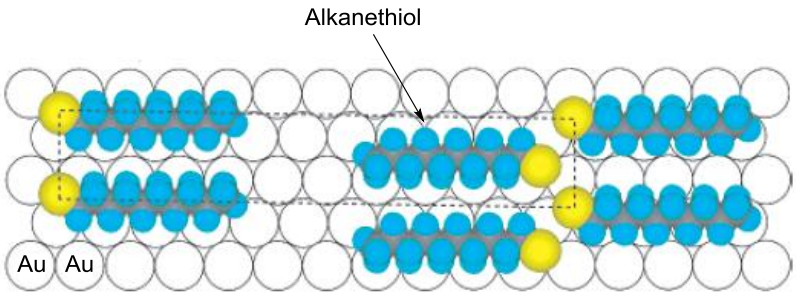

Figure 9: Alkanethiol molecules in the 'lying down' phase, parallel to the Au surface. Figure modified from reference 18. Dashed line is the unit cell.

Despite their ease of preparation and widespread use, alkanethiol based SAMs often face stability issues.[52-53] Their poor long term stability is due to oxidation of the Au-S bond to either sulfinates ($-SO_2$) or sulfonates ($-SO_3$)[52, 54] with the rate of oxidation varying significantly with chain length.[55-56] Alkanethiol based SAMs also suffer from low thermal stability as the desorption of thiols from the Au surface occurs at ~60 °C, which means that any modification of thiolate SAMs on Au must be performed below this temperature to keep the SAM intact.[57-59]

1.3.2 Applications of SAMs on Au

Despite the aforementioned disadvantages, alkanethiol based SAMs are still the most popular system for forming molecular assemblies where a molecular level control is desired. These type of SAMs are suited towards a wide variety of applications including electron transfer processes,[60-61] protein resistant surfaces, [62-63] immobilisation of DNA,[64-65] carbohydrates arrays for use in glycomics,[66-67] and antibody immobilisation[68-69]

Ozoemena and co-workers have reported the use of thiol based SAMs on Au as an electrochemical sensor for the recognition of anti-mycolic acid antibody, which is present in tuberculosis positive human serum co-infected with human immunodeficiency virus (HIV).[70] The authors were able to attach a SAM of steric acid *via* an amide coupling reaction and subsequently integrate a mycolic acid (MA) antibody **14** into the Au electrode (Figure 10). This electrode was then able to discriminate between TB-positive and TB-negative serum. The results show that the Au electrode **15** could detect HIV^{+}-TB^{+} serum diluted as high as 1:2000, indicating that this particular immunosensor has a high degree of sensitivity. The authors also conduct cyclic voltammetry scans and show no detectable deviations even after 20 repetitive scans indicating electrochemical stability.

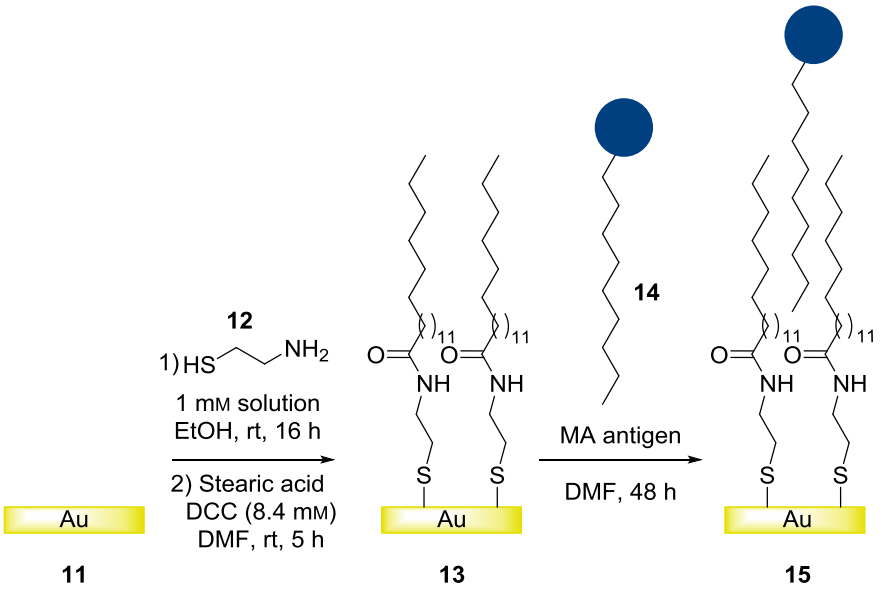

Figure 10: Fabrication of a mycolic acid antibody onto a Au surface *via* a SAM.

Leigh and co-workers have fabricated a photo-responsive Au surface based on a switchable fluorinated molecular shuttle.[71] The authors deposited a pre-synthesised rotaxane onto a carboxylic acid terminated Au surface and tested the effects of a photo-induced wetting/de-wetting protocol (Figure 11). A drop of diiodomethane was placed on the rotaxane surface and irradiated with a perpendicular beam of 240-400 nm light focused on one side of the drop. After

irradiation for 900 s the droplet had elongated 0.8 mm and the contact angle decreased from 35 ±2° to 13 ±2°. Amazingly, transport of the entire droplet occurred at a mean speed of ~1 μm s^{-1} signifying that discrete changes in surface polarity can translate to the macroscopic level.

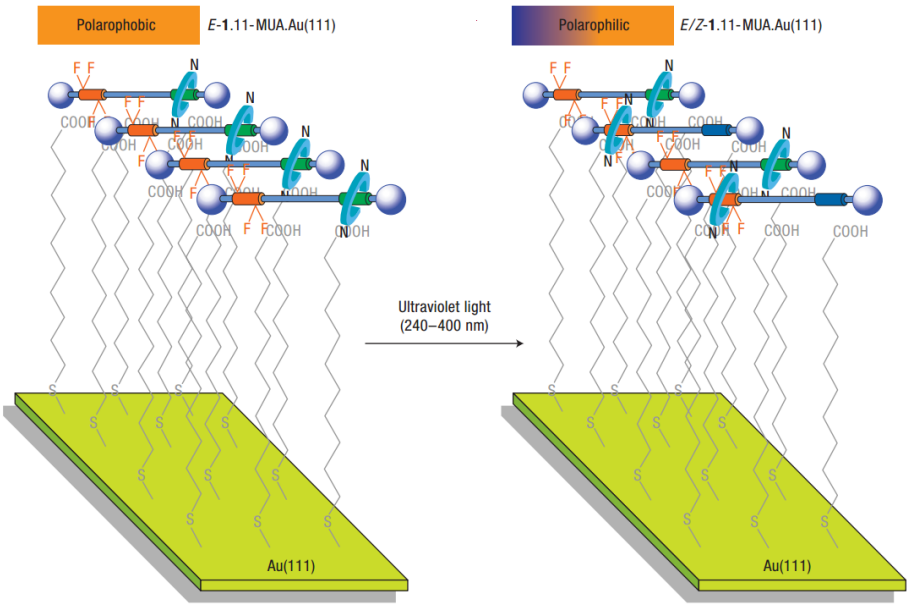

Figure 11: A photo-responsive surface based on switchable molecular shuttles. Reprinted with permission from reference 73. Copyright 2016 Nature Publishing Group.

1.4 Modification of other oxide surfaces

Gademann and co-workers have developed a molecular surface modification platform based on nitrocatechol derivatives that allows functionalisation of TiO_2 and efficient release of a nanoparticle bound cargo by photoinduction using UV light at 366 nm.[72] The authors designed a nitrocatechol derivative which was anchored to a TiO_2 nanoparticle (Figure 12) and used HPLC analysis to measure the increase in concentration of fluorophore **18** upon photocleavage of **16**. The features of this protocol are the ease of functionalisation of TiO_2 particles, the stability of the resulting particle and rapid release of the bound cargo (*ca*. 50% in 46 min).

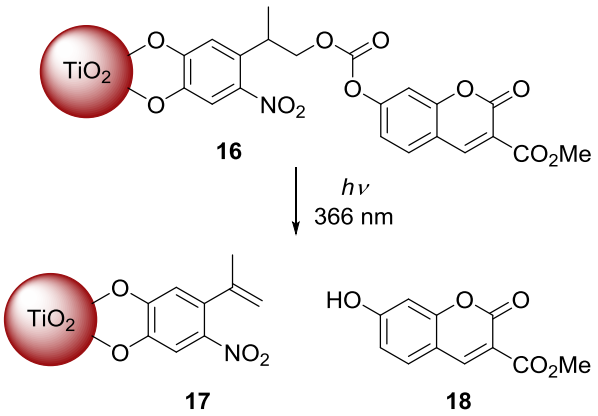

Figure 12: Photocleavage of nitrocatechol 16 under UV light at 366 nm.

Talham and co-workers have developed a Mn^{III} porphyrin catalyst **21** supported on zirconium phosphonate films and evaluated its catalytic efficiency in the epoxidation of cyclooctene.[73] The authors impressively deposited a series of organic monolayers using a combination of Langmuir-Blodgett and SAM methodologies to afford a Zr^{4+} surface. A pre-synthesised Mn^{III} porphyrin complex was then anchored to the surface *via* phosphonate moieties where each Zr^{4+} site is bound to a single octadecylphosphonic acid moiety. The macrocycle plane is believed to be oriented almost parallel to the surface. The surface bound porphyrin was evaluated in the epoxidation of cyclooctene **19** as well as that of its homogeneous equivalent. The results showed that thin films of the Mn^{III} porphyrin **21** were more effective, in terms of TON, than the homogeneous reaction. This is in part due to the deactivation of the homogeneous system after a certain time due to the formation of dimers in solution. While the authors cite that monolayers on flat surfaces have limited utility as practical catalysts due to the difficulty in achieving large surface areas, these types of systems can be useful tools in the study of heterogeneous reactions.

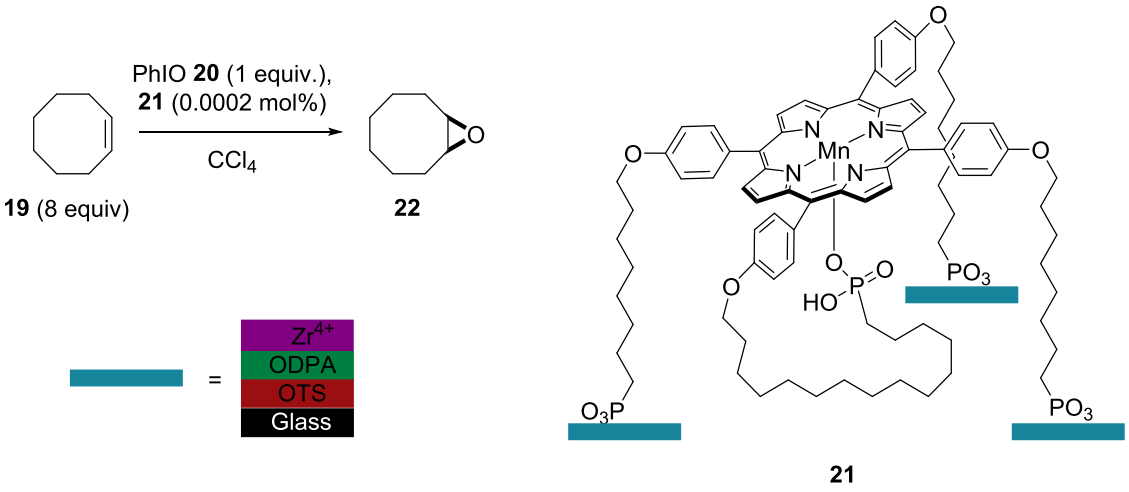

Figure 13: Epoxidation of cyclooctene using supported Mn^{III} porphyrin catalyst 21. OTS = octadecyltrichlorosilane. ODPA = octadecylphosphonic acid.

1.5 Analytical techniques

With surface science many spectroscopic and analytical techniques can be employed to investigate various properties of surfaces and nanostructures. During the course of this work four main techniques were employed to assess the success of the self-assembly process as well as the subsequent reactions performed on the surface. These include X-ray photoelectron spectroscopy (XPS), atomic force microscopy (AFM), ellipsometry and static water contact angle (CA) and are discussed in detail in the following section.

1.5.1 Atomic force microscopy

Atomic force microscopy (AFM) is a type of scanning probe microscopy and can demonstrate resolutions on the nanometre scale. The sensing part of an AFM consists of a microcantilever that is fixed at one end, connected to a support chip which is held in place by the AFM system while the other end of the cantilever has a sharp tip attached. When the tip is brought into proximity with the sample surface, intermolecular forces, such as van der Waals, between the tip and sample lead to a deflection of the cantilever.[74-75] This movement is detected by a laser which is reflected off the back of the cantilever and relays back information to the detector (Figure 14). If the tip is scanned over the surface and the response of cantilever movement is monitored then a topographic image of the surface can be generated.[78]

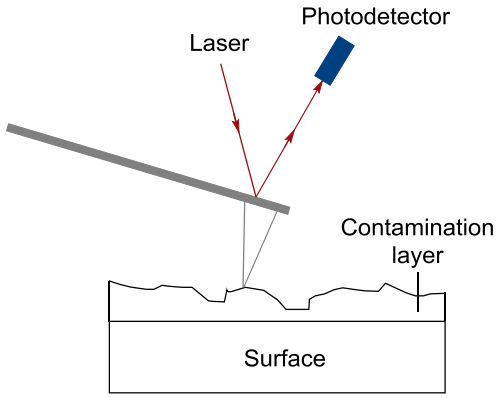

Figure 14: Main components of an AFM setup.

There are several different operational modes in AFM; static, and dynamic mode. In static mode the feedback system of the instrument keeps a set force between the tip and surface by monitoring the microcantilevers static bending and moving.[77] Essentially the tip is dragged across the surface and the resulting image is a contour of constant force. In tapping mode the tip oscillates up and down, contacting the surface then retracting.[78] In tapping mode there is often no hard contact between the tip and surface, which makes damage to the tip and/or surface much less likely. AFM can provide a topographic image of the surface and helps the user ascertain the roughness and cleanliness level of the surface under inspection.

1.5.2 X-Ray photoelectron spectroscopy (XPS)

XPS is one the most important spectroscopic methods used for analysing surfaces.[79-80]XPS is based on the photoelectric effect, where the binding energy of a core-level electron is overcome by the energy of an X-ray photon and the core level electron is ejected from the surface.[81] The kinetic energies (E_K) of the ejected electrons are measured by an electron spectrometer. Since the total energy is conserved, $E_K = h\nu - E_B$, where $h\nu$ is the energy of the photons and E_B is the binding

energy. The binding energy of each photoelectron is characteristic of the orbital from which the photoelectron came and the binding energy depends on the final state configuration after photoemission. The final state is characterised by full relaxation of all atomic orbitals towards the hole in the core level (Figure 15).

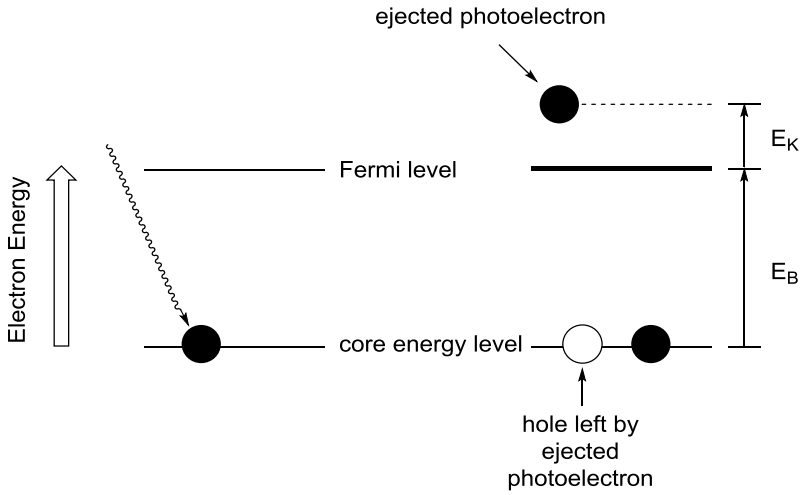

Figure 15: Photoelectron emission process.

The study of ejected photoelectrons can provide a wealth of information about the composition of a surface. Identification of the surface can be obtained through survey scans that scan over the entire range of binding energies (measured in eV) that are relevant to the organic components and the surface. Each element has a characteristic set of peaks in the spectrum, with peak positions influenced by oxidation state of the element and its chemical environment.

1.5.3 Contact angle

The static water contact angle of a solid surface can be used to establish its hydrophilicity or hydrophobicity. It is a basic technique that measures the resulting angle of a drop of deionised water on a surface that can indicate changes in the terminal functional groups of a monolayer.[82] Depending on the roughness and interactions on a surface, the contact angle can be lower than 90°, which is considered hydrophilic, or greater than 90°, which is considered hydrophobic (Figure 16).

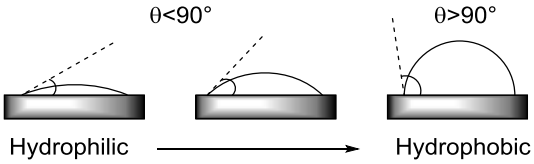

Figure 16: Degrees of hydrophilicity and hydrophobicity on a solid surface.

1.5.4 Ellipsometry

Ellipsometry is an optical spectroscopic technique that is used to determine the thickness of thin films on solid surfaces. The film thickness can be calculated by measuring changes of an elliptically polarised light beam resulting from an interaction with the sample (Figure 17). A beam of monochromatic light, which is polarised in a known state, is released upon a sample and the state of the polarized light is examined.[83] Ellipsometry measures the change in phase shift and amplitude component of the light that is reflected or transmitted by the sample and from this a monolayer thickness, relative to the known oxide layer (in the case of Si/SiO_2), can be calculated.[84]

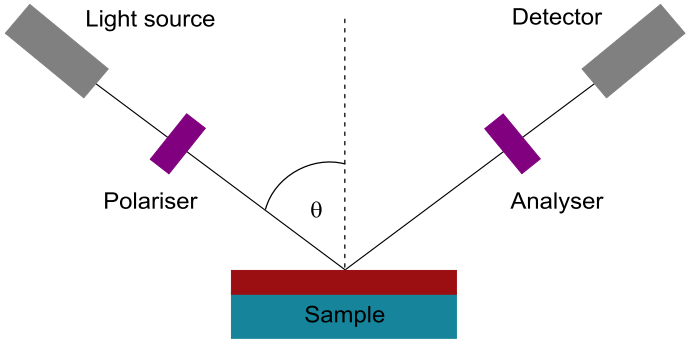

Figure 17: Schematic representation of a typical ellipsometry experiment.

1.6 Catalytic surface functionalisation

Most of the methods reported for the functionalisation of oxide surfaces are based on stoichiometric reactions between the surface and alkoxy- or allylsilanes and are usually carried out at high temperatures and sometimes harsh conditions.[85-86] Therefore, the development of catalytic methods that offer facile and mild conditions for the functionalisation of oxide surfaces, which also circumvent the use of moisture sensitive silane reagents commonly employed in the deposition process, are highly desirable.

Jun and co-workers reported a one-step grafting procedure for the preparation of azide, chloride, cyano and aldehyde terminated silica surface at room temperature using a catalytic amount of $Sc(OTf)_3$ to promote the reaction.[87] The authors synthesised a range of silanes and through the grafting procedure, derivatives of **24** were attached to a silica surface in a one-pot process (Figure 18). The grafting process is thought to proceed through a carbocation intermediate **29** and following attack of silanol **28** on organosilane **29** to release isobutene, a Si-O bond is formed to the surface forming **30**. Subsequent repetition of this reaction sequence, confirmed by disappearance of ^{13}C resonances associated with the methallyl group in the CP-MAS ^{13}C NMR spectrum, afforded **25** with both methallylsilyl groups covalently bonded to the surface.

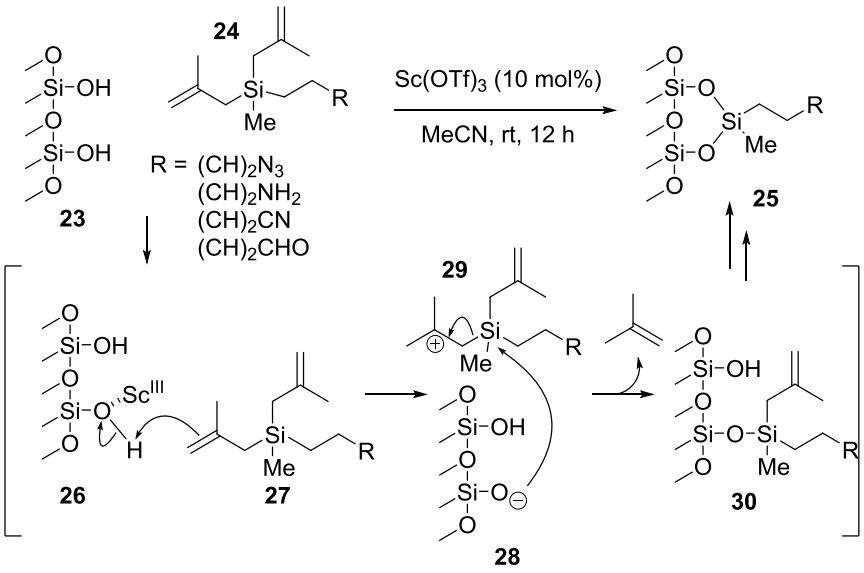

Figure 18: Grafting of organomethylallylsilane to a silica surface in the presence of catalytic $Sc(OTf)_3$ proposed to proceed *via* carbocation 29.

Another report from the research group of Jun has shown that hydroxyl-terminated Si/SiO_2 surfaces (glass) can be functionalised with vinylsilanes in the presence of catalytic $[Ir(COE)_2Cl]_2$ **33** to afford various alkyl terminated surfaces.[88] The authors deposited a series silanes on hydroxyl-terminated glass surfaces in the presence of $[Ir(COE)_2Cl]_2$ **33** and *N*,*N*-dimethylacetamide HCl **34** , which successfully promoted the grafting of silanes to the surface as confirmed by contact angle (CA) analysis (Figure 19).

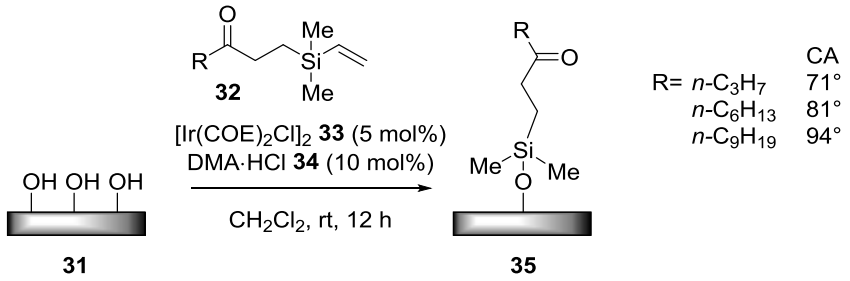

Figure 19: Grafting of vinylsilanes onto hydroxyl terminated silicon surfaces promoted by catalytic $[Ir(COE)_2Cl]_2$. COE = cyclooctene.

Nakanishi and Shimada have shown the functionalisation of silica can proceed in the presence of catalytic $B(C_6F_5)_3$ **38** through an organocatalytic Si-H activation of hydrosilanes.[89] The reaction is thought to proceed initially by complexation of hydrosilane **37** with $B(C_6F_5)_3$ catalyst **38** to form **40**. This highly reactive intermediate then reacts with surface silanol **36** to form complex **41**. One of the possible reasons for such a fast reaction between silane **40** and surface silanol **36** is the acidity of the surface silanol (pK_a = 4.9-8.5),[90] which makes the silanol oxygen prone to electrophilic attack by the silicon in complex **40**. Finally borane hydride **41b** deprotonates the

acidic proton in **41a**, forming H_2 and regenerating the $B(C_6F_5)_3$ catalyst **38**. This procedure was tolerant of a variety of functional groups including halogens, azides, amines, esters, carboxylic acids and ketones, some of which are readily reduced in the presence of hydrosilanes in homogeneous reactions.[91-93]

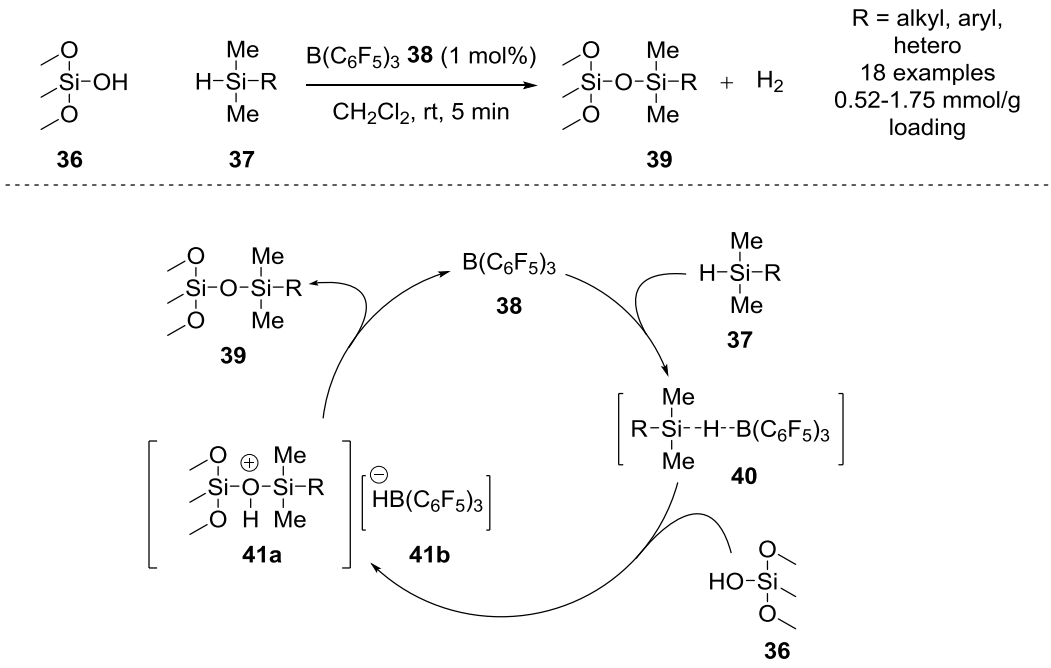

Figure 20: Functionalisation of silica in the presence of catalytic $B(C_6F_5)_3$ 38 through an organocatalytic Si-H activation of hydrosilanes and plausible mechanism.

While the grafting of various functionalities directly onto an oxide surface is a desirable property, the post-deposition functionalisation of monolayers can also be useful as the molecular control SAMs provide is tuneable and a variety of known procedures are available for this process. This type of surface modification has not yet been fully acknowledged because of low yields and the fact that little is known about the rules that govern organic reactions on surfaces.[59, 94] Despite this potential disadvantage, several transition metal-catalysed reactions have been developed for the functionalisation of SAMs on silicon, gold and germanium surfaces. Several research groups have reported the use of catalytic Pd in various cross-coupling reactions on SAMs.[95-98] For example, Nguyen and Bedzyk sought to establish whether sequential Pd-catalysed Sonogashira cross coupling reactions would occur on acetylene terminated SAMs to afford conjugated organic surfaces.[96] The authors synthesised an aryl iodide terminated SAM **42** on Si and performed a Sonogashira coupling on the surface using a microwave assisted procedure (Figure 21). The authors achieved high conversion in short reaction times with no noticeable over coupling of bromoacetylene **44** to give the diacetylated product.

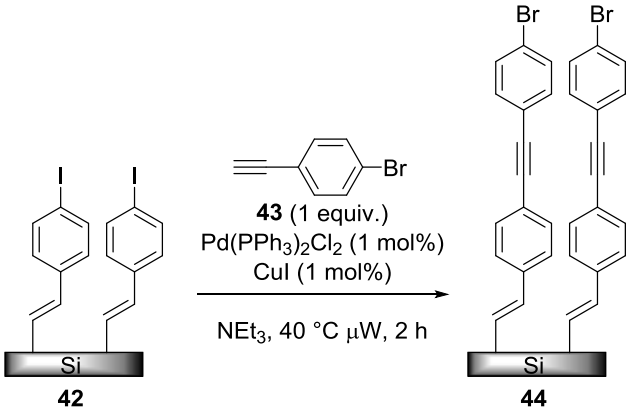

Figure 21: Pd-catalysed Sonogashira cross-coupling of aryl iodide terminated SAM with *p*-bromoacetylene 43.

Lewis and co-workers have utilised the well-known Pd-catalysed Heck reaction to couple olefins to a mixed monolayer surface.[98] A silicon surface comprised of a thiophenyl and methyl mixed monolayer was subjected to catalytic $Pd(PPh)_4$ followed by immersion in a solution of the appropriate terminal olefin to afford the Heck coupled product (Figure 22). The reaction proceeded cleanly, as no residual surface bound Pd was detected by XPS. Electrochemical studies also showed that the surface bound thiophene linker did not shift the electrochemical potential or impede electron transfer from the Si surface to the bound redox moieties when tested with Co, Cu and Zn.

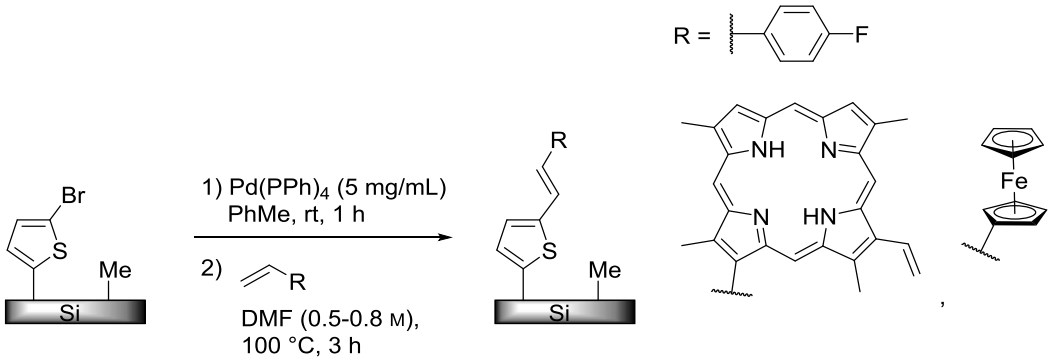

Figure 22: Synthesis of redox active mixed monolayers by the Pd-catalysted Heck reaction.

Choi and co-workers have used an in-plane enyne metathesis strategy and subsequent Diels-Alder reaction sequence to afford tetracyano, maleic anhydride and maleimide groups on the surface of Au based SAMs.[59] Based on previous work,[99] they postulated that an in-plane dimerization reaction may take place in the presence of Ru metathesis catalyst **48**. The authors synthesised a mixed surface consisting of a terminal alkyne and alkenes and subjected it to olefin cross-metathesis conditions using catalyst **48** (Figure 23). FTIR, XPS and time-of-flight secondary-ion mass spectrometry (TOF-SIMS) confirmed the presence of enyne metathesis products, which

were then subjected to a Diels-Alder reaction with tetracyanoethylene **50**, maleic anhydride and malemide which afforded the corresponding surfaces.

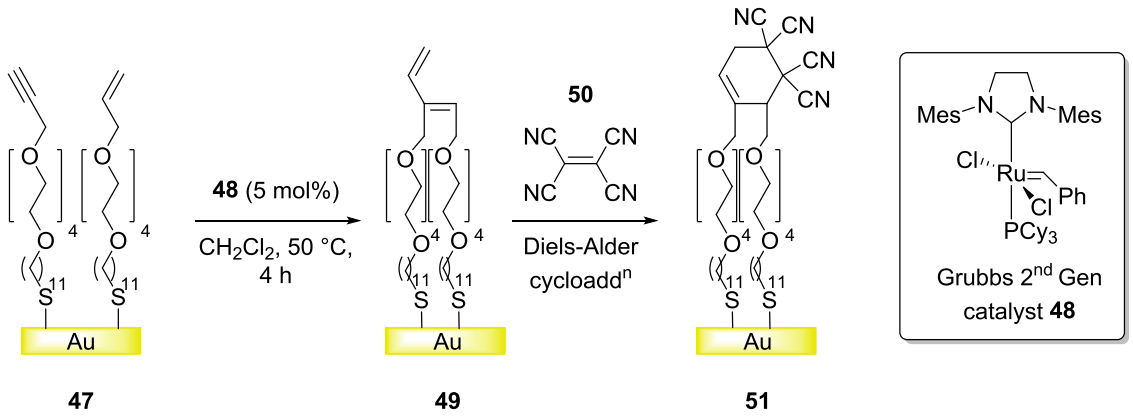

Figure 23: Enyne metathesis followed by a Diels-Alder reaction sequence.

Other transition metals have also been used in surface modification reactions on SAMs. Locklin and co-workers have reported the formation of electroactive polymer brushes on a surface *via* a surface-initiated Kumada-type polycondensation reaction.[100] The authors used an *in situ* formed $Ni(COD)(PPh_3)_2$ complex to initiate the polymerisation reaction. The Ni^0 inserts into the C-Br bond of the thiophene to form Ni^{II} complex **54** on the surface. Following the addition of Grignard **55** and intramolecular transfer of the Ni^{II} species into the C-I bond of the thiophene, $Ni^{II}I$ surface **56** is formed. Addition of another equivalent and repetition of the previous steps, using dilute HCl as a termination agent, affords a conjugated polymer brush on the surface with a measured thickness of 42 nm.

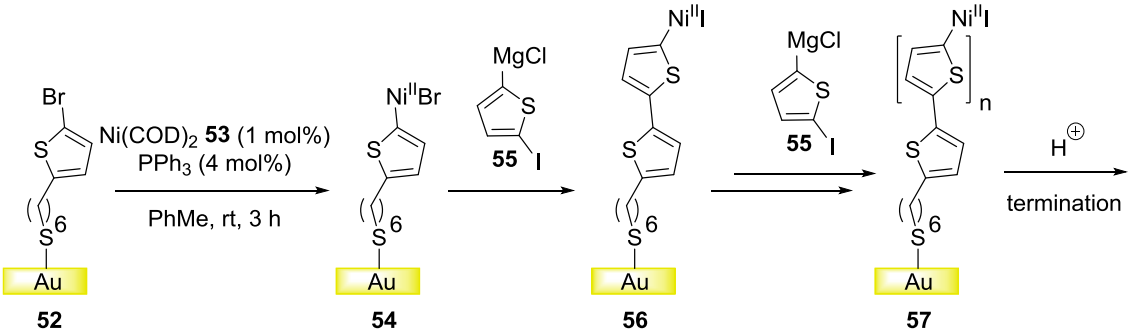

Figure 24: Synthesis of thiophene-based polymer brushes on a surface using a Ni-catalysed Kumada-type polycondensation method.

1.7 Previous work within the Smith group

The Smith group have previously investigated the generation and uses of ammonium enolates formed from carboxylic acid derivatives and Lewis basic isothiourea (ITU) organocatalysts. For

example, ammonium enolates generated from arylacetic acids and achiral isothioureas undergo Michael addition-lactonisation reactions with trifluoromethylenones, affording racemic dihydropyranones (DHPs) in solution with moderate to high diastereoselectivity (Figure 25).[101]

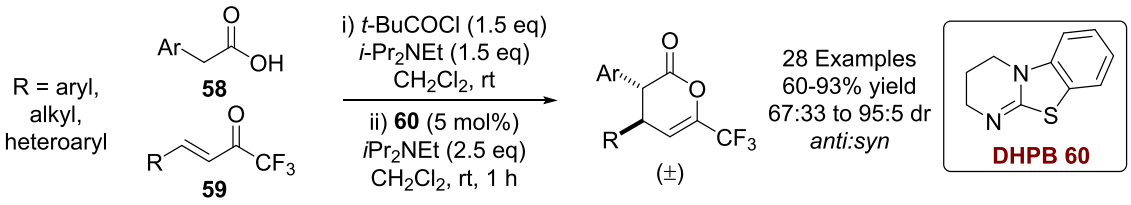

Figure 25: Generation of racemic DHPs with high diastereoselectivity in solution using DHPB.

Furthermore, chiral isothioureas such as HyperBTM-(2*S*,3*R*) **61** catalyse the enantioselective Michael addition-lactonisation of trifluoromethylenones in solution, yielding *anti*-DHPs with high diastereo-and enantiocontrol (Figure 26).[101]

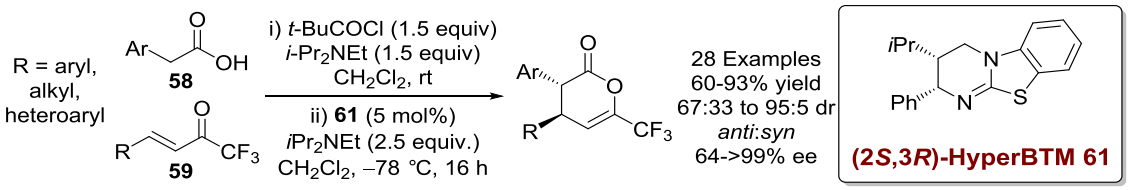

Figure 26: Generation of enantiopure DHPs in solution using HyperBTM.

The proposed mechanism of the Michael addition-lactonisation proceeds *via* initial formation of a mixed anhydride **62** formed *in situ* from pivaloyl chloride and the appropriate phenylacetic acid. Subsequent *N*-acylation with HyperBTM-(2*S*,3*R*) **61** generates the corresponding acyl isothiouronium **63**, with deprotonation generating the (*Z*)-ammonium enolate **64**. This undergoes a stereoselective Michael addition with the trifluormethylenone **59**, followed by intramolecular cyclisation, to generate DHP **66** (Figure 27).

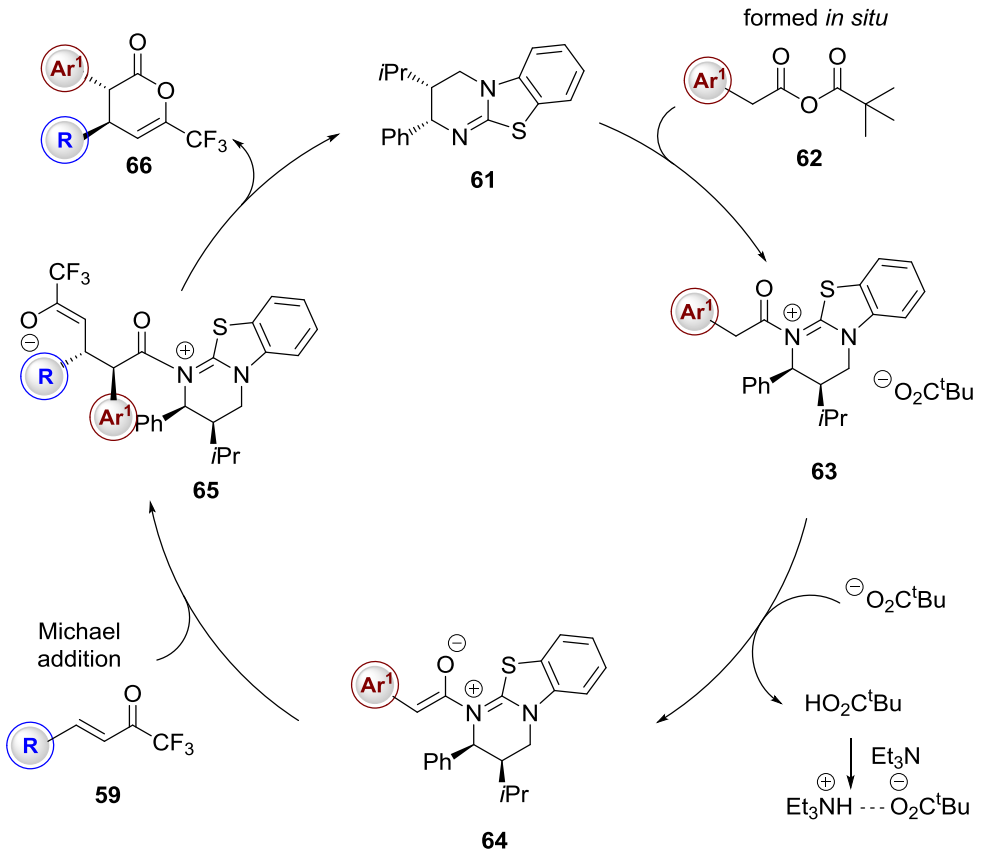

Figure 27: Proposed catalytic cycle for the enantioselective Michael-lactonisation process.

Detailed DFT calculations were used to investigate the minimum energy transition state(s) involved in the conjugate addition step of the reaction (Figure 28).[102] The structure of **69** highlights the preference for the intermediate isothiouronium enolate **64** to adopt a half-chair type confirmation with the phenyl component pseudo-axial. The enantioselectivity of the process arises from the stereodirecting groups on the isothiourea that block the *Si* face of the enolate favouring addition onto the *Re* face, while the diastereoselectivity comes from enolate geometry ((*E*) *vs* (*Z*)). The 1,5-planar geometry associated with O···S interactions allows for the orbital containing the non-bonding lone pair of electrons on the donor atom to overlap more effectively with the σ^* orbital of C-S bond (n_o to $\sigma^*_{C\text{-}S}$).[103] Tantillo and Romo have shown that n_o to $\sigma^*_{C\text{-}S}$ interactions can govern the selectivity of Diels-Alder cycloadditions by restricting rotation about the C-N bond of the acylammonium salt intermediate (**64** in this case) giving high *endo* selectivity in the products.[104] Birman and Houk have also used computational studies to model the origin of enantioselectivity in benzotetramisole-catalysed dynamic kinetic resolution of azalactones.[105] The authors postulate that the oxygen atom of the acyl carbonyl is nearly coplanar with the thiazolium moiety and points towards the sulfur atom, basing their arguments on non-bonding S-O interactions.

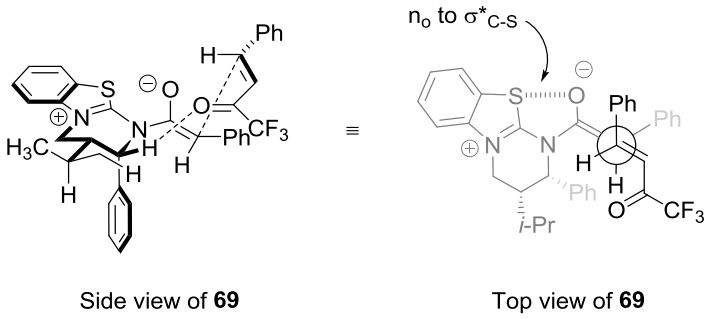

Figure 28: Possible pre-transition state assembly for conjugate addition step

Such n_o to $\sigma^*_{C\text{-}S}$ interactions have been reported by others in reaction processes utilising isothioureas[106-107] and is well precedented in the literature.[108] Stahl and co-workers have shown, through a comprehensive study of small molecule crystals, that carbonyl groups display a strong preference for 1,5-O···S interactions.[109] An example of a non-covalent O···S interaction was elegantly shown by Nagao and co-workers where the authors show, through analysis of X-ray crystal structures and *ab initio* calculations, that (acylamino)thiadiazoline derivatives exhibit an O···S attractive force.[110] This attractive force holds the thiadiazoline in a in rigid *cis* conformation (**70**b) and reduces the bond distance to 2.65 Å, which is significantly shorter than the sum of the Van der Waals radii (3.32 Å) (Figure 29).

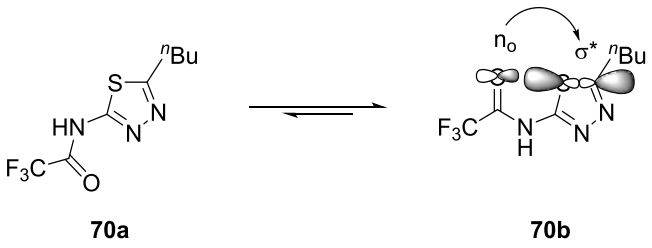

Figure 29: n_o to $\sigma^*_{C\text{-}S}$ interactions in thiadiazoles.

In the context of isothioureas, Birman and co-workers have proposed that the 1,5-O···S interaction present in acylated isothioureas may provide enhanced activity compared with their amidine derivatives due to a conformational lock being present (Figure 30 (a)).[107] This view was corroborated by Romo and co-workers who postulated the reason for high selectivity in their nucleophile-catalysed aldol lactonisation (NCAL) process using (*S*)-HBTM **73** was due to a conformation lock in the pre-transition state assembly between the sulfur atom of the *N*-acylated catalyst and the oxygen atom on the carbonyl group (Figure 30 (b)).

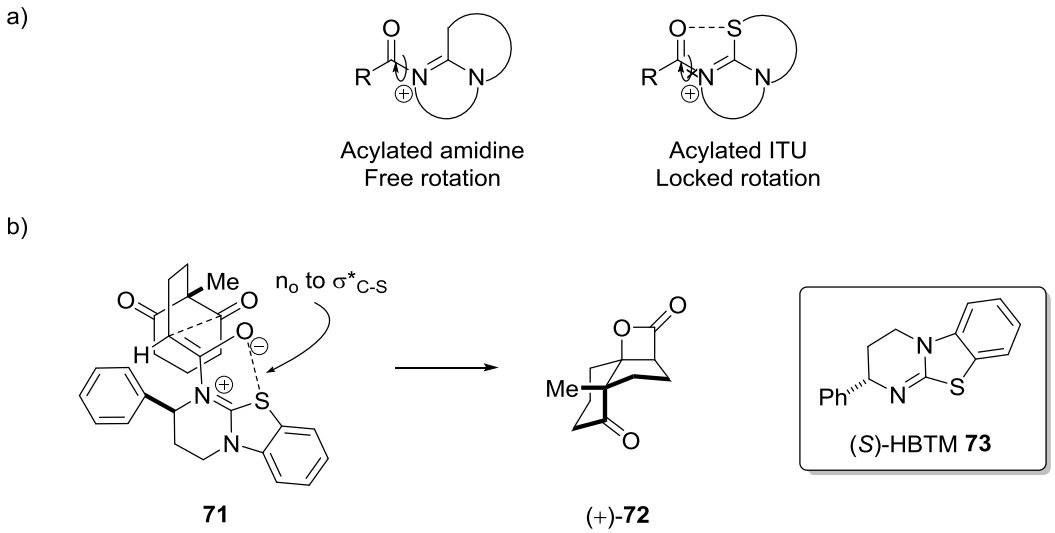

Figure 30: Rotation in acylated amidines and isothioureas.

The challenges associated with transferring a well studied homogeneous reaction to the heterogenous state are many. How the enantioselection process will proceed is a large unknown. How will the reaction proceed mechanistically? Indeed chiral molecules on surfaces have been shown to form complex two-dimensional structures with specific enantiomeric chracteristics, different from what might be expected when considering the single molecule itself.[111] As surfaces can lower the symmetry of the adsorbates, chiral molecules can display more complex behaviours on surfaces than in the gas/liquid phase and prochiral molecules can become chiral upon adsorption, also displaying specific enantiomeric chracteristics.[111] How this intrinsic feature of surfaces may play a role in the development of new enantioselective processes on surfaces is unknown. The concept of homo and heterochirality may come into play where particular domains of the monolayer on a surface posseses different chirality, possibly influencing the reaction pathway and potentially increasing or decreasing the resulting enantioselectivity. As homochirality is proposed to have originated from specific enantioselective processes occurring on chiral surfaces [112] this may potentially play a major role in the selectivity of the reaction. One of the main challenges associated with the analysis of chiral surfaces is the measurement and quantification of the resulting selectivity. These difficulities arise from the limitations of the current state-of-the-art methodologies, not allowing for quantification of the reaction selectivity on the surface. These limitations must be overcome in order to obtain a clearer picture of what is occurring during the reaction process.

The generality and scope of this Michael addition-lactonisation procedure led us to believe that it would be a suitable candidate for optimisation on a surface functionalised with SAMs. Moreover, the potential for the generation of enantioenriched surfaces from an achiral starting material on a

surface *via* enantioselective organocatalysis offers a direct route towards highly functionalised SAMs with what is hoped to be high levels of selectivity.

1.8 Previous work within the Hähner group

Previous studies within the Hähner group has shown that a series of vinyl terminated SAMs can be deposited on SiO_2 using vapour phase methodology.[31][111] Vapour phase deposition can be conducted by vapourising a volatile silane in the presence of freshly cleaned SiO_2 surfaces and in a sealed reaction vessel (Figure 12 (a)). This demonstrated that a suitable silane precursor could be utilised in a vapour deposition process to afford virtually identical results to that of the solution based analogue.

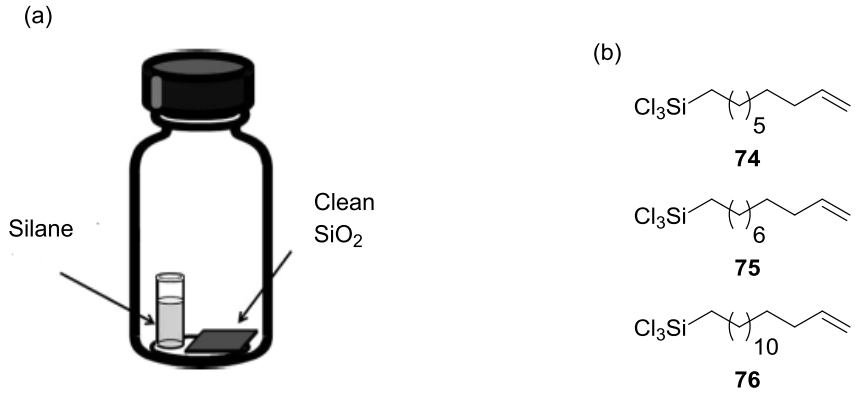

Figure 12: (a) Experimental set-up for vapour phase deposition, (b) vinyl silanes used in the deposition process.

While this report was a proof of concept study and no subsequent reaction was performed on the surface, follow up reports show that vinyl-terminated SAMs can be exploited in a gas phase in a C-C bond forming reaction with bis(trifluoromethyl)carbenes (Figure 31).[114] In this study the vinyl terminated SAMs were treated with hexfluoroacetone azine (HFAA) **78** in the gas phase with the resulting films being consistent with the presence of a bis(trifluoromethyl) cyclopropane group on the surface after nitrogen extrusion.

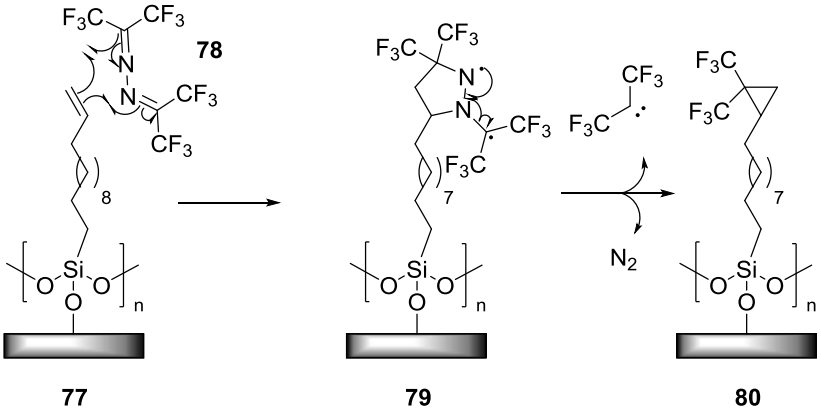

Figure 31: Postulated mechanism for Bis(trifluoromethyl) cyclopropane formation on a surface.

Further work in the area, has also shown that a range of dihalocarbenes can be added across vinyl terminated SAMs (Figure 32).[113] The reactive species (dihalocarbenes) were generated from $CHCl_3$, $CHBr_3$ and TMS-CF_3 (Ruppert-Prakash reagent) and were reacted with vinyl terminated SAMs to afford the subsequent dihalocarbene surfaces. XPS analysis showed that after reaction with the carbene species the overall surface coverage was around 30%.

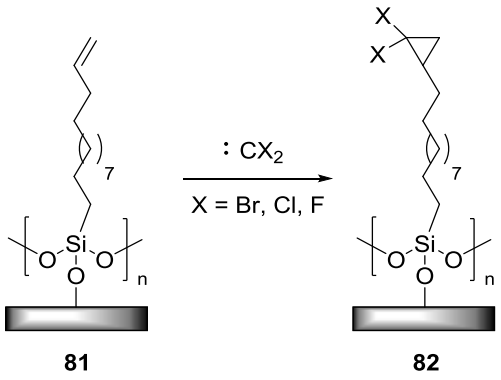

Figure 32: Previous work showing synthesis of dihalocarbene terminated SAMs.

1.9 Project aims & objectives

Organocatalysis has become one of the main methods for selective carbon-carbon bond formation over the last decade and can provide products with high levels of stereocontrol. At the beginning of this PhD there was no example of using organocatalysis to immobilise a reactive species onto a surface. We therefore sought to modify pre-existing SAMs using isothiourea organocatalysis in the late-stage formation of functionalised trifluoromethyldihydropyranones on a Si/SiO_2 surface (Figure 33 (a)). Initial work focused on a proof of concept study where racemic DHPs were generated using the achial isothiourea catalyst DHPB **60**. The ultimate aim for this work was the *in situ* generation of enantiomerically enriched surfaces using the chiral isothiourea HyperBTM-(2*R*,3*S*) **61** (Figure 33 (b)). A second aim was to develop a procedure for the immobilisation of reactive isothiourea organocatalysts onto a solid support and evaluate their use as heterogeneous Lewis base catalysts in a range of processes.

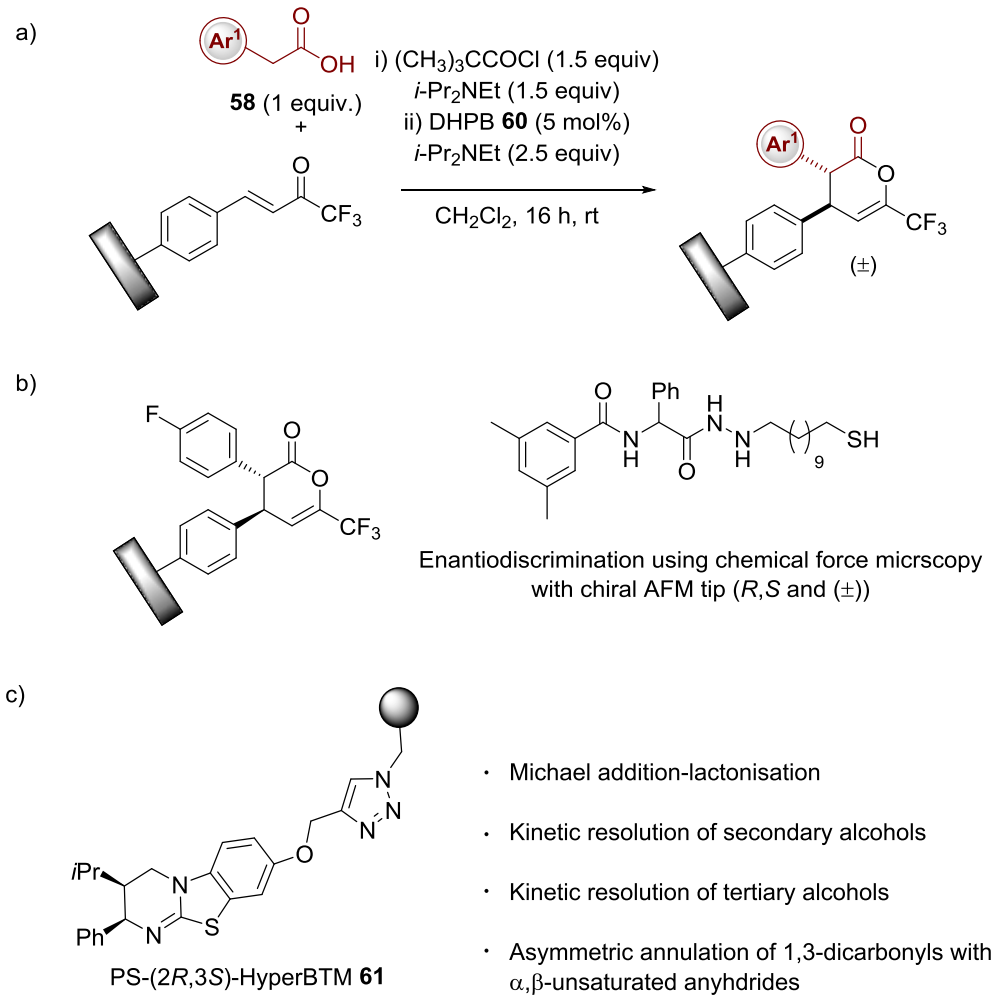

Figure 33: (a) Synthesis of racemic DHP using isothiourea organocatalysis (b) Chiral discrimination of enatioenriched surfaces using chemical force microscopy (c) immobilisation of isothiourea catalyst on a polystyrene support.

1.1 References and Notes

[1] S. Zhang, *Nat Biotech* **2003**, *21*, 1171-1178.
[2] R. Bogue, *Assembly Autom.* **2008**, *28*, 211-215.
[3] G. M. Whitesides, B. Grzybowski, *Science* **2002**, *295*, 2418-2421.
[4] D. Philp, J. F. Stoddart, *Angew. Chem. Int. Ed.* **1996**, *35*, 1154-1196.
[5] J.-C. Loudet, P. Barois, P. Poulin, *Nature* **2000**, *407*, 611-613.
[6] J. Aizenberg, A. J. Black, G. M. Whitesides, *Nature* **1999**, *398*, 495-498.
[7] J. A. Shapiro, *Annu. Rev. Microbiol* **1998**, *52*, 81-104.
[8] N. Shimoyama, K. Sugawara, T. Mizuguchi, Y. Hayakawa, M. Sano, *Phys. Rev. Lett.* **1996**, *76*, 3870-3873.
[9] J. J. Gooding, S. Ciampi, *Chem. Soc. Rev.* **2011**, *40*, 2704-2718.
[10] A. Ulman, *Chem. Rev.* **1996**, *96*, 1533-1554.
[11] W. C. Bigelow, D. L. Pickett, W. A. Zisman, *J. Coll. Sci.* **1946**, *1*, 513-538.
[12] W. C. Bigelow, L. O. Brockway, *J. Coll. Sci.* **1956**, *11*, 60-68.
[13] L. S. Bartell, R. J. Ruch, *J. Phys. Chem.* **1956**, *60*, 1231-1234.
[14] L. S. Bartell, R. J. Ruch, *J. Phys. Chem.* **1959**, *63*, 1045-1049.
[15] O. Levine, W. A. Zisman, *J. Phys. Chem.* **1957**, *61*, 1068-1077.
[16] J. Sagiv, *J. Am. Chem. Soc.* **1980**, *102*, 92-98.

[17] S. Onclin, B. J. Ravoo, D. N. Reinhoudt, *Angew. Chem. Int. Ed.* **2005**, *44*, 6282-6304.
[18] J. C. Love, L. A. Estroff, J. K. Kriebel, R. G. Nuzzo, G. M. Whitesides, *Chem. Rev.* **2005**, *105*, 1103-1170.
[19] S. P. Pujari, L. Scheres, A. T. M. Marcelis, H. Zuilhof, *Angew. Chem. Int. Ed.* **2014**, *53*, 6322-6356.
[20] N. Herzer, S. Hoeppener, U. S. Schubert, *Chem. Comm.* **2010**, *46*, 5634-5652.
[21] R. Tian, O. Seitz, M. Li, W. Hu, Y. J. Chabal, J. Gao, *Langmuir* **2010**, *26*, 4563-4566.
[22] S. R. Walter, J. Youn, J. D. Emery, S. Kewalramani, J. W. Hennek, M. J. Bedzyk, A. Facchetti, T. J. Marks, F. M. Geiger, *J. Am. Chem. Soc.* **2012**, *134*, 11726-11733.
[23] K. Wen, R. Maoz, H. Cohen, J. Sagiv, A. Gibaud, A. Desert, B. M. Ocko, *ACS Nano* **2008**, *2*, 579-599.
[24] A. Y. Fadeev, T. J. McCarthy, *J. Am. Chem. Soc.* **1999**, *121*, 12184-12185.
[25] H. Sano, H. Maeda, T. Ichii, K. Murase, K. Noda, K. Matsushige, H. Sugimura, *Langmuir* **2009**, *25*, 5516-5525.
[26] Y.-a. Cheng, B. Zheng, P.-h. Chuang, S. Hsieh, *Langmuir* **2010**, *26*, 8256-8261.
[27] B. D. Booth, S. G. Vilt, J. B. Lewis, J. L. Rivera, E. A. Buehler, C. McCabe, G. K. Jennings, *Langmuir* **2011**, *27*, 5909-5917.
[28] R. Maoz, H. Cohen, J. Sagiv, *Langmuir* **1998**, *14*, 5988-5993.
[29] R. Maboudian, W. R. Ashurst, C. Carraro, *Sensor Actuat. A-Phys.* **2000**, *82*, 219-223.
[30] L. T. Zhuravlev, *Langmuir* **1987**, *3*, 316-318.
[31] M. Adamkiewicz, T. O'Hara, D. O'Hagan, G. Hähner, *Thin Solid Films* **2012**, *520*, 6719-6723.
[32] D. A. Hook, J. A. Olhausen, J. Krim, M. T. Dugger, *J. Microelectromech. S.* **2010**, *19*, 1292-1298.
[33] H. O. Finklea, L. R. Robinson, A. Blackburn, B. Richter, D. Allara, T. Bright, *Langmuir* **1986**, *2*, 239-244.
[34] P. Silberzan, L. Leger, D. Ausserre, J. J. Benattar, *Langmuir* **1991**, *7*, 1647-1651.
[35] T. Vallant, H. Brunner, U. Mayer, H. Hoffmann, T. Leitner, R. Resch, G. Friedbacher, *J. Phys. Chem. B.* **1998**, *102*, 7190-7197.
[36] N. Rozlosnik, M. C. Gerstenberg, N. B. Larsen, *Langmuir* **2003**, *19*, 1182-1188.
[37] Y. Liu, L. K. Wolf, M. C. Messmer, *Langmuir* **2001**, *17*, 4329-4335.
[38] T. Balgar, R. Bautista, N. Hartmann, E. Hasselbrink, *Surf. Sci.* **2003**, *532–535*, 963-969.
[39] J. V. Davidovits, V. Pho, P. Silberzan, M. Goldmann, *Surf. Sci.* **1996**, *352–354*, 369-373.
[40] C. Carraro, O. W. Yauw, M. M. Sung, R. Maboudian, *J. Phys. Chem. B.* **1998**, *102*, 4441-4445.
[41] Q. Li, G. Mathur, S. Gowda, S. Surthi, Q. Zhao, L. Yu, J. S. Lindsey, D. F. Bocian, V. Misra, *Adv. Mater.* **2004**, *16*, 133-137.
[42] G. E. Steve P. Beeby, M. Kraft, N. M. White, *MEMS Mechanical Sensors*, Artech House London, **2004**.
[43] M.-H. Bao, *Micro mechanical transducers: pressure sensors, accelerometers and gyroscopes, Vol. 8*, Elsevier, **2000**.
[44] M. C. Pirrung, *Angew. Chem. Int. Ed.* **2002**, *41*, 1276-1289.
[45] D. S. Wilson, S. Nock, *Angew. Chem. Int. Ed.* **2003**, *42*, 494-500.
[46] S. P. Pujari, E. Spruijt, M. A. Cohen Stuart, C. J. M. van Rijn, J. M. J. Paulusse, H. Zuilhof, *Langmuir* **2012**, *28*, 17690-17700.
[47] A. S. P. Kalimuthu, S. A. John, *J. Chem. Sci.* **2012**, *124*, 1315-1325.
[48] M. Yoshioka, Y. Mukai, T. Matsui, A. Udagawa, H. Funakubo, *J. Chromatogr. B* **1991**, *566*, 361-368.
[49] R. G. Nuzzo, D. L. Allara, *J. Am. Chem. Soc.* **1983**, *105*, 4481-4483.
[50] M. Hasan, D. Bethell, M. Brust, *J. Am. Chem. Soc.* **2002**, *124*, 1132-1133.
[51] C. Vericat, M. E. Vela, R. C. Salvarezza, *Phys. Chem. Chem. Phys.* **2005**, *7*, 3258-3268.
[52] G. Yang, N. A. Amro, Z. B. Starkewolfe, G.-y. Liu, *Langmuir* **2004**, *20*, 3995-4003.

[53] E. Cortés, A. A. Rubert, G. Benitez, P. Carro, M. E. Vela, R. C. Salvarezza, *Langmuir* **2009**, *25*, 5661-5666.
[54] A. B. Horn, D. A. Russell, L. J. Shorthouse, T. R. E. Simpson, *J. Chem. Soc., Faraday Trans.* **1996**, *92*, 4759-4762.
[55] D. A. Hutt, G. J. Leggett, *J. Phys. Chem.* **1996**, *100*, 6657-6662.
[56] E. Cooper, G. J. Leggett, *Langmuir* **1998**, *14*, 4795-4801.
[57] N. Camillone, C. E. D. Chidsey, G. Y. Liu, G. Scoles, *J. Chem. Phys.* **1993**, *98*, 3503-3511.
[58] J. B. Schlenoff, M. Li, H. Ly, *J. Am. Chem. Soc.* **1995**, *117*, 12528-12536.
[59] J. K. Lee, Y. S. Chi, J. S. Lee, Y.-G. Kim, Y. H. Jung, E. Oh, S.-B. Ko, H. J. Jung, P.-S. Kang, I. S. Choi, *Langmuir* **2005**, *21*, 10311-10315.
[60] C. E. D. Chidsey, C. R. Bertozzi, T. M. Putvinski, A. M. Mujsce, *J. Am. Chem. Soc.* **1990**, *112*, 4301-4306.
[61] S. B. Sachs, S. P. Dudek, R. P. Hsung, L. R. Sita, J. F. Smalley, M. D. Newton, S. W. Feldberg, C. E. D. Chidsey, *J. Am. Chem. Soc.* **1997**, *119*, 10563-10564.
[62] K. L. Prime, G. M. Whitesides, *J. Am. Chem. Soc.* **1993**, *115*, 10714-10721.
[63] K. Prime, G. Whitesides, *Science* **1991**, *252*, 1164-1167.
[64] M. Riepl, K. Enander, B. Liedberg, M. Schäferling, M. Kruschina, F. Ortigao, *Langmuir* **2002**, *18*, 7016-7023.
[65] J. S. Shumaker-Parry, M. H. Zareie, R. Aebersold, C. T. Campbell, *Anal. Chem* **2004**, *76*, 918-929.
[66] K. R. Love, P. H. Seeberger, *Angew. Chem. Int. Ed.* **2002**, *41*, 3583-3586.
[67] D. M. Ratner, E. W. Adams, J. Su, B. R. O'Keefe, M. Mrksich, P. H. Seeberger, *ChemBioChem* **2004**, *5*, 379-383.
[68] M. Schäferling, M. Riepl, P. Pavlickova, H. Paul, D. Kambhampati, B. Liedberg, *Microchim. Acta* **2003**, *142*, 193-203.
[69] A. Bruckbauer, D. Zhou, D.-J. Kang, Y. E. Korchev, C. Abell, D. Klenerman, *J. Am. Chem. Soc.* **2004**, *126*, 6508-6509.
[70] N. S. Mathebula, J. Pillay, G. Toschi, J. A. Verschoor, K. I. Ozoemena, *Chem. Comm.* **2009**, 3345-3347.
[71] J. Berna, D. A. Leigh, M. Lubomska, S. M. Mendoza, E. M. Perez, P. Rudolf, G. Teobaldi, F. Zerbetto, *Nat Mater* **2005**, *4*, 704-710.
[72] R. Wehlauch, J. Hoecker, K. Gademann, *ChemPlusChem* **2012**, *77*, 1071-1074.
[73] I. O. Benítez, B. Bujoli, L. J. Camus, C. M. Lee, F. Odobel, D. R. Talham, *J. Am. Chem. Soc.* **2002**, *124*, 4363-4370.
[74] PhD thesis, John D. Parkin, University of St Andrews, 2012
[75] B. Cappella, G. Dietler, *Surf. Sci. Rep.* **1999**, *34*, 1-104.
[76] F. J. Giessibl, *Rev. Mod. Phys.* **2003**, *75*, 949-983.
[77] F. J. Giessibl, G. Binnig, *Ultramicroscopy* **1992**, *42–44, Part 1*, 281-289.
[78] S. Yongho, J. Wonho, *Rep. Prog. Phys.* **2008**, *71*, 016101.
[79] J. F. Watts, *Surface science techniques* **1994**, 5-23.
[80] J. M. Walls, R. Smith, *Surface Science Techniques*, Elsevier Science, **2013**.
[81] J. M. Hollander, W. L. Jolly, *Acc. Chem. Res.* **1970**, *3*, 193-200.
[82] D. Samanta, A. Sarkar, *Chem. Soc. Rev.* **2011**, *40*, 2567-2592.
[83] H. Fujiwara, *Spectroscopic Ellipsometry: Principles and Applications*: J. Wiley and Sons, **2007**.
[84] H. G. Tompkins, *A User's Guide to Ellipsometry*, Dover Publications Inc., **2007**.
[85] J.-W. Park, Y. J. Park, C.-H. Jun, *Chem. Comm.* **2011**, *47*, 4860-4871.
[86] C. Haensch, S. Hoeppener, U. S. Schubert, *Chem. Soc. Rev.* **2010**, *39*, 2323-2334.
[87] Y.-R. Yeon, Y. J. Park, J.-S. Lee, J.-W. Park, S.-G. Kang, C.-H. Jun, *Angew. Chem. Int. Ed.* **2008**, *47*, 109-112.
[88] J.-W. Park, C.-H. Jun, *J. Am. Chem. Soc.* **2010**, *132*, 7268-7269.

[89] N. Moitra, S. Ichii, T. Kamei, K. Kanamori, Y. Zhu, K. Takeda, K. Nakanishi, T. Shimada, *J. Am. Chem. Soc.* **2014**, *136*, 11570-11573.
[90] M. Sulpizi, M.-P. Gaigeot, M. Sprik, *J. Chem. Theory. Comput.* **2012**, *8*, 1037-1047.
[91] D. Addis, S. Das, K. Junge, M. Beller, *Angew. Chem. Int. Ed.* **2011**, *50*, 6004-6011.
[92] J. M. Blackwell, E. R. Sonmor, T. Scoccitti, W. E. Piers, *Org. Lett.* **2000**, *2*, 3921-3923.
[93] D. J. Parks, W. E. Piers, *J. Am. Chem. Soc.* **1996**, *118*, 9440-9441.
[94] Y. Kwon, M. Mrksich, *J. Am. Chem. Soc.* **2002**, *124*, 806-812.
[95] G. Collins, C. O'Dwyer, M. Morris, J. D. Holmes, *Langmuir* **2013**, *29*, 11950-11958.
[96] J.-C. Lin, J.-H. Kim, J. A. Kellar, M. C. Hersam, S. T. Nguyen, M. J. Bedzyk, *Langmuir* **2010**, *26*, 3771-3773.
[97] Y. Yamanoi, J. Sendo, T. Kobayashi, H. Maeda, Y. Yabusaki, M. Miyachi, R. Sakamoto, H. Nishihara, *J. Am. Chem. Soc.* **2012**, *134*, 20433-20439.
[98] L. E. O'Leary, M. J. Rose, T. X. Ding, E. Johansson, B. S. Brunschwig, N. S. Lewis, *J. Am. Chem. Soc.* **2013**, *135*, 10081-10090.
[99] J. K. Lee, K.-B. Lee, D. J. Kim, I. S. Choi, *Langmuir* **2003**, *19*, 8141-8143.
[100] S. K. Sontag, N. Marshall, J. Locklin, *Chem. Comm.* **2009**, 3354-3356.
[101] L. C. Morrill, J. Douglas, T. Lebl, A. M. Z. Slawin, D. J. Fox, A. D. Smith, *Chem. Sci.* **2013**, *4*, 4146-4155.
[102] PhD thesis, Louis Christian Morrill, University of St Andrews, 2014.
[103] B. R. Beno, K.-S. Yeung, M. D. Bartberger, L. D. Pennington, N. A. Meanwell, *J. Med. Chem.* **2015**, *58*, 4383-4438.
[104] M. E. Abbasov, B. M. Hudson, D. J. Tantillo, D. Romo, *J. Am. Chem. Soc.* **2014**, *136*, 4492-4495.
[105] P. Liu, X. Yang, V. B. Birman, K. N. Houk, *Org. Lett.* **2012**, *14*, 3288-3291.
[106] C. A. Leverett, V. C. Purohit, D. Romo, *Angew. Chem. Int. Ed.* **2010**, *49*, 9479-9483.
[107] V. B. Birman, X. Li, Z. Han, *Org. Lett.* **2007**, *9*, 37-40.
[108] X. Zhang, Z. Gong, J. Li, T. Lu, *J. Chem. Info. Model.* **2015**, *55*, 2138-2153.
[109] K. A. Brameld, B. Kuhn, D. C. Reuter, M. Stahl, *J. Chem. Info. Model.* **2008**, *48*, 1-24.
[110] Y. Nagao, T. Hirata, S. Goto, S. Sano, A. Kakehi, K. Iizuka, M. Shiro, *J. Am. Chem. Soc.* **1998**, *120*, 3104-3110.
[111] D. Rampulla, A. J. Gellman, Dekker Encyclopedia of Nanoscience and Nanotechnology, ed. J. A. Schwarz, C. I. Contescu and K. Putyera, Marcel Dekker, New York, **2004**, 1113–1123.
[112] Hazen, R.M.; Filley, T. R.; Goodfriend, G.A. *Proc.Natl. Acad. Sci*. **2001**, *98*, 5487–5490.
[113] PhD thesis, Malgorzata Adamkiewicz, University of St Andrews, 2013
[114] M. Adamkiewicz, D. O'Hagan, G. Hähner, *Langmuir* **2014**, *30*, 5422-5428.
[115] M. Adamkiewicz, D. O'Hagan, G. Hahner, *Beilstein J. Org. Chem.* **2014**, *10*, 2897-2902

Chapter 2 : Isothiourea-catalysed Michael addition-lactonisation on a surface

Introduction

This chapter describes the post-deposition functionalisation of alkylsilane based self-assembled monolayers, deposited on Si/SiO_2, using organocatalytic methodology previously developed within the Smith group.[101] The achiral isothiourea catalyst, 3,4-dihydro-2*H*-pyrimido[2,1-*b*]benzothiazole (DHPB **60**), promotes the intermolecular Michael addition-lactonisation using a trifluoromethylenone terminated SAM and a variety of arylacetic acids affording *C*(6)-trifluoromethyldihydropyranones (DHP) tethered to a surface (Figure 34). X-ray photoelectron spectroscopy, atomic force microscopy, contact angle and ellipsometry analysis were conducted to confirm the presence of the substituted dihydropyranone (DHP) on the surface.

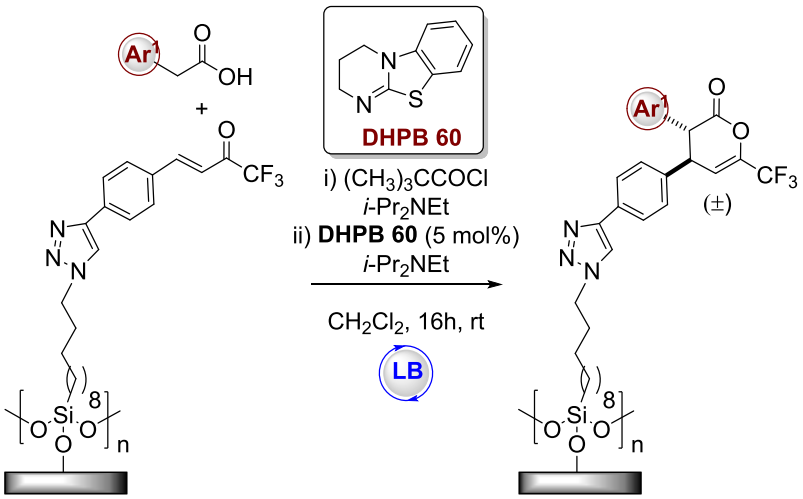

Figure 34: Michael addition-lactonisation of trifluoromethylenones using DHPB as a catalyst.

2.1 Aims

As previous work has shown that isothioureas can catalyse the intermolecular Michael addition-lactonisation of arylacetic acids and trifluoromethylenones, we envisaged that this methodology could be applicable to the late stage functionalisation of SAMs *in situ* on Si/SiO_2 surfaces. Commercially available arylacetic acids containing marker atoms which are clearly visible in the XPS spectrum of a surface would give a good indication of the conversion obtained in the reaction. In solution, this system is robust, and tolerant of a variety of functional groups in either the arylacetic acid portion or the trifluoromethylenone component of the reaction ranging from para-substituted electron withdrawing and electron-donating groups to heteroaromatic and alkyl groups. We hoped that our investigations into this system would provide a proof of concept

regarding Michael addition-lactonisation on a Si/SiO_2 surface for generating racemic DHPs with high selectivity. We also hoped that using DHPB **60** in the synthesis of racemic DHPs would serve as a model system for optimisation of a similar enantioselective process using a chiral isothiourea catalyst. The enantioinduction obtained from the asymmetric process can be probed on the surface using chemical force microscopy, which will be discussed in detail in Chapter 3.

2.2 Initial strategy – formation of vinyl-terminated SAMs

Previous work in the Hähner group has shown that vinyl-terminated SAMs can be easily prepared from the appropriate alkyl chain length trichlorosilane and subsequently functionalised using a variety of organic reactions.[31][115] Based on this work the initial strategy was to synthesise several vinyl-terminated trichlorosilanes and deposit them on an Si/SiO_2 surface. Following this, oxidation to the aldehyde using an ozonolysis approach would be pursued with the aim of attaching a suitable Michael acceptor to the surface *via* a modified Horner-Wadsworth-Emmons reaction (Figure 35).

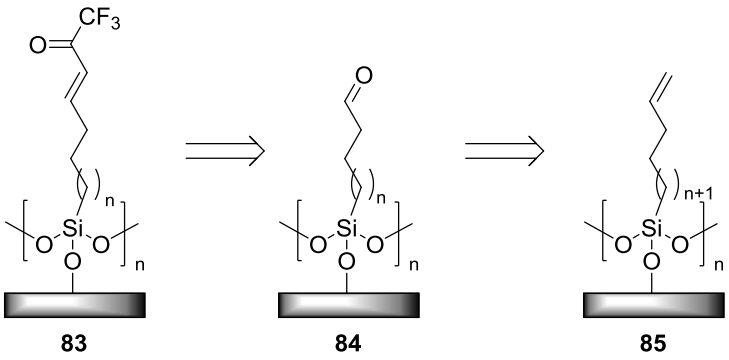

Figure 35: Retrosynthetic route towards trifluomethylenone terminated surface 83.

2.2.1 Synthesis of starting materials for SAM formation

In order to obtain vinyl-terminated monolayers the requisite alkylsilane precursors needed to be synthesised. Self-assembling molecules, with different alkyl chain lengths and reactive head groups *i.e.* $SiCl_3$, $Si(OMe)_3$ and $Si(OEt)_3$, can affect the overall SAM quality by altering the self-assembly process.[10] Wöll and co-workers[116] have shown that the optimum molecular chain length is eighteen carbons to form a well ordered, homogeneous SAM. Moverover, short alkyl chain silanes with three[116] or eight[117] carbons form disordered films, whereas longer chain silanes *ca*. thirty[116] carbons also form less ordered monolayers. Based on these parameters we decided that the synthesis of two alkyltrichlorosilane derivatives, C_{11} and C_{15} would be prepared and deposited to decide on the most appropriate chain length for further modification. The target molecules were vinyl-terminated trichlorosilanes with alkyl chain lengths of eleven (trichloro(undec-10-en-1-yl)silane **86**, and fifteen (trichloro(tridec-14-en-1-yl)silane **76**.

For the synthesis of **86** commercially available undec-10-en-1-ol **87** was transformed to the corresponding bromide under Appel conditions to afford 11-bromoundec-1-ene **88** in 82% yield after chromatographic purification. Following on from bromide **88** the corresponding trichlorosilane was synthesised using a Grignard reaction, and purification by Kugelrohr distillation afforded **86** in low yield 26% but high purity (Figure 36).

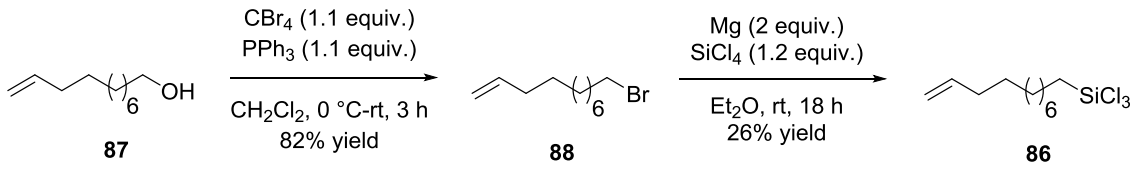

Figure 36: Synthesis of trichloro(undec-10-en-1-yl)silane 86.

For the synthesis of **76** a procedure outlined by Hähner and co-workers was used.[115] Starting from commercially available ω-pentadecalactone **89** an acid catalysed ring opening was used to afford the corresponding methyl ester **90** in 90% yield, which was used in the next step without further purification. Alcohol **90** was then subjected to PPh_3 and *N*-bromo succinimide in DMF at 55 °C for 0.5 h, which afforded the desired bromide in 77% yield (Figure 37).

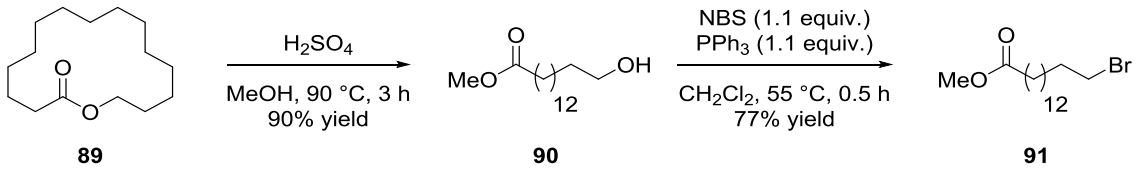

Figure 37: Synthetic route towards bromide 91.

Bromide **91** was then treated with a 1 M solution of KO^{t}Bu which gave the corresponding alkene **92**, with slightly lower yield than previous steps. Subsequent reduction of *tert*-butyl ester **92** using $LiAlH_4$ afforded desired alcohol **93** in a 71% yield after purification (Figure 38).

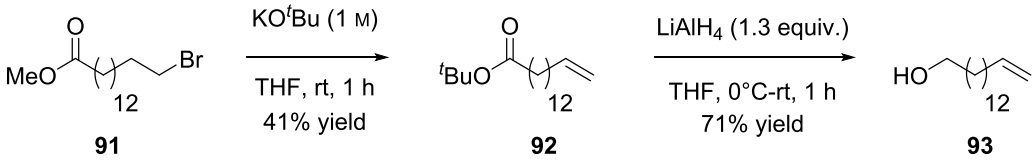

Figure 38: Synthetic route towards alkyl alcohol 93.

With alkenyl alcohol in hand, the desired trichlorosilane was synthesised in a further two steps. Alcohol **93** was treated with PPh_3 and *N*-bromo succinimide in DMF at 55 °C for 0.5 h, which afforded the desired bromide in 80% yield. Upon treatment of alkyl bromide **94** with Mg, the corresponding Grignard was formed which was treated with an excess of $SiCl_4$ to form trichlorosilane **76** in low yield (Figure 39).

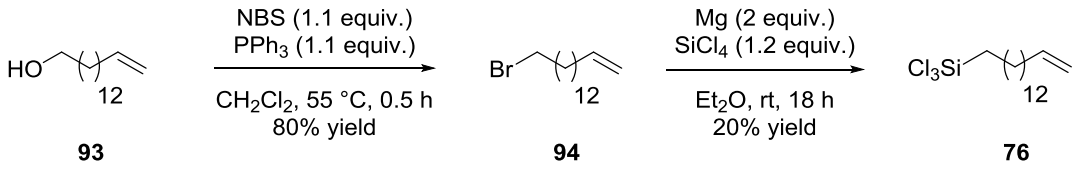

Figure 39: Synthesis of trichlorosilane 76.

2.3 Deposition of vinyl-terminated SAMs

2.3.1 Cleaning procedure

It is established in the literature that in order for a well-ordered, smooth, homogeneous monolayer to be deposited on Si/SiO_2 in solution or vapour phase there needs to be a clean hydroxy terminated surface devoid of any external contaminants.

There are two main methods, wet and dry, used to achieve this kind of hydrophilic surface. As wet methods are the focus of this chapter, only these are discussed. Liquid phase (wet) cleaning procedures usually employ hot acidic and alkali solutions, however the immersion time, order of reagents and temperature may vary.[116] The silicon wafers are first immersed in a mixture of H_2SO_4 and H_2O_2 known as 'Piranha solution' which removes any organic contaminant on the surface. The next step uses a mixture of H_2O_2, NH_4OH and H_2O, also known as SC-1 which removes inorganic contaminants such as heavy metal complexes that includes Au, Cu, Ag, Cd, Zn and Cr.[117] In the last step, a mixture of H_2O, H_2O_2 and HCl, also known as SC-2, removes residual trace metals such as Au and metal hydroxides such as $Mg(OH)_2$, $Fe(OH)_3$ and $Al(OH)_3$. This cleaning process should, in theory, generate a thin hydrophilic oxide layer.

A procedure outlined by Hähner and co-workers was used as a starting point for the cleaning procedure.[115] This procedure did not give consistent results as contaminants such as nitrogen and chlorine were noted in the N 1s and Cl 2p regions of the XPS spectra and attributed to NH_4OH and HCl respectively. As such several modifications were made to the original procedure which are outlined below:

1. The SiO_2 wafer was immersed in Piranha solution (conc. H_2SO_4/30% H_2O_2 – 2:1) at 70°C for 15 mins.
2. The wafer was then removed and transfered directly into a solution of NH_4OH, deionised (DI) water and 30% H_2O_2 (1:5:1) at 70°C for 15 mins
3. The wafer was removed again and transferred straight into a solution of conc. HCl, DI water and 30% H_2O_2 (1:6:1) at 70°C for 15 mins.
4. After cleaning the wafer was washed with copious amounts of DI water and placed in an oven at 130 °C for 30 mins to remove all but a single layer of water on the surface.

5. Once dried, the wafer was immersed in a 1mM solution of silane precursor in toluene for 16 h.
6. After deposition the wafers were removed from solution and sonicated in vials of toluene, CH_2Cl_2 and DI water respectively for 5 mins. Finally they were dried under a stream of Ar.

AFM images of the SiO_2 surface after the cleaning procedure were obtained to assess the success of the cleaning procedure (Figure 40). The AFM image showed a clean surface devoid of any artefacts and the high resolution scans of the N 1s and Cl 2p region shows no sign of contaminants.

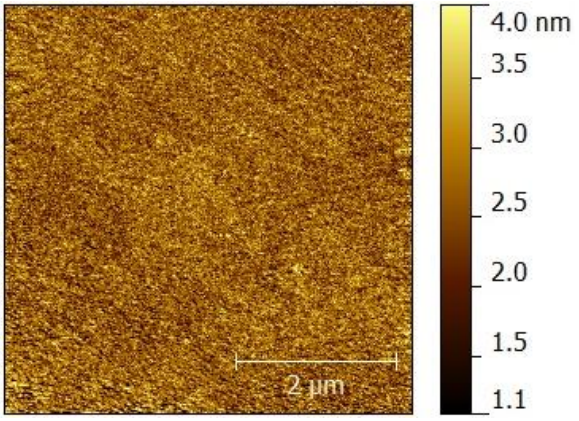

Figure 40: AFM image of 5 µm × 5 µm area of clean Si/SiO_2.

XPS spectra of clean Si/SiO_2 surfaces after oven drying were also obtained and characterised showing the presence of several different chemical environments for silicon and oxygen as expected (Figure 41). A large asymmetric peak appears in the Si 2p spectrum which is attributed to the combination of the Si $2p_{1/2}$ (98.7 eV) and Si $2p_{3/2}$ (98.1 eV) components in the elemental bulk silicon of the substrate. A peak with a binding energy of 102.0 eV also appears in the spectrum and is assigned to the Si 2p of the silicon in the silicon oxide layer. XPS survey scans also showed no sign of any unwanted contaminants and as such the surface was deemed sufficiently clean.

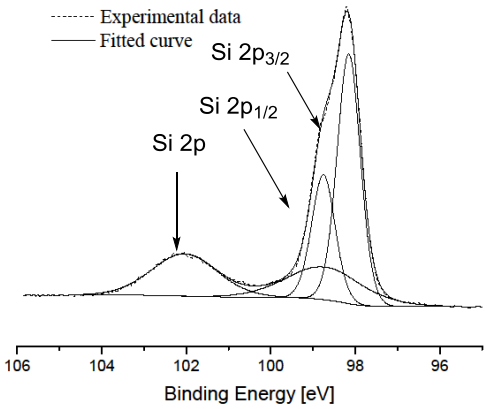

Figure 41: High resolution XPS scans of Si 2p region of clean Si/SiO_2.

2.3.2 Deposition of SAMs in solution

Solution phase deposition is by far the most common method of preparing SAMs on a small scale.[118] Although it is relatively simple to produce SAMs of good quality, it can be difficult to reproduce the results as SAM formation is very dependent on reaction parameters such as solvent,[119-120] solution age,[120] water content,[121-122] deposition time[123-124] and temperature.[125] Rozlosnik and co-workers have shown[120] that using a wide range of concentrations (25 μM to 2.5 mM) of octadecyltrichlorosilane (OTS) **2** faciltates the formation of a full-coverage self-assembled monolayer on hydrophilic silicon oxide. Other studies have shown that using toluene as a deposition solvent can produce SAMs of full coverage and of reproducible quality.[126] This was used as a starting point for monolayer deposition in solution.

SAMs were prepared from trichlorosilane self-assembling molecules **76** and **86**. Freshly cleaned SiO_2 wafers (as per the cleaning procedure outlined in 2.3.1) were placed in a glass vial and 5 mL of a 1 mM solution of the appropriate silane was added to the vial (Figure 42). The silicon wafers were left immersed in the solution for 16 h at room temperature. It should also be noted that solutions of surfactants had to be freshly prepared in order to avoid possible contaminants such as water. Water contamination can result in silane polymerisation which in turn results in a non-homogeneous film on the surface.

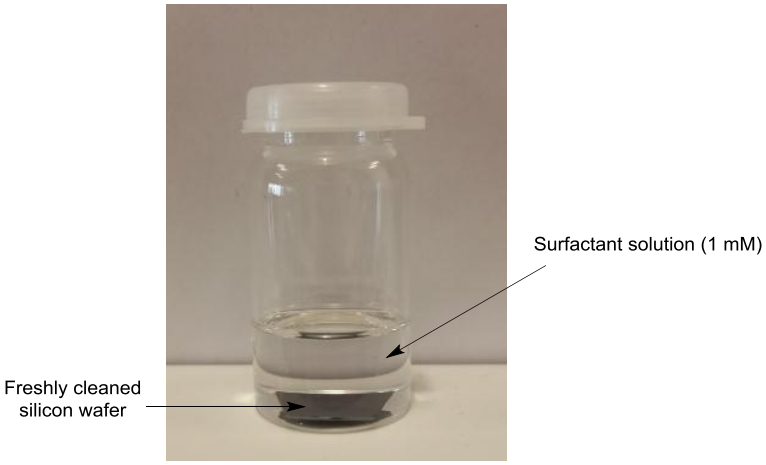

Figure 42: Experimental set-up for SAM deposition in solution.

2.4 Vinyl-terminated SAMs

As previously stated, the initial strategy focused on the deposition of two alkylsilane based SAMs with a vinyl group as a functional handle and assessed their viability as precursors for further surface chemistry. Vinyl-terminated monolayers have shown promise as model systems for study of the interactions of atmospheric oxidants with boundary layer surfaces.[127] In the present study two different SAMs were deposited on Si/SiO_2 surfaces from the solution phase and assessed. The self-assembling molecules both contain the same vinyl terminal group and $-SiCl_3$ reactive head group but varied in alkyl chain length (Figure 43).

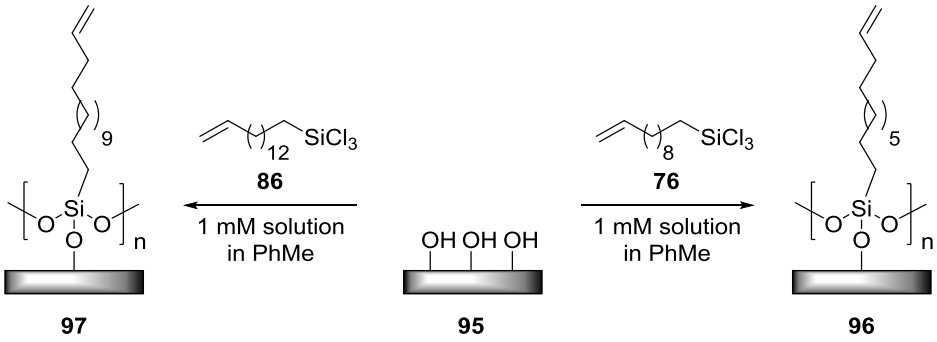

Figure 43: Deposition of vinyl terminated SAMs from precursor molecules 76 and 86.

2.4.1 X-Ray Photoelectron Spectroscopy

The XPS spectra of each of the vinyl terminated SAMs in this study showed the presence of Si (2s 151.6 eV, 2p 99.6 eV), C (1s 284.6 eV) and O (1s 532.7 eV) as expected. A typical survey scan of vinyl terminated SAM **96** is shown in Figure 44. There were no unexpected elements detected from XPS scans of the surface such as unreacted silane (no Cl signal was detected). The data obtained for C 1s, Si 2s and Si 2p was consistent with monolayer films in the literature.

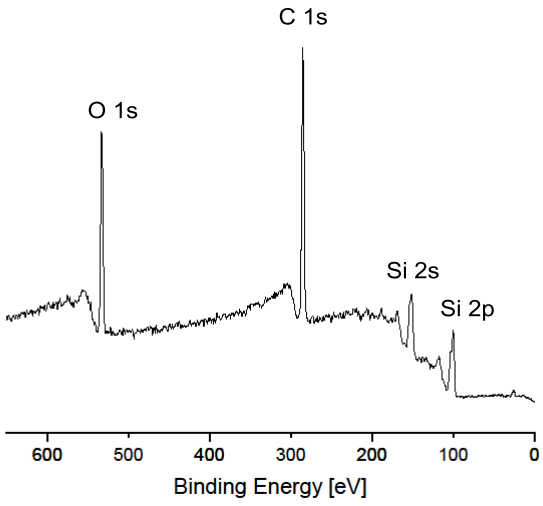

Figure 44: XPS survey scan of vinyl terminated SAM 96.

High resolution scans of each element were taken to reveal their elemental composition. An example single region scan of the C 1s of SAMs **97** is shown in Figure 45. As photoelectrons are lost during the photoemission process a positive charge builds up on the sample, known as sample charging. As this happens, the kinetic energy of the emitted photoelectrons decrease in energy resulting in a shift to a higher binding energy. All analysed samples were shifted and corrected for sample charging. The main C 1s aliphatic peak in SAM **97** appears at a binding energy of 284.6 eV. On the majority of samples a shoulder peak was fitted at a higher binding energy (286.4 eV) to the main C 1s peak. Based on the polarity of the double bond it is possible that this is the more electropositive carbon in the olefin moiety which shifts its overall binding energy higher in the XPS spectrum. It is difficult to definitively detect the different chemical states of carbon in alkene moieties using XPS and as such the shoulder peak could not be conclusively assigned.[128-130]

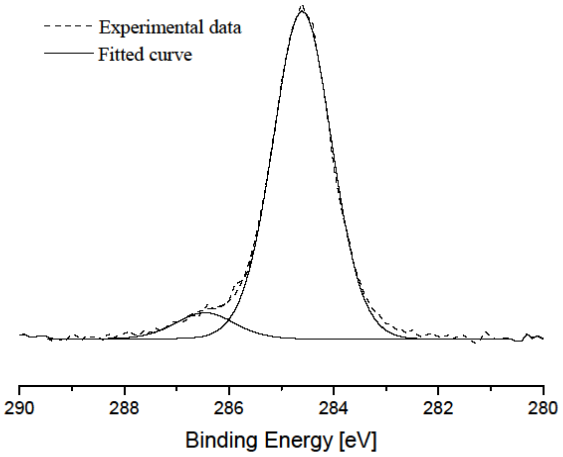

Figure 45: XPS C 1s high resolution scan of vinyl terminated SAM 97.

2.4.2 Contact Angle

The vinyl terminated SAMs **96** and **97** gave similar water contact angle values within several degrees of each other which is expected given the idetical surface termination. Experimental and literature values are shown in Table 1. Reported values were measured directly after placing drops of water onto modified silicon samples. These results are consistent with values reported for similar films.[131]

Water Contact Angle (°)

Surfactant	Liquid deposition	Literature
C_{11}-vinyl **96**	97±1.5	96±1.4
C_{15}-vinyl **97**	101±1	101±1.0 [115, 132]

Table 1: Comparison of experimental and literature values

2.4.3 Atomic Force Microscopy

Atomic Force Microscopy was used to determine the quality of the deposited SAMs as well as the overall topography of the surface. AFM is also useful for determining whether any aggregations from the self-assembly process are present on the surface. A typical AFM image of a vinyl terminated SAM **97** is shown in Figure 46. The AFM image shows a relatively smooth surface with a root mean squared (RMS) value of ~96 pm averaged over a 1 µm × 1 µm area for the solution phase deposited SAM of **97**. In this case the RMS value gives an estimate of how homogeneous the resulting surface is after SAM deposition. The majority of vinyl terminated

surfaces imaged gave smooth surfaces with RMS roughness values in the range of 48-250 pm which agrees with the literature. For comparison, a clean Si/SiO_2 surface has an RMS of ~50 pm. These results, coupled with results from the other surface analysis techniques, suggest the presence of a dense, well-ordered and homogeneous SAM on the surface.

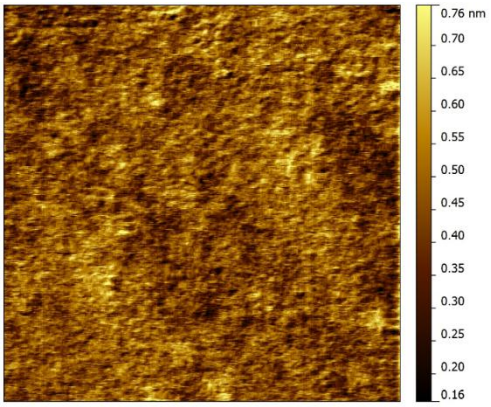

Figure 46: AFM image of 1 µm × 1 µm area of C_{15}-vinyl SAM 97.

2.4.4 Reactivity of vinyl terminated SAM

Pd-mediated cross-coupling reactions are a valuable method for the construction of C-C bonds. In particular the Mizoroki-Heck reaction[133] is a useful method for the construction of substituted alkenes and has widespread use in organic synthesis[134] as well as on solid supports.[135] Mizoroki-Heck reactions have been reported on a variety of functionalised silicon surfaces[98][136-137] and as such seemed a suitable candidate to test the reactivity of the vinyl group on the surface. Vinyl terminated SAM **97** was subjected to Heck conditions using *p*-bromophenylacetic acid **98** as a coupling partner (Figure 47). Reaction at 125 °C for 2 h gave the corresponding phenylacetic acid on the surface as confirmed by XPS and contact angle.

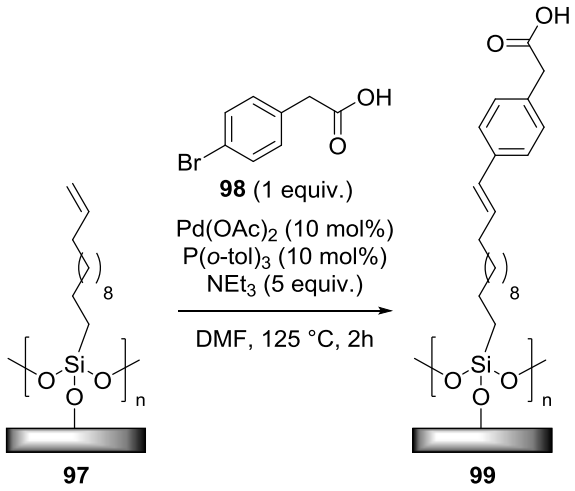

Figure 47: Mizoroki-Heck reaction of aryl bromide with vinyl terminated SAM 97.

High resolution scans of the C 1s region of the XPS spectrum show the appearance of a peak at 288.6 eV and this is attributed to the C in the C=O of the newly attached phenylacetic acid component(Figure 48)

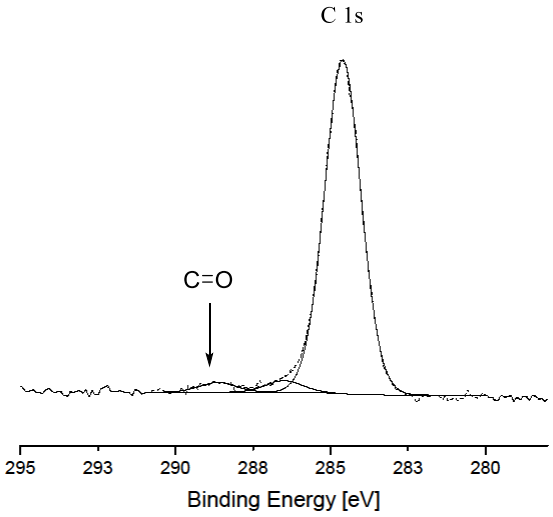

Figure 48: High resolution XPS scans of C 1s region of phenylacetic acid terminated SAM 99.

The contact angle of the sample was also measured, with a significant decrease, from 97 to 55 °, attributed to the change in hydrophilicity of the monolayer. This, coupled with XPS results, suggested successful attachment of the phenylacetic acid unit thus confirming the reactivity of the vinyl group in the monolayer.

2.5 Modification of vinyl-terminated SAMs using ozonolysis

The aldehyde functional group is one of particular importance as it can partake in a variety of reactions based on its electrophilic character. It is also important as the aldehyde carbonyl serves as an anchoring site for amines, and has shown to be useful in microarray technology and chemical biology.[138] Following a procedure outlined by Sukenik and co-workers,[136] the appropriate vinyl terminated SAM was subjected to a solution phase ozonolysis reaction which afforded the subsequent aldehyde terminated SAM in quantitative conversion after quenching with dimethyl sulfide (Figure 49). Complete monolayer cleavage from the surface and possible over oxidation to the carboxylic acid and/or anhydride may occur,[139-140] neither of these being observed in our case based on comparative contact angle and XPS analysis of the resulting SAMs with the literature.

The ozonolysis was almost instantaneous, indicated by a significant colour change from colourless to blue, which is indicative of the CH_2Cl_2 solution being saturated with unreacted

ozone. This colour change indicated complete consumption of any alkene present. Simple quenching of the reaction with excess dimethyl sulfide afforded aldehyde terminated SAMs in quantitative conversion as measured by XPS, contact angle and ellipsometry. AFM was also performed to assess the resulting surfaces for possible contaminants from the reaction.

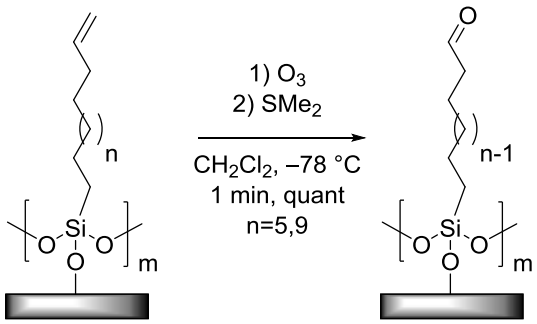

Figure 49: Heterogeneous ozonolysis reaction on vinyl terminated SAMs 76 and 86.

2.5.1 Contact angle and ellipsometry

In this particular transformation, the water contact angle can be extremely useful as it operates on the basis of hydrophobic and hydrophilic interactions on the surface. Therefore, transformation from a hydrophobic vinyl terminated SAM to a hydrophilic SAM, based on hydrogen bonding interactions, can be easily ascertained.[132] Vinyl terminated SAMs **96** and **97** were subjected to ozonolysis in solution with the results presented in Table 2. The initial contact angles of the vinyl terminated SAMs **96** and **97** are similar so it could be assumed that upon treatment with ozone the subsequent contact angle would also be similar. The contact angle obtained from aldehyde terminated SAM **96** is in good agreement with the literature[132] and gave a solid basis for further exploration into SAMs consisting of longer alkyl chains.

However, upon treatment of vinyl terminated SAM **97** with ozone in CH_2Cl_2 the resulting contact angles did not correspond in the same fashion as **96**. This could possibly be explained by the molecular packing density in the monolayer. At the terminal end of a SAM, there needs to be conformational mobility available to interact with an incoming molecule.[141] In the case of the vinyl terminated SAM **96** the contact angle, ellipsometry and XPS would suggest a highly ordered and densely packed monolayer which in turn could possibly restrict the interaction of the terminal alkene with the ozone.[142-143] The results may suggest that the ozone could not get sufficient access to react with the alkene, causing the subsequent contact angle to be higher than expected.

Water Contact Angle (°) and ellipsometry

SAM precursor	CA vinyl (°) SAM[a,b]	CA aldehyde (°) SAM[a,b]	Film thickness (Å) vinyl SAM	Film thickness (Å) aldehyde SAM
96	98 ±1.0	60 ±1.5	15.3	13.7
97	97 ±1.1	81 ±1.9	19.2	17.1

Table 2: Comparison of contact angle and ellipsometry values for vinyl and aldehyde terminated SAMs. [a]Average taken over a minimum of five samples. [b]Standard deviation between different samples.

2.5.2 X-Ray Photoelectron Spectroscopy

High resolution scans of the C 1s region of the resulting aldehyde terminated SAMs **96a** and **97a** were obtained and a typical spectrum is shown below in Figure 50. The main C 1s aliphatic peak appears at a binding energy of 284.6 eV which is shifted to account for sample charging as before. There is clear evidence of a peak at 288.3 eV which is attributed to the C=O π bond and conclusive evidence of an aldehyde moiety. This specific set of binding energies is consistent with other aldehyde terminated SAMs on Si/SiO_2 in the literature.[144-145] It is also worth noting that there was no evidence of any other possible contaminants, such as sulfur, present in the XPS spectra.

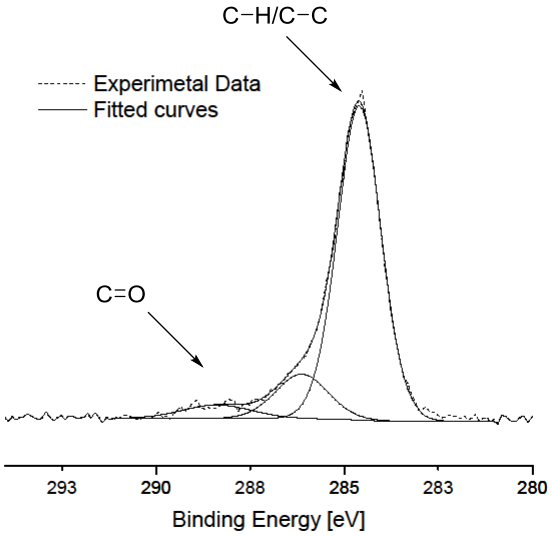

Figure 50: XPS C 1s high resolution scan of aldehyde terminated SAM 96a.

2.5.3 Aldehyde reactivity

A common method for the detection of aldehydes is by reaction with dinitrophenylhydrazine (DNPH) to form the corresponding hydrazone which is usually accompanied by a characteristic colour change in solution. This methodology was used to gain an insight into the reactivity of the newly generated aldehyde (Figure 51). Although a significant colour change was not detected in

the reaction mixture, subsequent analysis by XPS, ellipsometry and contact angle suggested the presence of the hydrazine moiety on the surface.

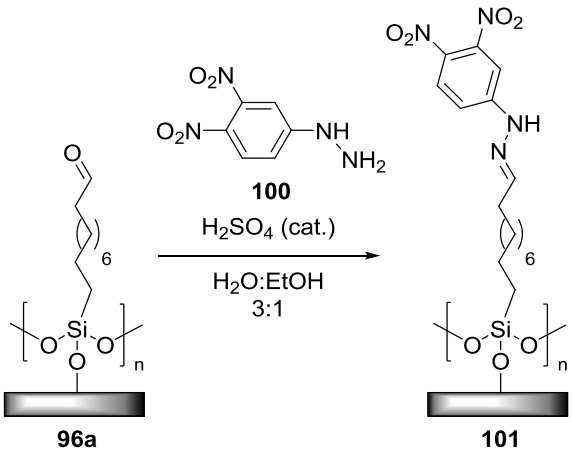

Figure 51: Reaction of aldehyde terminated surface with DNPH.

High resolution scans of the C 1s region of the resulting hydrazone terminated SAM **101** were obtained (Figure 52). A peak at 288.3 eV appears in the C 1s spectrum which can be assigned to the newly formed C=N bond in the hydrazone moiety. A shoulder peak also appears next to the main C 1s aliphatic peak in the spectrum which can be attributed to either advantageous atmospheric carbon contaminants or possibly the aromatic region in the hydrazone moiety or a combination of both.[132] A peak at 400.2 eV appears in the N 1s spectrum which can be attributed to the amine in the monolayer, while a peak with a binding energy of 406.1 eV also appears and is assigned to the more electronegative nitro group.[132] This confirms that that the aldehyde on the surface is reactive, at least towards nucleophilic amines.

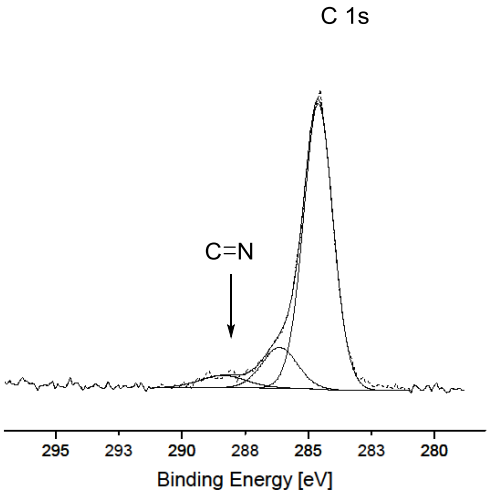

Figure 52: High resolution scans of the C 1s region of hydrazone terminated SAM 101.

2.5.4 Attempted synthesis of Michael acceptor on the surface

Having shown that ozonlysis can afford aldehyde terminated SAMs *via* oxidation of the corresponding vinyl-terminated monolayer, initial attempts sought to use aldehyde surface **96a** to afford a suitable CF_3 enone terminated surface. Previous work within the Smith group has shown that the use of imidoyl chloride **102,** in a modified Horner-Wadsworth-Emmons reaction,[146-147] can afford a series of CF_3 enone Michael acceptors for use in a Michael addition-lactonisation procedure (Figure 53).

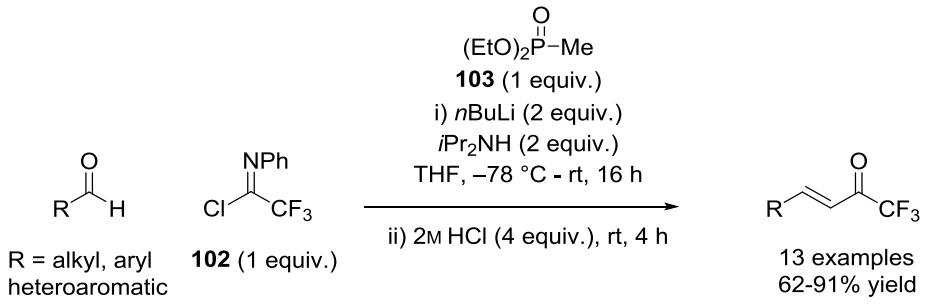

Figure 53: Synthesis of a series of CF_3 enones using a modified HWE reaction.

Following a procedure from Uneyama[148] reaction of trifluoroacetic acid with aniline in the presence of PPh_3 and NEt_3 using CCl_4 as solvent afforfded *N*-phenyltrifluoroacetimodoyl chloride **102** in 62% overall yield (Figure 54). Imidoyl chloride **102** was used as starting material in the synthesis of the required CF_3 enone on the surface.

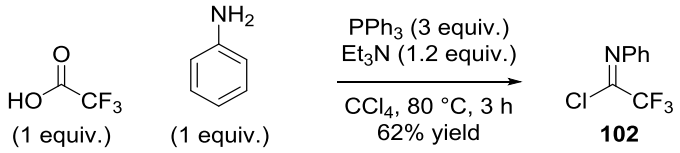

Figure 54: Synthesis of *N*-phenyltrifluoroacetimodoyl chloride 102.

With starting materials in hand, synthesis of the desired CF_3 Michael acceptor was attempted using a modified HWE reaction. Diethyl methylphosphonate **103** was reacted aldehyde surface **96a** in the presence of imidoyl chloride **102** and *n*BuLi but disappointingly gave no observable conversion to enone surface **104** as judged by XPS, contact angle and ellipsometry analysis. As this route gave no conversion to the desired surface it was no longer pursued and a different approach towards the fabrication of the enone surface was adopted.

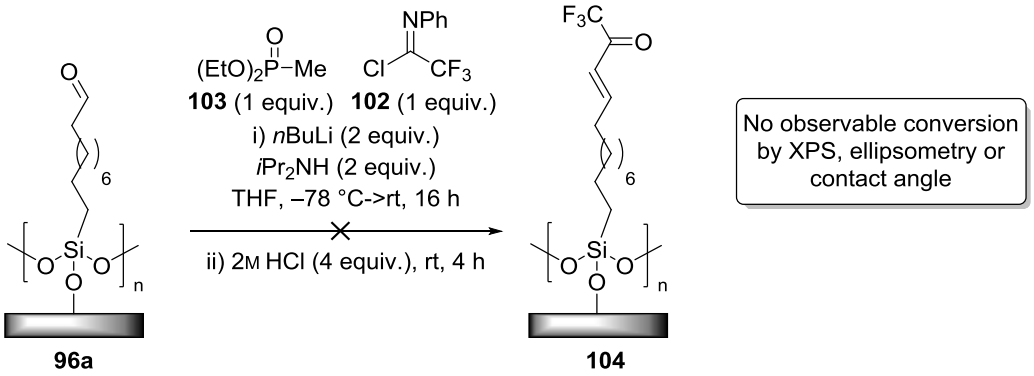

Figure 55: Attempted synthesis of CF_3 enone terminated surface.

2.6 Click Chemistry

Click chemistry can be used to build upon a molecular framework that is already in place and structured molecular layers can be constructed from a bottom up approach. The advantage of using click chemistry to functionalise a surface is that large bulkier groups can be introduced on the surface that would be otherwise difficult using classical organic chemistry methods.

One of the first examples of using click chemistry on SAMs was carried out by Choi *et al*.[149] where the authors used alkyne-terminated SAM **105** on Au for the formation of 1,2,3-traizoles on the surface while varying the azide used (Figure 56). The success of the reaction was determined by analysis using XPS, FTIR, ellipsometry and contact angle.

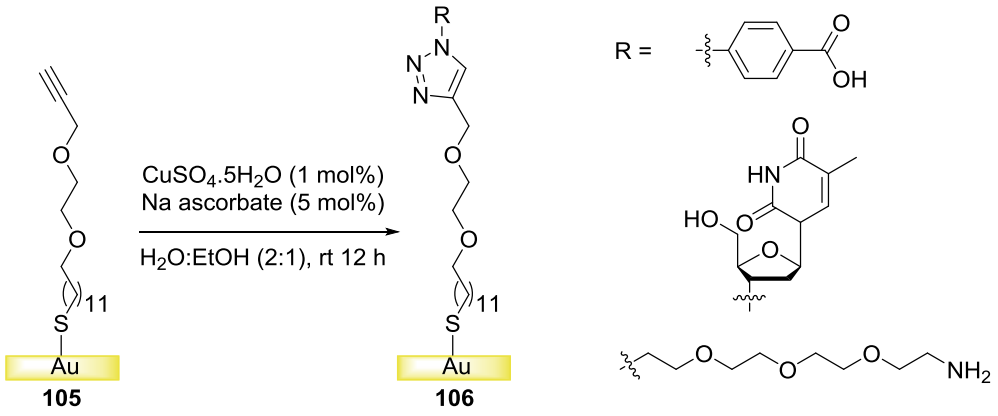

Figure 56: Formation of 1,2,3-triazoles on Au surfaces using click chemistry.

Coster *et al*. have also deposited alkyne terminated SAMs but on a Si-H terminated surface.[150] The authors proceeded to attach pre-synthesised polypeptide **108** to the surface using a CuAAC reaction (Figure 57).

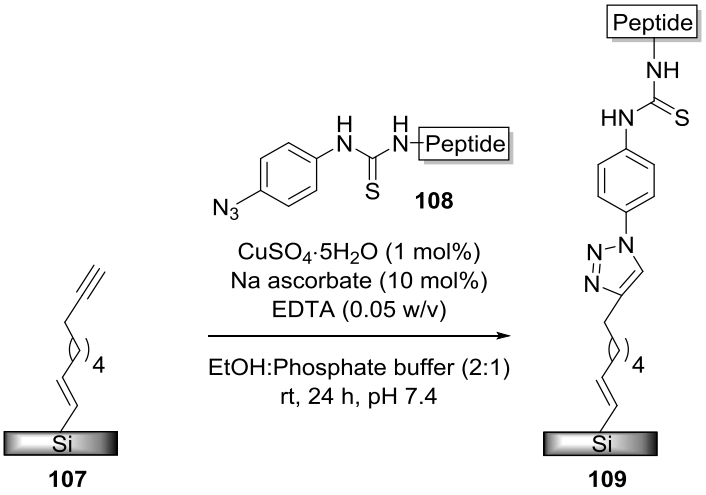

Figure 57: Attachment of polypeptide 107 to an alkyne terminated SAM on Si.

Mi *et al*. has shown the utility of azide-terminated SAMs, readily derived from the corresponding bromine-terminated SAMs, in click chemistry to attach a zwitterionic polymer **111** to a surface (Figure 58 (a)).[151] Using a similar approach Hacker and co-workers[152] have shown that click chemistry can be used to attach redox active diruthenium complex **113** to a Si/SiO_2 or Au based azide SAM (Figure 58 (b)).

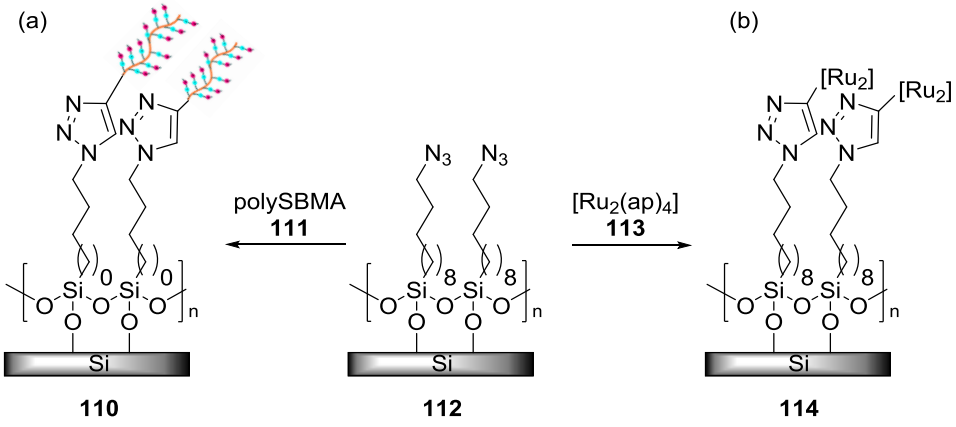

Figure 58:(a) Attachment of zwitterionic polymer to the surface and (b) attachment of a diruthenium complex, both using click chemistry.

Our strategy for the construction of a suitable enone terminated surface consisted of using an initial bromine terminated SAM which can be easily transformed into an azide terminated surface using NaN_3. From the resulting azide surface, a click reaction can be performed using catalytic $CuSO_4$ in the presence of (+)-sodium ascorbate with a suitable enone tethered alkyne (Figure 59). This route would allow for the fabrication of an enone terminated surface in three steps which could then be optimised for the organocatalytic Michael-addition lactonisation process.

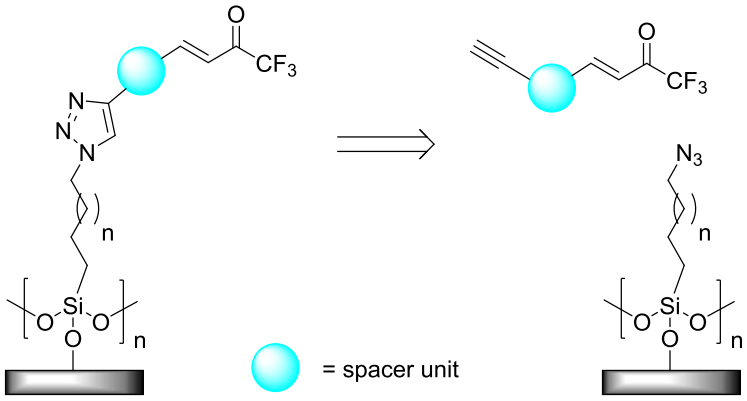

Figure 59: Retrosynthetic analysis of CF_3 Michael acceptor on the surface.

2.7 Optimisation of bromine terminated monolayer deposition

2.7.1 Deposition of 11-bromoundecyltrichlorosilane in solution

Commercially available 11-bromoundecyltrichlorosilane **115** was chosen as a potential starting material for the deposition of the bromine-terminated monolayer **116**. Initial studies focused on deposition conditions for the formation of a well-ordered homogeneous SAM. Reports have shown that an ideal Br-terminated SAM should have a contact angle of 83° ±1[153] and a film thickness of 1.9 nm.[153] Several different deposition conditions were tested including deposition solution concentration and solvent. Initial studies focused on toluene as a deposition solvent in a 1 mM concentration which provided the most consistent ellipsometry and contact angle values over the largest sample range (entry 1 Table 3). Several of the results using bicyclohexane as a deposition solvent gave reasonable contact angles but displayed thickness values that were considered either too high (entries 3,5), or were one-off results that could not be reproduced under the same experimental conditions (entry 4). Other deposition solvents such as hexane (entry 6), heptane:$CHCl_3$ (entry 7) and hexadecane (entry 8) gave unacceptable contact angles and were deemed unsuccessful. Overall entry 1 (Table 1) gave the most reproducible and consistent results for solution-phase deposition.

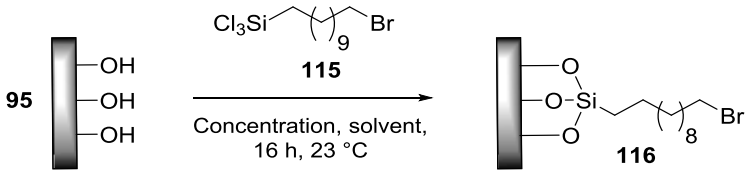

Entry	Deposition solvent	Concentration (mM)	Contact Angle (std. dev.)	Ellipsometry (Å)
1	Toluene	1	83.2 (±0.9)	1.90
2	Toluene	2	87.2(±1.2)	n/a[a]

3	Bicyclohexane	1	83.7(±1.5)	5.3
4	Bicyclohexane	5	83.7(±0.8)	1.3
5	Bicyclohexane	10	83.0(±2.2)	4.4
6	Hexane	1	86.2(±0.8)	n/a[a]
7[b]	Heptane:$CHCl_3$ (7:3)[c][160]	1	90.3(±4.1)	n/a[a]
8	Hexadecane	1	81.3 (±4.0)	0.83

Table 3: Optimisation of deposition of 11-bromoundecyltrichlorosilane in solution. [a]If the contact angle was not deemed sufficient no ellipsometry measurement was obtained. [c]Deposition time was 4 h and temperature was 6 °C. Standard deviation of contact angle is between at least two samples or more of similar quality.

Survey scans of the Br terminated surface were obtained and a typical spectrum is shown below (Figure 60). In addition to the expected Si and O signals the XPS spectrum showed three additional peaks consistent with the presence of bromine SAM. A peak at a binding energy of 71 eV was assigned to Br 3d[153], and a peak at a binding energy of 190 eV which is attributed to the Br 3p signal.[155] A more intense peak, relative to the Br signals, is shifted to 284.6 eV which is to account for sample charging and this is assigned to the C 1s signal. Overall this data suggests the presence of a bromine-terminated SAM.[154, 156]

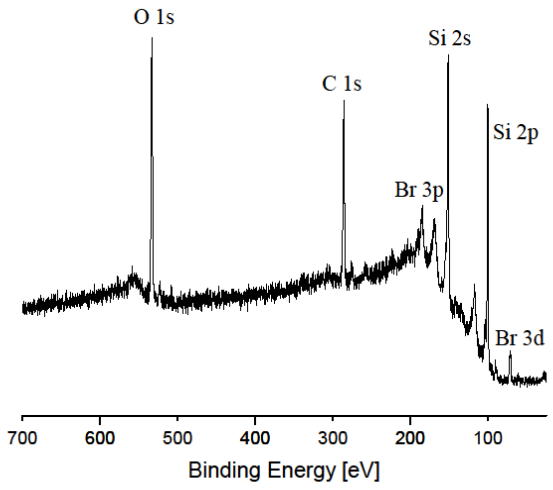

Figure 60: XPS survey scan of Br terminated surface 115.

2.7.2 Deposition of 11-bromoundecyltrichlorosilane from the vapour phase

While solution-phase deposition offered a route towards the desired bromine terminated SAM **115**, vapour phase deposition could provide a viable alternative. Vapour phase deposition has the potential to eliminate some of the common problems associated with solution-phase deposition

such as the inability to wet all parts of a microstructure due to the presence of microscopic air bubbles from the air-water interface.[157-158] Higher quality SAMs can also be obtained from the vapour phase as aggregated organosilanes, which may be deposited in the solution phase, do not vapourise and therefore are not deposited on the surface.[159]

Commercially available 11-bromoundecyltrichlorosilane **115** was chosen as a suitable starting material for vapour-phase deposition as it had already shown promising results in the analogous solution phase deposition procedure. The deposition procedure was performed using a reduced pressure set-up and carried out in a sealed reaction vessel (Figure 61).

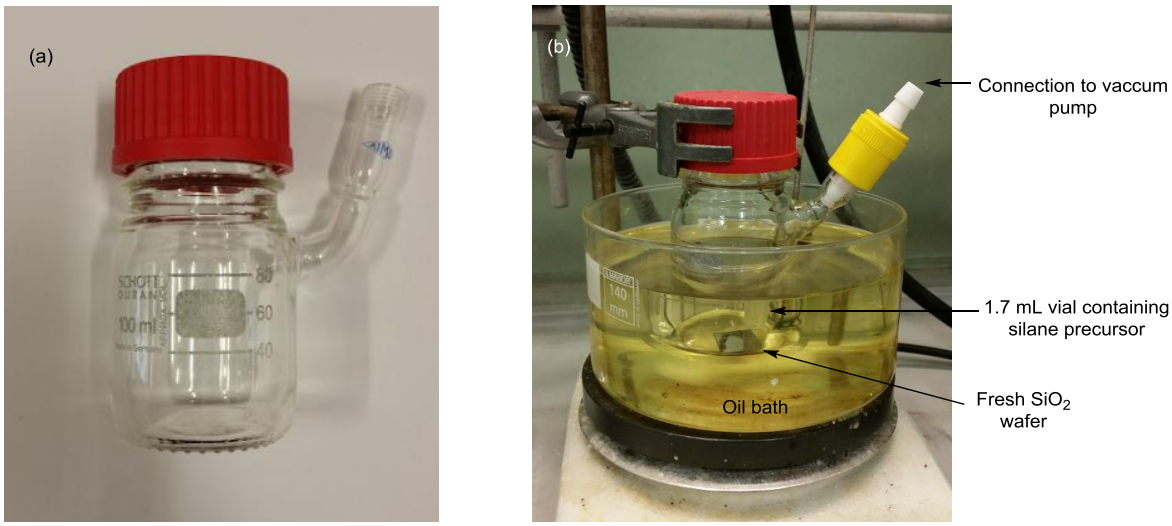

Figure 61(a): Reaction vessel for vapour phase deposition, (b) experimental set-up for vapour phase deopsition

Following a procedure outlined by Hähner[115] a freshly cleaned SiO_2 wafer was placed in the reaction vessel shown in Figure 61(a) and subjected to varying reaction parameters including solvent concentration, deposition time and temperature (Table 4).[1] Several of the resulting contact angles were promising (entries 4-6, 9,11) but interrogation by AFM revealed a variety of unusual features present on the surface depending on the reaction conditions. Entry 4 (Table 4) gave a contact angle within range (*ca.* 82.7°) but upon examination with AFM a series of small depositions roughly 5 nm in height were detected (Figure 62(a)). This is indicative of an inhomogeneous SAM and which could not be used in subsequent reactions. Entry 9 (Table 4) also gave a contact angle within the usual range and was examined using AFM. The AFM image showed a particularly large membrane type structure on the surface over a large area (Figure

[1] Several samples prepared by project student Baptiste Fasseau.

62(b)). This was attributed to polymerisation of the silane precursor and as such was could not be used for subsequent functionalisation.

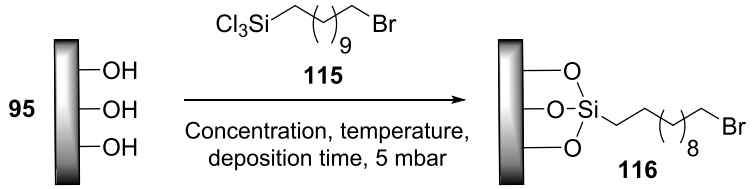

Entry	Concentration (mM)	Temperature (° C)	Deposition time (h)	Contact Angle (Std. dev.)[a]
1	10	60	24	89.6(±2.4)
2	10	60	36	84.3(±0.7)
3	10	60	48	84.5(±0.9)
4	10	60	72	82.7(±1.3)
5	10	70	72	83.0(±1.0)
6	10	80	72	82.0(±1.0)
7	20	85	72	85.3(±0.8)
8	10	60	96	89.1(±1.3)
9	10	70	96	82.0(±1.0)
10	10	80	96	79.0(±1.0)
11	10	60	120	83.0(±1.0)

Table 4: Summary of vapour phase deposition of 11-bromoundecyltrichlorosilane.[a]Standard deviation of contact angle is between at least two samples or more of similar quality.

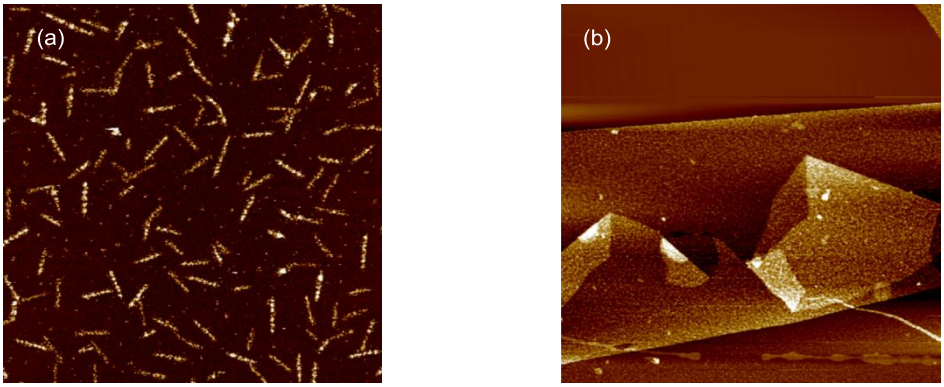

Figure 62(a): 5×5 μm^2 AFM image of small features of unknown origin on the surface, (b) 40×40 μm^2 AFM image of membrane type structure on the surface.

Although both solution phase and vapour phase methodologies gave suitable bromine terminated SAMs that could be used in subsequent modification, the solution phase methodology was carried forward as it produced more reliable and reproducible films.

2.8 Conversion of bromine to azide surface

With optimised conditions in hand (entry 1, Table 3) Br terminated monolayer **116** was subjected to a saturated solution of NaN_3 in DMF for 24 h which afforded azide terminated surface **112**, usually in >80% conversion (Figure 63).

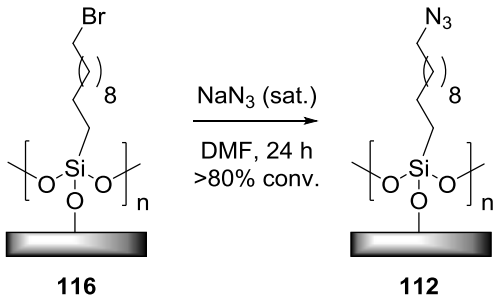

Figure 63: Conversion of Br-terminated SAM to azide terminated monolayer.

Pleasingly this protocol was reproducible and conversions of >80% were routinely obtained. Ellipsometry measurements gave a thickness value of 1.7 ±0.2 nm and a roughness of 0.1 ±0.02 nm which suggests the presence of a smooth homogenous surface after reaction with NaN_3. High resolution scans of the N 1s region of the azide terminated SAM **112** were obtained and a typical spectrum is shown in Figure 64. Two major components at a lower binding energy and a single component at higher binding energy are evident in the high resolution scans and can be attributed to the electron-rich and electron-poor nitrogen atoms respectively.[160] The first of three components relating to the azide moiety appears at a binding energy of 399.5 eV and is attributed to N**3**. There is also another peak close in binding energy that appears at 400.1 eV and is attributed to N**1**. Based on the resonance forms of the azide functionality shown in Figure 64, both N**1** and N**3** are chemically very similar and as a result have a closely related binding energy. The peak at a higher binding energy of 403.4 eV can be attributed to the electron-poor nitrogen (N**2**) in the azide moiety. All of the peaks associated with the azide are consistent with azide terminated monolayers in the literature.[167-168]

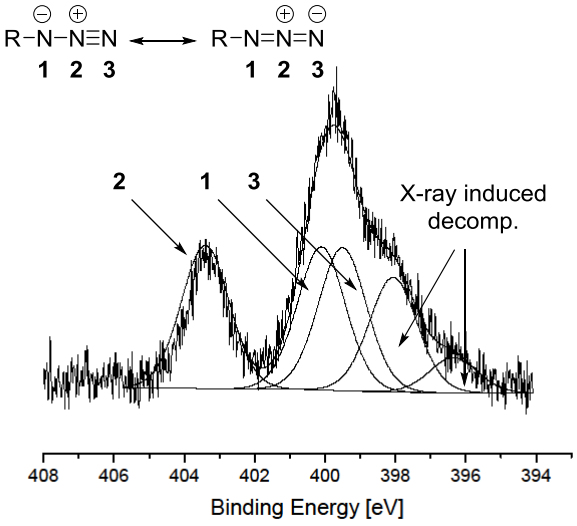

Figure 64: High resolution scan of N 1s region of azide terminated SAM 112.

A peak at 398.1 eV is also present in the XPS spectrum which cannot be attributed to the azide moeity. Unger and Schalley have shown that during the irradiation process of azide terminated monolayers on Au, a new peak at 399.0 eV appears in the XPS spectrum.[161] The authors recorded multiple XPS spectra of azide terminated monolayers over a period of 142 min and detailed XPS data showed that significant decomposition of the azide occurs. Given that the azide samples in this study are typically irradiated by X-rays for a minimum of 30-40 mins during XPS analysis it is reasonable to assume that these surfaces are experiencing the same degradation as those in the Unger and Schalley report. The authors suggest a potential mechanism for degradation, whereby decomposition of azide **112** and subsequent N_2 extrusion gives a nitrene on the surface. This reactive intermediate undergoes a subsequent [1,2]-hydride shift which affords an imine on the surface (Figure 65). Analysis by XPS and NEXAFS spectroscopy shows a peak at a binding energy 399.0 eV which is consistent with the presence of an imine moiety.[162]

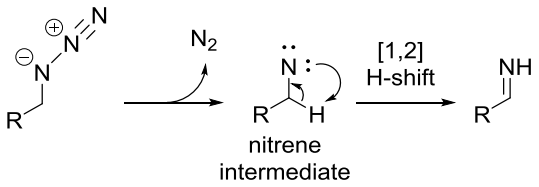

Figure 65: Possible mechanistic pathway for the degradation of azide terminated surface 112.

2.9 Synthesis of starting materials

2.9.1 Synthesis of DHPB 60

Following a procedure outlined by Smith,[164] DHPB **60** was obtained *via* a two-step procedure. Reaction of 2-chlorobenzothiazole **117** with 3-aminopropan-1-ol **118** and *i*Pr$_2$NEt in *o*-

dichlorobenzene gave the corresponding amino alcohol **119** in excellent yield. Subsequent treatment of alcohol **119** with methanesulfonyl chloride and Et_3N in CH_2Cl_2 afforded DHPB **60** in 70% yield after recrystallisation from toluene (Figure 66).

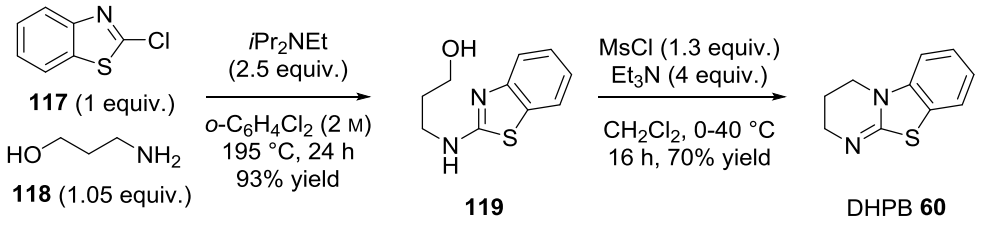

Figure 66: Synthesis of isothiourea DHPB 60.

2.9.2 Synthesis of alkyl trifluoromethyl enone

Initial attempts focused on the preparation of alkyl trifluoromethylenone **124**. Starting with commercially available 4-pentyn-1-ol **120**, this was subjected to *n*BuLi and TMS-Cl to afford the corresponding TMS protected alkyne **121** in 61% yield. Reaction under Swern conditions gave the corresponding aldehyde **122** in 44% yield (Figure 67).

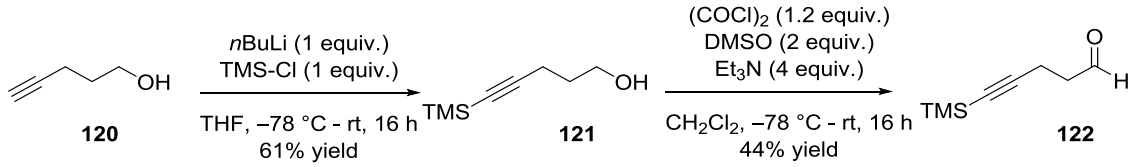

Figure 67: Synthesis of alkynyl aldehyde 121.

Aldehyde **122** was then subjected to an aldol reaction using trifluoroacetone **123** and piperidine as a base but disappointingly this gave no trace of product and returned only starting material. Aldehyde **122** was also subjected to a modified Horner-Wadsworth-Emmons reaction[146-147] using acetimidoyl chloride **102** and diethylmethylphosphonate **103** but again this returned only starting material with no sign of any of the desired enone (Figure 68). As none of the conditions were successful when tested on this substrate, this route was not pursued further and an alternative β-aryl Michael acceptor was synthesised.

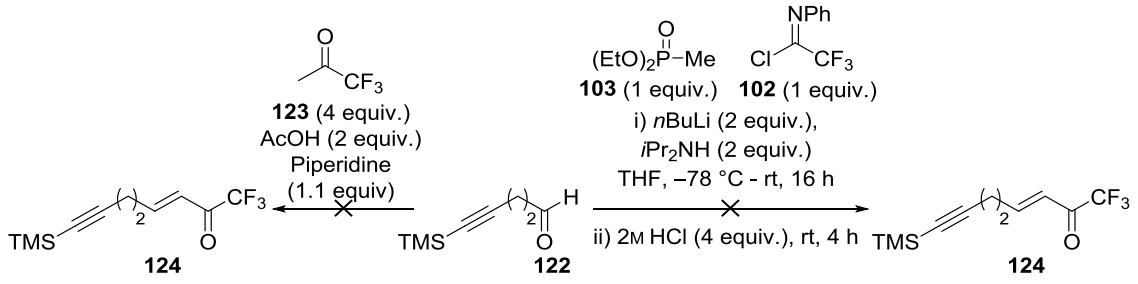

Figure 68: Attempted synthesis of α,β-unsaturated enone 124.

2.9.3 Synthesis of aryl trifluoromethylenone

Commercially available 4-bromobenzaldehyde was subjected to Sonogashira cross coupling conditions with trimethylsilylacetylene to afford **125** in 75% yield. The TMS-protected alkyne **125** was treated with imidoyl chloride **102** in the presence of phosphonate **103** and *n*BuLi which afforded (*E*)-enone **126** in 29% yield. Finally, treatment of TMS alkyne **126** with K_2CO_3 in MeOH afforded alkyne **127** in 32% yield as a precursor for the click reaction (Figure 69).

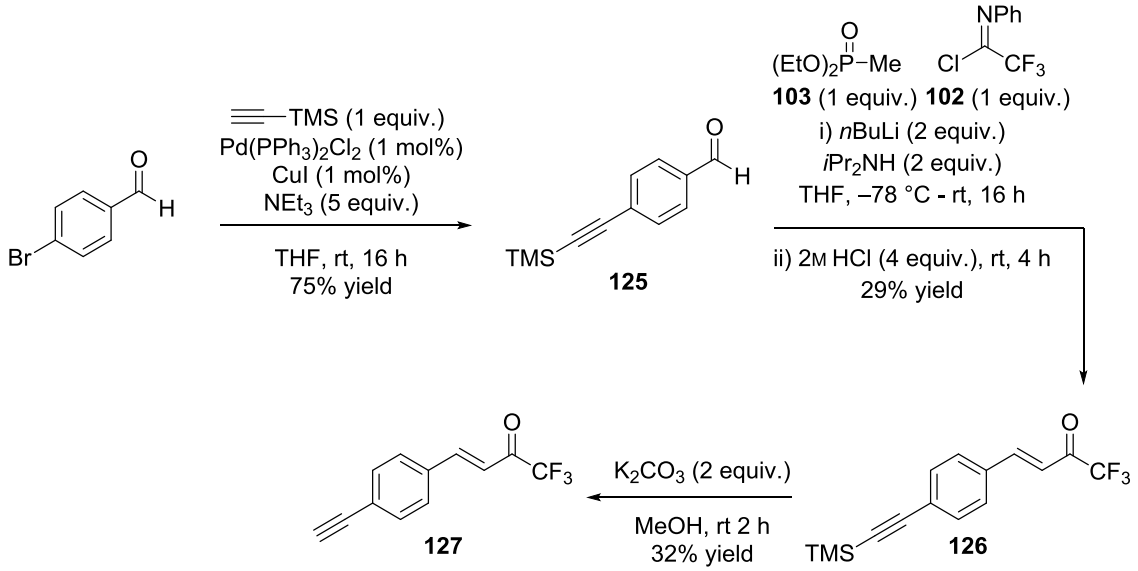

Figure 69: Synthesis of aryl CF_3 enone 127.

2.10 Generation of trifluoromethylenone 128 on the surface

With azide terminated surface in hand, alkyne **127** was attached to the surface *via* a CuAAC reaction using catalytic $CuSO_4{\cdot}5H_2O$ and (+)-sodium ascorbate (Figure 70).

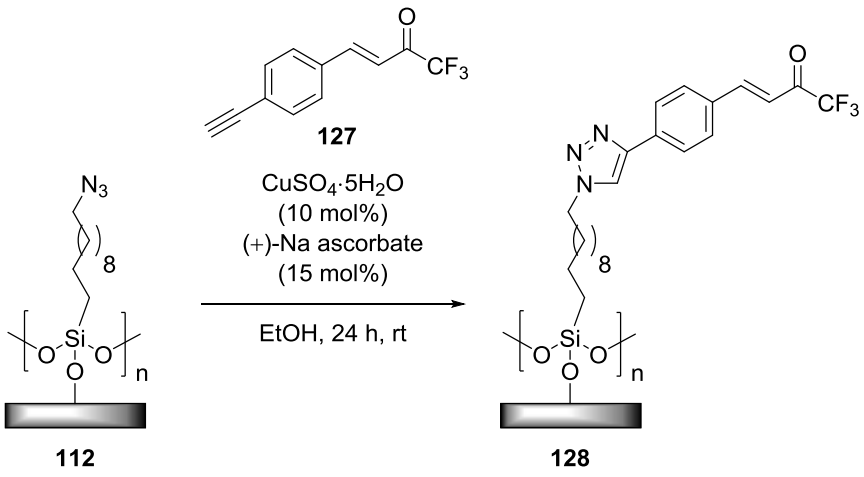

Figure 70: CuAAC using enone 127 and azide terminated monolayer 112.

A clear change in the contact angle, thickness, and surface roughness accompanied this step. The contact angle decreased from 79.1±1.0 to 72.6±2.5 nm after addition of the enone moiety. Ellipsometry measurements gave a thickness of 2.64 nm which is consistent with the addition of the enone moiety. The roughness was calculated to be 0.16 ±0.04 nm which suggested the presence of a smooth homogenous surface after the click reaction. High resolution XPS spectra of the N 1s region were obtained that included characteristic peaks suggesting the presence of a 1,2,3-triazole (Figure 71). Often peaks from the nitrogen atoms in the residual unreacted azide groups were also observed with a reproducible conversion from azide to enone in the region 89%. It is evident from the peak fitting that there are three different chemical environments present in the N 1s region that can be attributed to the triazole. Two peaks close in binding energy, 399.4 and 400.1 eV, can be assigned to N**2**/N**3** respectively.[165-166] The last peak present appears at a binding energy of 401.4 eV and is attributed to the slightly more electropositive N**1**.[167-1168]

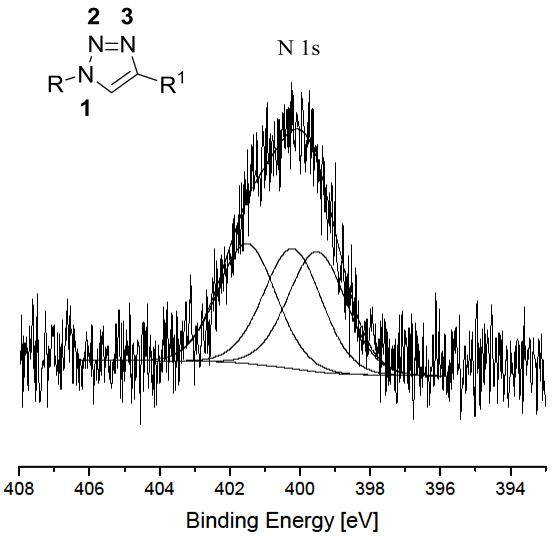

Figure 71: High resolution XPS scans of the N 1s region in 128.

High resolution XPS scans from the C 1s region further supported the claim that enone **127** had been successfully clicked onto the surface (Figure 72 (a)). Apart from the main C 1s aliphatic peak there are three peaks that appear in the C 1s spectrum. The first is at a binding energy of 286.1 eV, and can be attributed to the near neighbours of the nitrogen atoms and the aromatic regions.[169] Peaks at 292.5 eV and 288.3 eV were assigned to the C**1** and C**2** respectively. Both these peaks suggest the presence of a CF_3 containing carbonyl functionality on the surface. AFM also showed a clean smooth homogeneous surface that also further suggested a successful click reaction as no unexpected features or tip modifications were detected in the majority of samples tested (Figure 72 (b)).

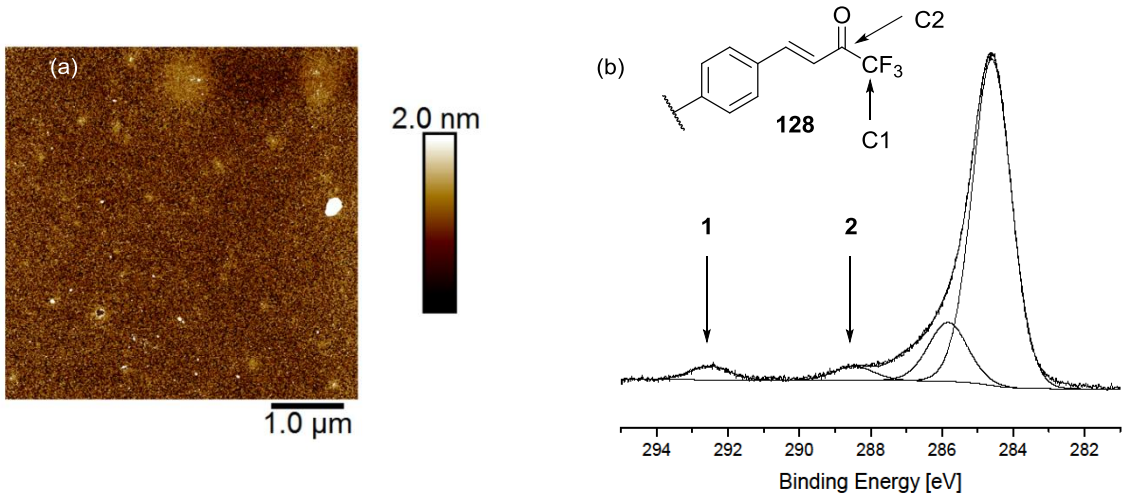

Figure 72 (a): 5×5 µm^2 AFM image of enone terminated surface 128. (b) High resolution XPS scans of C 1s region of enone-terminated SAM 128.

2.10.1 Summary of enone generation

Clean Si/SiO_2 surfaces, bromine, azide and enone terminated SAMs were all tested using contact angle, ellipsometry, XPS and AFM. The cleaned Si/SiO_2 surface gave between 5-20 ° contact angle value which is expected given the hydroxyl termination on the surface.[170] After deposition of the Br-terminated SAM, there was an increase in the contact angle to 82.9 ±0.8 consistent with the formation of a well ordered SAM. The thickness was also well within range for the expected presence of a Br-terminated SAM. Upon reaction with NaN_3 the thickness decreased slightly to 1.76 nm (entry 3, Table 5). This observation can be attributed to the decrease in bond lengths of C-Br *vs* N-N≡N (1.966 and 1.216 Å respectively) and also that bromine has a larger atomic radius compared to azides.[171] After the click reaction with enone **127** the thickness increases to 2.76 nm (Entry 4, Table 5) which is within range given the introduction of a number of carbon units. The contact angle also decreases which is slightly surprising as SAMs with fluorine as the terminal group tend to display higher contact angles, attributed to the hydrophobic fluorine atoms.[172] Coupled with data from the N 1s region it can be inferred that the click reaction was successful and enone **127** was covalently attached to the surface (Table 5).

Entry	Sample type	CA (°)[a]	Thickness (nm)[a,b]	Roughness[a] (nm)	Conv.(%)[a,c]
1	Clean Si/SiO_2 **95**	5-20	1.70 ±0.1	0.09 ±0.01	n/a
2	Bromine (Br) **115**	82.9 ±0.8	1.90 ±0.25	0.1 ±0.02	n/a
3	Azide (N_3) **112**	79.1 ±1.0	1.76 ±0.22	0.11 ±0.02	~80
4	CF_3 Enone **128**	72.6 ±2.5	2.64 ±0.23	0.16 ±0.04	~89

Table 5: Summary of the film parameters after each reaction step. [a]Average values from at least two samples of each type are shown. [b]Thicknesses quoted are for that of the oxide layer for silica and total thickness of the organic layer thereafter. [c]Calculated by XPS analysis of N 1s region.

2.11 Model study in solution

As none of the methods of characterisation (XPS, ellipsometry, contact angle or AFM) allow the diastereoselectivity of the organocatalytic process on the surface to be evaluated a solution based approach was evaluated. To show that productive ITU catalysis works with a triazole functionality present and to estimate the level of diastereocontrol that may be expected in this process, a model system was devised whereby a system analogous to that assumed on the Si/SiO_2 surface was subjected to the same reaction conditions in solution. A solution analogue of the surface tethered trifluoromethylenone was designed to undergo an analogous Michael addition-lactonisation. Commercially available 1-bromooctane **129** was treated with NaN_3 at 100 °C in DMF to afford the corresponding azide **130** in 90% yield. Reaction with enone **127** in the presence of catalytic $CuSO_4{\cdot}5H_2O$ gave the corresponding 1,2,3-triazole in a moderate 47 % yield (Figure 73)

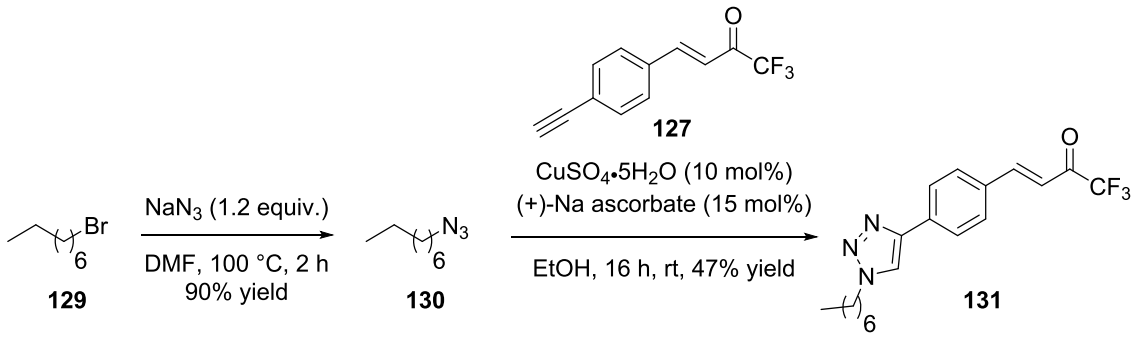

Figure 73: Synthesis of triazole 131 using click methodology.

Reaction of 4-bromophenylacetic acid **98** with pivaloyl chloride, *i*Pr_2NEt and enone **127** in the presence of catalytic DHPB **60** (5 mol%) gave ring-opened product **132** in 70% yield. The diastereoselectivity of the solution phase Michael addition-lactonisation reaction, after ring opening with MeOH, was measured by ^1H NMR spectroscopy, with a dr of 80:20 (*anti:syn*) obtained from the crude reaction mixture (Figure 74 (a)). The diasteroselectivity remained the same after purification of the crude reaction mixture by column chromatography. This diastereoselectivity is in line with what was obtained in the previous work with a variety of

substituted phenylacetic acid components.[101] This level of relative stereocontrol, combined with the $^{1}H–^{1}H$ coupling constants of ^{3}J=10.9 and 3.8 Hz for the major diastereoisomers, corresponding to the C(3)*H* and C(5)*H* resonances respectively, is consistent with the expected "*anti*"-stereocontrol observed in previous solution based studies (**133** Figure 73 (b)). This result suggests that DHPB **60** catalyses the reaction of phenylacetic acid **98** with enone **127**.

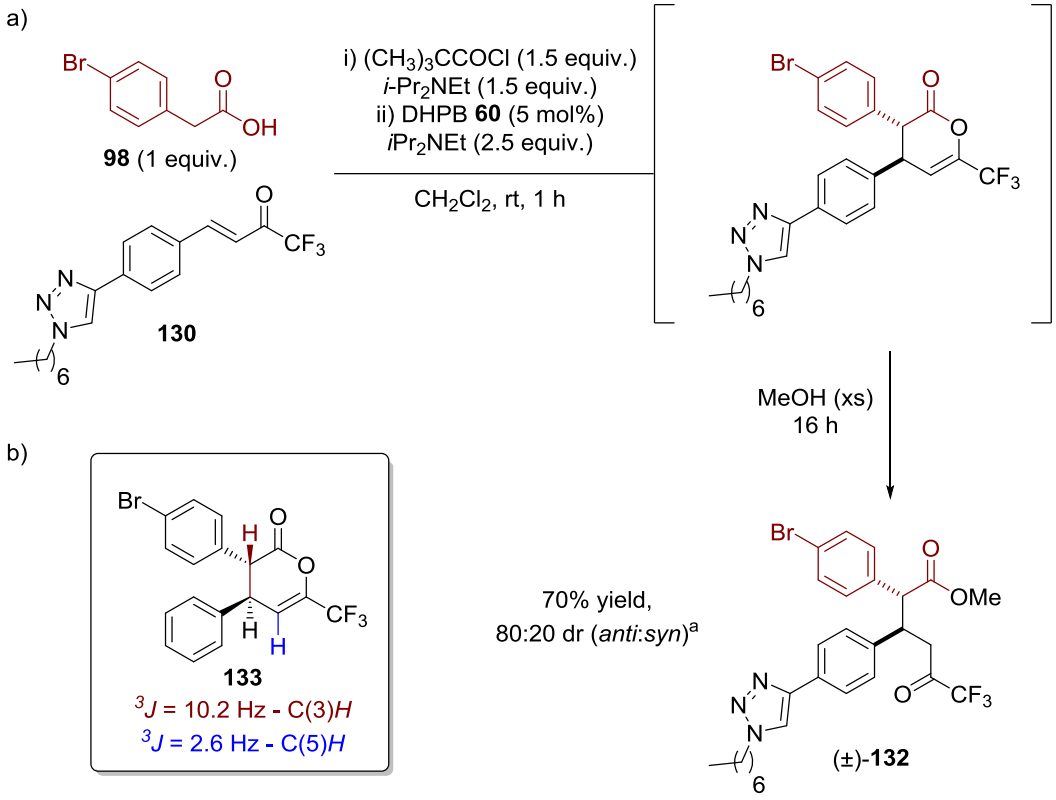

Figure 74: (a) Synthesis of ring-opened DHP (±)-132 (b) Analogous DHP 133 with corresponding ^{1}H NMR spectroscopic resonances. [a]Determined by ^{1}H NMR spectroscopy of the purified reaction mixture.

2.12 Michael addition-lactonisation on a surface

2.12.1 Initial results

With the starting material for catalysis, enone **128**, in hand, a Michael addition-lactonisation protocol was developed to allow for surface functionalisation. Pleasingly, reaction of 3-thiophenylacetic acid **134** with pivaloyl chloride, *i*Pr$_2$NEt and enone **128** in the presence of catalytic DHPB **60** (5 mol%) gave DHP terminated surface **135** (Figure 78).

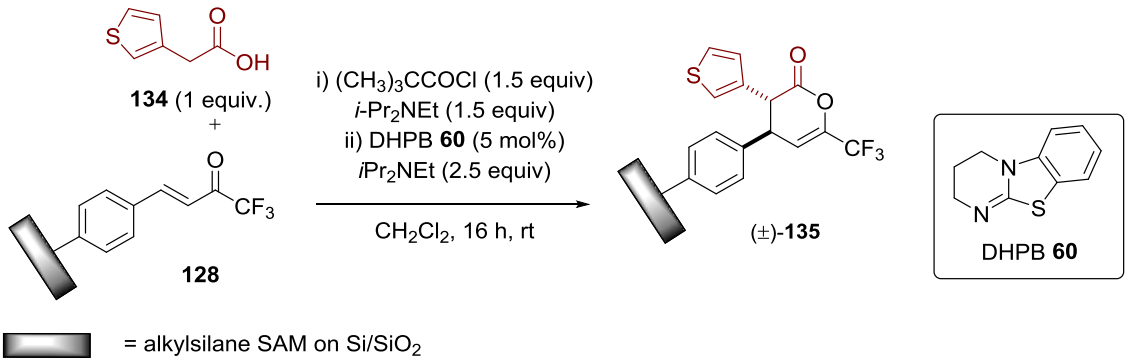

Figure 75: Initial investigation into the Michael addition-lactonisation process using 3-thiophenylacetic acid 134 and enone surface 128.

The formation of thiophene-substituted DHP **135** was confirmed by the appearance of a peak corresponding to the sulfur atom in the thiophene moiety (Figure 76(b)). A peak with a binding energy of 286.2 eV was detected in the C 1s spectrum and this was attributed to the near neighbours of the aromatic substituents in the monolayer. The peak at 288.1 eV was assigned as $\mathbf{C2_L}$ in the DHP ring.[169] The peak at 289.6 eV is assigned as $\mathbf{C1_L}$ and differs slightly in binding energy to the carbonyl peak in enone **128** and this can be taken as indication that the lactonisation process was successful. Ellipsometry measurements gave a thickness of 3.87 ±0.24 nm (entry 1, Table 6) which is consistent with the expected monolayer thickness. The expected monolayer thickness was determined using the equation proposed by Whitesides *et al*. where *L* is the length of a methyl-terminated monolayer containing *n* methylene units (Equation 2).[173]

$$L = 1.26n + 4.78$$

Equation 2: Equation used to calculate the theoretical thickness of a SAM.

AFM gave a roughness of 0.247 ±0.04 nm (entry 1, Table 6) which is in the expected region given the number of reaction steps performed on the surface. AFM also showed a clean surface over a 5×5 μm^2 area in thiophene-substituted DHP **135** (Figure 76 (c)).

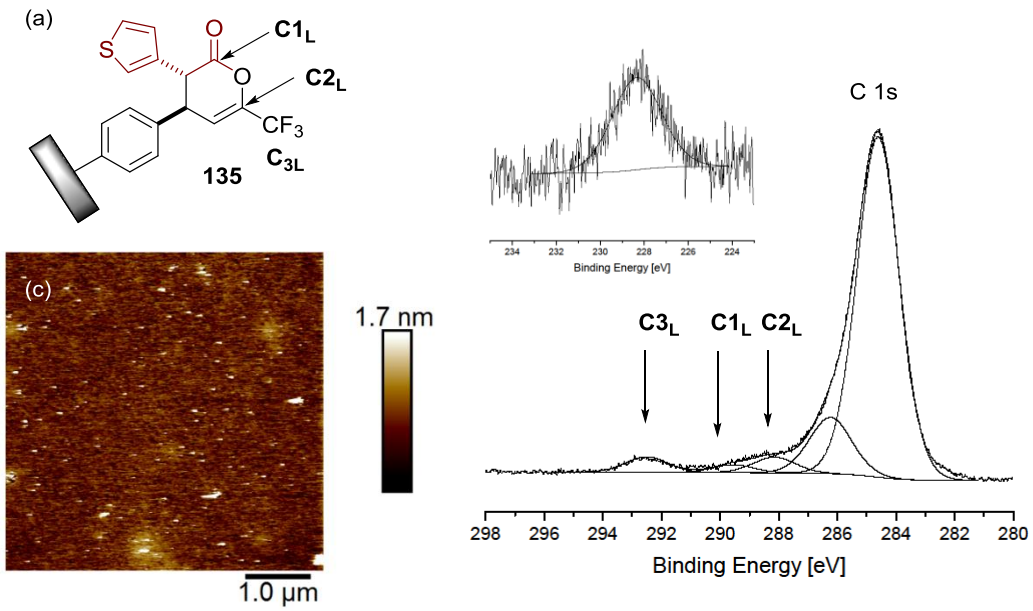

Figure 76: Thiophenyl terminated surface 135. (b) High resolution C 1s nd S 2s XPS scans of thiophene terminated surface 135. (c) 5×5 µm^2 AFM image of thiophene terminated surface 135.

As not all of the enone terminations were converted to DHPs, there remained some residual signals in the C 1s spectrum associated with the starting enone. This was used to calculate the conversion from enone to DHP by comparison of the relative peaks areas in the XPS spectra (Figure 77).

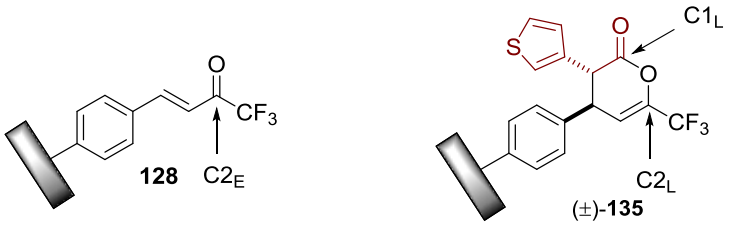

Figure 77: Estimation of conversion in the Michael addition-lactonisation process.

The conversion for the reaction of enone **128** to 3-thiophenyl DHP surface **135** was calculated to be ~54% according to **Equation 2**. Furthermore, no unidentified sulfur or nitrogen was detected in the XPS spectra, consistent with the catalyst **60** being successfully removed from the surface by the post-deposition cleaning procedure. To further probe the catalytic necessity of the isothiourea for surface functionalisation, a control reaction was performed where a CF_3 enone sample **128** was subjected to the same Michael addition-lactonisation conditions with the omission of the catalyst DHPB **60**. Formation of a DHP was not observed and the surface had properties equivalent to that of other trifluoromethylenone surfaces.

$$c = \text{Area}(C1_L)/\text{Area}(C2_E + C2_L)$$

Equation 2: Equation used to calculate conversion from enone 128 to DHP terminated surfaces.

2.13 Scope of the phenylacetic acid component

The generality of the Michael addition-lactonisation process was investigated through variation of the arylacetic acid component. The arylacetic acids were chosen specifically as they contained marker atoms that would give characteristic peaks in the XPS spectra and made it possible to obtain a conversion for the catalysis. Using the standard conditions the reaction readily tolerates heteroaryl (3-thiophenyl) as well as 4-aryl substitution, including electron-donating (4-NMe_2) and electron-withdrawing (4-CF_3) substituents giving moderate to good conversions in the reactions on the surface.

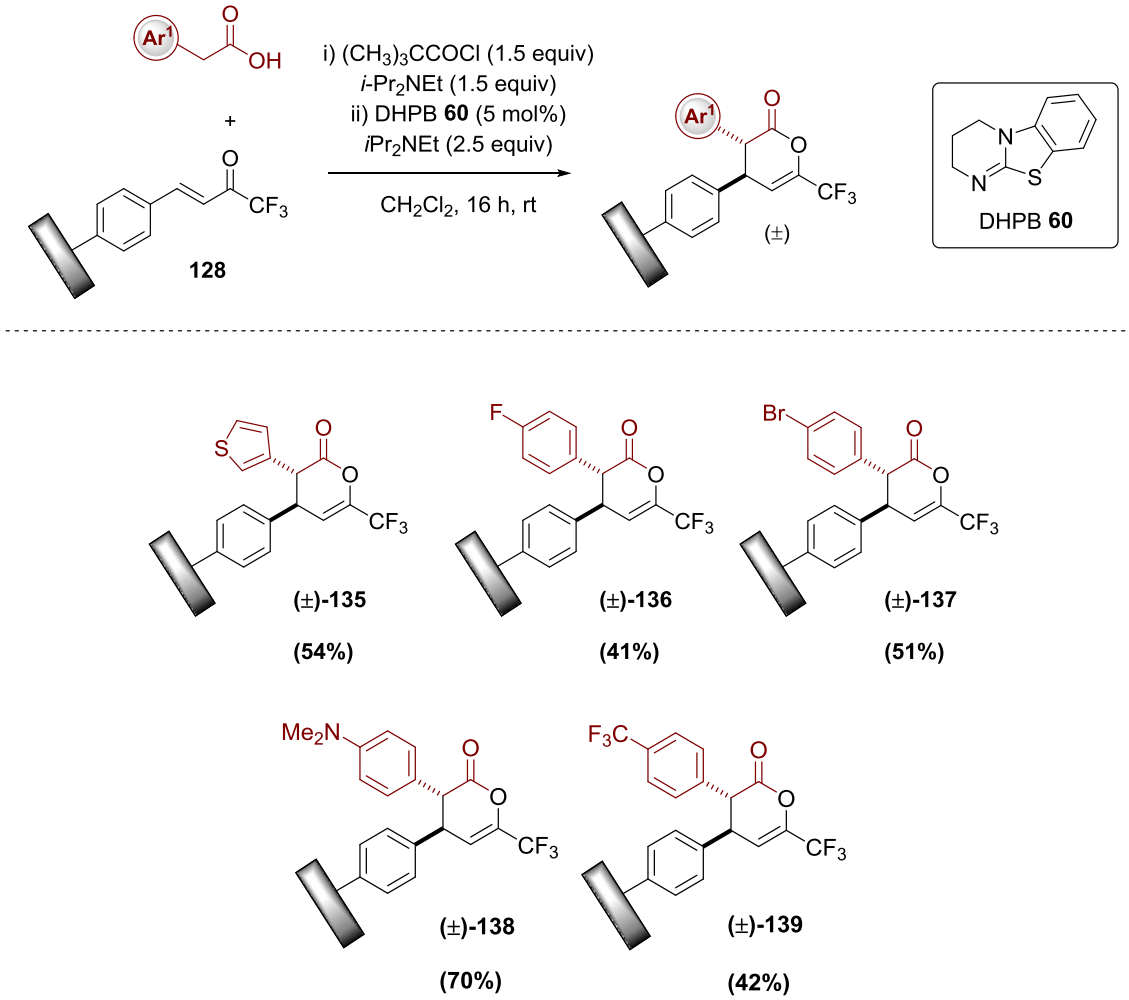

Figure 78: Michael addition-lactonisation of trifluoromethylenones on the surface using DHPB. Major diastereoisomer shown.

Formation of the DHP species was confirmed by XPS in all cases based on the appearance of a peak at 289.6 eV in the C 1s XPS spectra, corresponding to the carbonyl species ($C1_L$, Figure 77),

along with the appearance of the marker atoms in the XPS spectra. Formation of DHP terminated samples was generally accompanied by a small drop in contact angle compared to that of the enone samples. The Michael addition-lactonisation step increased the thickness of the organic layer by around 0.5−1.3 nm in comparison to the enone samples to a total value of around 3.1−3.9 nm. The roughness of the DHP samples was greater that for the corresponding enone sample, as a result of the additional reaction step which is expected. 4-Fluorine **136** 4-bromine **137**, 4-dimethylamino **138** and 4-trifluoromethyl **139** terminated samples were all analysed in an analogous fashion, using the marker atoms for an estimate of conversion (Table 6). The conversions from the reaction of enone terminated surface **128** with the appropriate arylacetic acids to afford DHP terminated surfaces **135-139** were not as high yielding as their solution-phase analogues. For example, in the solution-phase reaction of 3-thiophenylacetic acid to afford (±)-**135** occurred with full conversion and a 75% yield, lower than the conversion on the surface, possibly due to lower reactivity. (Table 6). The relative conversions of enone **128** to DHP terminated surfaces are within approximately 10% of each other (with the expection of **138**). This reactivity may indicate that regardless of phenylacetic acid, consumption of the starting material can only proceed to a certain conversion. A possible sterics based explaination for the lack of reactivity, compared to the homogeneous system, could be that the surface bound DHPs formed in the reaction begin to form domains or islands and this does not allow access for the incoming nucleophile to react with the remaining enone functionalities. However, at the present time there is no evience for this claim and further experiments are needed in order to confirm this hypothesis.

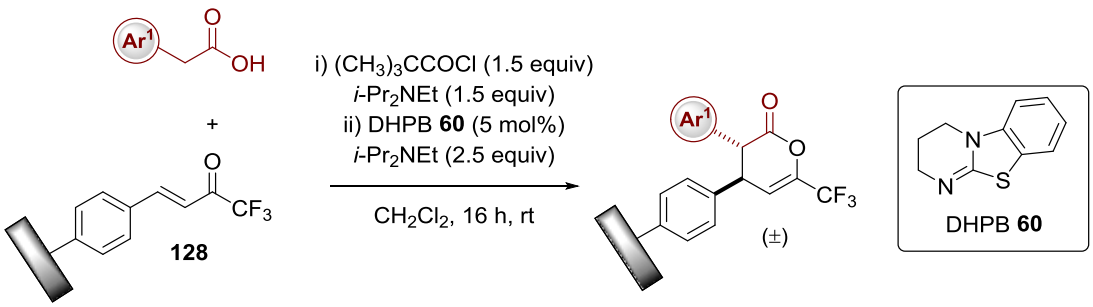

Entry	Sample	CA (°)[a]	Thickness (nm)[a,b]	Roughness[a] (nm)	Conv. (%)[a]	Conv./Yield (%)[c]
1	**3-thiophene 135**	69.8 ±2.4	3.87 ±0.24	0.247 ±0.04	~54	100/75
2	**4-FC$_6$H$_4$ 136**	71.3 ±1.1	3.60 ±0.12	0.178 ±0.05	~41	100/81
3	**4-BrC$_6$H$_4$ 137**	68.6 ±1.0	3.10 ±0.28	0.162 ±0.02	~51	100/72
4	**4-NMe$_2$C$_6$H$_4$ 138**	70.0 ±2.2	3.89 ±0.15	0.155 ±0.06	~70	100/80
5	**4-CF$_3$C$_6$H$_4$ 139**	72.8 ±1.5	3.76 ±0.24	0.16 ±0.05	~42	100/60

Table 6: Summary of the film parameters of different dihydropyranone species. [a]Average values from at least two samples of each type are shown. [b]Thicknesses quoted are for that of the oxide layer for silica and total thickness of the organic layer thereafter. [c]Conversion and yields of analogous solution phase Michael addition-lactonisation reactions.

2.14 Conclusions and Future Work

In this work a small library of dihydropyranones have been synthesised on a surface through an isothiourea-mediated Michael addition-lactonisation procedure using a range of arylacetic acids. The conversions were in the range of 40-70% and as such this methodology offers an effective route to build a variety of complex surfaces containing this functionality. As this was a proof of concept study only a small range of arylacetic acids were tested but the consistency of this methodology suggests that a wide range of phenylacetic acid derivatives could be applied providing a flexible methodology for surface functionalisation.

It has also been shown in solution that these types of dihydropyranone motifs are prone to ring opening by a range of nucleophiles [174] which opens up the possibility for covalent attachment of an external nucleophile, such as a protein or amino acid. Such strategies may have applications in biosensor technologies. Several of the resulting dihydropyranones also contain useful functional handles that may allow for further modification, such as transition metal mediated cross-coupling and S_NAr reactions.

2.15 References and Notes

[116] K. Bierbaum, M. Kinzler, C. Woell, M. Grunze, G. Haehner, S. Heid, F. Effenberger, *Langmuir* **1995**, *11*, 512-518.
[117] T. Ohtake, N. Mino, K. Ogawa, *Langmuir* **1992**, *8*, 2081-2083.
[116] D. K. Aswal, S. Lenfant, D. Guerin, J. V. Yakhmi, D. Vuillaume, *Anal. Chim. Acta* **2006**, *568*, 84-108.
[117] W. Kern, *J. Electrochem. Soc.* **1990**, *137*, 1887-1892.
[118] D. K. Schwartz, *Annu. Rev. Phys. Chem.* **2001**, *52*, 107-137.
[119] N. Rozlosnik, M. C. Gerstenberg, N. B. Larsen, *Langmuir* **2003**, *19*, 1182-1188.
[120] T. Vallant, H. Brunner, U. Mayer, H. Hoffmann, T. Leitner, R. Resch, G. Friedbacher, *J. Phys. Chem. B.* **1998**, *102*, 7190-7197.
[121] Y. Liu, L. K. Wolf, M. C. Messmer, *Langmuir* **2001**, *17*, 4329-4335.
[122] J. V. Davidovits, V. Pho, P. Silberzan, M. Goldmann, *Surf. Sci.* **1996**, *352–354*, 369-373.
[123] L. Sanga, K. M. Knesting, A. Bulusuc, A. K. Sigdel, A. J. Giordanoe, S. R. Marder, J. J. Berry, S. Graham, D. S. Ginger, J. E. Pemberton, *Appl. Surf. Sci*., **2016**, *389*, 190-198.
[124] W. Gao , L. Dickinson, C. Grozinger, F. G. Morin, L. Reven, *Langmuir*, **1996**, *12*, 6429-6435.
[125] C. Carraro, O. W. Yauw, M. M. Sung, R. Maboudian, *J. Phys. Chem. B.* **1998**, *102*, 4441-4445.
[126] Y. Cheng, B. Zheng, P. Chuang, S. Hsieh, *Langmuir* **2010**, *26*, 8256-8261.
[127] S. G. Moussa, B. J. Finlayson-Pitts, *Phys. Chem. Chem. Phys.* **2010**, *12*, 9419-9428.
[128] F. Bournel, F. Jolly, F. Rochet, G. Dufour, F. Sirotti, P. Torelli, *Phys. Rev. B.* **2000**, *62*, 7645-7653.
[129] A. P. Dementjev, A. de Graaf, M. C. M. van de Sanden, K. I. Maslakov, A. V. Naumkin, A. A. Serov, *Diamond Relat. Mater.* **2000**, *9*, 1904-1907.

[130] F. R. McFeely, S. P. Kowalczyk, L. Ley, R. G. Cavell, R. A. Pollak, D. A. Shirley, *Phys. Rev. B.* **1974**, *9*, 5268-5278.
[131] D. Janssen, R. De Palma, S. Verlaak, P. Heremans, W. Dehaen, *Thin Solid Films* **2006**, *515*, 1433-1438.
[132] A. Razgon, R. G. Bergman, C. N. Sukenik, *Langmuir* **2008**, *24*, 2545-2552.
[133] R. F. Heck, J. P. Nolley, *J. Org. Chem.* **1972**, *37*, 2320-2322.
[134] I. P. Beletskaya, A. V. Cheprakov, *Chem. Rev.* **2000**, *100*, 3009-3066.
[135] R. Franzén, *Can. J. Chem.* **2000**, *78*, 957-962.
[136] S. R. Puniredd, O. Assad, T. Stelzner, S. Christiansen, H. Haick, *Langmuir* **2011**, *27*, 4764-4771.
[137] K. E. Plass, X. Liu, B. S. Brunschwig, N. S. Lewis, *Chem. Mater.* **2008**, *20*, 2228-2233.
[138] M. C. Pirrung, *Angew. Chem. Int. Ed.* **2002**, *41*, 1276-1289.
[139] Y. Dubowski, J. Vieceli, D. J. Tobias, A. Gomez, A. Lin, S. A. Nizkorodov, T. M. McIntire, B. J. Finlayson-Pitts, *J. Phys. Chem. A.* **2004**, *108*, 10473-10485.
[140] L. R. Fiegland, M. McCorn Saint Fleur, J. R. Morris, *Langmuir* **2005**, *21*, 2660-2661.
[141] A. W. Snow, G. G. Jernigan, M. G. Ancona, *Analyst* **2011**, *136*, 4935-4949.
[142] J. W. Lu, L. R. Fiegland, E. D. Davis, W. A. Alexander, A. Wagner, R. D. Gandour, J. R. Morris, *J. Phys. Chem. C.* **2011**, *115*, 25343-25350.
[143] J. Vieceli, O. L. Ma, D. J. Tobias, *J. Phys. Chem. A.* **2004**, *108*, 5806-5814.
[144] C. Rogero, B. T. Chaffey, E. Mateo-Martí, J. M. Sobrado, B. R. Horrocks, A. Houlton, J. H. Lakey, C. Briones, J. A. Martín-Gago, *J. Phys. Chem. C.* **2008**, *112*, 9308-9314.
[145] A. Hozumi, H. Taoda, T. Saito, N. Shirahata, *Surf. Interface Anal.* **2008**, *40*, 408-411.
[146] L. Horner, H. Hoffmann, H. G. Wippel, G. Klahre, *Chem. Ber.* **1959**, *92*, 2499-2505.
[147] L. Horner, H. Hoffmann, H. G. Wippel, *Chem. Ber.* **1958**, *91*, 61-63.
[148] K. Tamura, H. Mizukami, K. Maeda, H. Watanabe, K. Uneyama, *J. Org. Chem.* **1993**, *58*, 32-35.
[149] J. K. Lee, Y. S. Chi, I. S. Choi, *Langmuir* **2004**, *20*, 3844-3847.
[150] F. Shamsi, H. Coster, K. A. Jolliffe, *Surf. Sci.* **2011**, *605*, 1763-1770.
[151] S. Zheng, Q. Yang, B. Mi, *Appl. Surf. Sci.* **2016**, *363*, 619-626.
[152] S. Pookpanratana, I. Savchenko, S. N. Natoli, S. P. Cummings, L. J. Richter, J. W. F. Robertson, C. A. Richter, T. Ren, C. A. Hacker, *chem*, *30*, 10280-10289.
[153] N. Balachander, C. N. Sukenik, *Langmuir* **1990**, *6*, 1621-1627.
[154] J. Böhmler, A. Ponche, K. Anselme, L. Ploux, *ACS Appl. Mater. Inter.* **2013**, *5*, 10478-10488.
[155] Y. S. Cohen, A. Vilan, I. Ron, D. Cahen, *J. Phys. Chem. C.* **2009**, *113*, 6174-6181.
[156] S. Zhang, J. T. Koberstein, *Langmuir* **2012**, *28*, 486-493.
[157] W. R. Ashurst, C. Carraro, R. Maboudian, *IEEE T. Device. Mat. Re.* **2003**, *3*, 173-178.
[158] Y. X. Zhuang, O. Hansen, T. Knieling, C. Wang, P. Rombach, W. Lang, W. Benecke, M. Kehlenbeck, J. Koblitz, *J. Microelectromech. Syst.* **2007**, *16*, 1451-1460.
[159] T. Koga, M. Morita, H. Ishida, H. Yakabe, S. Sasaki, O. Sakata, H. Otsuka, A. Takahara, *Langmuir* **2005**, *21*, 905-910.
[160] E. Darlatt, A. Nefedov, C. H. H. Traulsen, J. Poppenberg, S. Richter, P. M. Dietrich, A. Lippitz, R. Illgen, J. Kühn, C. A. Schalley, C. Wöll, W. E. S. Unger, *J. Electron. Spectrosc. Relat. Phenom.* **2012**, *185*, 621-624.
[161] T. Heinrich, C. H. H. Traulsen, E. Darlatt, S. Richter, J. Poppenberg, N. L. Traulsen, I. Linder, A. Lippitz, P. M. Dietrich, B. Dib, W. E. S. Unger, C. A. Schalley, *RSC Adv.* **2014**, *4*, 17694-17702.
[162] C. H. Haensch, S.; Schubert, U. S., *Nanotechnology* **2008**, *19*, 035703.
[163] X. Song, Y. Ma, C. Wang, P. M. Dietrich, W. E. S. Unger, Y. Luo, *J. Phys. Chem. C.* **2012**, *116*, 12649-12654.
[164] D. S. B. Daniels, S. R. Smith, T. Lebl, P. Shapland, A. D. Smith, *Synthesis* **2015**, *47*, 34-41.

[165] M. James, S. Ciampi, T. A. Darwish, T. L. Hanley, S. O. Sylvester, J. J. Gooding, *Langmuir* **2011**, *27*, 10753-10762.
[166] J. Wang, F. Wu, M. Watkinson, J. Zhu, S. Krause, *Langmuir* **2015**, *31*, 9646-9654.
[167] T. Palacin, H. L. Khanh, B. Jousselme, P. Jegou, A. Filoramo, C. Ehli, D. M. Guldi, S. Campidelli, *J. Am. Chem. Soc.* **2009**, *131*, 15394-15402.
[168] P.-J. Wei, G.-Q. Yu, Y. Naruta, J.-G. Liu, *Angew. Chem. Int. Ed.* **2014**, *53*, 6659-6663.
[169] M. Giesbers, A. T. M. Marcelis, H. Zuilhof, *Langmuir* **2013**, *29*, 4782-4788.
[170] S. Diegoli, P. M. Mendes, E. R. Baguley, S. J. Leigh, P. Iqbal, Y. R. Garcia Diaz, S. Begum, K. Critchley, G. D. Hammond, S. D. Evans, D. Attwood, I. P. Jones, J. A. Preece, *J. Exp. Nanosci.* **2006**, *1*, 333-353.
[171] F. H. Allen, O. Kennard, D. G. Watson, L. Brammer, A. G. Orpen, R. Taylor, *J. Chem. Soc. Perkin Trans. 2* **1987**, S1-S19.
[172] S. P. Pujari, E. Spruijt, M. A. Cohen Stuart, C. J. M. van Rijn, J. M. J. Paulusse, H. Zuilhof, *Langmuir* **2012**, *28*, 17690-17700.
[173] S. R. Wasserman, Y. T. Tao, G. M. Whitesides, *Langmuir*, **1989**, *5*, 1074–1087.
[174] N. Attaba, J. E. Taylor, A. M. Z. Slawin, A. D. Smith, *J. Org. Chem.* **2015**, *80*, 9728-9739.

Chapter 3 :Synthesis and chiral discrimination of enantioenriched *C*(6)-trifluoromethyldihydropyranones by chemical force microscopy

Introduction

Having demonstrated the use of an achiral isothiourea organocatalyst for the generation of racemic *C*(6)-trifluoromethyldihydropyranone-terminated surfaces (Chapter 2), this chapter describes the use of a either enantiomer of a chiral isothiourea catalyst, HyperBTM **61**, to give either enantiomer of the dihydropyranone (DHP) on a surface (Figure. 79).The enantioinduction imparted on the surface was analysed using chemical force microscopy, including the development of a novel chiral AFM probe, which gave a clear level of enantiodiscrimination between different enantiomers of DHPs attached to the surface.

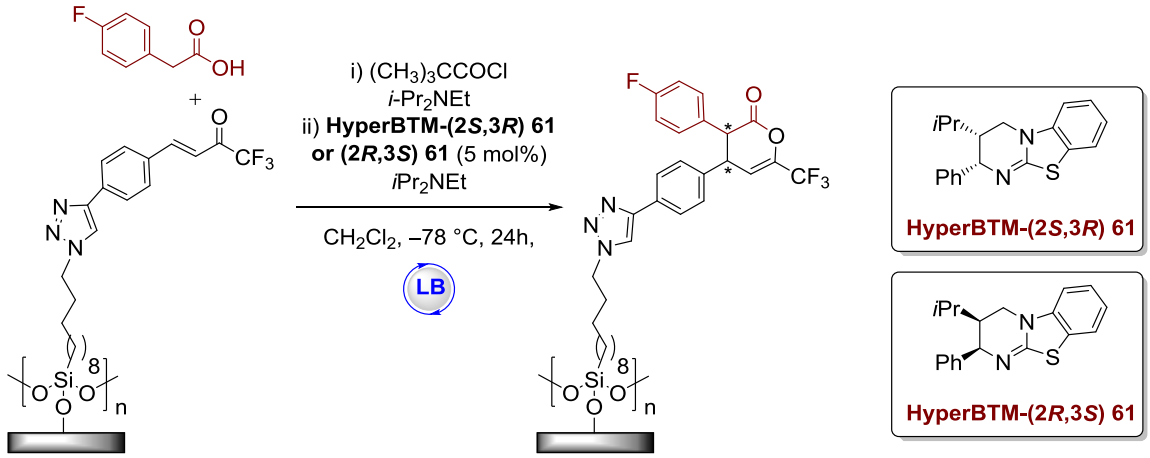

Figure 79: Michael addition-lactonisation of enones using either HyperBTM-(2*S*,3*R*) 61 or HyperBTM-(2*R*,3*S*) 61.

The generation of chiral surfaces is an area of great interest and they are finding uses in fields such as chiral selectors,[175] selective crystallisation[176] and enantioselective heterogeneous catalysis.[177-178] Surfaces can be considered chiral if they are based on chiral crystals or on templates with chiral molecules.[179] For example, chiral selectors are used to separate the two enantiomers of a racemate, with the most widespread use of chiral selectors being in high performance liquid chromatography (HPLC).[180] Chiral resolution on chiral stationary phases (CSPs) is realised through the formation of non-covalent diastereomeric complexes between the chiral selector and the enantiomers in a racemic mixture resulting in discrimination between the two enantiomers.[175] These transient diasteromeric interactions result in a difference in binding affinity with the chiral selector and hence a difference in retention time (t_R). Chiral surfaces have also found use in the study of biomaterials, as certain cell types are known to attach themselves

differentially to surfaces based on the chirality of the surface, demonstrating sensitivity at the angstrom scale.[179, 181]

3.1 Aims

The aim of this project was to investigate whether a chiral isothiourea catalyst could be used to induce asymmetry onto a surface through a catalytic enantioselective transformation. As enantioinduction on a surface is difficult to quantify and detect using classical organic chemistry methods (HPLC, optical polarimetry etc.) chiral force microscopy was used to obtain a quantitative picture of the enantioenrichement on the surface. We hoped that the design of a novel chiral AFM tip and its subsequent use in chiral force microscopy would provide a clear discrimination between different enantiomerically-enriched surfaces, to confirm that asymmetry can be induced using enantioselective catalysis on a surface

3.2 Measuring molecular chirality at surfaces

Classically, there are two main approaches to induce chirality at surfaces: the deposition of enantiopure molecules directly onto a surface or *via* careful cutting of the crystal to expose chiral kinked and stepped surfaces.[182] It was envisaged that the modification of a surface with a prochiral termination using enantioselective means could be used as a third novel method to create a chiral environment on a surface. To the best of our knowledge, to date there has been no example in the literature of using catalytic enantioselective methodology on a SAM to generate enantioenriched surfaces. Consequentially, measuring the enantioinduction imparted on the surface, as a result of enantioselective catalysis has not been demonstrated. Many different techniques have been developed to measure the level of chirality on a surface.[183] The following section offers a review of different approaches to measuring chirality at surfaces.

3.2.1 Second harmonic generation circular dichroism (SHG-CD)

Circular dichroism (CD) detects the slight differences in optical absorption between left and right circularly polarised light interacting with enantiomers in solution.[184] The theory behind this type of spectroscopy centres on the rotational strength which results from a weak interaction between the electric and magnetic dipole transition moments within a given molecule.[185] However, CD cannot be used to detect chirality in ultrathin films of small molecules as the response is too weak.[186] SHG-CD is an effect that depends on the handedness of the chromophore, thereby revealing chirality and can be used to detect chirality at surfaces of ultrathin films.[185] McGilp and co-workers have shown that SHG-CD can be used to detect the chiral nature of thin films of (*R*)-and (*S*)-1,1'-binaphthlene-2,2'-diol.[186] A small difference in chirality can been seen in this system demonstrating the potential for the use of SHG-CD in the detection and quantification of chirality of ultrathin organic films.

3.2.2 Enantioselective crystallisation

As early as 1858 Pasteur discovered that the crystals of (±)-sodium ammonium tartrate **140**, isolated from the overheated deposition of fermented grape juice, consisted of two different kinds of enantiomorphic shapes (Figure 80).[187] He could manually sort these crystals into each type of shape using a pair of tweezers, and found that each type of crystal rotated polarised light in opposite directions. This experiment, and those that followed spawned the field of resolution and selective crystallisation.

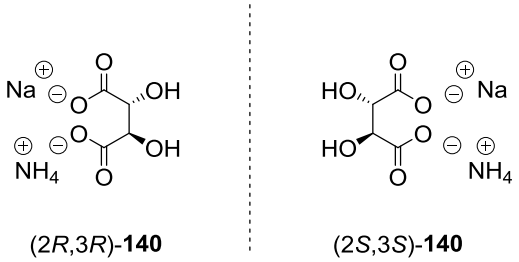

Figure 80: Ammonium sodium tartaric acid enantiomers separated by Pasteur in 1858.

The basic assumption of enantioselective crystallisation on surfaces follows that of classical resolution, where the chiral surface will serve as a selective chiral nucleus, lowering the energy needed for crystal formation of one of the enantiomers.[188] This particular enantiomer will then crystallise in excess on the surface and can easily be separated from the mixture. Mastai and Dressler have shown that both enantiomers of (±)-glutamic acid **141** can be selectively crystallised using surfaces of L-and D-cysteine.[176] The authors selectively crystallised D-glutamic acid in 31% ee from (±)-glutamic acid on an L-cysteine surface **142** (Figure 81) while also selectively crystallising L-glutamic acid on a D-cysteine surface in 27% ee. This demonstrated the potential of chiral surfaces for the resolution of racemates, albeit in low to moderate ee.

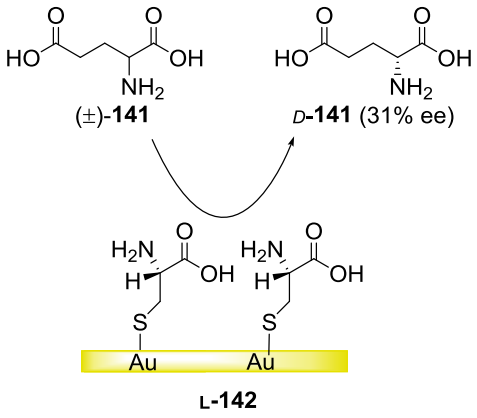

Figure 81: Selective crystallisation of *D*-glutamic acid from (±)-glutamic acid on *L*-cysteine surface 142.

Mastai *et al.* reported the first example of a chiral nanosized metal oxide surface based on chiral SAMs coated with a metal oxide.[189] The authors deposited a known enantiomer of cysteine on an Au coated glass surface and subsequently grew a TiO_2 film on the cysteine SAM using atomic layer deposition (ALD) and $[Ti\{N(CH_3)_2\}_4]$ **144** as a promoter (Figure 82). TiO_2 was used as a protective nanolayer for SAM **143** while also preserving the chirality of the surface. SHG-CD was used to assess the chiral nature of the surface and the results showed a significant difference in the polarisation of light by each of the different enantiomers indicating a chiral surface. An enantioselective crystallisation experiment was also employed to assess the chirality of the surface. The surface was immersed vertically in a super saturated solution of (±)-threonine and macro sized crystals formed on the surface where they were carefully removed and tested for ee. The results showed a modest ee of 38%, for L-enantiomer **146**, was obtained from (±)-threonine on an L-cysteine derived surface which further suggested that the surfaces were indeed chiral.

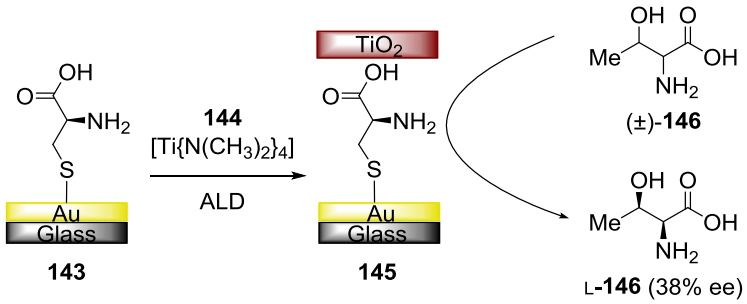

Figure 82: Deposition of enantiopure cysteine onto an Au followed by ALD of TiO_2.

3.2.3 Chemical force microscopy

Chemical force microscopy (CFM) has proven a useful tool in the detection of different functional groups on surfaces since its introduction by Lieber and co-workers in the mid 1990's.[190] CFM works by measuring the adhesive and friction forces between molecularly modified AFM probe tips and organic SAMs with a suitable terminal functional group.[191] It builds on the classical area of force microscopy where information about adhesion and friction may be obtained but it cannot directly probe the specific chemical groups on the sample.[192] CFM can overcome this obstacle by the introduction of chemically modified probes which makes them sensitive to specific molecular interactions (Figure 83).

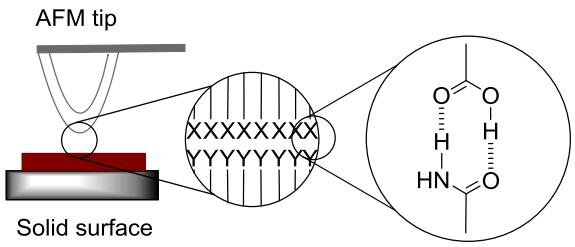

Figure 83: Illustrative example of specific molecular interactions in CFM (hydrogen bonding between a primary amide and carboxylic acid).

Since the introduction of CFM it has been applied to various studies including the binding of biotin and streptavadin,[193-194] binding between DNA base pairs[195] and most importantly, with reference to this work, been used as a method for the discrimination of chiral surfaces.[196]

Abell and co-workers were the first to demonstrate a proof of principle study on the chiral discrimination of enantiopure Au surfaces using CFM.[196] A novel chiral precursor **147** was synthesised based on Pirkle's resin[197], used originally in chiral HPLC, and deposited on an Au coated micro cantilever (Figure 84(a)). This chiral AFM tip was then tested against a series of Au surfaces functionalised with enantiopure mandelic acids (Figure 84(b)). The authors showed that discrimination (measured in nN) can be obtained in the cases of the (*S*)-functionalised tip **147** vs both (*R*)-**148** and (*S*)-**148** ether surfaces (1.1 ±0.1 and 0.4 ±0.1 nN respectively) and the same tip vs both (*R*)-**149** and (*S*)-**149** aromatic surfaces (0.9 ±0.2 and 0.5 ±0.1 nN respectively). Similar discrimination was observed in the case of (*R*)-functionalised tip **147** vs both (*R*)-**148** and (*S*)-**148** ether surfaces (0.5 ±0.1 and 1.2 ±0.1 nN respectively) and the same tip vs both (*R*)-**149** and (*S*)-**149** aromatic surfaces (0.6 ±0.1 and 1.1 ±0.2 nN respectively). Experiments with (*R*)-**150** and (*S*)-**150** surfaces (ester) were inconclusive and gave no discrimination using any of the enantiopure or racemic tips. This study showed that CFM was sufficiently sensitive to permit discrimination between enantiomers of simple chiral molecules. The authors also hypothesise that the chiral discrimination observed must arise from the differing non-covalent complexes formed between the probe tip and the surface but do not give any stereochemical model to support this theory.

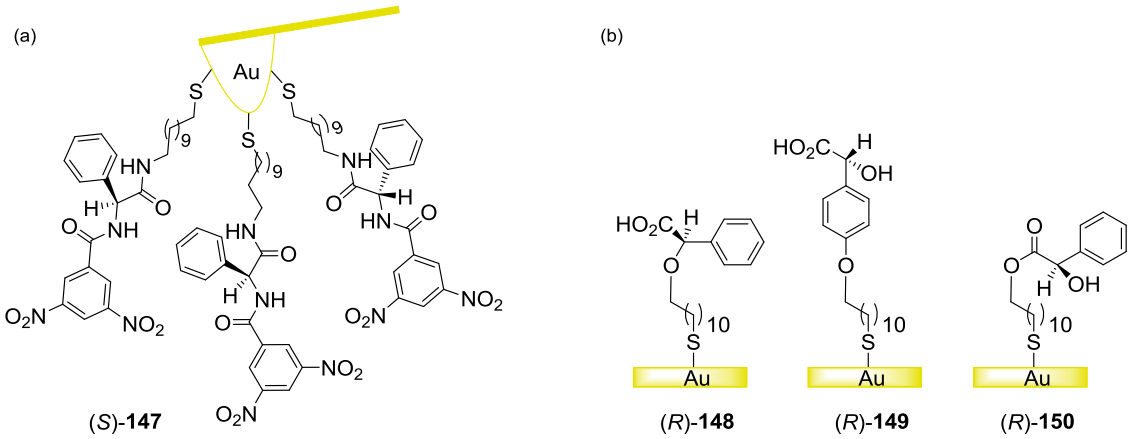

Figure 84 (a): Deposition of enantiopure chiral benzamide onto an Au coated AFM tip; (b) a series of enantiopure (*R*)-mandelic acids deposited on separate Au coated wafers.

Another report from the research group of Abell showed that chiral discrimination can also be achieved using either enantiomer of Pirkle's resin (Figure 84(a)), deposited on a probe tip, when tested against a series of hydrophobic coated Au surfaces derived from enantiopure amino

acids.[198] The study showed that chiral discrimination could be demonstrated in all cases when measuring the adhesion forces between the (*R*)-or (*S*)-tip and the surfaces **151** to **154** (Table 7). A greater adhesion force was measured for the chiral amines **151** and **152** (Entries 1-8, Table 7) and it was theorised that the amines on the surface were protonated under experimental conditions, resulting in adhesion with the probe tip due to the presence of a net positive charge. Surfaces **153** and **154** showed less of an adhesion force overall but still gave a large enough difference in adhesion to suggest discrimination.

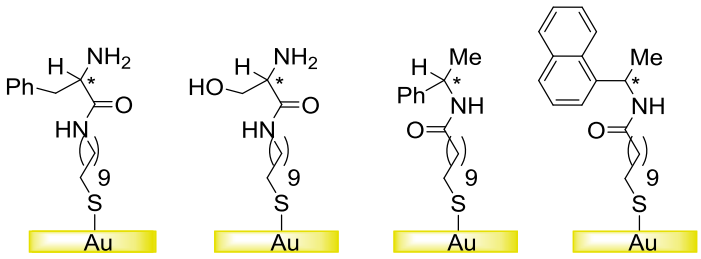

151 **152** **153** **154**

Entry	Tip enantiomer	Surface	Adhesion (nN)
1	(*R*)-**147**	(*R*)-**151**	0.2 ±0.1
2	(*R*)-**147**	(*S*)-**151**	0.7 ±0.1
3	(*S*)-**147**	(*R*)-**152**	0.5 ±0.1
4	(*S*)-**147**	(*S*)-**152**	0.2 ±0.1
5	(*R*)-**147**	(*R*)-**153**	0.9 ±0.1
6	(*R*)-**147**	(*S*)-**153**	1.2 ±0.1
7	(*S*)-**147**	(*R*)-**154**	0.4 ±0.1
8	(*S*)-**147**	(*S*)-**154**	0.2 ±0.1

Table 7: Adhesion forces for phenalynine and serine derived surfaces tested against both (*R*)- and (*S*)-147.

Takahara and co-workers have also shown that chiral discrimination can be achieved by depositing simple enantiopure molecules on a probe tip and on a surface.[191] The authors used 2,2,2-trifluoro-1-(9-anthryl)ethanol (TFAE) **155** and *N*-(3,5-dinitrobenzoyl)phenylglycine (DNPB) **156** as the enantiomeric pairs, which were immobilised to a Si-based probe tip and a Si/SiO_2 surface respectively using an aminosilane anchor (Figure 85). The authors examined all four possible combinations *i.e.* (*R*)-TFAE **155** vs. (*R*)-DNBP **156**, (*R*)-TFAE **155** vs. (*S*)-DNBP**156**, (*S*)-TFAE **155** vs. (*R*)-DNBP **156**, (*S*)-TFAE **155** vs. (*S*)-DNBP **156** and showed that chiral discrimination events were occurring between the probe tip and the surface. The authors also hypothesised that the interactions that lead to chiral discrimination must be coming from weak non-covalent interactions such as hydrogen bonding and charge transfer between the two

entities and elude to these types of systems being used for the rational design of novel silica based chiral columns.

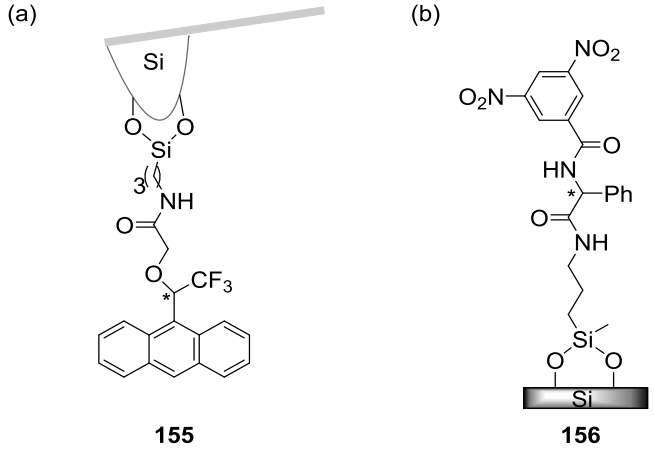

Figure 85 (a): Deposition of enantiopure TFAE 155 onto a silicon based cantilever, (b) Deposition of enantiopure DNPB 156 onto a Si/SiO_2 surface.

Hodacova *et al*. have demonstrated that CFM can be performed using enantiopure trianglamines deposited onto both a silicon surface and a Si_3N_4 based AFM tip.[199] The authors grafted enantiopure triangleamine **158** to a surface through reaction with an isocyanate moiety **157** to give a urea **159a** and subsequently measured the adhesion forces between the surface and a probe tip **159b** (Figure 86). The results showed that chemical force discrimination could be achieved in this system with the adhesion force values showing a matched and mismatched effect between the probe and the surface. Weaker interactions occurred between the enantiomers of the trianglamines than with trianglamines of the same configuration.

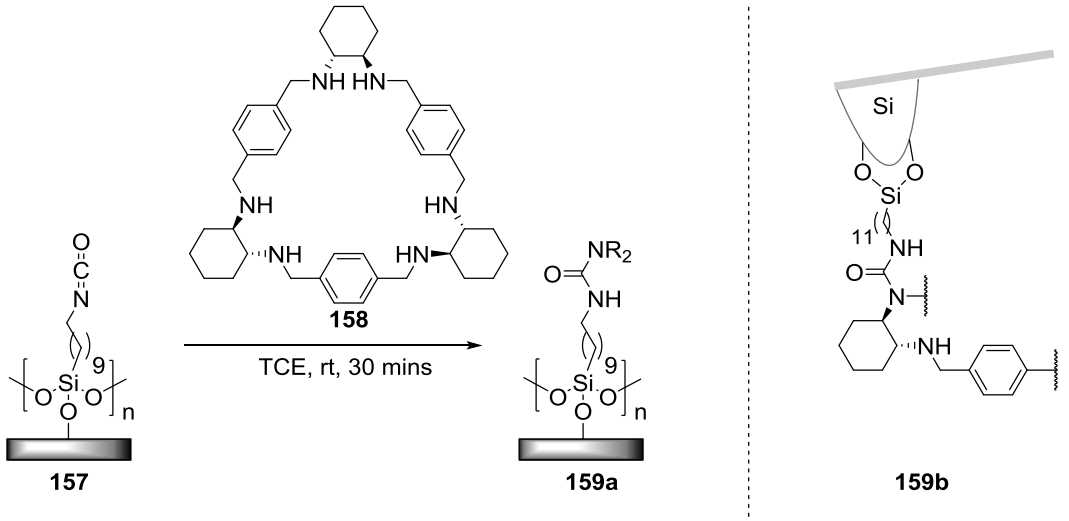

Figure 86: Direct attachment of trianglamine 158 to the surface *via* an isocyanate functionality.

Kimura *et al*. have shown that chiral discrimination can also be achieved using an AFM tip bearing optically active crown ethers and a Au surface coated with cysteine derivatives.[200] The authors deposited a perchlorate cysteine derivative of known enantiomeric purity on the Au surface. The adhesions forces were measured for the surface vs the probe tip and the results show that the chiral recognition ability of the crown ether modified tip, (*R*,*R*,*R*,*R*)-**161**, was opposite to that of its enantiomer (*S*,*S*,*S*,*S*)-**161** on the tip (Table 8).

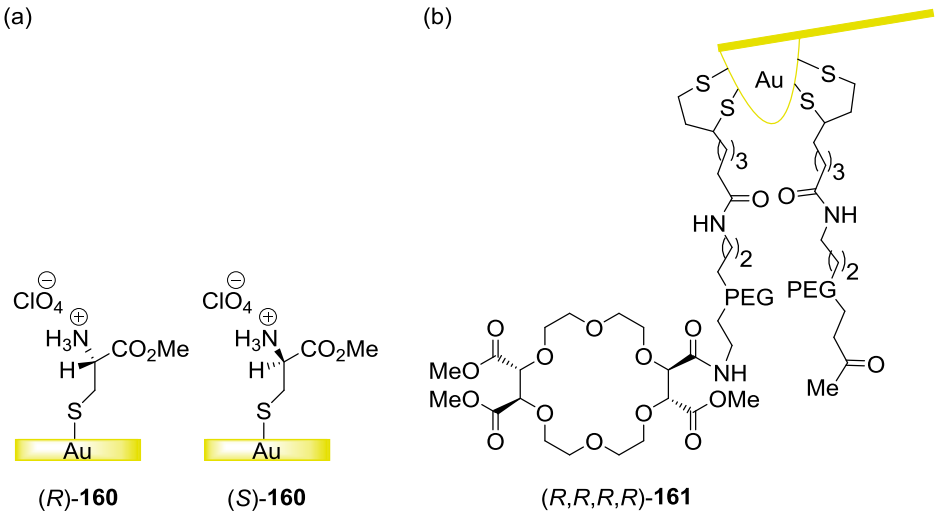

(*R*)-**160** (*S*)-**160** (*R*,*R*,*R*,*R*)-**161**

Entry	Tip enantiomer	Surface	Adhesion (nN)
1	(*R*,*R*,*R*,*R*)-**161**	(*R*)-**160**	0.22 ±0.08
2	(*R*,*R*,*R*,*R*)-**161**	(*S*)-**160**	0.26 ±0.08
3	(*S*,*S*,*S*,*S*)-**161**	(*R*)-**160**	0.25 ±0.08
4	(*S*,*S*,*S*,*S*)-**161**	(*S*)-**160**	0.21 ±0.08

Table 8: Summary of the adhesion forces obtained when testing both enantiomers of crown ether functionalised AFM tip against both enantiomers of cysteine derivatives (*R*)-160 and (*S*)-160 on the surface.

3.2.4 Enantiospecific wetting

Ducker and co-workers recently introduced a new technique known as enantiospecific wetting where either enantiomer of a chiral liquid can be placed onto a chiral surface and the resulting contact angles are measured.[201] In one experiment the authors placed a drop of (*S*)-leucinol **162** onto a silicon surface functionalised with (*R*)-leucinol **162** and measured the resulting contact angle. The results showed a clear difference in contact angle (Table 9) suggesting chiral discrimination. The same was also shown for the opposite case where (*S*)-leucinol **162** was deposited on a surface and both enantiomers of leucinol were tested. The measurements were also carried out in hexadecane as this provided a clearer visual result with respect to the contact angles and also indicated that contact angles are dependent on environment.

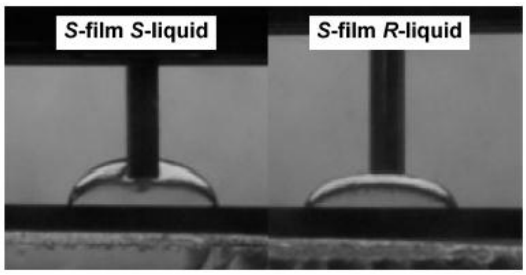

Entry	Film	Liquid	Contact Angle (°)
1	(*R*)-**162**	(*S*)-**162**	74 ±1
2	(*R*)-**162**	(*R*)-**162**	82 ±2
3	(*S*)-**162**	(*S*)-**162**	86 ±1
4	(*S*)-**162**	(*R*)-**162**	75 ±1

Table 9: Contact angles of leucinol droplets on a leucinol modified surface measured in a hexadecane medium. Taken from reference 201.

Shundo and Tanaka have shown enantioselective wetting of a chiral polymer on quartz and silicon surfaces that involves conformational reorganisation at the surface and a subsequent change in the contact angle.[202] The (*R*)-and (*S*)-enantiomers of polymer **163** (Figure 87(a)) were deposited on a surface and the contact angles probed using (*R*)-and (*S*)-1,2-propanediol **164** (Figure 87(b)). The results showed that a contact angle of 63 ° was obtained for (*S*)-**164** being placed on an (*S*)-**163** film, whilst a contact angle of 41 ° was obtained when (*R*)-**164** was placed on the same film. Importantly this trend was also observed for the opposite case where (*R*)-and (*S*)-**164** were placed on an (*R*)-**163** film. The authors attribute this inherent difference in contact angle to the reorganisation of the chiral polymer when it comes into contact with the chiral liquid ((*R*)-or (*S*)-**164**) which is induced by the hydrogen bonding between the carbonyl in the polymer and the hydroxyl group in the chiral liquid.

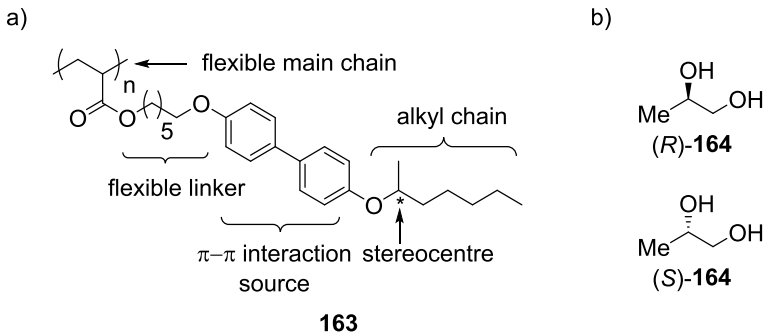

Figure 87: (a) Chiral polymer deposited on the surface, (b) chiral aliphatic diols used to probe the chiral surfaces.

3.3 Synthesis of dihydropyranones using HyperBTM 61 on a surface

3.3.1 Re-optimisation of bromine terminated SAM deposition

As the deposition of 11-bromoundecyltrichlorosilane **115** on the Si/SiO_2 did not give consistent results, a new approach was targeted using 11-bromoundecyltrimethoxysilane **165**. The advantage of using alkoxysilanes over chlorosilanes is the increased stability of the Si-O vs Si-Cl bond (799 vs 406 kJ mol^{-1})[203] during monolayer preparation, although because of this inherent stability they do not form SAMs as readily as halosilanes.[204-205]Following a procedure from Braun,[206] 11-bromoundecyltrimethoxysilane **165** was used, along with NEt_3 as an additive, for the formation of a bromine-terminated SAM (Table 10).

During the optimisation process several solvents were tested in the formation of a bromine terminated SAM. As NEt_3 is known to aid the self-assembly process it was used as an additive in some cases.[206] Although several entries show a reasonable contact angle (*ca*. 83°), ellipsometry gave a low (entries 1,2 and 4) or unreliable value (entries 6 and 7). When using bicyclohexyl or hexadecane as the deposition solvent (Entries 3 and 5) the ellipsometry value was close to the optimum reported in the literature (*ca*.1.9 nm) but unfortunately these were isolated results and disappointingly could not be reproduced. As toluene gave the most consistent results, with respect to ellipsometry and contact angle, over the largest sample range (Entry 1), this was taken forward as the optimum conditions for deposition for all of the samples discussed in the following sections. A potential reason for the low thickness value could be due to the lack of complete monolayer formation in the self-assembly process. Alkoxysilanes are not as reactive as the corresponding chlorosilanes and as such may not allow for the complete hydrolysis of the Si-OMe groups.[207-208]

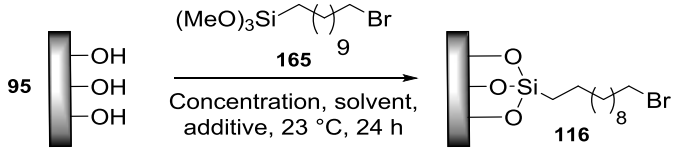

Entry	Deposition solvent	Concentration (mM)	Additive (mmol)	Contact Angle (°)	Elipsometry (nm)
1	Toluene	10	NEt_3 (15)	83.7	0.85
2	Toluene	10	-	81.5	0.61
3	Bicyclohexane	10	NEt_3 (15)	82.2	1.37
4	Hexadecane	1	-	81.3	0.80
5	Hexadecane	5	-	83.7	1.30
6	Hexadecane	10	-	84.5	n/a[b]

7	Hexadecane	10	NEt_3 (15)	84.0	n/a[b]

Table 10: Optimisation of deposition of 11-bromoundecyltrimethoxysilane in solution.[a]If the contact angle was not deemed sufficient, no ellipsometry measurement was obtained.[b]Ellipsometry data could not be fitted reasonably.

All subsequent reactions to afford the CF_3 trifluoromethylenone surface **128** remained unchanged from the original procedure as they gave reproducible results. These surfaces displayed similar characteristics to that of surfaces derived from 11-bromoundecyltrichlorosilane **115**. AFM showed a clean surfaces devoid of any external contaminants for all cases considered which suggested a smooth homogeneous SAM. Ellipsometry gave an increase in thickness from 0.9-1.7 nm for the reaction of **112** with **127**. The resulting contact angle for **128** was 76 °±1.2. Furthermore, XPS showed the expected elemental composition for surface **128** (C, N, O, Si and F) as well as routine conversions of 85% for the click reaction (Figure 88).

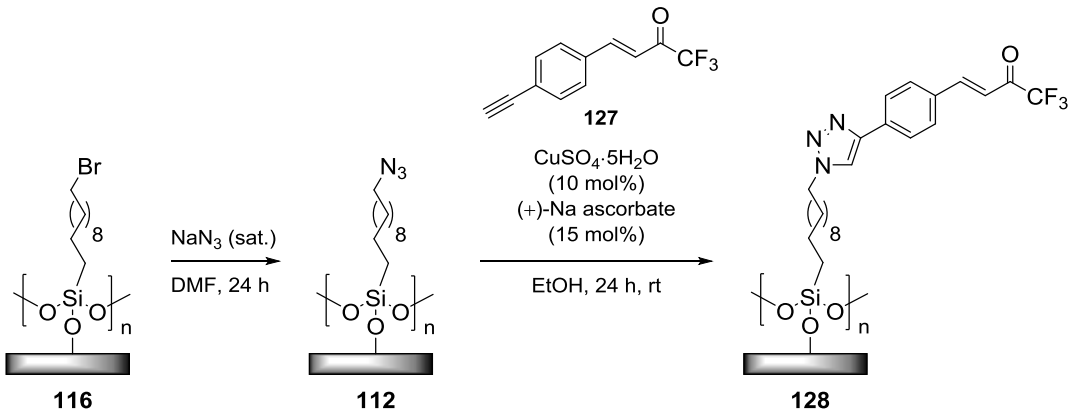

Figure 88: Generation of CF_3 Michael acceptor from bromine terminated SAM.

Having demonstrated the capability of achiral isothiourea to successfully promote the catalytic Michael addition-lactonisation of trifluoromethylenones with arylacetic acids, attention was focused on the synthesis of enantioenriched *C*(6)-trifluoromethyldihydropyranones. In an attempt to generate enriched (3*R*,4*R*) and (3*S*,4*S*) surfaces, a simple modification of the protocol developed in chapter 2, using either enantiomer of the chiral isothiourea catalyst HyperBTM **61**, was applied (Figure 89). The resulting characteristics of the surfaces were similar to that of the surfaces obtained from reaction with DHPB **60**. AFM showed a smooth surface in most of the surfaces examined, giving an RMS roughness of 0.14 nm which is in line with previous results. XPS showed the expected elemental composition (Si, O, N, C and F) with an increase in fluorine content as expected upon successful Michael addition-lactonisation, while the value obtained from ellipsometry was lower, 2.0 nm, given the lower value from the initial bromine-terminated SAM while the contact angle dropped slightly to 73° ±1.5.

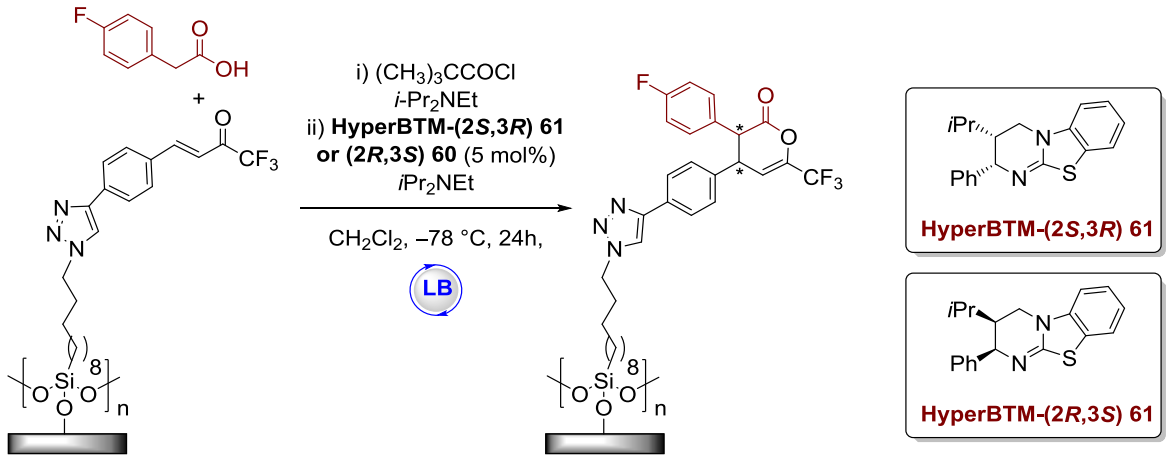

Figure 89: Synthesis of enantioenriched DHPs on the surface using a Michael addition-lactonisation procedure.

3.4 Synthesis of chiral precursor for AFM probe

In donor-acceptor type chiral stationary phases in HPLC, π-π stacking interactions between electron poor and electron rich aromatic groups play a significant part in discriminating chiral compounds, in addition to hydrogen bonding, and steric interactions.[209] It was envisaged that a chiral probe could be devised based on the stationary phase of a Chiracel™ OD-H column (Figure 90) and used to probe a surface comprised of enantioenriched DHPs. As these type of CSPs, based on Pirkle's resin,[210] are known to possess capabilities for enantiomeric separation within the realm of chiral HPLC, we hoped this property would translate across to our system and manifest as a strong adhesion force when attached to an AFM probe tip and tested against a surface comprised of DHPs synthesised using the chiral isothiourea catalyst **61**.

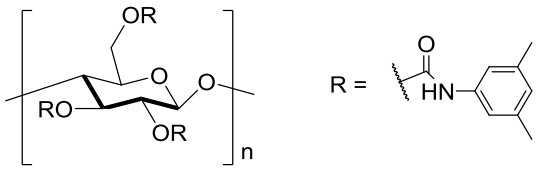

Figure 90: Cellulose tris(3,5-dimethylphenylcarbamate) coated on silica gel used as a stationary phase in a Chiracel™ OD-H HPLC column.

As thiols are known to form well-ordered monolayers on Au surfaces (discussed detail in Section 1.3), initial attempts focused on synthesising a thiol based chiral phenylglycine precursor **166** for use as an AFM probe, based on the CSP reported by Pirkle.[210] Conceptually this chiral precursor could be accessed *via* a series of amino acid coupling reactions starting with commercially available (*S*)-phenylglycine **169** and amine **168** which could potentially be accessed from a variety of routes (Figure 91).

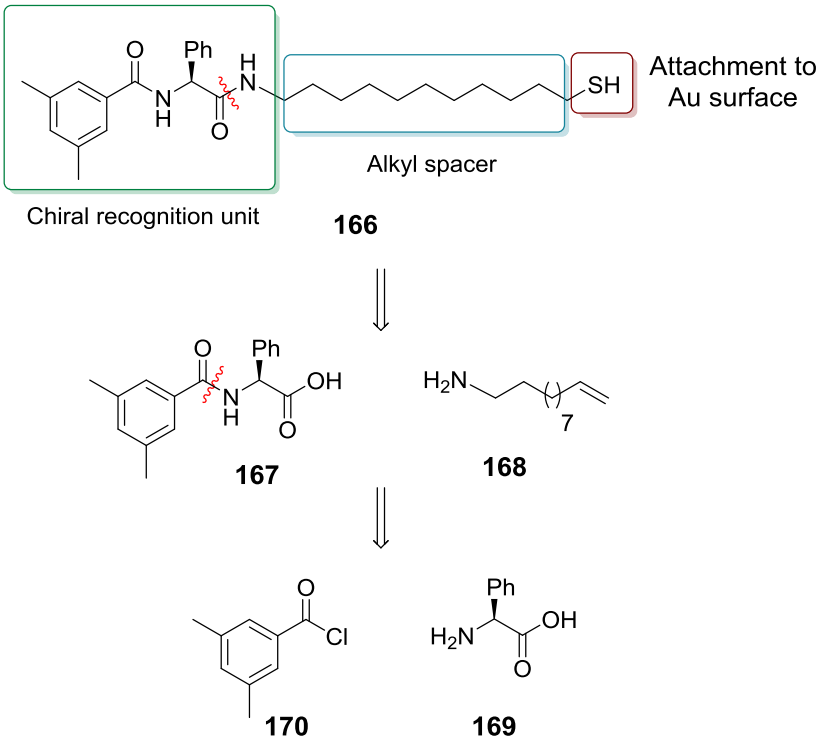

Figure 91: Retrosynthetic analysis of chiral AFM tip precursor 166.

Commercially available 3,5-dimethyl benzoic acid **171** was reacted with thionyl chloride at reflux which afforded the corresponding acid chloride **170** in 85% yield. Commercially available (*S*)-phenylglycine **169** was then reacted with acid chloride **170** in the presence of NaOH to give (*S*)-**172** in a good 82% yield (Figure 92).

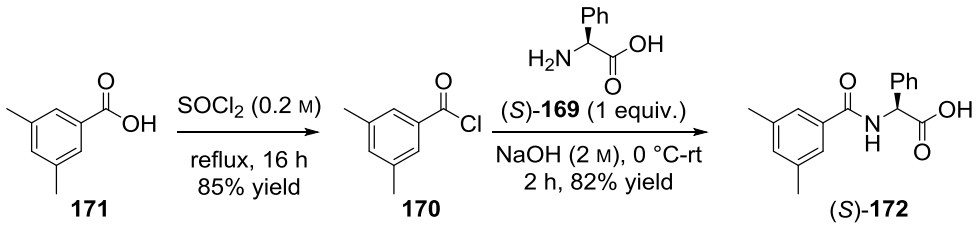

Figure 92: Synthesis of phenylglycine derivative 172.

Next, the coupling partner was synthesised in two steps using a Gabriel amine synthesis[211] starting from 11-bromoundecene **174** and potassium phthalimide **173**. Alkyl phthalimide **175** was obtained in a 75% yield and then subsequently reduced to the corresponding amine using hydrazine monohydrate in refluxing EtOH in 75% yield (Figure 93).

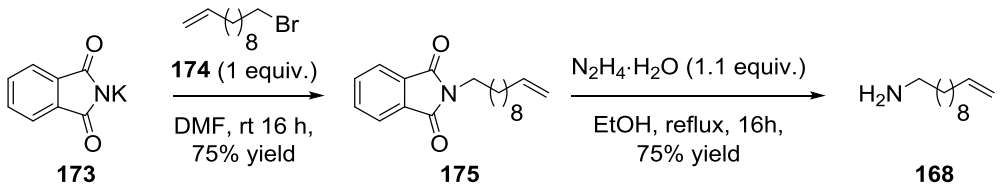

Figure 93: Gabriel amine synthesis of alkyl amine 168.

Following the synthesis of both coupling partners, carboxylic acid **172** and amine **168** were subjected to *N*-ethyl-*N*′-(3-dimethylaminopropyl)carbodiimide hydrochloride (EDCI) and 1-hydroxybenzotriazole hydrate (HOBt) to afford amide **176** in 66% yield. With amide **176** in hand, the thiol group needed to anchor the molecule to the Au surface was ready to be installed. Treatment with thioacetic acid in the presence of catalytic benzoyl peroxide and irradiation under UV light afforded the desired thioacetate **177** in a low 10% yield but afforded enough material to proceed with the synthetic route (Figure 94).

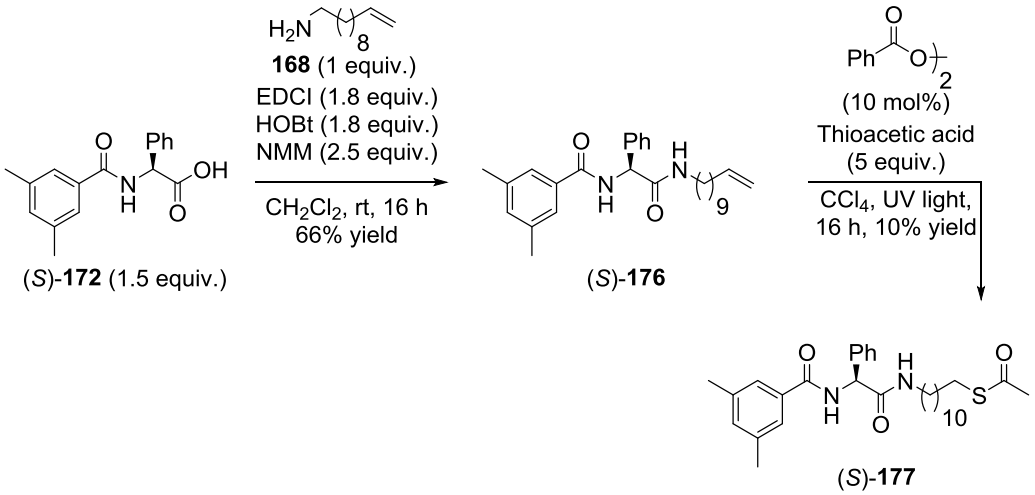

Figure 94: Synthesis of thioacetate 177.

Deprotection of thioacetate (*S*)-**177** was attempted using a variety of nucleophiles to cleave the acetate group in several different solvent systems, but disappointingly the thiol could not be obtained, and in most cases only starting material was recovered. Reaction of (*S*)-**177** with the nucleophilic acylation catalyst DMAP in MeOH gave only 60% recovered starting material after work up with no trace of product (entry 1, Table 11). Next, treatment with hydride reducing agents $LiBH_4$ (entry 2, Table 11) and $LiAlH_4$ (entry 3, Table 11) gave 28% recovered starting material and decomposition products respectively. Attempted deprotection with conc. HCl in MeOH at reflux gave back mostly starting material (entry 4, Table 11) while hydrolysis using LiOH (entry 5, Table 11) and NaOH (entry 6, Table 11) disappointingly gave no trace of desired product. Cleavage of thioacetate **177** was attempted using MeMgBr in THF but gave only decomposition products (entry 7, Table 11) and finally treatment with $N_2H_4 \cdot H_2O$ gave only starting material after work up (entry 8, Table 11).

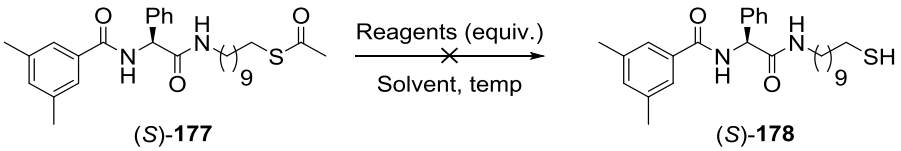

(*S*)-**177** (*S*)-**178**

Entry	Reagents (equiv.)	Reaction time (h)	Solvent	Temperature (° C)	Result
1	DMAP (0.5)	48	MeOH	rt	60% SM recovered
2	$LiBH_4$ (1.0)	1	MeOH:CH_2Cl_2	0-rt	28% SM recovered
3	$LiAlH_4$ (1.3)	3	THF	0-rt	Decomp
4	Conc. HCl (0.1)	16	MeOH	reflux	84% SM recovered
5	LiOH (6.5)	10	MeOH:THF	rt	95% SM recovered
6	NaOH (2 M)	16	MeOH	rt	73% SM recovered
7	MeMgBr (3.0)	16	THF	rt	Decomp
8	$N_2H_4 \cdot H_2O$ (1.0)	16	EtOH	reflux	91% SM recovered

Table 11: Reaction conditions tested for the deacylation of 177. SM = starting material. Decomp = decomposition.

As none of the reaction conditions produced the desired product, a modification of the initial strategy was envisaged where a reactive hydrazide moiety would be used, in combination with phenylglycine derivate **172**. This synthesis involved a change in polarity from the original strategy and also relied on leaving the thiol unprotected (Figure 95).

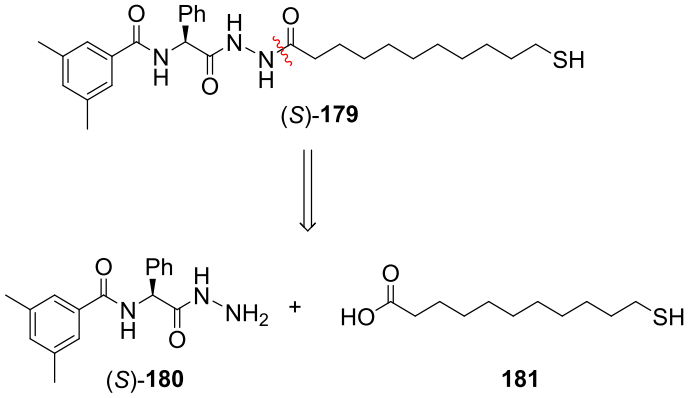

(*S*)-**179** (*S*)-**180** **181**

Figure 95: Retrosynthetic analysis of benzamide 179 utilising hydrazide 180 and acid 181.

Treatment of acid **172** with catalytic H_2SO_4 in the presence of MeOH afforded the corresponding methyl ester **182** in 79% yield. Reaction with hydrazine monohydrate in refluxing EtOH at reflux gave the desired hydrazine **180** in reasonable yield (Figure 96).

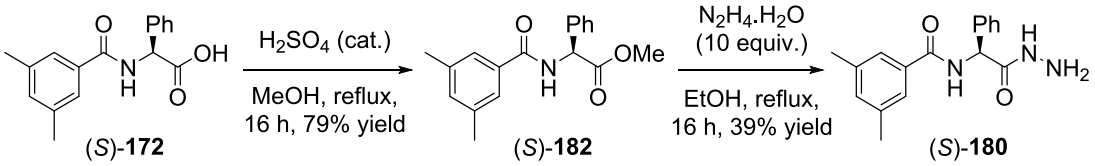

Figure 96: Synthesis of hydrazine 180 from phenylglycine derivative 182.

Commercially available 11-bromoundecanoic acid **183** was heated with thiourea at reflux in H_2O which afforded the corresponding thiol **181** in an excellent 90% yield (Figure 97). This gave both coupling partners in relatively good yields over all reaction steps.

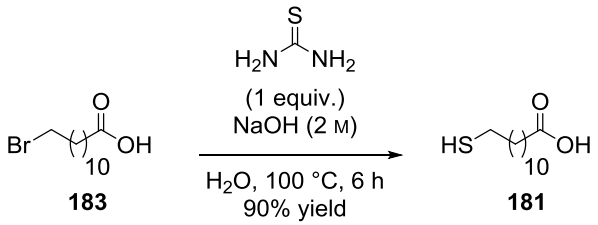

Figure 97: Synthesis of 11-mercaptoundecanoc acid 181 using thiourea.

Pleasingly, using conditions described previously for the coupling of **168** with **172**, pure amide **179** was synthesised after recrystallisation from EtOH (Figure 98). This synthetic protocol was reliable and was used for the synthesis of the (*R*)-**179** and (±)-**179**, starting from (*R*)-and (±)-phenylglycine.

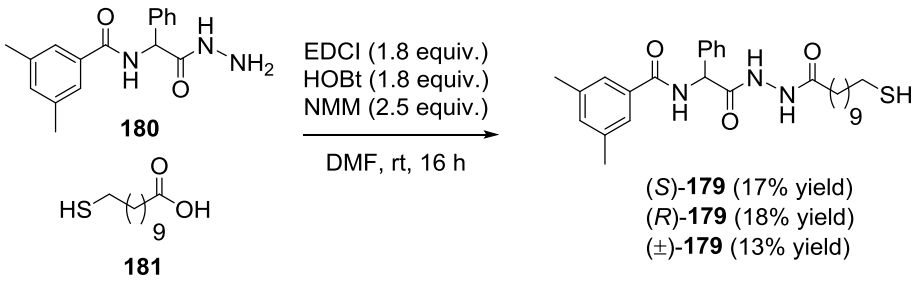

Figure 98: Synthesis of precursor 179 for AFM probe using an amide coupling reaction.

3.5 Synthesis of alkyne substituted DHPs

To assess the potential viability of the CFM methodology, both enantiomers of 4-fluoro DHP derivative **182** were synthesised in solution and attached to a surface. Reaction of 4-fluorophenylacetic acid **182** with enone **127** in the presence of (2*R*,3*S*)-HyperBTM **61** or

HyperBTM-(2*S*,3*R*)-**61** gave (3*S*,4*S*)-**183** and (3*R*,4*R*)-**183** enantiomers of DHP, in 87% and 90% ee respectively (Figure 99).

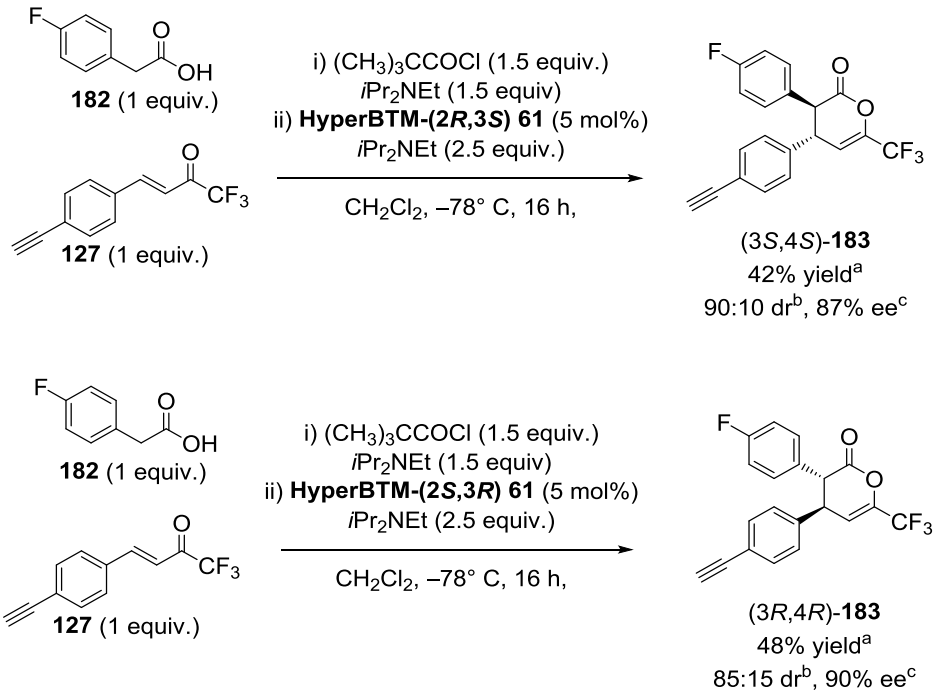

Figure 99: Synthesis of enantioenriched DHPs using both enantiomers of HyperBTM. [a]Isolated yield of major diastereoisomer of **183** (>95:5 dr). [b]Determined by ^{1}H NMR spectroscopy analysis of the crude reaction mixture. [c]Determined by chiral HPLC analysis.

With enantioenriched products (3*S*,4*S*)-**183** and (3*R*,4*R*)-**183** in hand, both were attached to separate azide terminated surfaces **112** using the standard conditions for click chemistry affording enantioeniched DHP terminated surfaces (3*S*,4*S*)-**184** and (3*R*,4*R*)-**184** (Figure 100).

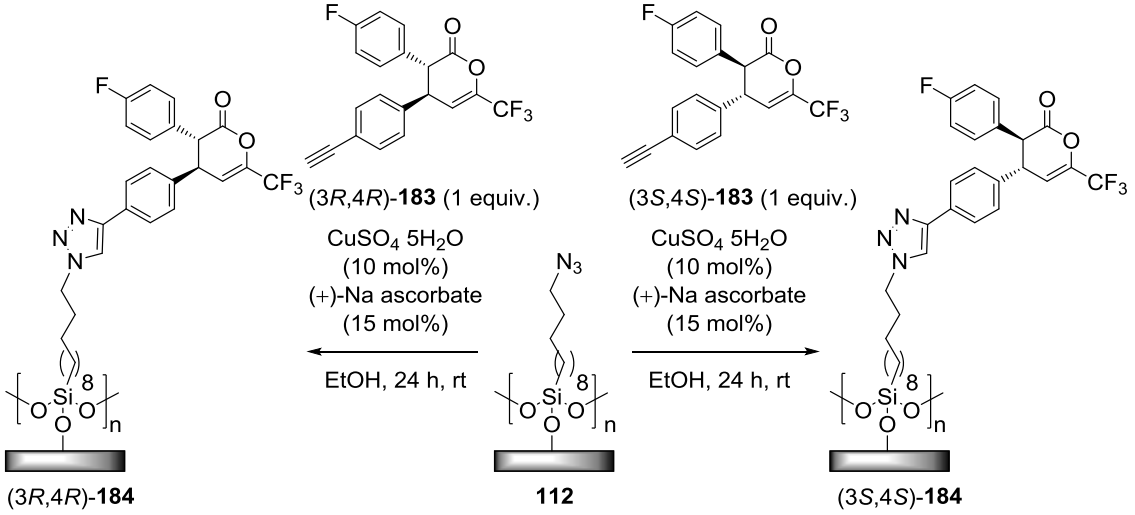

Figure 100: Attachment of enantioenriched DHP derivatives onto azide terminated surfaces using click methodology.

3.6 Model system for chiral force microscopy

To assess whether this methodology was suitable for analysis of our system, a model system consisting of Au surfaces and Au coated AFM probe tips functionalised with both L-and D-cysteine was devised and subjected to chiral force microscopy (Figure 101). In this model study D-cysteine and L-cysteine were deposited onto separate Au coated Si surfaces (Figure 101(a)) and also onto separate Au coated AFM probe tips (Figure 101(b)) and assessed using chiral force microscopy. Cysteines deposited onto Au surfaces gave static water contact angles of 33.8 ±1.1 ° (L-cysteine) and 29.2 ±1.7 ° (D-cysteine) which are within the range for SAMs of cysteine reported in the literature.[212-213]

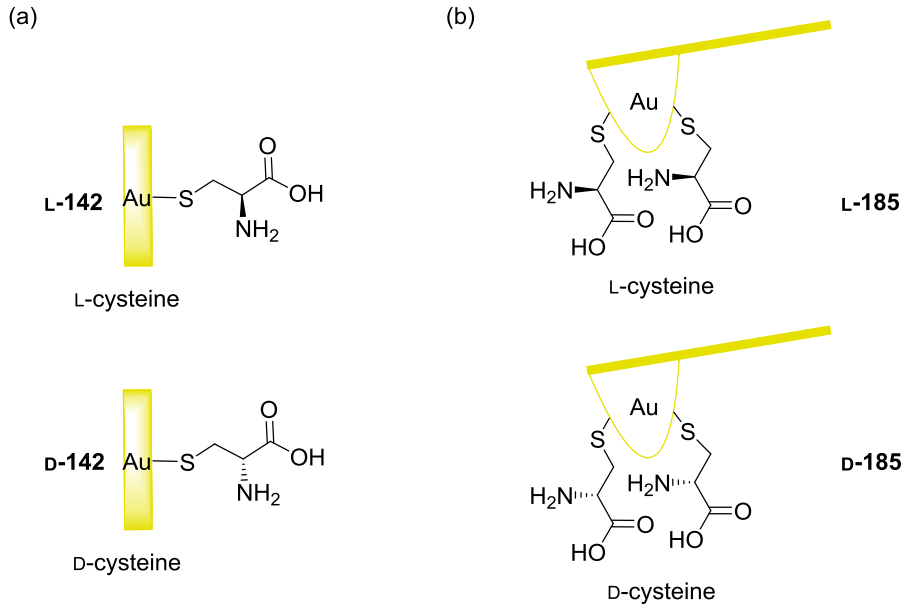

Figure 101 (a): Both enantiomers of cysteine deposited on an Au surface, (b) both enantiomers of cysteine deposited on an Au coated AFM tip.

The results of measurements between both combinations of surface and probe tip of the adhesion force are shown in Table 12.† The adhesion histogram shows the distribution of adhesion or pull-off forces (measured in nN) for an L-cysteine coated AFM tip L-**185** tested against both L-cysteine L-**142** and D-cysteine D-**142** deposited on Au-coated surfaces. The model system shows a clear difference in adhesion values arising from the different interactions of the L-cysteine tip L-**185** with both L-cysteine L-**142** (0.9 ±0.3 nN, Entry 2, Table 12) and D-cysteine D-**142** (2.4 ±1.0 nN, Entry 1, Table 12) terminated surfaces. A second set of measurements were taken between the L-cysteine tip L-**185** and D-cysteine surface D-**142** in order to eliminate the possibility of

† All AFM measurement and analysis performed by PDRA Dr John Parkin.

experimental error as AFM cantilevers are prone to blunting and can be easily damaged during operational conditions, which results in larger adhesion values as the tip-surface contact area is larger.[214-215] Although the adhesion value was slightly higher (1.3 nN vs 0.9 nN) suggesting some possible tip blunting, the value obtained (1.3 nN) was still significantly lower than that using the D-cysteine surface (2.4 nN) validating the chiral discrimination. The peaks for the adhesion histograms were fit using a normal distributionusing the 'hisfit' MATLAB function.†

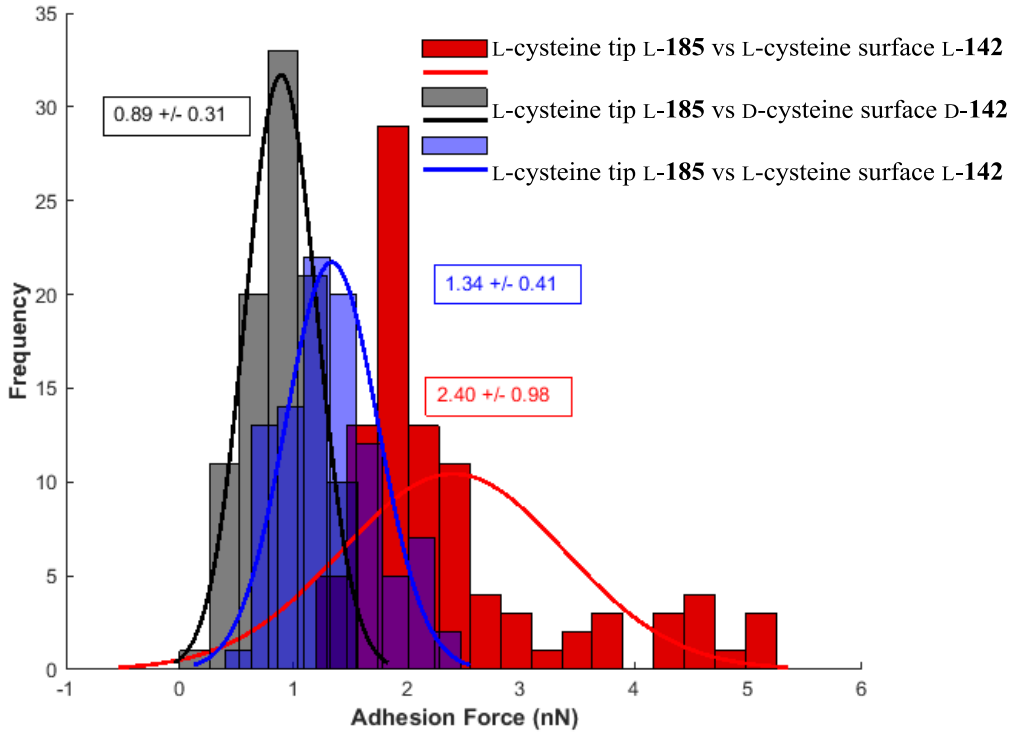

Figure 102: Adhesion histogram of L-cysteine coated AFM tip tested against separate samples of both L-and D-cysteine on Au. All measurement were taken using the same D-cysteine coated AFM tip. Measurements are snap out of contact. At least four areas tested per sample.

To further assess the reliability of the model system, an Au-coated AFM tip was functionalised with D-cysteine and tested against both L-cysteine L-**142** and D-cysteine D-**142** deposited on Au coated surfaces (Figure 103). Pleasingly, when D-cysteine tip D-**185** was tested against a D-cysteine surface D-**142** a reasonable discrimination value was obtained (0.8 ±0.6 nN, Entry 4, Table 12) which is similar to L-cysteine tip L-**185** vs L-cysteine surface L-**142** (0.9 ±0.3 nN). When D-cysteine tip D-**185** was tested against an L-cysteine surface L-**142** a value of 2.0 ±0.7 nN (Entry 5, Table 12) was obtained which is lower, but similar to, that of L-cysteine tip L-**185** vs D-cysteine D-**142** surface (2.4 ±1.0 nN). Both results show a similar trend indicating similar chiral discrimination in each case with opposite enantiomers giving the largest interaction. These results

show that chemical force microscopy is sufficiently sensitive to allow for discrimination between enantiomers of simple chiral molecules.

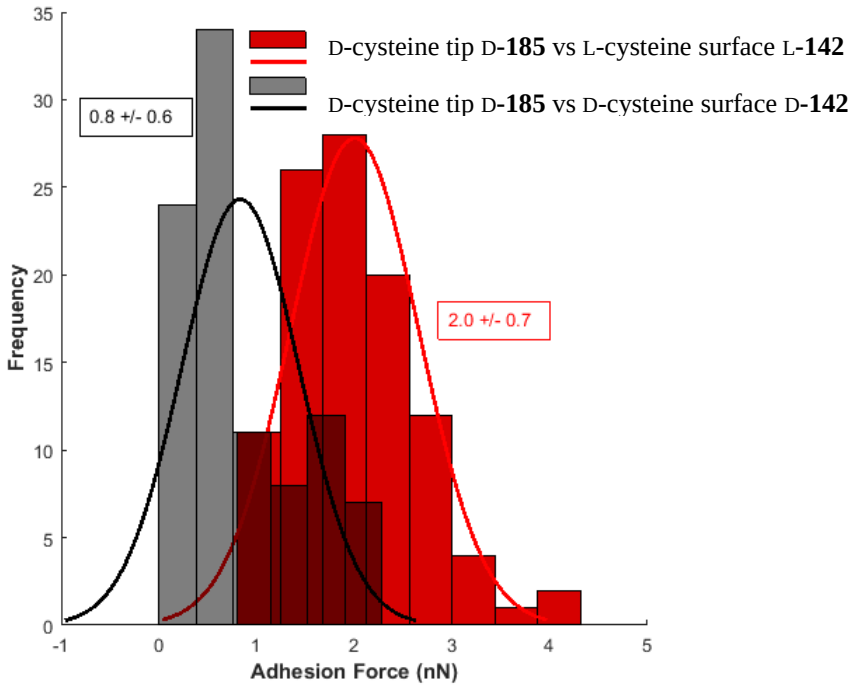

Figure 103: Adhesion histogram of D-cysteine coated AFM tip tested against separate samples of both L-and D-cysteine on Au. All measurement were taken using the same D-cysteine coated AFM tip. Measurements are snap out of contact. At least four areas tested per sample.

Entry	Probe tip	Surface	Mean (nN)[a]	Std. dev. (nN)
1	L-cysteine L-**185**	D-cysteine D-**142**	2.4	1.0
2	L-cysteine L-**185**	L-cysteine L-**142**	0.9	0.3
3	L-cysteine L-**185**	L-cysteine L-**142** (2)	1.3	0.4
4	D-cysteine D-**185**	D-cysteine D-**142**	0.8	0.6
5	D-cysteine D-**185**	L-cysteine L-**142**	2.0	0.7

Table 12: Summary of adhesions forces from L-cysteine derived AFM tips tested against L-and D-cysteine surfaces.

3.7 Cysteine coated AFM tips vs 'clicked' enantioenriched DHPs

With a reliable model system and both enantiomers of DHP **183** in hand, attention was focused on the chiral discrimination of enatioenriched surfaces (3*S*,4*S*)-**184** and (3*R*,4*R*)-**184** using the developed CFM methodology with L/D-cysteine as probe tips. When L-cysteine functionalised tip L-**185** was tested against a (3*S*,4*S*)-**184** surface (87% ee) an adhesion value of 1.9 ±0.1 nN (entry 2, Table 13) was obtained. When L-cysteine functionalised tip L-**185** was tested against a (3*R*,4*R*)-**184** surface (90% ee) an adhesion value of 1.5 ±0.1 nN (entry 1, Table 13) was obtained.

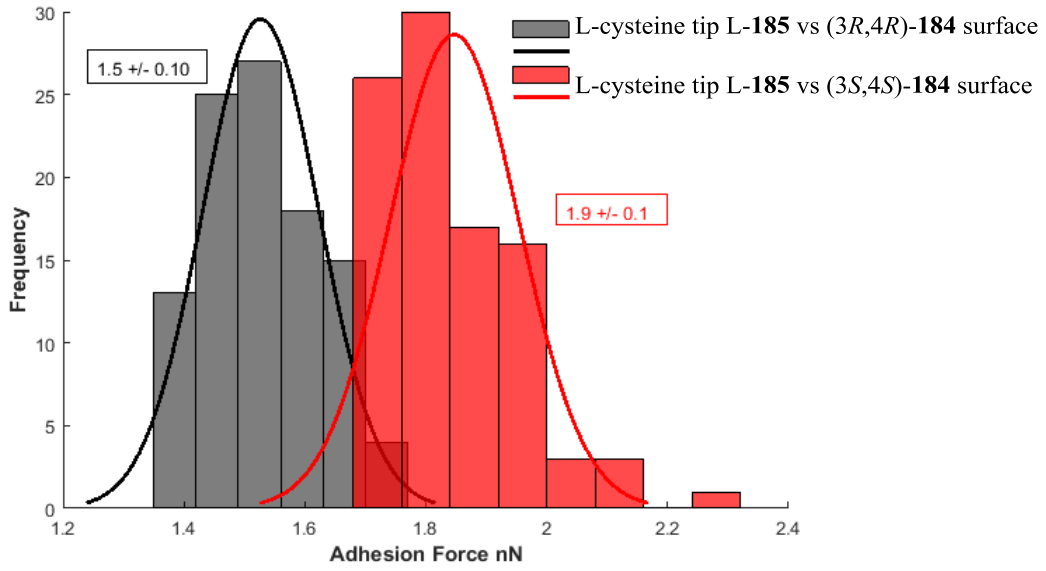

Figure 104: Adhesion histogram of L-cysteine coated AFM tips tested against separate samples of both (3*R*,4*R*)-184 and (3*S*,4*S*)-184 clicked DHP surfaces respectively. All measurement were taken using the same L-cysteine coated AFM tip. Measurements are snap out of contact.

When a D-cysteine functionalised tip D-**185** was tested against a surface comprised of (3*S*,4*S*)-**184** DHPs (90% ee) an adhesion value of 1.3 ±0.2 nN (entry 3, Table 13) was obtained. Finally, a D-cysteine functionalised tip D-**185** was tested against a surface comprised of (3*R*,4*R*)-**184** DHPs (87% ee) an adhesion value of 1.9 ±0.2 nN (entry 4, Table 13) was obtained. From the measurements obtained (Figure 104 and Figure 105) it can be said that there is a clear chiral discrimination event occurring on the surfaces in question. It is a clear that when the enantiomer of the AFM probe tip is changed, the magnitude of values is reversed, indicating that a chiral discrimination event is occurring specific to the enantiomeric/diasteromeric pairing.

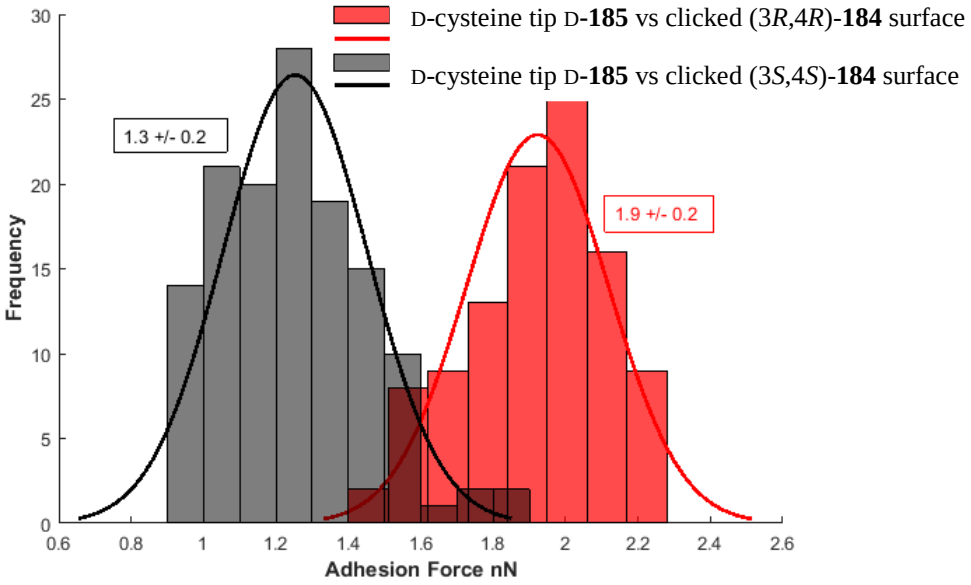

Figure 105: Adhesion histogram of D-cysteine coated AFM tips tested against separate samples of both (3*R*,4*R*)-184 and (3*S*,4*S*)-184 clicked DHP surfaces respectively. All measurement were taken using the same L-cysteine coated AFM tip. Measurements are snap out of contact.

3.8 Chiral benzamide tips vs 'clicked' enantioenriched DHPs

As shown in Section 3.4, two enantiomerically pure thiol based benzamides, and a racemic version, were synthesised to evaluate their capacity as chiral probes in chemical force microscopy. The (*R*)-and (*S*)-enantiomers, as well as the racemic functionalised tips were tested against enantioenriched surfaces (3*R*,4*R*)-**184** and (3*S*,4*S*)-**184** (Figure 106).

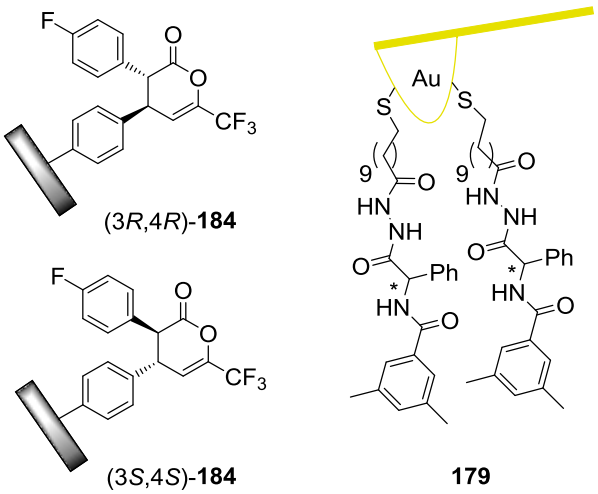

Figure 106: (*R*)/(*S*)-179 modified AFM tips evaluated against DHPs terminated surfaces prepared from enantiomerically enriched starting materials.

When (*S*)-benzamide tip **179** was tested against a surface comprised of (3*S*,4*S*)-**184** DHPs (90% ee) an adhesion value of 5.7 ±1.0 nN (entry 6, Table 13) was obtained. When (*S*)-benzamide tip

179 was tested against a surface comprised of (3*R*,4*R*)-**184** DHPs (87% ee) an adhesion value of 3.5 ±0.3 nN (entry 5, Table 13) was obtained which shows a clear difference in adhesion values for this system

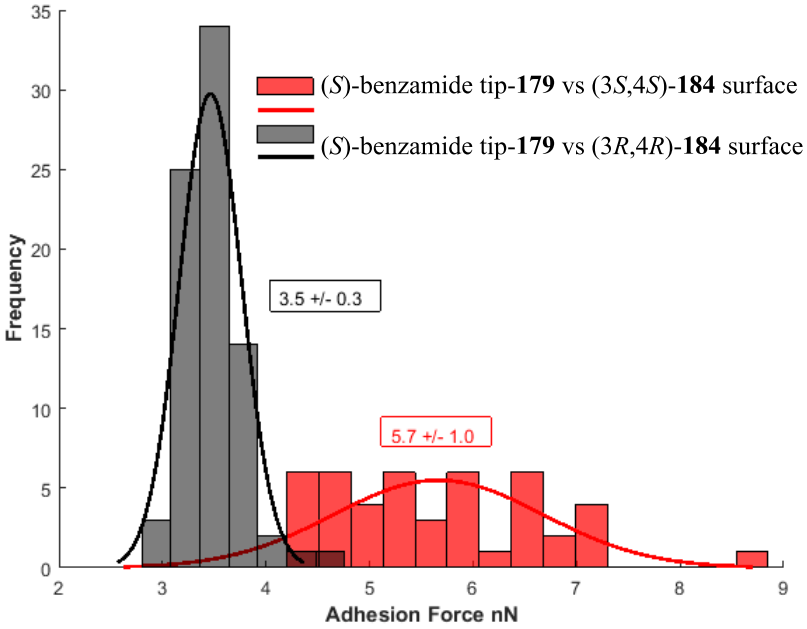

Figure 107: Adhesion histogram of (*S*)-benzamide coated AFM tips tested against separate samples of both (3*R*,4*R*)-184 and (3*S*,4*S*)-184 clicked DHP surfaces respectively. All measurement were taken using the same L-cysteine coated AFM tip. Measurements are snap out of contact.

When (*R*)-benzamide tip **179** was tested against a surface comprised of (3*S*,4*S*)-**184** DHPs (90% ee) an adhesion value of 4.6 ±0.4 nN (entry 7, Table 13) was obtained. When (*S*)-benzamide tip **179** was tested against a surface comprised of (3*R*,4*R*)-**184** DHPs (87% ee) an adhesion value of 7.0 ±0.8 nN (entry 8, Table 13). This result agrees with the trend observed in the previous system, that is when the enantiomer of the AFM probe tip is changed, the magnitude of values is reversed, indicating a diasterospecific event occurring.

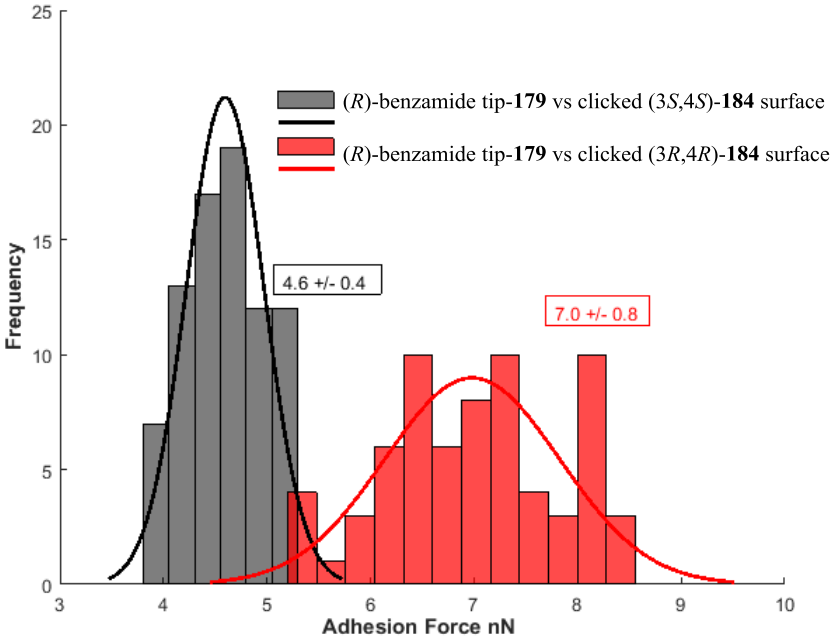

Figure 108: Adhesion histogram of (*R*)-benzamide coated AFM tips tested against separate samples of both (3*R*,4*R*)-184 and (3*S*,4*S*)-184 clicked DHP surfaces respectively. All measurement were taken using the same L-cysteine coated AFM tip. Measurements are snap out of contact

Entry	Probe tip	Surface	Mean ± Std. dev. (nN)
1	L-cysteine L-**185**	(3*R*,4*R*)-**184**	1.5 ± 0.1
2	L-cysteine L-**185**	(3*S*,4*S*)-**184**	1.9 ± 0.1
3	D-cysteine D-**185**	(3*S*,4*S*)-**184**	1.3 ± 0.2
4	D-cysteine D-**185**	(3*R*,4*R*)-**184**	1.9 ± 0.2
5	(*S*)-benzamide **179**	(3*R*,4*R*)-**184**	3.5 ± 0.3
6	(*S*)-benzamide **179**	(3*S*,4*S*)-**184**	5.7 ± 1.0
7	(*R*)-benzamide **179**	(3*S*,4*S*)-**184**	4.6 ± 0.4
8	(*R*)-benzamide **179**	(3*R*,4*R*)-**184**	7.0 ± 0.8

Table 13: Summary of adhesions forces from L-and D-cysteine and (*S*)/(*R*)-benzamide derived AFM tips tested against (3*R*,4*R*)-184 and (3*S*,4*S*)-184 surfaces.

3.9 Cysteine coated AFM tips vs DHPs prepared using HyperBTM 61

Having demonstrated a proof of principle with respect to the cysteine model study and pre-synthesised enantioenriched DHPs attached to the surface, attention was then focused on chiral discrimination of DHP surfaces functionalised using enantioselective catalysis. For a direct comparison with the model system, L-cysteine was deposited onto an AFM tip and evaluated in CFM against two modified SAM surfaces prepared using the previously described Michael addition-lactonisation methodology using either enantiomer of isothiourea HyperBTM **61** as the catalyst (Figure 109).

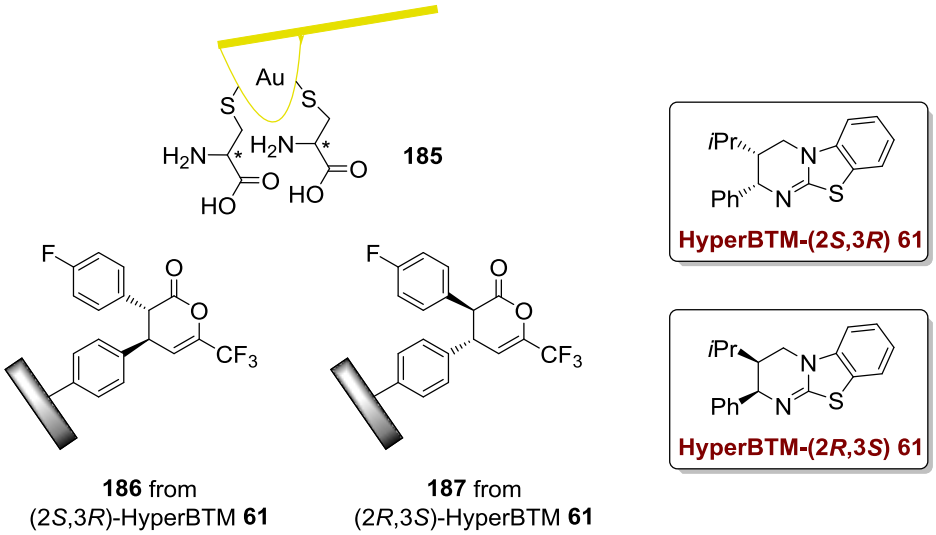

Figure 109: L-and D-cysteine modified AFM tip evaluated against DHPs generated from the Michael addition-lactonisation procedure using both enantiomers of HyperBTM 61.

Initial results showed some discrimination between the L-cysteine tip L-**185** and the **186** and **187** surfaces (Figure 110). Adhesion values obtained for the L-cysteine tip L-**185** tested against the **186** surface gave a value of 2.8 ±0.7 nN (Entry 1, Table 14) while adhesion values obtained for the L-cysteine tip L-**185** tested against **187** surface gave a value of 3.8 ±0.8 nN (Entry 2, Table 14). This shows a reasonable difference in adhesion values for this specific case but also noteworthy was the presence of significant overlap in adhesion values. This may suggest possible tip blunting during AFM measurements or homogeneity of the SAMs may be an issue.

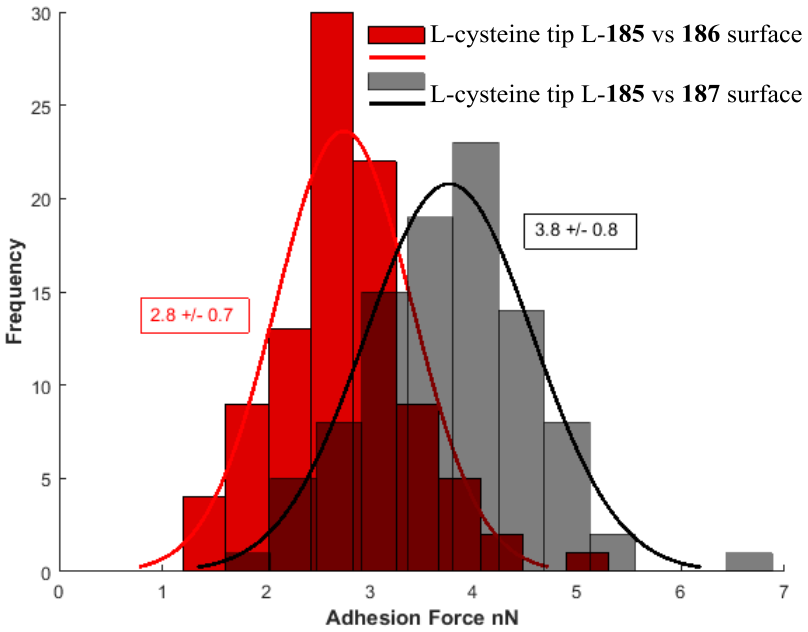

Figure 110: Adhesion histogram of L-cysteine coated AFM tips tested against separate samples of both 186 and 187 surfaces respectively. All measurement were taken using the same L-cysteine coated AFM tip. Measurements are snap out of contact. At least four areas tested per sample.

When D-cysteine functionaised AFM tip D-**185** was tested against both **186** and **187** surfaces a small difference in adhesion force was detected (Figure 111). Adhesion values obtained for the D-cysteine tip D-**185** tested against surface **186** gave an adhesion value of 2.3 ±0.3 nN (Entry 4, Table 14) while adhesion values obtained for the D-cysteine tip D-**185** tested against surface **187** gave a value of 1.8 ±0.3 nN (Entry 3, Table 14). These results show an overall decrease in adhesion values for this system when compared to the L-**185** tested against the same surfaces (Figure 110). Moreover the adhesion values obtained for the D-cysteine tip D-**185** seem to be the 'opposite' to that of the L-cysteine tip L-**185**. The D-cysteine tip D-**185** has a higher affinity for the **186** surface whereas the L-cysteine tip L-**185** has a higher affinity for the **187** surface.

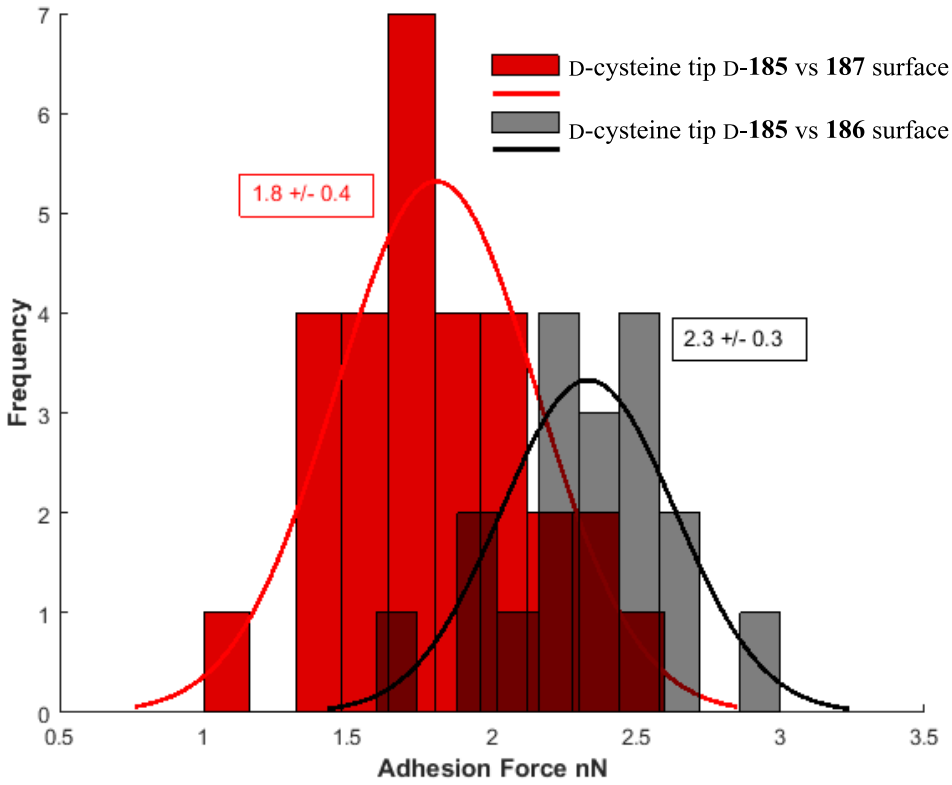

Figure 111; Adhesion histogram of D-cysteine coated AFM tips tested against separate samples of both 186 and 187 surfaces respectively. All measurement were taken using the same D-cysteine coated AFM tip. Measurements are snap out of contact.

Entry	Probe tip	Surface	Mean (nN)	Std. dev. (nN)
1	L-cysteine L-**185**	**186**	2.8	0.7
2	L-cysteine L-**185**	**187**	3.8	0.8
3	D-cysteine D-**185**	**187**	1.8	0.4
4	D-cysteine D-**185**	**186**	2.3	0.3

Table 14: Summary of adhesions forces from L-cysteine derived AFM tips tested against surfaces 186 and 187.

3.10 Chiral benzamide tip vs DHPs prepared using HyperBTM 61

CFM measurements showed discrimination in all cases. The previously developed chiral AFM tip **179** was tested against surfaces **186**, **187** and **188** obtained from the *in situ* Michael addition-lactonisation procedure using HyperBTM **61** (Figure 112).

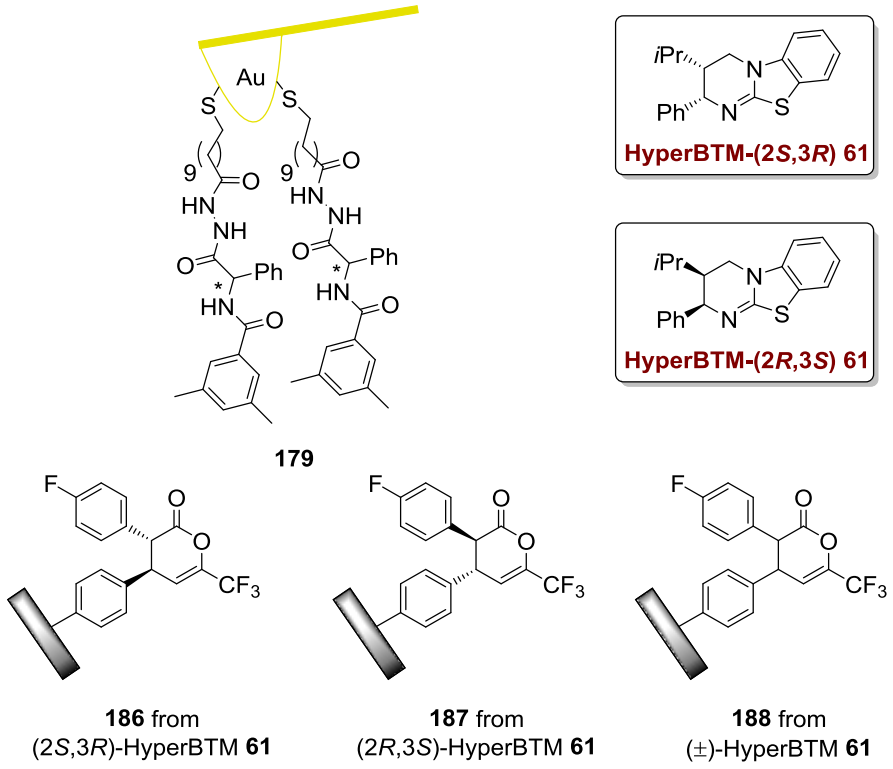

Figure 112: (*R*)/(*S*) and (±)-179 modified AFM tips evaluated against DHPs terminated surfaces prepared from a Michael addition-lactonisation procedure using both enantiomers and (±)-HyperBTM 61.

The (*S*)-benzamide tip **179** vs surface **186** gave an adhesion value of 4.7 ±2.1 nN (Entry 1 Table 15) while the same probe tip tested against a **187** surface gave an adhesion value 9.6 ±3.0 nN (Entry 2 Table 15). When (*S*)-benzamide **179** was tested against surface **188** an adhesion value of 11.3 ±4.5 nN was obtained (Entry 3 Table 15). In theory, when (*S*)-benzamide **179** is tested against surface **188** an adhesion value halfway between those obtained for **186** and **187** surfaces should be obtained. However this discrimination was not observed, which may suggested that the **188**

surface may have particular domains consisting of either enantiomer and not an equal mixture of both distributed on the surface as expected.[216-217]

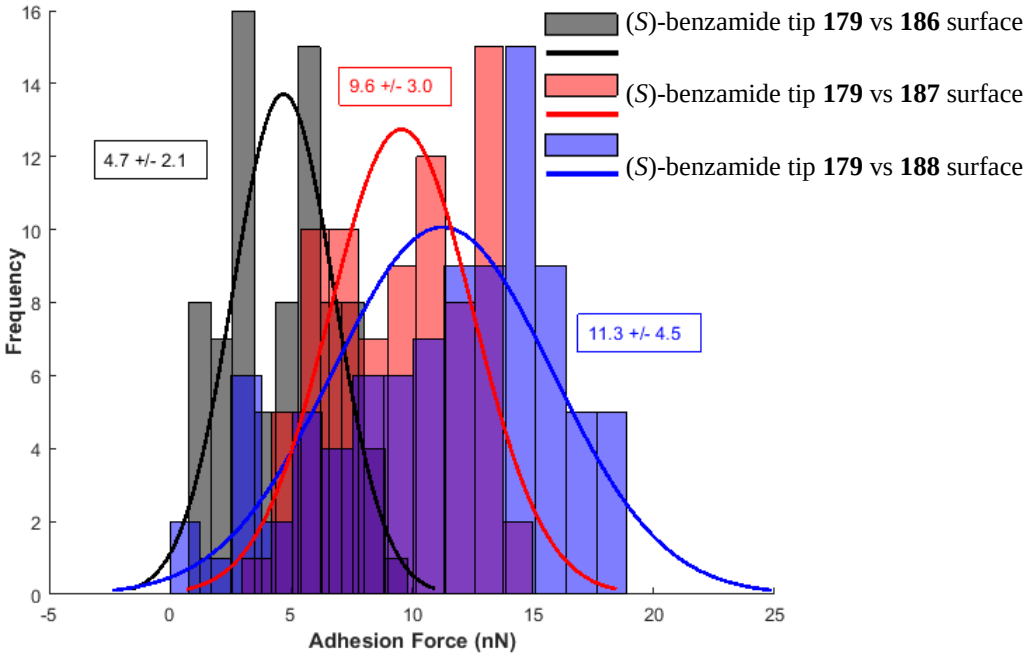

Figure 113: Adhesion histogram of (*S*)-benzamide coated AFM tip tested against separate samples of 186, 187 and 188 DHP terminated surfaces respectively. All measurement were taken using the same (*S*)-benzamide coated AFM tip. Adhesion force before snap out of contact. At least four areas tested per sample.

When (*R*)-benzamide **179** was tested against surfaces **186** and **187** a notably larger set of adhesion values were obtained than in the previous measurements (Table 14). The (*R*)-benzamide **179** vs **186** gave an adhesion value of 4.8 ± 4.2 nN (Entry 4 Table 15). The same probe tip tested against a **187** surface gave a mean adhesion value 28.5 ± 9.6 nN (Entry 5 Table 15) which greatly differs from that of the corresponding (*S*)-benzamide **179** tested against the same surface (Entry 2 Table 15). Finally, when the surface **188** was tested against (*R*)-benzamide **179**, a mean adhesion value of 28.9 ± 9.6 nN (Entry 6, Table 15) which is the same as that obtained for the **187** surface. The higher adhesion values may be a result of a greater interaction between tip and surface which may be expected given the magnitude of values observed when (*S*)-benzamide **179** was tested. These results suggest that chiral discrimination is not as clear with this combination of probe tip and surface and are not consistent with what has been observed in the previous measurements using L-and D-cysteine as probe tips. In previous measurements the magnitude of the interactions are reversed upon the use of a different enantiomer of AFM probe tip, suggesting different chiral interactions events are happening. It is not obviously clear why this is the case and due to time constraints, this particular set of measurements could not be repeated. A possible reason for the lack of chiral discrimination of these surfaces may be due to the homogeneity of the SAM.

Lattanzi and co-workers have shown using DFT calculations that the introduction of large bulky groups to the terminal end of a SAM ((6-(2-triptycenylcarboxy)hexylphosphonic acid in this case) can interfer with homogenenity and result in irregular and rough surfaces.[218] The preparation of these surfaces most likely play a crucial role in the overall quality and final distribution of molecules on the surface. Conversely, as the distribution and molecular packing on the (*R*)-**179** tip is unknown and cannot be verified it may potentially be that the AFM tip used added to anomalous results. Repeat experiments are needed in order to validate these measurements and as such these results may not be relied upon to draw any conclusions at the present time.

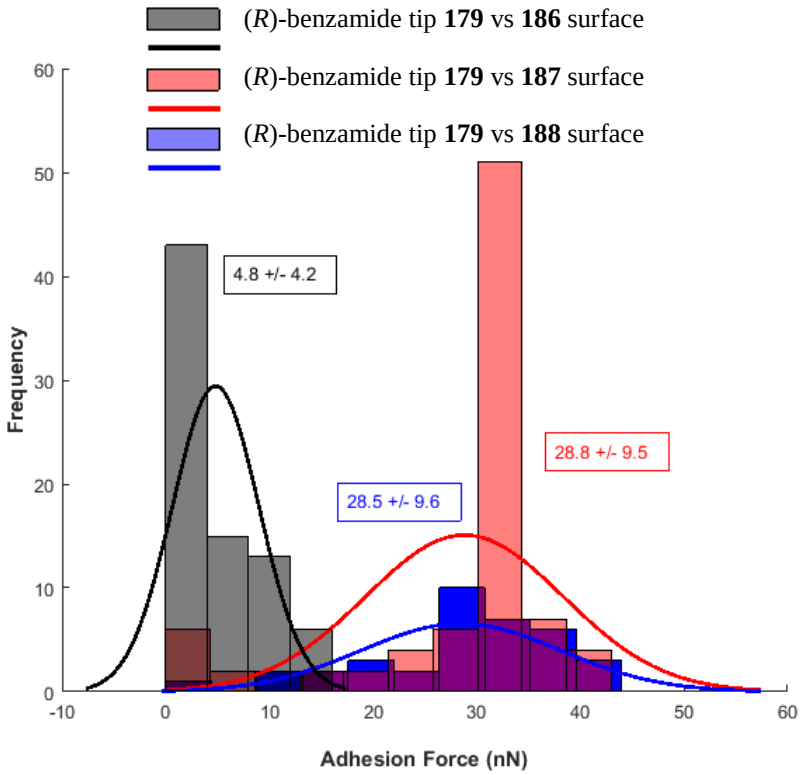

Figure 114: Adhesion histogram of (*R*)-benzamide coated AFM tips tested against separate samples of 186, 187 and 188 DHP terminated surfaces respectively. All measurement were taken using the same (*R*)-benzamide coated AFM tip. Measurements are snap out of contact. At least four areas tested per sample.

To complete the measurements and obtain a clearer picture of the discrimination occurring on the surfaces, a racemic variant of the probe tip was constructed by depositing (±)-**179** on an Au coated AFM tip. When (±)-benzamide **179** was tested against surfaces **186** and **187** no discrimination was observed (Figure 115) Adhesion values obtained were similar and with error of each other (Entries 7 and 8 Table 15). Similarly when the (±)-**179** tip was tested against the surface **188** an adhesion value between the two, 3.5 ± 1.5 nN, was obtained (entry 9, Table 15). Overall this was the expected result from the measurement of surfaces **186**, **187** and **188** using the (±)-**179** tip and no discrimination was observed in any of the cases.

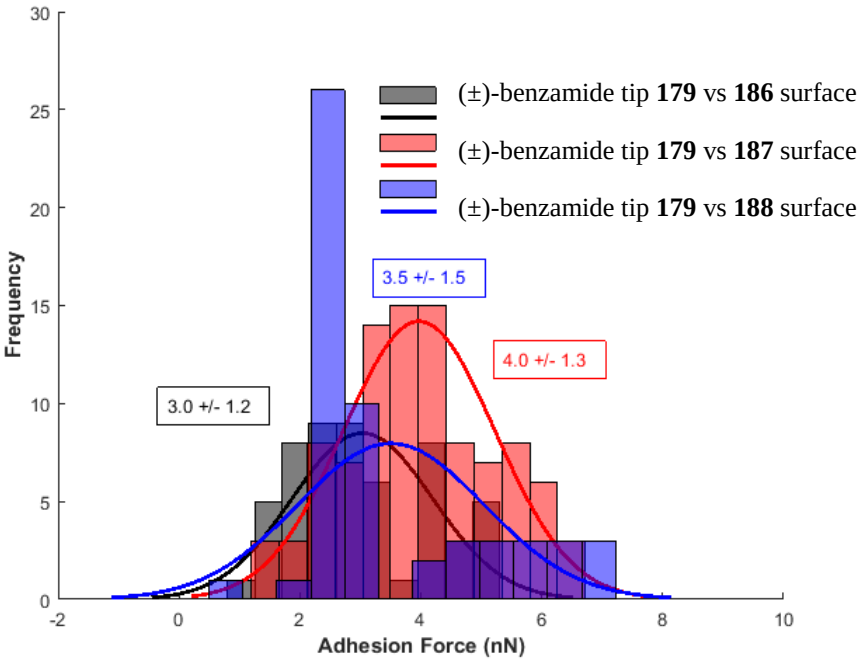

Figure 115: Adhesion histogram of (±)-benzamide coated AFM tips tested against separate samples of 186, 187 and 188 DHP terminated surfaces respectively. All measurement were taken using the same (*R*)-benzamide coated AFM tip. Measurements are snap out of contact. At least four areas tested per sample.

Entry	Probe tip	Surface	Mean (nN)[a]	Std. dev. (nN)
1	(*S*)-benzamide **179**	**186**	4.7	2.1
2	(*S*)-benzamide **179**	**187**	9.6	3.0
3	(*S*)-benzamide **179**	**188**	11.3	4.5
4	(*R*)-benzamide **179**	**186**	4.8	4.2
5	(*R*)-benzamide **179**	**187**	28.5	9.6
6	(*R*)-benzamide **179**	**188**	28.9	9.6
7	(±)-benzamide **179**	**186**	4.0	1.3
8	(±)-benzamide **179**	**187**	3.0	1.2
9	(±)-benzamide **179**	**188**	3.5	1.5

Table 15: Summary of adhesions forces from (*R*)-179, (*S*)-179 and racemic 179 derived AFM tips tested against surfaces 186, 187 and 188.

As it is not particular informative to directly compare adhesion values obtained using different AFM tips, ratios of the adhesion force obtained with one particular enantiomer of the AFM tip tested against the same surface termination was calculated e.g. L-cysteine tip **185** tested against **186** and (3*R*, 4*R*)-**184**, importantly keeping the AFM tip constant. A ratio of 1.0:2.3 for the measurement an L-cysteine tip **185** vs (3*R*,4*R*)-**184** and **186** was obtained which corresponded to

double the magnitude of adhesion force (entry 1, Table 16). A possible reason for the increase in magnitude may be due to the roughness and/or homogeneity of the surfaces. A ratio of 1.0:1.1 for an L-cysteine tip **185** vs (3*S*,4*S*)-**184** and **187** surface was obtained indicating surfaces of similar molecular packing (entry 2, Table 16). Similar trends are observed when the same D-cysteine tip D-**185** was used to probe the (3*S*,4*S*)-**184**, (3*R*,4*R*)-**184**, **186** and **187** surfaces. A ratio of 1.0:1.2 for the same D-cysteine tip D-**185** vs (3*R*,4*R*)-**184** and **187** surfaces again indicating consistent films on the surfaces (entry 3, Table 16). When D-cysteine tip L-**185** was tested against (3*S*,4*S*)-**184** and **187** surfaces a ratio of 1.3:1.0 was obtained (entry 4, Table 16). When (*S*)-benzamide tip **179** was tested against surfaces **186** and **187** similar ratios were obtained to that of the previous measurements. A ratio of 1.0:1.3 was obtained for an (*S*)-benzamide tip **179** vs (3*R*,4*R*)-**184** surface and **187** (entry 5, Table 16) and a ratio of 1.7:1.0 for a (3*S*,4*S*)-**184** and **187** surface indicating consistent films on both surfaces. As the results from the (*R*)-benzamide tip **179** in the *in situ* Michael addition lactonisation protocol were inconclusive they will not be compared in further detail but are presented below for completeness (entries 7-8, Table 16). It should be mentioned however, that the results obtained from the (*R*)-benzamide tip **179** tested against the 'clicked' surfaces followed the same trend as previously observed, that is the magnitude of the adhesion values were reversed, and as such may be a true reflection of the discrimination events on the surface. Based on these results we can suggest that the molecular packing of the DHPs is similar on some of the surfaces concerned regardless of fabrication method.

Entry	Probe tip	Surfaces	'Clicked' mean (nN)	*In situ* mean (nN)	Ratio
1	L-cysteine L-**185**	(3*R*,4*R*)-**184**/**186**	1.5 ± 0.1	2.8 ± 0.7	1.0:2.3
2	L-cysteine L-**185**	(3*S*,4*S*)-**184**/**187**	1.9 ± 0.1	3.8 ± 0.8	1.0:1.1
3	D-cysteine D-**185**	(3*S*,4*S*)-**184**/**187**	1.3 ± 0.2	1.8 ± 0.4	1.0:1.2
4	D-cysteine D-**185**	(3*R*,4*R*)-**184**/**186**	1.9 ± 0.2	2.3 ± 0.3	1.3:1.0
5	(*S*)-benzamide **179**	(3*R*,4*R*)-**184**/**186**	3.5 ± 0.3	4.7 ± 2.1	1.0:1.3
6	(*S*)-benzamide **179**	(3*S*,4*S*)-**184**/**187**	5.7 ± 1.0	9.6 ± 3.0	1.7:1.0
7	(*R*)-benzamide **179**	(3*S*,4*S*)-**184**/**187**	4.6 ± 0.4	28.5 ± 9.6	1.0:6.2
8	(*R*)-benzamide **179**	(3*R*,4*R*)-**184**/**186**	7.0 ± 0.8	4.8 ± 4.2	1.5:1.0

Table 16: Summary of adhesions forces from L-and D-cysteine and (*S*)/(*R*)-benazamide derived AFM tips tested against (3*R*,4*R*)-184 and (3*S*,4*S*)-184 surfaces.

3.11 Enantiospecific wetting on enantioenriched DHPs

An enantiospecific wetting experiment was undertaken using the synthesised assumed enantioenriched surfaces to evaluate a possible chiral interaction with a chiral probe liquid.[†] Following a procedure from Ducker[201], the chiral surface was tested using a leucinol by placing ~3 µL drop on the appropriate surface synthesised from the *in situ* Michael addition-lactonisation procedure (Figure 116). Initially the contact angle was measured using (*S*)-leucinol **190** as a chiral liquid. This gave a small difference in contact angle on the surface when tested against all assumed enantioenriched surfaces (**186-189**) (Table 17). In the Ducker report hexadecane was used as a surrounding medium for the measurements to allow a more measureable contact angle. Unfortunately this was not the case in these set of experiments and only a slight difference in angle was measured between all surfaces. Practically it is difficult to measure contact angles below 15-20 ° as they do not give a large contact angle (θ) with the surface and tend to have large experimental error. However, a small difference is noticed and this may tentatively be attributed to the chiral interactions taking place on the surface between the assumed enantioenriched DHPs and the leucinol.

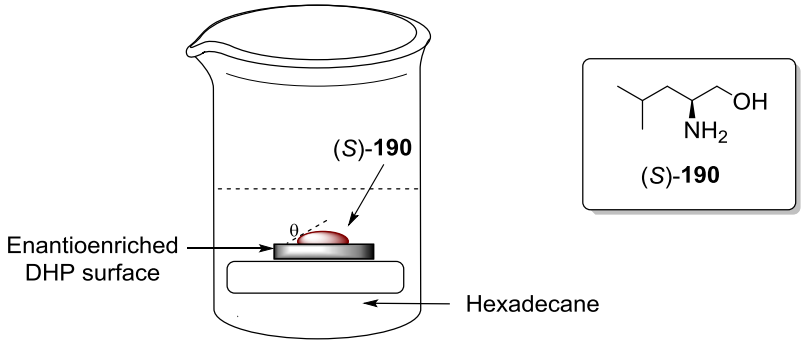

Figure 116: Experimental set-up for contact angle measurement using enantiospecific wetting methodology.

Entry	Surface	Leucinol	Surrounding medium	Contact Angle (°)[a,b]
1	**186**	(*S*)-leucinol **190**	Atmosphere	11.5 ±1.0
2	**186**	(*S*)-leucinol **190**	Hexadecane	16.6 ±2
3	**187**	(*S*)-leucinol **190**	Hexadecane	19.9 ±1.2
4	**188**	(*S*)-leucinol **190**	Hexadecane	11 ±0.8

Table 17: Contact angles of enantiospecific wetting experiments of (*S*)-leucinol tested against all the combinations of chiral surfaces.[a]Average of two samples of the same termination.[b]Average of at least two measurements on the same sample.

[†] Enantiospecific wetting experiment performed by Dr John D. Parkin.

3.12 Conclusion and future outlook

In this work enantioenriched surfaces were synthesised using a Michael addition-lactonisation the chiral isothiourea catalyst HyperBTM in both (2*S*,3*R*) and (2*R*,3*S*) **61** enantiomeric forms A model system was developed that gave reliable and reproducible results when used in chemical force microscopy measuring chiral discrimination. A novel chiral AFM probe tip was also developed and tested in our system against the enantioenriched surfaces giving a reasonable level of discrimination.

Both enantiomers of the enantioenriched DHP **184** were also synthesised and attached to the surface using click chemistry. The results from this show that regardless of fabrication method, both types of surfaces give similar adhesion values, within error of each other, suggesting that similar chiral discrimination events are happening on the surfaces as well as comparable molecular packing of the surfaces.

Additional experiments measuring contact angles using a chiral, enantiopure liquid were also undertaken to ascertain the possible differing diastereomeric interactions occurring between the liquid and solid interface. These results did not show a huge difference in the resulting contact angles, and this was attributed to practical issues with the measurements, although some information may be tentatively taken from this.

The limitations of the current methodology include the inability of the chiral force measurements to allow for quantification of the levels of enantioselectivity imparted on the surface. Non-linear effects in ee generation [219] (on the surface) may come into play but this is difficult to measure using classical methods. A possible remedy to this would be to prepare a series of surfaces using enantioenriched catalysts of varying ee's, that is, with the idea of creating a series of surfaces with DHPs present in increasing levels of ee and testing using the aforementioned methodology. This may provide insight into the sensitivity of the CFM methodology developed in this work.

Future work in this area could include the derivatisation of these surfaces to attach desired functional groups in a selective manner and possibly even be used as chiral selectors in enantioselective reactions.

3.13 References and Notes

[175] R. Arjumand, I. I. Ebralidze, M. Ashtari, J. Stryuk, N. M. Cann, J. H. Horton, *J. Phys. Chem. C.* **2013**, *117*, 4131-4140.
[176] D. H. Dressler, Y. Mastai, *Chirality* **2007**, *19*, 358-365.
[177] H.-U. Blaser, *Catal. Today* **2000**, *60*, 161-165.
[178] T. Mallat, E. Orglmeister, A. Baiker, *Chem. Rev.* **2007**, *107*, 4863-4890.
[179] K. Baranes, H. Moshe, N. Alon, S. Schwartz, O. Shefi, *ACS Chem. Neurosci.* **2014**, *5*, 370-376.
[180] Y. Okamoto, T. Ikai, *Chem. Soc. Rev.* **2008**, *37*, 2593-2608.

[181] D. Hanein, B. Geiger, L. Addadi, *Science* **1994**, *263*, 1413-1416.
[182] R. Raval, *Chem. Soc. Rev.* **2009**, *38*, 707-721.
[183] K.-H. Ernst, *Phys. Status Solidi B.* **2012**, *249*, 2057-2088.
[184] L. Persechini, J. F. McGilp, *Phys. Status Solidi B.* **2015**, *252*, 95-99.
[185] J. D. Byers, H. I. Yee, T. Petralli-Mallow, J. M. Hicks, *Phys. Rev. B.* **1994**, *49*, 14643-14647.
[186] L. Persechini, J. F. McGilp, *Phys. Status Solidi B.* **2012**, *249*, 1155-1159.
[187] L. Pasteur, *C. R. Acad. Sci* **1848**, *34*, 535.
[188] Y. Mastai, *Chem. Soc. Rev.* **2009**, *38*, 772-780.
[189] H. Moshe, M. Vanbel, V. K. Valev, T. Verbiest, D. Dressler, Y. Mastai, *Chem. Eur. J.* **2013**, *19*, 10295-10301.
[190] C. D. Frisbie, L. F. Rozsnyai, A. Noy, M. S. Wrighton, C. M. Lieber, *Science* **1994**, *265*, 2071-2074.
[191] H. Otsuka, T. Arima, T. Koga, A. Takahara, *J. Phys. Org. Chem.* **2005**, *18*, 957-961.
[192] Aleksandr Noy, a. Dmitri V. Vezenov, C. M. Lieber, *Annu. Rev. Mater. Sci.* **1997**, *27*, 381-421.
[193] G. U. Lee, D. A. Kidwell, R. J. Colton, *Langmuir* **1994**, *10*, 354-357.
[194] M. Ludwig, W. Dettmann, H. E. Gaub, *Biophys. J.* **1997**, *72*, 445-448.
[195] T. Boland, B. D. Ratner, *PNAS* **1995**, *92*, 5297-5301.
[196] R. McKendry, M.-E. Theoclitou, T. Rayment, C. Abell, *Nature* **1998**, *391*, 566-568.
[197] W. H. Pirkle, J. M. Finn, J. L. Schreiner, B. C. Hamper, *J. Am. Chem. Soc.* **1981**, *103*, 3964-3966.
[198] M. Mahapatro, C. Gibson, C. Abell, T. Rayment, *Ultramicroscopy* **2003**, *97*, 297-301.
[199] J. Hlinka, J. Hodacova, L. Raehm, M. Granier, M. Ramonda, J.-O. Durand, *CR Chemie.* **2010**, *13*, 481-485.
[200] Y. Nakahara, H. Mitani, S. Kado, K. Kimura, *RSC Adv.* **2014**, *4*, 57850-57854.
[201] M. Rapp, W. A. Ducker, *J. Am. Chem. Soc.* **2010**, *132*, 18051-18053.
[202] A. Shundo, K. Hori, T. Ikeda, N. Kimizuka, K. Tanaka, *J. Am. Chem. Soc*. **2013**, *135*, 10282−10285.
[203] J. B. Pedley, E. M. Marshall, *J. Phys. Chem. Ref. Data* **1983**, *12*, 967-1031.
[204] Y. Barness, O. Gershevitz, M. Sekar, C. N. Sukenik, *Langmuir* **2000**, *16*, 247-251.
[205] Y. Yang, A. M. Bittner, S. Baldelli, K. Kern, *Thin Solid Films* **2008**, *516*, 3948-3956.
[206] M. D. Losego, M. E. Grady, N. R. Sottos, D. G. Cahill, P. V. Braun, *Nat Mater* **2012**, *11*, 502-506.
[207] M. J. Stevens, *Langmuir* **1999**, *15*, 2773-2778.
[208] K. Wen, R. Maoz, H. Cohen, J. Sagiv, A. Gibaud, A. Desert, B. M. Ocko, *ACS Nano*, **2008**, *2*, 579–599.
[209] C. R. Martinez, B. L. Iverson, *Chem. Sci.* **2012**, *3*, 2191-2201.
[210] W. H. Pirkle, D. W. House, *J. Org. Chem.* **1979**, *44*, 1957-1960.
[211] S. Gabriel, *Ber. Deut. Chem. Ges.* **1887**, *20*, 2224-2236.
[212] A.-D. Filimon, P. Jacob, R. Hergenröder, A. Jürgensen, *Langmuir* **2012**, *28*, 8692-8699.
[213] X. Yao, Y. Hu, B. Cao, R. Peng, J. Ding, *Biomaterials* **2013**, *34*, 9001-9009.
[214] J. L. Hutter, J. Bechhoefer, *Rev. Sci. Instrum.* **1993**, *64*, 1868-1873.
[215] R. W. Carpick, N. Agraït, D. F. Ogletree, M. Salmeron, *J. Vac. Sci. Technol. B.* **1996**, *14*, 1289-1295.
[216] D. Alberga, G. F. Mangiatordi, A. Motta, O. Nicolotti, G. Lattanzi, *Langmuir*, **2015**, *31*, 10693–10701
[217] M. Rachel, T. Maria-Elena, A. Chris, R. Trevor, *Jpn. J. Appl. Phys.* **1999**, *38*, 3901.
[218] F. Stevens, D. J. Dyer, D. M. Walba, *Angew. Chem. Int. Ed.* **1996**, *35*, 900-901.
[219] Kagan, H. B. *Synlett* **2001**, 888-899.

Chapter 4 : Synthesis and immobilisation of isothiourea catalysts onto polystyrene supports

Introduction

This chapter describes the immobilisation of reactive isothiourea-based organocatalysts onto Merrifield-type polystyrene supports (Figure 117). At the onset of this study there was no examples of a solid support isothiourea-based organocatalyst in the literature. In this study, two polymer-supported (PS) isothioureas synthesised (PS-(*R*)-BTM **191** and PS-(2*R*,3*S*)-HyperBTM **61**) have been evaluated in heterogeneous Michael addition-lactonisation reactions, kinetic resolutions of secondary aryl-alkyl alcohols, kinetic resolutions of heteroaromatic tertiary alcohols and stereoselective annulations of α,β-unsaturated acyl ammonium intermediates with 1,3-dicarbonyls. These separate protocols all provide excellent selectivity, comparable with the corresponding homogeneous system, with good yields in most cases. A recyclability study of PS-(2*R*,3*S*)-HyperBTM **61** as a catalyst for the kinetic resolution of tertiary alcohols was also undertaken and this showed that the catalyst can be recycled up to 8 times with only a small loss in selectivity.

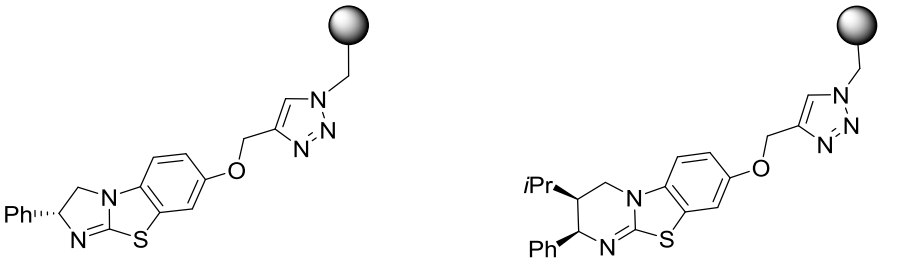

Figure 117: Polymer-supported isothioureas synthesised and used in this work.

4.1 Aims

The aim of this chapter was to immobilise reactive isothiourea-based organocatalysts onto a polystyrene support and perform studies to test the robustness and recyclability of the resulting catalytic resins. Secondly, we wanted to assess the applicability of these catalysts to a wide range of enantioselective processes that are known to be mediated by (2*R*,3*S*)-HyperBTM **61** and PS-(*R*)-BTM **191**. Comparison of the efficiency and selectivity with the homogeneous counterparts was also an initial aim of this work.

4.2 Polymer-supported synthesis

Since the introduction of insoluble polymer-supports by R. Bruce Merrifield in 1963[220] there has been a huge uptake in their use as a solid-support for reagent and catalyst immobilisation.[221]

Originally these polymer-supports were to be used for solid-phase peptide synthesis, but their generality and applications in chemical synthesis quickly caught on and is now widespread.[222-223] Insoluble polymer-supports offer the advantage of being easily removed from reaction mixtures by filtration, rinsing and drying allowing them to be readily reusable. This is a desirable property for any system where the aim is to minimise waste products and abide by the principles of green chemistry.[224] After initial research by Merrifield using several different polymeric materials, the chloromethyl and divinylbenzene (DVB) crosslinked PS were introduced, commonly known at Merrifield resin **192** (Figure 118).

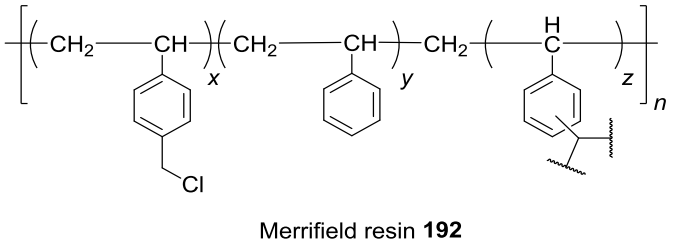

Merrifield resin **192**

Figure 118: Polymer-support (PS) introduced by R. B. Merrifield in 1963.

Favourable properties of Merrifield resin **192** included swelling in non-polar organic solvents altough this proved restrictive when synthesising long peptide sequences.[225] As a result several improvements were made to make the resin more compatible with a wider range of reagents/catalysts. The most notable was the introduction of a tetrahydrofuran-derived cross-linker to enhance swelling characteristics by Toy and Janda,[225] known as JandaJel™ (**193**), which is now commercially available (Figure 119).

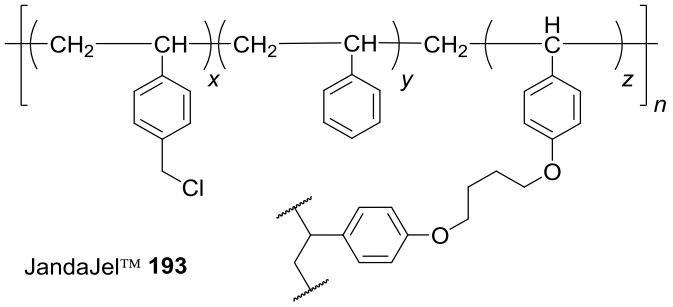

JandaJel™ **193**

Figure 119: JandaJel™ containing a THF derived cross-linker introduced by Toy and Janda.

Polymer swelling is a major characteristic of polystyrene derived resins which can play an important role in the reactivity. Swelling of a gel-like resin is considered a prerequisite for facilitating reactions to occur within the solid support.[226-227] Early research in the area focused on enhancing the swelling properties by introducing polymeric regions that are more compatible with polar solvents, thus increasing the scope of reactions that can performed using polymer-supports. The introduction of polyethylene glycol (PEG) units into the polymer-support gave the

desired swelling properties and a series of resins was developed from this methodology.[228] TantaGel™ **194** and later ArgoGel™ **195** received the most significant commercial success and both are prepared by grafting the PEG chains through polymerisation and not installing prefabricated PEG linkers (Figure 120).

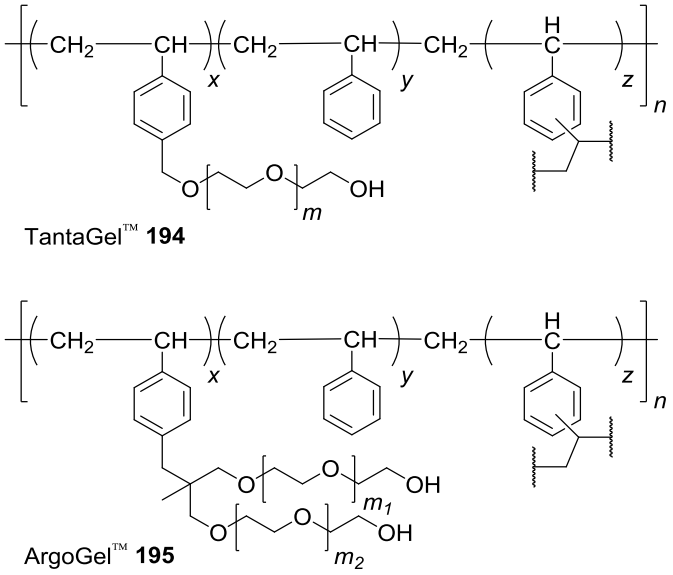

Figure 120: Typical examples of the PEG-PS family of resins.

4.3 Polymer-supported tertiary Lewis base organocatalysts

The section offers a brief history of the development of immobilised tertiary amine Lewis basic organocatalysts, with particular emphasis on chiral derivatives and their use in stereoselective synthesis. An overview of recent noteworthy developments within the area is also given.

4.3.1 Polymer-supported *Cinchona* alkaloids

The first example of a polymer-supported Lewis basic organocatalyst for use in enantioselective synthesis was reported by Nakamura and co-workers in 1974.[229] Following from the original work by Pracejus, who used phenylmethyketene **196** in the synthesis of (−)-α-phenyl methylpropionate, [230] the authors immobilised a *Cinchona* derived catalyst onto a polymer-support using AIBN as initiator in a co-polymerisation procedure. PS-(1*S*,2*R*,4*S*,5*R*)-**197** was examined in the enantioselective addition of methanol to phenylmethyketene **196** affording ester **198**, in 35% ee (Figure 121). Unfortunately the recyclability of this system was not tested. Although the ee's are mediocre by today's standards, this example served as a starting point for organocatalyst immobilisation.

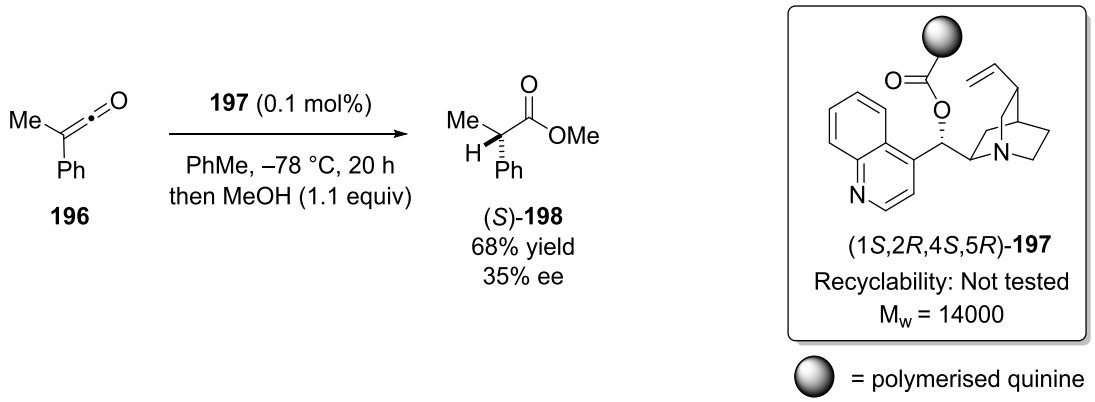

Figure 121: Seminal work by Nakamura and co-workers using PS Cinchona derivative 197 for enantioselective addition to ketenes.

Although this particular catalyst class went through several incremental improvements,[231-234] it was not until a report from d'Angelo and co-workers in 1999 that showed that PS *Cinchona* alkaloids could compete with their non-supported counterparts.[235] As such, PS-(1*S*,2*R*,4*S*,5*S*)-**201** was an efficient catalyst for the enantioselective Michael addition of **199** to methyl vinyl ketone (MVK) **200**, forming (*R*)-**202** in an 85% yield and 87% ee (Figure 122). This was the highest ee value for this reaction obtained by using either a non-supported or polymer-support catalyst.

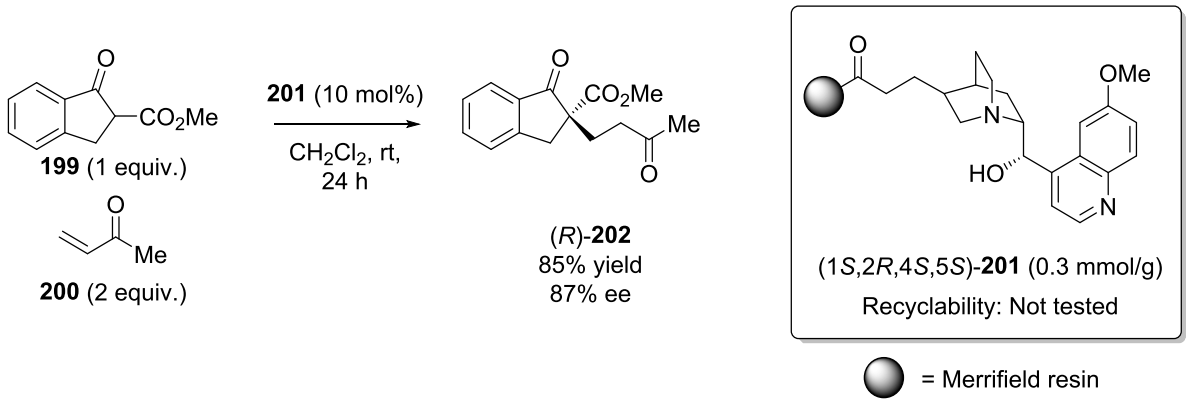

Figure 122: PS quinine derivative 201 catalysed Michael addition

Lectka and co-workers have shown that PS-*Cinchona* alkaloids catalyse the formation of β-lactams in a [2+2] cycloaddition between ketenes and *N*-tosyl imines.[236] In this report the authors packed solid phase reagents into sequentially linked columns and eluted the reagents through using gravity. Reaction of acid chloride **203** with PS-BEMP generates the corresponding ketene **204** *in situ*, which in the presence of imine **205** and PS-**206** undergoes a [2+2] cycloaddition to afford a range of β-lactams in moderate yields, good dr and excellent ee's (Figure 123). Interestingly, the catalyst took between five and 10 runs to 'equilibrate' and afford consistent

results, after which the system could be recycled up to 60 times without erosion of yield or selectivity.

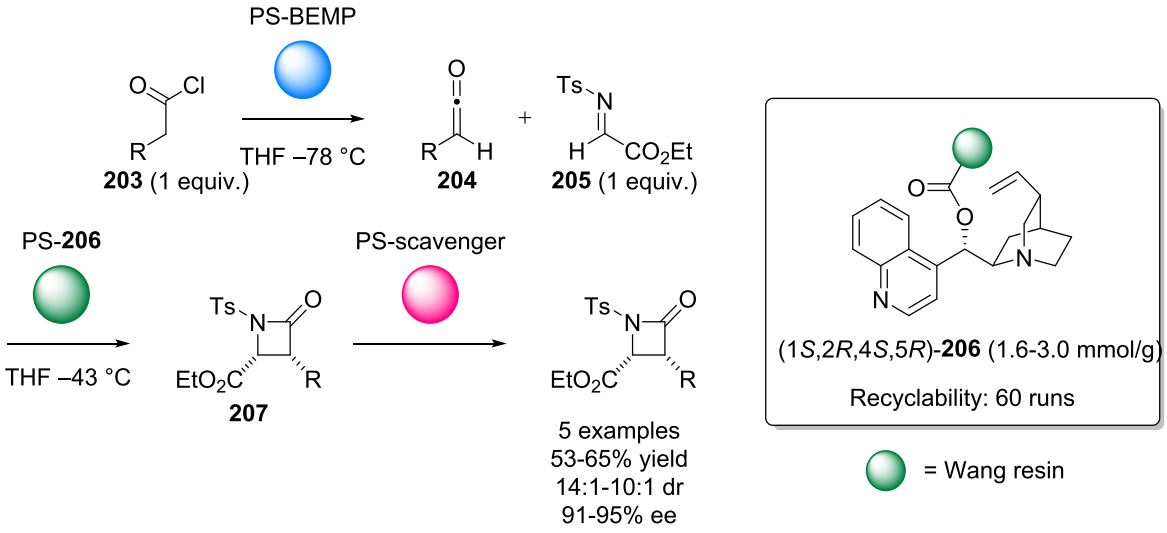

Figure 123: Lectka's synthesis of β-lactams using PS Cinchona 206 on sequentially linked columns

4.3.2 Polymer-supported amidines

Nagai and Endo have reported the use of a polymer-supported amidine in the catalytic synthesis of a range of 1*H*-quinazoline-2,4-diones from 2-aminobenzonitriles.[237] The authors synthesised the polymer support using a radical polymerisation procedure. The polymer-supported catalyst **209** was able to fix CO_2 from the atmosphere and subsequently react with 2-aminobenzonitriles **208** to afford the products in low to excellent yield (Figure 124). The authors report that PS-**209** could be recycled at least twice without loss in activity.

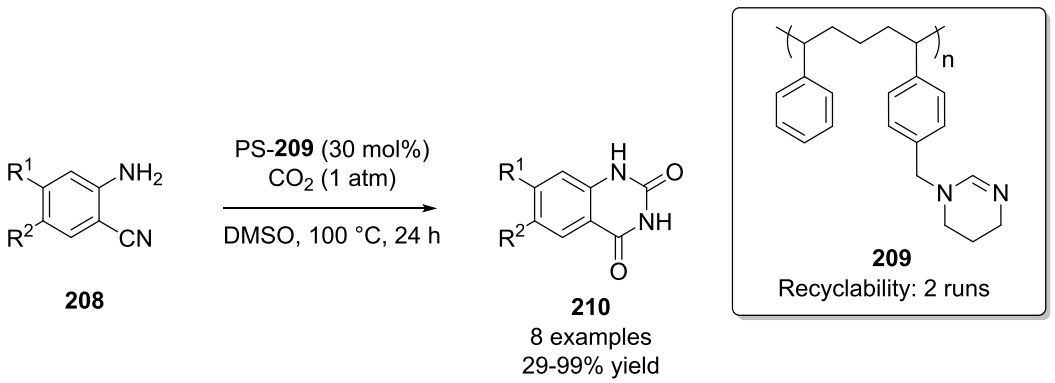

Figure 124: Use of PS amidine 209 in CO_2 fixation and synthesis of 1*H*-Quinazoline-2,4-diones.

A more recent example of using amidines in polymer-supported synthesis was reported by Khalafi-Nezhad and co-workers who used PS-PEG-DBU **215** as an organocatalytic base in the multi-component one-pot synthesis of a range of 8-substitited pyro[2,3-*d*]-pyramidine-6-carbonitriles in water (Figure 125).[238] The reaction of barbituric acid **211**, malonitrile **212**, benzaldehyde **213** and adeonside **214** in the presence of PS-**215** affords the corresponding

substituted pyramidines in high yields. PS-**215** can be recycled up to 12 times without any loss of selectivity.

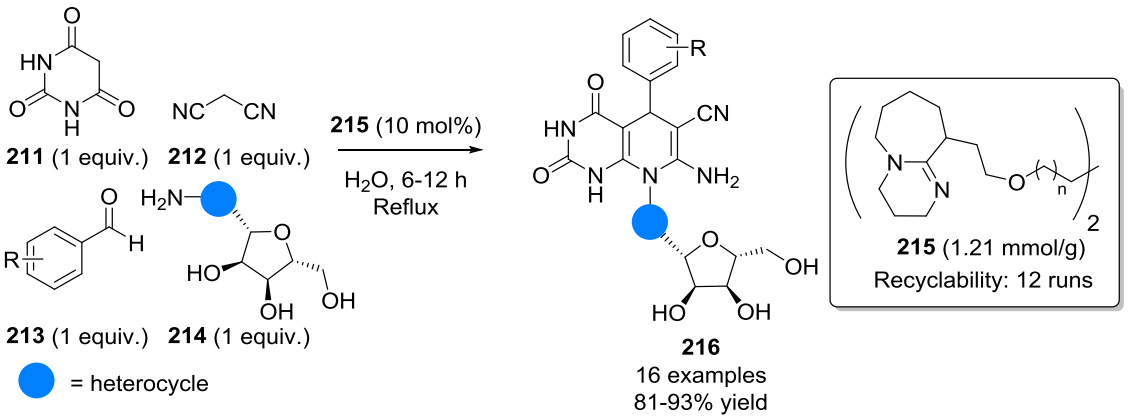

Figure 125: One-pot multicomponent synthesis of pyro[2,3-*d*]-pyramidine-6-carbonitriles using PS-215.

4.3.3 Polymer-supported guanidines

Matsukawa and co-workers have shown that a PS-TBD organocatalyst can be used in the regioselective ring-opening of racemic aziridines with silylated nucleophiles, giving good yields and generally excellent regioselectivity (Figure 126).[239] The authors also comment that the PS-TBD **219** used gave better regioselectivity than a previously reported PS-TBD catalyst in the ring-opening of epoxides under similar conditions.[240-241]

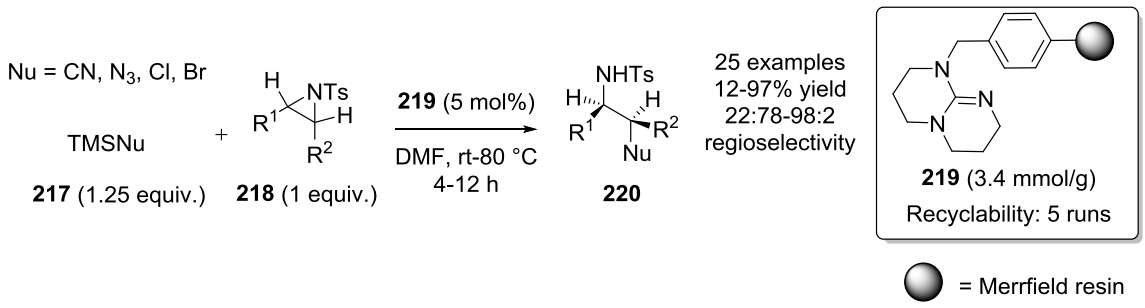

Figure 126: PS-219 assisted ring opening of aziridines with a variety of nucleophiles.

Ishikawa and co-workers have shown the use of PS guanidine 'superbases' in the enantioselective Michael reaction of glycine imine **221** with methyl vinyl ketone **199** to afford the corresponding Michael product **223** in good yield and good ee (85% ee).[242] Reaction of PS-(*R*,*R*)-**222** with imine **221** is thought to generate the corresponding enolate, which undergoes a stereoselective Michael addition with MVK **199** to give (*S*)-**223** with good stereocontrol. The authors recycled PS-(*R*,*R*)-**222** three times with only a slight loss in yield and negligible loss of stereoinduction. A stereochemical model was not proposed for the polymer-support system, however the same authors have proposed one for the analogous homogeneous system. In this case, the guanidine derivative blocks the *Si* face of the enolate allowing addition from the *Re* face (Figure 127).[243]

As the same sense of enantioselectivity in both non-supported and PS-(*R*,*R*)-**222** is similar (91% vs 85% ee) the same sterochemical rationale may potentially be assumed.

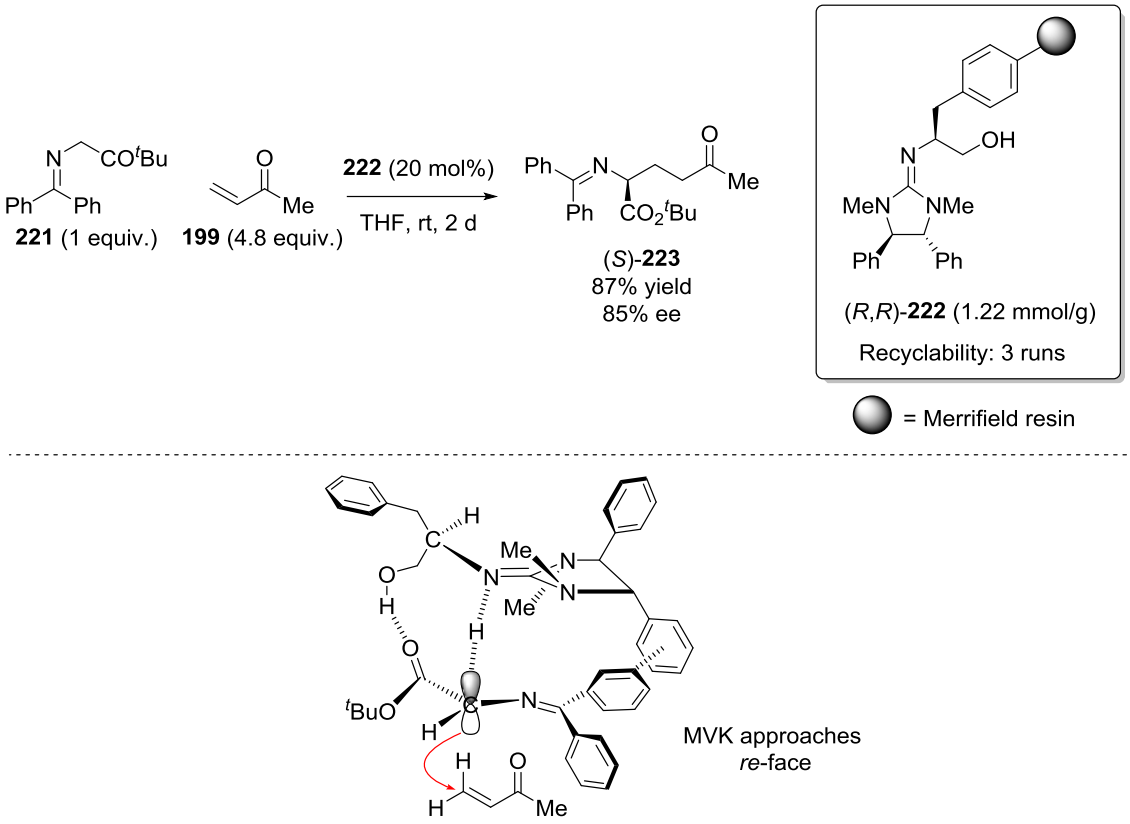

Figure 127: Enantioselective Michael addition of glycine imine 221 to MVK using PS-222.

4.3.4 Polymer-supported DMAP derivatives

Since the first report of a polymer-supported DMAP derivative[244] there have been many reports of their use in a variety of useful transformations.[245-249] It was not until 2003 that a chiral analogue of DMAP was immobilised onto a polymer-support and evaluated in the kinetic resolution of secondary alcohols (Figure 128).[248] Kinetic resolution of racemic alcohol **224** using PS-(*S*)-**225** and isobutyric anhydride allowed the unreacted alcohol **224** to be isolated in 93% ee at 67% conversion . This corresponds to a low selectivity factor (s = k_{fast}/k_{slow}), suggesting that the enantiodiscrimination between the enantiomers of **224** is low. No significant effects were found regarding changes in catalyst loading or nature of the support. Recycling of PS-(*S*)-**225** showed a decrease in efficiency after four runs as selectivity dropped significantly.

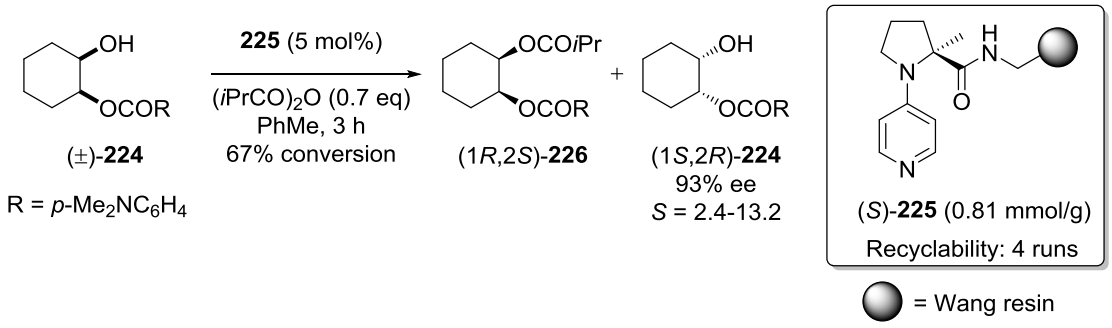

Figure 128: Use of PS-(*S*)-225 DMAP derivative for the kinetic resolution of secondary alcohols.

4.3.5 Polymer-supported isothioureas

During the course of this thesis, Pericàs and co-workers published a report using a polymer-supported derivative of the isothiourea (*R*)-benzotetramisole (BTM) **229**.[251] PS-(*R*)-**229** can efficiently catalyse the enantioselective formation of a series of DHP derivatives as well as several saccharin-derived products in a Michael addition-lactonisation protocol (Figure 129). PS-(*R*)-**229** can also be recycled at least 6 times without any loss of selectivity. The distereoselectivity obtained from these processes are reportedly generally higher than those of the original homogeneous system, originally reported by the Smith group.[101] This is attributed to the introduction of the substituent at C3 on PS-(*R*)-BTM that possibly destabilises the transition state that leads to the formation of the minor diastereoisomer.

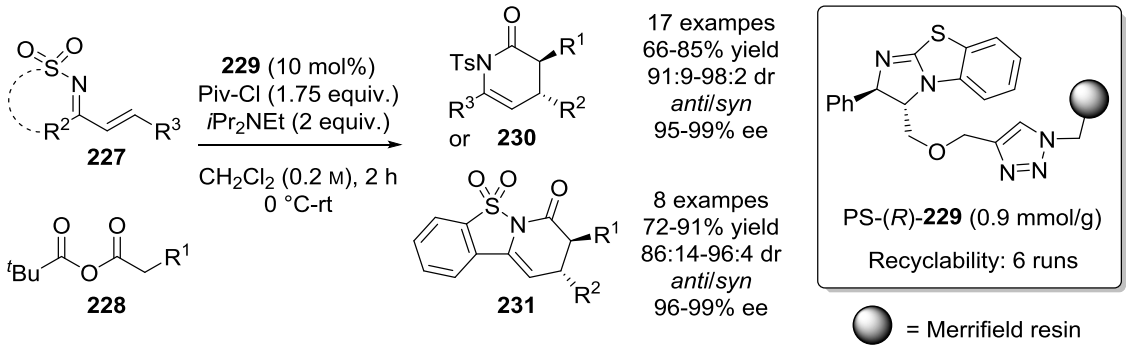

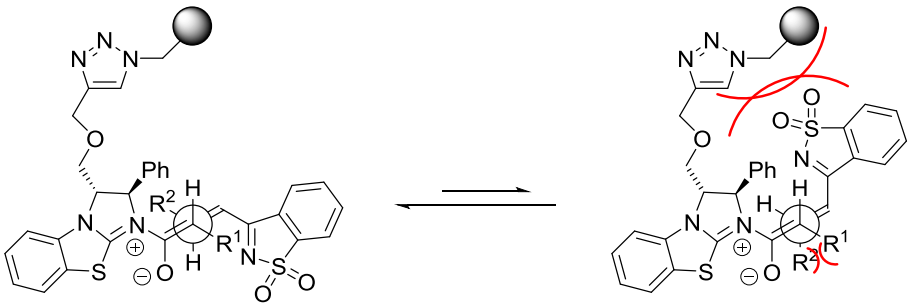

Figure 129: Michael addition-lactonisation protocol using PS-229 and rationale for the increase in diastereoselectivity over the homogeneous system.

4.4 Synthesis of starting materials for PS-(*S*)-benzotetramisole analogue

The CuAAC reaction is a versatile method for the regioselective construction of 1,2,3-triazoles. Several reports have shown that the CuAAC reaction can be used to attach alkynes to azide terminated polymer supports.[250-254] We envisaged that the synthesis of an alkyne BTM-**234** analogue would give a species that could react with a polymer-supported azide, affording the desired immobilised isothiourea organocatalysts (Figure 130).

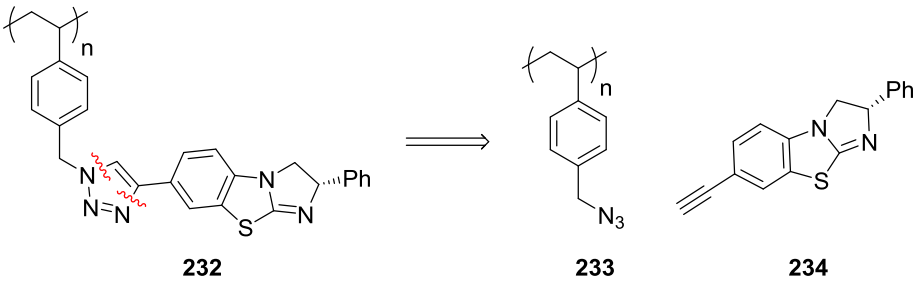

Figure 130: Retrosynthetic analysis of polymer-supported (*S*)-BTM 232.

We envisaged the synthesis of a 2-aminobenzothiazole core **235** *via* an oxidative ring closing reaction using the appropriate thiourea **236** (Figure 131).

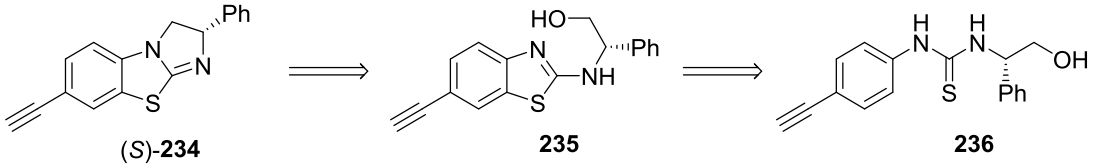

Figure 131: Retrosynthetic analysis of (*S*)-234 using the Hugerschoff reaction

4.4.1 Benzothiazole synthesis from thioureas

Initial attempts focused on the synthesis of the benzothiazole core from the corresponding thiourea with the pre-installation of an alkyne moiety, which would circumvent the need for any late stage installation of this functionality. The most important strategy for the synthesis of benzothiazoles is the condensation of *ortho*-amino-phenol, thiophenol or aniline with a carboxylic acid, aldehyde, acyl chloride or acid anyhdride (Figure 132).[255]

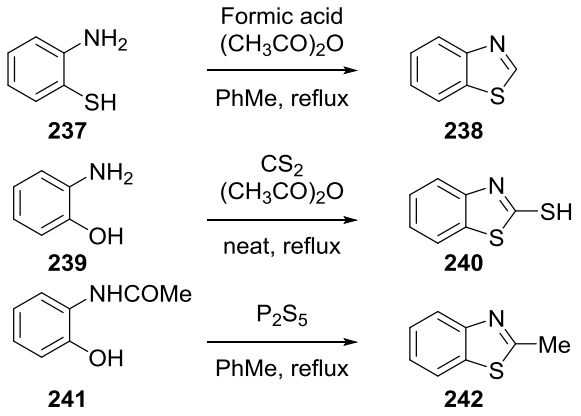

Figure 132: Various *ortho*-condensation reactions for the synthesis of 2-benzothizoles.

Another important reaction for the synthesis 2-benzothiazoles is the oxidative ring closure of arylamine-thioamides affording 2-aminobenzthiazoles, known as the Hugershoff reaction.[256-257] In the original report, Hugershoff used 1-phenylthiourea **243** and elemental bromine in the presence of acetic acid, which cyclised to give the corresponding 2-aminobenzothiazole **244** (Figure 133(a)).

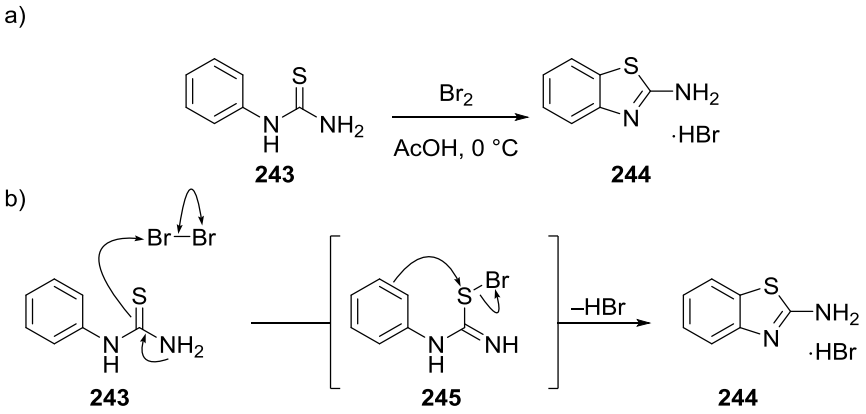

Figure 133 (a): Original conditions reported by Hugershoff for the formation of 2-aminobenzothiazoles, (b) Proposed mechanism of the Hugerschoff reaction.

Synthesis of thiourea **236** began with commercially available 4-iodoaniline **246**. TMS-acetylene was reacted with **246** under Sonogashira conditions to afford the corresponding alkynyl aniline **247** in excellent yield. Treating **247** with 1,1-thiocarbonyldiimidazole **248** in $CHCl_3$ gave the isothiocyanate **249** in excellent 92% yield (Figure **134**).

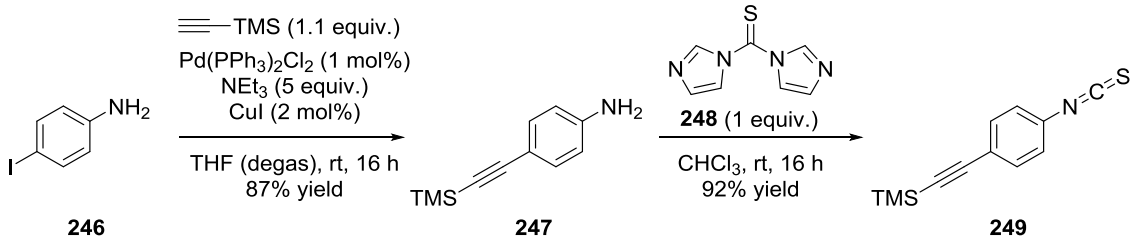

Figure **134: Synthesis of isothiocyanate 249.**

As aryl thioureas can be generated from addition of a primary or secondary amine to the appropriate isothiocyanate, a variety of amino alcohols were used for the synthesis of several substituted thioureas. In this protocol, the appropriate amino alcohol **250** was reacted with isothiocyanate **249** neat for 10 mins then toluene was added and the reaction stirred for 20 mins. This procedure gave thioureas **251**-**253** in moderate to excellent yields (Figure 135).

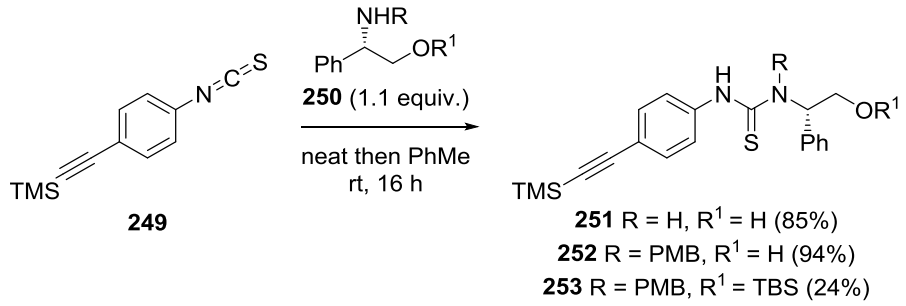

Figure 135: General scheme for the synthesis of substituted thioureas.

With a variety of substituted thioureas in hand, the oxidative cyclisation into 2-aminobenzothiazoles was evaluated. Initial attempts focused on the use of Br_2 in AcOH with LiBr as an additive using AcOH as a solvent, but this gave no observable conversion in any of the cases (entries 1-3,Table 18). Switching the solvent to CH_2Cl_2 and using Br_2 also gave no conversion (entries 4-6,Table 18). Catalytic $Pd(OAc)_2$ was next trialled with 1,10-phenanthroline as an additive but again no conversion was observed (entry 7, Table 18). Patel and co-workers have reported the use of catalytic $Cu(OTf)_2$ in the formation of intramolecular C-S bonds.[258] Therefore catalytic $Cu(OTf)_2$ (10 mol%) was used under an O_2 atmosphere, but again none of the desired cyclised product was observed (entries 8-11,Table 18). Use of $Cu(OTf)_2$ with (*S*)-**252** gave none of the desired benzothiazole, however gave several isolable products were obtained after column chromatography (entry 11,Table 18). Using ^1H and ^{13}C NMR spectroscopic analysis alongside high-resolution mass spectrometry, the isolated products were identified as oxazolidine **254** and thiazolidine **255**, respectively[2] (Figure 136). Heinelt *et al*. have also reported similar findings in the synthesis of aza-heterocycles where O- *vs* S-cyclisation of substituted thioureas occurs in

[2] Assigned with the assistance of Dr James Taylor.

differing ratios depending on the substitution of the nitrogen atoms.[259] As this methodology gave no conversion to the desired aminobenzothiazole a new strategy was developed involving the use of commercially available benzothiazole derivatives.

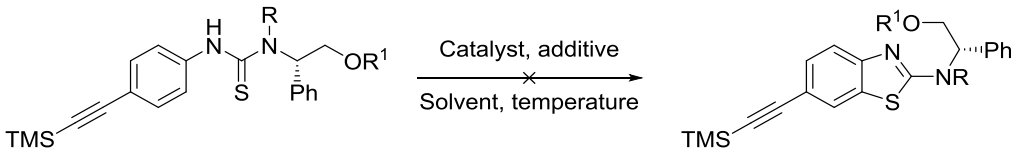

Entry	R	R^1	Reagents (equiv.)	Additive	Solvent	Temperature (° C)	SM recovered (%)
1	H	H	Br_2 (1.0)	LiBr	AcOH	rt	70
2	PMB	H	Br_2 (1.0)	LiBr	AcOH	rt	75
3	PMB	TBS	Br_2 (1.0)	LiBr	AcOH	rt	72
4	H	H	Br_2 (1.0)	n/a	CH_2Cl_2	reflux	55
5	PMB	H	Br_2 (1.0)	n/a	CH_2Cl_2	reflux	64
6	PMB	TBS	Br_2 (1.0)	n/a	CH_2Cl_2	reflux	43
7	PMB	H	$Pd(OAc)_2/K_2CO_3$	1,10-phen	DMF	85 °C	0
8	H	H	$Cu(OTf)_2$ (10 mol%)	O_2	PhMe	reflux	48
9	H	TBS	$Cu(OTf)_2$ (10 mol%)	O_2	PhMe	reflux	66
10	PMB	TBS	$Cu(OTf)_2$ (10 mol%)	O_2	PhMe	reflux	84
11	PMB	H	$Cu(OTf)_2$ (10 mol%)	O_2	PhMe	reflux	0[a]

Table 18: Conditions tested for the oxidative cyclisation of thioureas to 2-aminobenzothiazoles. Conversion determined by ^{1}H NMR spectroscopic analysis of the crude reaction mixture. PMB = *para*-methoxybenzyl. TBS = *tert*-butyldimethylsilyl. Phen = phenanthroline. [a] Several products isolated after column chromatography.

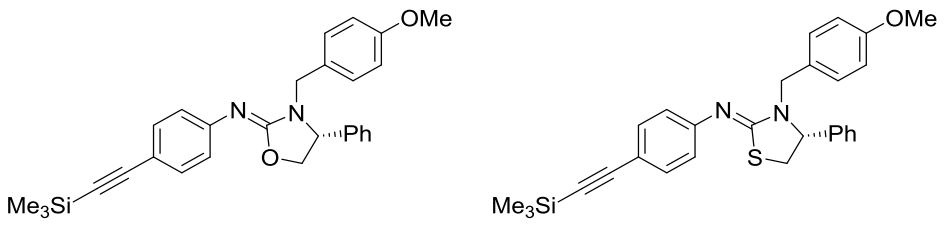

Major product **254** (45 %)

Minor product **255** (22%)

Figure 136: Structures of major and minor products obtained from reaction in Table 18.

4.4.2 Sonogashira cross-coupling methodology

As a scalable and chromatography free method for the synthesis of (*R*), (*S*), and (±)-BTM **191** has been reported within the Smith group,[164] it was decided that this methodology would next be used towards the synthesis of PS-(*S*)-BTM. In the original BTM **191** synthesis

benzochlorothiazole **256** was reacted with a slight excess of phenylglycinol **257** at reflux, which gave the corresponding amino alcohol **258** in good yields (74-79%). Subsequent mesylation of **258** using MsCl and cyclisation gave BTM **191** over two steps in good yields (73-84%).

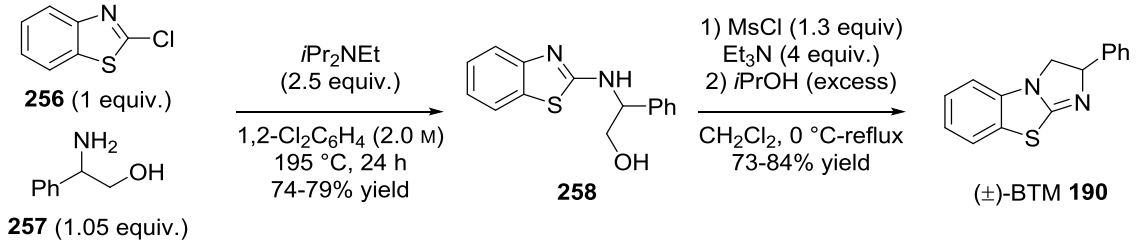

Figure 137: Scalable and chromatography free synthesis for the synthesis of (±)-BTM 191.

Initial attempts for the synthesis of an alkyne substituted PS-(*S*)-BTM **234** analogue focused on the installation of a protected acetylene to the benzothiazole core *via* a palladium catalysed cross-coupling reaction. Commercially available 6-bromo-2-benzothiazolinone **259** was subjected to Sonogashira conditions[260] using either NEt_3 or K_2CO_3 as base and TMS-acetylene as a coupling partner, but unfortunately neither conditions afforded the desired product (Figure 138).

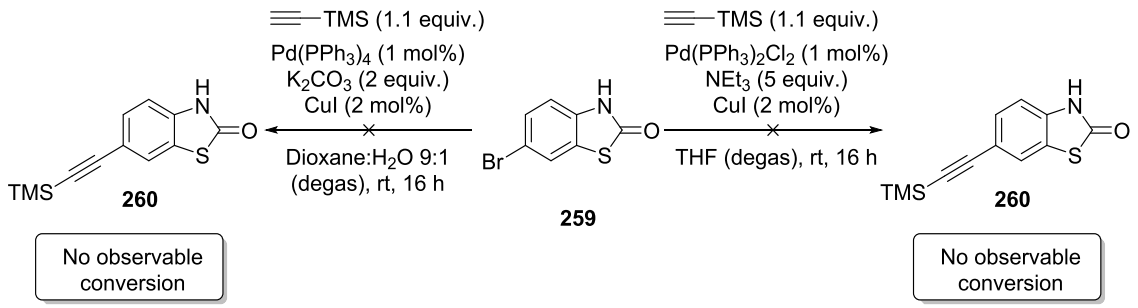

Figure 138: Unsuccessful synthesis of alkynyl benzothiazolinone.

It was thought that the nitrogen atom in the benzothiazolinone ring may be coordinating to the catalyst and hampering reactivity. Benzothiazolinone **259** was therefore Boc-protected using Boc-anydride and DMAP, which afforded Boc-protected amide **260** in 76% yield. This was subjected to the Sonogashira conditions, but as before no conversion into the product was observed and only starting material was returned (Figure 139).

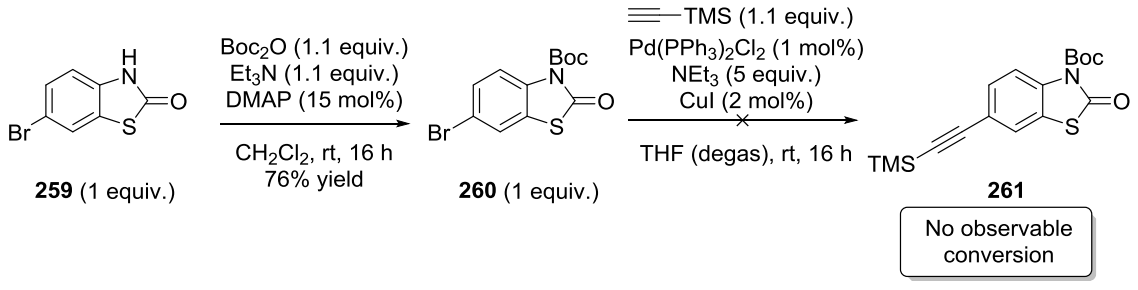

Figure 139: Unsuccessful Sonogashira cross-coupling of Boc-protected amide 260.

Next, lithium-halogen exchange using *t*BuLi was attempted on bromobenzothiazole **259**. Following a procedure from DeOrazia,[261] **259** was reacted with *t*BuLi and MeMgBr at −78 °C to generate the lithiated heterocycle. Quenching with DMF afforded the desired benzaldehyde **262** in 76% yield. This was reacted with the Ohira-Bestmann reagent **263** to try and obtain terminal acetylene in one pot, unfortunately, no **264** was obtained and only starting material was recovered. Aldehyde **262** was then reacted under Corey-Fuchs conditions[262] to synthesise vinyl dibromide **265**, which upon treatment with *n*BuLi should form terminal alkyne **264**. Unfortunately, no **265** was obtained and only starting material was recovered. (Figure 140).

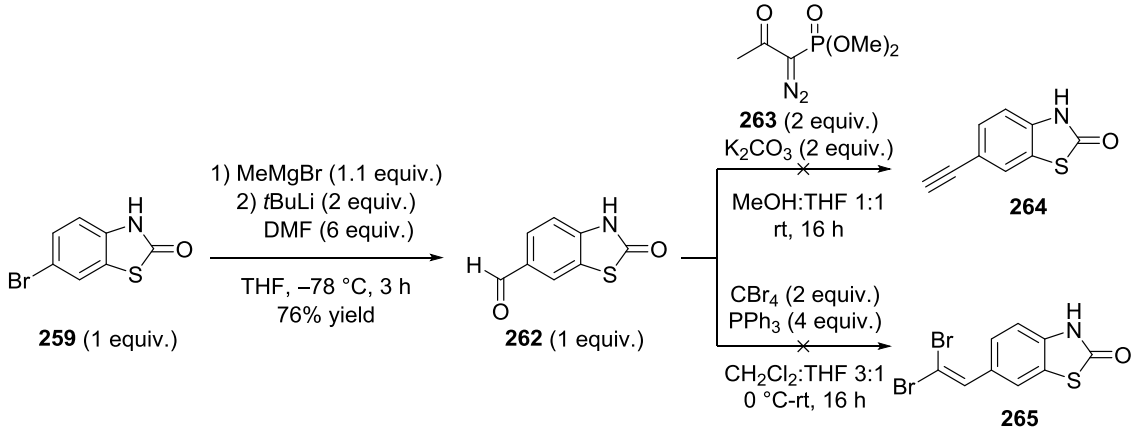

Figure 140: Attempted synthesis of alkyne 264 and vinyl dibromide 265.

As BTM **191** itself is known to be compatible with Pd-catalysts in cooperative dual-catalytic systems,[263-265] direct attachment of a protected acetylene to a bromo-(*S*)-BTM analogue **268**, using Pd-catalysed cross-coupling was investigated. Bromo-(*S*)-BTM analogue **268** was synthesised in three steps from commercially available 6-bromo-2-benzothiazolinone **259**. Chlorination using $POCl_3$ as solvent and catalytic DMF afforded the corresponding chlorobenzothiazole **266** in 82% yield. Reaction of chlorobenzothiazole **266** with (*S*)-phenylglycinol **257** and *i*Pr_2NEt in *o*-dichlorobenzene gave the amino alcohol **267** in good yield after recrystallisation from PhMe. Subsequent treatment of alcohol **267** with methanesulfonyl chloride and Et_3N in CH_2Cl_2 afforded (*S*)-**268** in good yield (Figure 141).

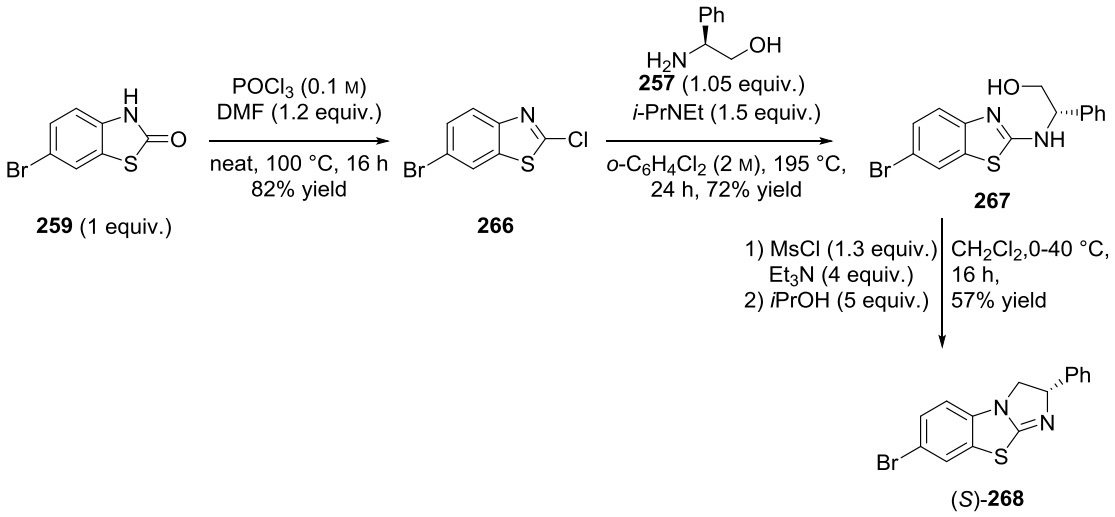

Figure 141: Synthesis of (*S*)-268.

Disappointingly, reaction of (*S*)-**268** with TMS-acetylene under Sonogashira conditions did not give any of desired alkyne (*S*)-BTM **269** and returned only starting material. As such, this route was no longer pursued and a different strategy utilising Suzuki-Miyaura methodology was adopted.

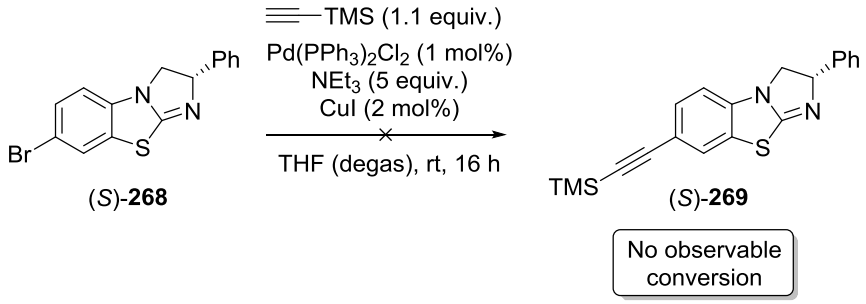

Figure 142: Attempted synthesis of alkyne tethered (*S*)-BTM.

4.4.3 Suzuki-Miyaura cross-coupling methodology

Next, an alternative strategy to introduce an alkyne onto BTM **191** was trialled using the Suzuki-Miyaura reaction.[266] Nolan and co-workers have shown that N-heterocyclic carbenes (NHCs) are good ligands for the Suzuki-Miyaura cross-coupling of aryl chlorides with aryl boronic acids at low catalyst loadings using a commercially available, air-stable [Pd(IPr)(cin)Cl] **272** pre-catalyst (Figure 144).[267] The reaction can tolerate of a wide variety of functional groups, most importantly *para*-acetylene substituted aromatics. Initial attempts focused on the synthesis of a suitable boronic acid coupling partner for reaction with (*S*)-**268** in the presence of a Pd catalyst. A triisopropylsilyl (TIPS) protecting group was chosen as TMS is typically not stable under the Suzuki-Miyaura reaction conditions.

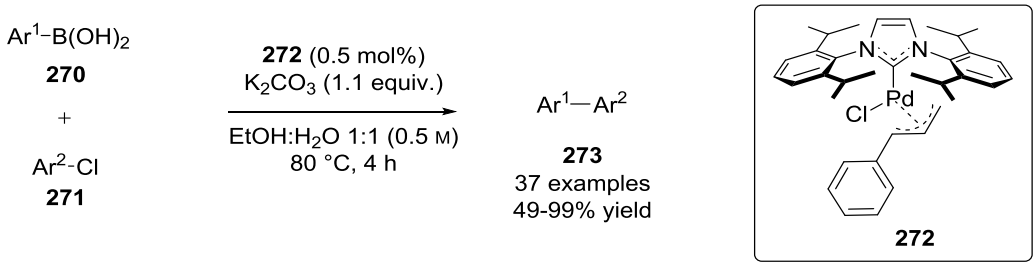

Figure 143: Suzuki-Miyaura reaction using aryl chloride and aryl boronic acids catalysed by NHC complex 272.

Synthesis of boronic acid **277** began with Sonogashira coupling of commercially available 1-bromo-4-iodobenzene **274** with TIPS-protected acetylene **275** to give **276** in 68% yield. Treatment with *n*BuLi generated the corresponding lithium anion, which was quenched *in situ* with B(O*i*Pr)$_3$ to give the isopropyl borate ester. Hydrolysis with 1 M HCl gave boronic acid **277** in a reasonable 43% yield (Figure 144).

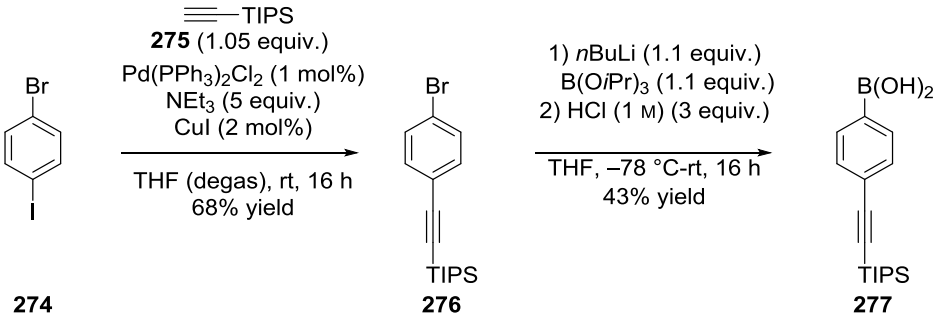

Figure 144: Synthesis of boronic acid 277 for use in Suzuki-Miyaura reactions.

With the desired boronic acid **277** in hand, Suzuki-Miyaura coupling was attempted with (*S*)-**268**. Disappointingly however, treatment of (*S*)-**268** and **277** in the presence of [Pd(IPr)(cin)Cl] **272** gave no observed product and returned only (*S*)-**268** along with degradation products (Figure 145).

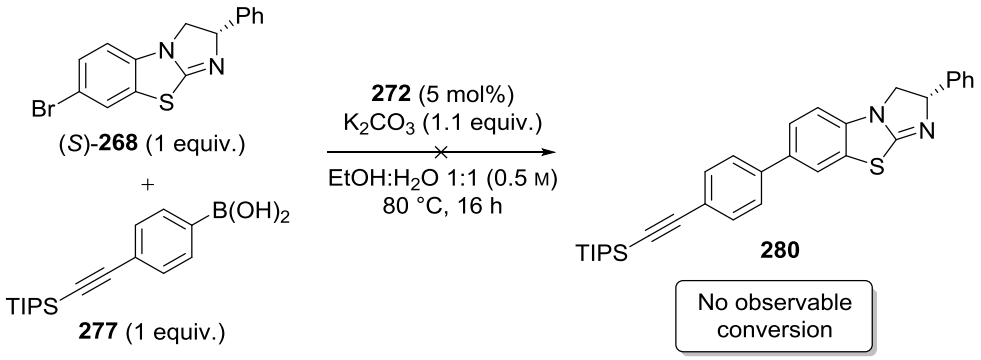

Figure 145: Attempted synthesis of (*S*)-BTM derivative 280 *via* Suzuki-Miyaura cross coupling.

Hiyama[268] and Hilt[269] have both reported the use of alkenyl halides for use in Suzuki-Miyaura cross-coupling reactions using aromatic boronic esters as coupling partners. Therefore, attempts were made to synthesise a boronic ester analogue of (*S*)-**268** and TMS protected alkynyl iodide **282**. Iodo TMS alkyne **282** was synthesised in one step from commercially available TMS-acetylene **281**. Reaction with *n*BuLi at −78 °C and subsequent quenching with I_2 afforded iodo-acetylene **282** in 82% yield (Figure 146). Synthesis of the boronic ester of (*S*)-**268** was attempted using both *n*-and *t*BuLi with a $B(OiPr)_3$ quench, but unfortunately this returned only degradation products after work up (Figure 147).

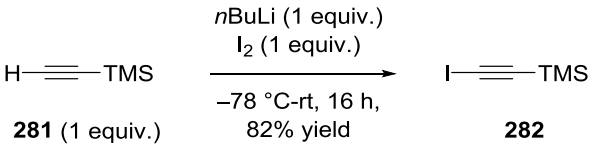

Figure 146: Synthesis of iodoalkyne 282.

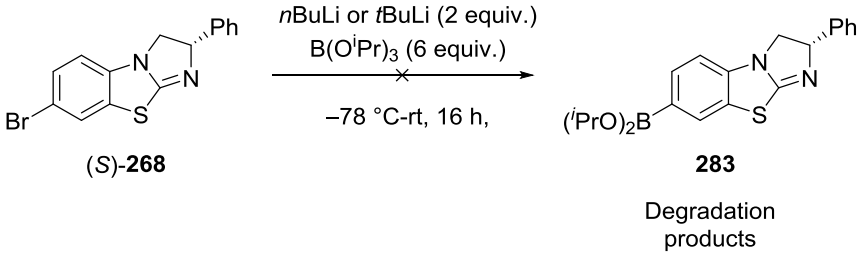

Figure 147: Attempted synthesis of boronic ester 283 using *t*BuLi.

4.4.4 Synthesis of PS-(*R*)-BTM using benzothiazole derivatives

As all attempts to introduce an alkyne directly onto BTM were unsuccessful, attention was turned to their incorporation *via* an oxygen linker. To this end, 2-amino-6-methoxybenzothiazole **286** was chosen as a viable starting point for the attempted synthesis of the (*R*)-**284**.

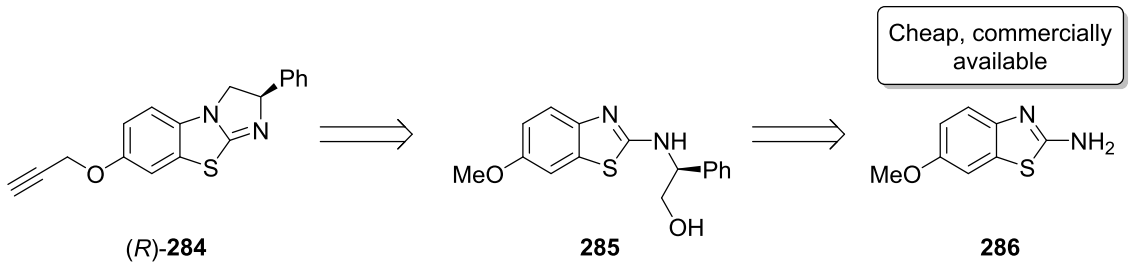

Figure 148: Retrosynthetic analysis of (*R*)-BTM analogue 284.

Initial attempts focused on the conversion of aniline **286** into aryl fluoride **289**, which may be capable of participating in an S_NAr reaction. Both the Sandmeyer[270] and Balz-Schiemann[271] reactions are known to afford aromatic halides *via* isolated or *in situ* formed diazonium

intermediates. This strategy was utilised to gain access to fluorbenzothiazole **289**. Commercially available 2-amino-6-methoxybenzothiazole **286** was tested under several reaction conditions using a variety of fluorine and nitrite sources (Table 19). Following a procedure outlined by Fukuhara,[272] a one-pot synthesis of fluorobenzothiazole **289** was attempted using HF·pyridine, however this protocol gave a mixture of products in the ^{1}H and ^{19}F NMR spectra (Table 19, Entry 1). A two-step procedure was next evaluated to try to isolate a stable tertrafluoroborate diazonium salt which, under thermal decomposition, are known to form aryl fluorides (Balz-Scheimann reaction). Several attempts to isolate the desired salt were unsuccessful (Table 19, entries 2-4) due to solubility issues. However, using *t*BuONO as a nitrite source allowed for the successful isolation of intermediate tetrafluoroborate salt **288** in 71% yield (Table 19, Entry 5).

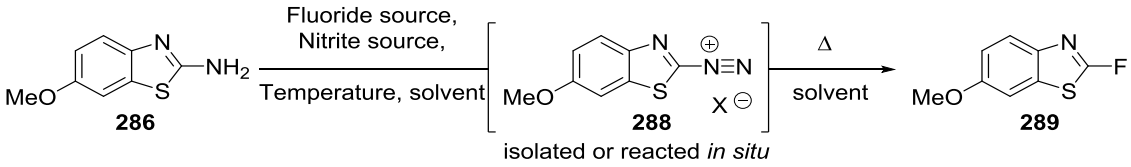

Entry	Fluoride source	Nitrite source	Solvent	Temperature (°C)	Diazonium 288 isolated (%)
1[a]	HF·pyridine	$NaNO_2$	neat	−30-rt then 50	No
2[b]	HBF_4 (8 M)	$NaNO_2$	HCl/H_2O	−5-rt	No
3[b]	HBF_4 (8 M)	$NaNO_2$	THF/H_2O	0	No
4[b]	HBF_4 (8 M)	$NaNO_2$	H_2O	0	No
5[b]	$BF_3{\cdot}OEt_2$	*t*BuONO	CH_2Cl_2	0	Yes (71)

Table 19: Conditions tested for the Sandmeyer and Balz-Schiemann reactions. [a]Conversion determined by ^{1}H NMR spectroscopic analysis of the crude reaction mixture after work up. [b]Conversion determined by ^{19}F and ^{11}B NMR spectroscopic analysis of the reaction mixture after work up.

Subsequent thermal decomposition was evaluated on diazonium salt **288**. Heating in *ortho*-dichlorobenzene at 135 °C gave small amounts of desired product **289**, but in low overall yield and as a mixture that included traces of starting material. Heating neat with a temperature increase of 80-130 °C showed no trace of product in the ^{1}H or ^{19}F NMR spectra.

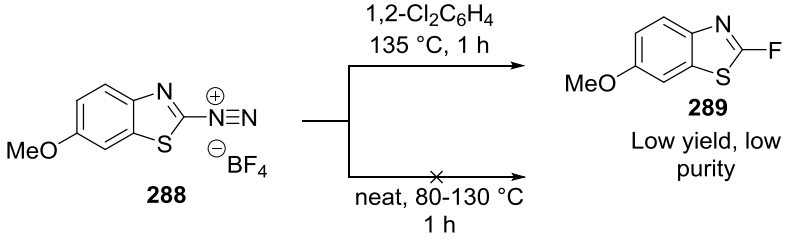

Figure 149: Attempted synthesis of fluorobenzothiazole 289.

As the conditions listed in Table 19 afforded only trace amounts of the product in low purity, synthesis of the analogous, but possibly less reactive, 2-chloro-6-methoxybenzo[*d*]thiazole **290** was attempted. 2-Amino-6-methoxybenzothiazole **286** was reacted with *tert*-butylnitrite in the presence of $CuCl_2$ and pleasingly this gave 2-chloro-6-methoxybenzo[*d*]thiazole **290** in 71% yield (Figure 150). This reaction can also be performed on a multi-gram scale with reproducible yields and purity.

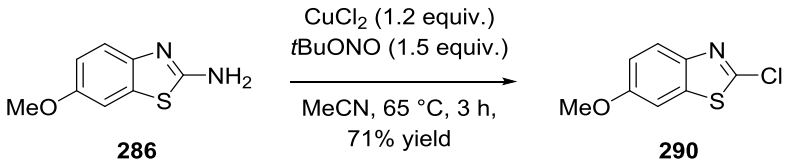

Figure 150: Synthesis of chlorobenzothiazole 290 using the Sandmeyer reaction.

With starting material in hand, 2-chloro-6-methoxybenzo[*d*]thiazole **290** was reacted with (*R*)-phenylglycinol **257** in the presence of *i*Pr_2NEt to afford amino alcohol **285** in a moderate 49% yield. Mesylation of alcohol (*R*)-**285** and heating gave the cyclised (*R*)-**291** BTM product in excellent yield (Figure 151).

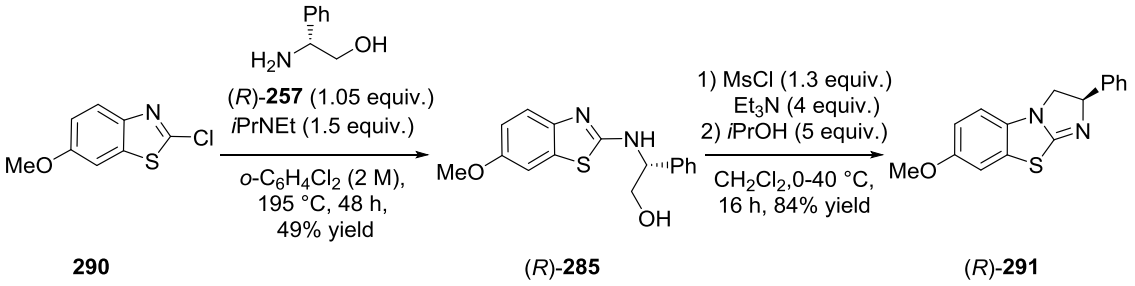

Figure 151: Synthesis of (*R*)-291 from the corresponding 2-chlorobenzothiazole.

With BTM derivative (*R*)-**291** in hand, a demethylation protocol was attempted using excess BBr_3. Pleasingly this gave the desired demethylated product (*R*)-**292** in good yield, isolated as the HBr salt (Figure 152).

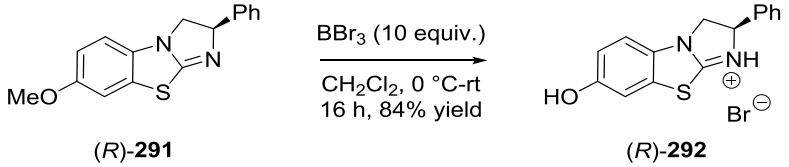

Figure 152: Synthesis of phenol BTM derivative (*R*)-292.

BTM derivative (*R*)-**292** was then subjected to a variety of conditions to attach the desired alkyne *via* an *O*-alkylation reaction. Propargyl bromide was used as the electrophile and a base screen

was conducted to obtain the optimum conditions. Initial attempts focused on milder bases such as K_2CO_3 which is known to facilitate *O*-alkylations.[251-253] However, reaction of (*R*)-**292** with propargyl bromide in the presence of K_2CO_3 in DMF gave no conversion (Table 20, entry 1). Increasing the amount of base, switching the solvent to acetone and using KI as an additive also gave no conversion (Table 20, entry 2). Increasing the equivalents of base used in DMF resulted in a small amount of conversion (15%) into the desired product **292** but this was not satisfactory. To obtain full deprotonation of the phenol, NaH was used in DMF but this gave a complex crude reaction mixture with no trace of product. Pleasingly, stirring in NaOH (2.2 equiv.) for 3 h prior to adding propargyl bromide gave a promising 60% conversion (Table 20, entry 5). Increasing the amount of base to four equivalents gave 80% conversion, allowed **292** to be isolated and a 41% yield (Table 20, entry 7) but five equivalents of NaOH resulted in decomposition products. Using Cs_2CO_3 as the base gave full conversion on a 0.1 mmol scale (Table 20, entry 9) but attempts to repeat this on a preparative scale were unsuccessful. The electrophile was then changed to the more reactive propargyl tosylate but this proved unsuccessful most likely due to solubility issues (Table 20, entry 10). Finally, the use of KO*t*Bu (2.6 equiv.) in a mixture of THF/DMSO at low temperature led to complete conversion, allowing **292** to be isolated in a good 68% yield after chromatography (Table 20, entry 11).

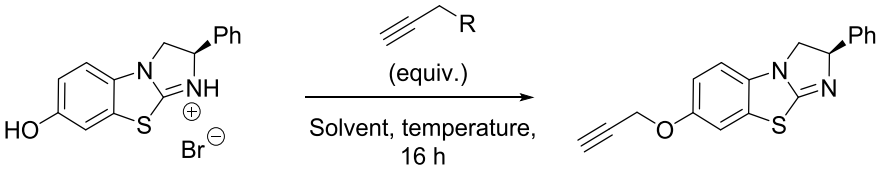

(*R*)-**292** (*R*)-**284**

Entry	Base (equiv.)	Solvent	R (equiv.)	Temperature (°C)	Conversion (%)[1] (yield %)
1	K_2CO_3 (2.2)	DMF	Br (1.1)	0-rt	0
2[a]	K_2CO_3 (5)	Acetone	Br (5.0)	rt	0
3	K_2CO_3 (6)	DMF	Br (1.1)	rt	15
4	NaH (6)	DMF	Br (1.1)	0-rt	0
5	NaOH (2.2)	DMSO	Br (1.05)	rt	60
6	NaOH (3)	DMSO	Br (1.5)	rt	74
7	NaOH (4)	DMSO	Br (1.1)	rt	80 (41)
8	NaOH (5)	DMSO	Br (1.1)	rt	0
9	Cs_2CO_3 (3)	DMF	Br (1.5)	rt	*c*
10[b]	KOH (3)	DMF/MeCN	OTs (1.3)	rt	0
11	KO*t*Bu (2.6)	THF/DMSO	Br	0-rt	100 (68)

Table 20: Reaction optimisation for *O*-alkylation of HBr salt (*R*)-292. Determined by ^{1}H NMR spectroscopic analysis of the crude reaction mixture. [a]KI (5 equiv.) was added to the reaction. [b]18-crown-6 (5 mol%) was used as an additive.[c]Only gave full conversion on small scale (0.1 mmol).

4.5 Synthesis of polymer-supported isothioureas

4.5.1 Attachment of propargyl BTM 292 to polymer support

Following a procedure outlined by Pericàs,[252] (azidomethyl)polystyrene **293** was synthesised in one step from commercially available (chloromethyl)polystyrene (Merrifield resin) (100-200 mesh). Merrifield resin **191** (*f* = 1.23 mmol/g) was treated with excess NaN_3 in DMSO resulting in the desired (azidomethyl)polystyrene **293** (Figure 153). Elemental analysis showed that the resulting functionalisation (*f*) was 1.20 mmol/g and a stretch in the IR spectum at 2094 cm^{-1} was indicative of an azide being present (Figure 154). The level of functionalisation (*f*) (mmol/g) was calculated based on nitrogen elemental analysis (% N) using the formula proposed by Pericàs (Equation 3).[273] This method of functionalisation calculation assumes 100% consumption of the starting azide (which is the case with **293**) based on the disppearence of the azide band in the IR spectrum. An alternative method for the calculation of functionalisation of PS-organocatalysts would be to subtract the expected contribution for the azide nitrogen atoms from the % N measured for the new organocatlayst resin using elemental analysis. This would give the increase in nitrogen content as a result of introducing the triazole appended functionalities and give an estimation of the % conversion of azides to the desired products.

$$f = \%N \times 1000 \times (\text{number of N atoms in functional unit})^{-1} \times (14.001)^{-1} \times 100^{-1}$$

Equation 3: Formula used to calculate catalyst loading on polystyrene resins

Figure 153: Conversion of Merrifield resin 191 to (azidomethyl)polystyrene 293.

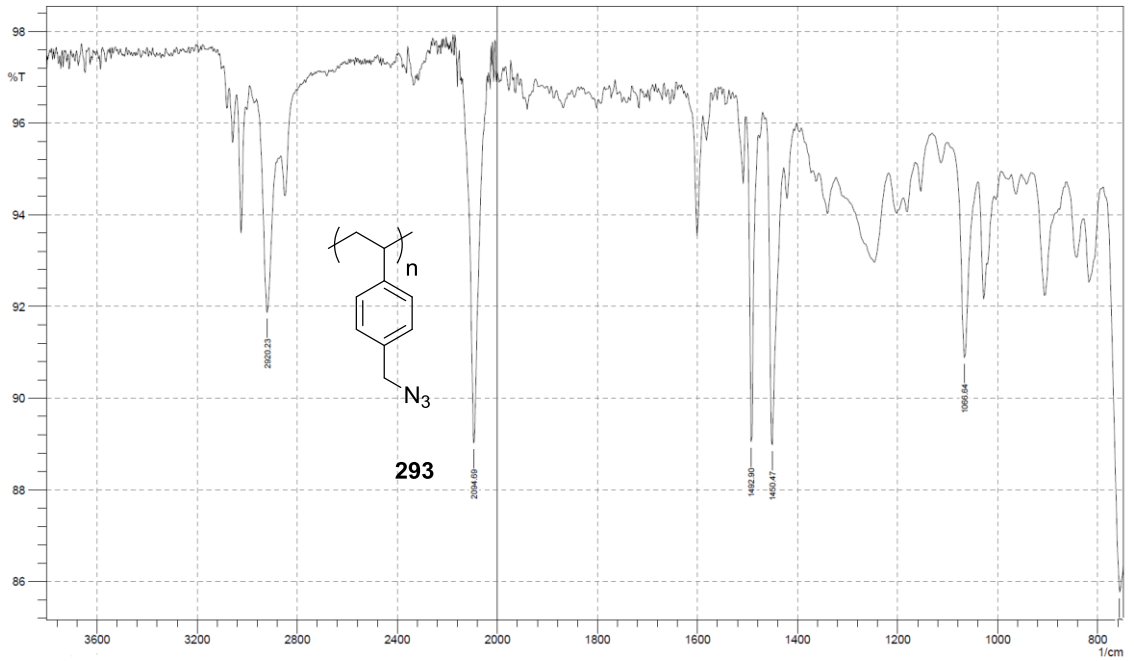

Figure 154: IR spectrum of azidomethyl(polystyrene) 293

With azidomethyl(polystyrene) in hand, propargyl BTM derivative **292** was attached to the PS *via* a click chemistry approach using a CuAAC reaction. In the presence of catalytic CuI and excess *i*Pr_2NEt, **292** was attached to PS-**293** and the progress of the reaction was conveniently monitored by disappearance of the azide band in the IR spectrum. A final loading of 0.93 mmol/g was calculated by nitrogen elemental analysis (Figure 155).

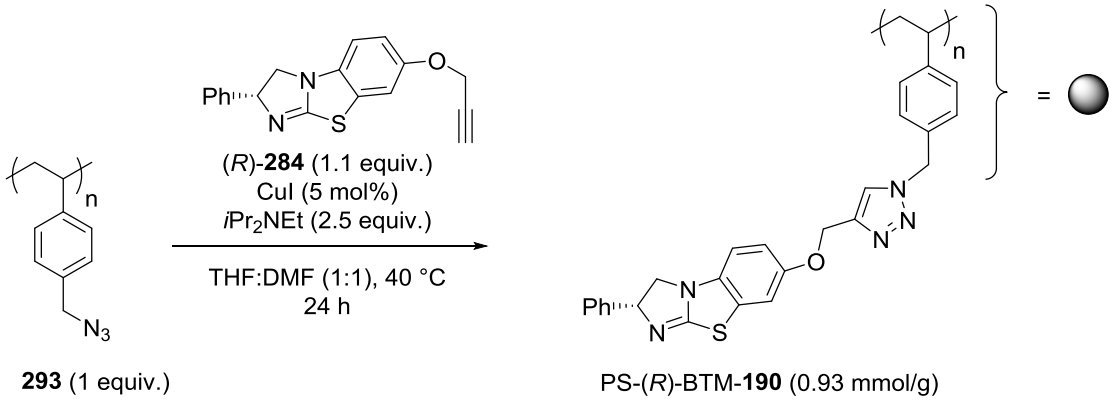

Figure 155: Attachment of propargyl BTM derivative 284 to azidomethyl(polystyrene) 293 using click methodology.

4.5.2 Attachment of propargyl HyperBTM 306 to polymer support

Using identical methodology developed for the synthesis of PS-(*R*)-BTM **191**, a propargyl derivative of (2*R*,3*S*)-HyperBTM was synthesised and attached to the same azidomethyl PS-**293**. Following the procedure outlined by Smith,[254] benzaldehyde **294** was reacted with *tert*-butyl carbamate **295** and sodium benzene sulfonate in the presence of formic acid to afford the carbamate **296** in excellent yield. Carbamate **296** was treated with K_2CO_3 in a CH_2Cl_2/H_2O

mixture to give the corresponding imine in good yield. Imine **297** was used immediately in an (*R*)-proline catalysed Mannich reaction with isovaleraldehyde **298** affording the *syn*-diastereoisomer of Boc-amino aldehyde (1*R*,2*R*)-**299** in excellent diastero and enantiocontrol (>95:5 dr, >99% ee). The absolute and relative configuration was assigned by comparison with the specific rotation and ^{1}H NMR spectroscopy in the literature.[101] Subsequent reduction of Boc-amino aldehyde (1*R*,2*R*)-**299** using $NaBH_4$ gave Boc-amino alcohol (1*R*,2*R*)-**300** in good yield. Finally, removal of the Boc-protecting group using HCl in dioxane afforded HCl salt (1*R*,2*R*)-**301** in 87% yield (Figure 156).

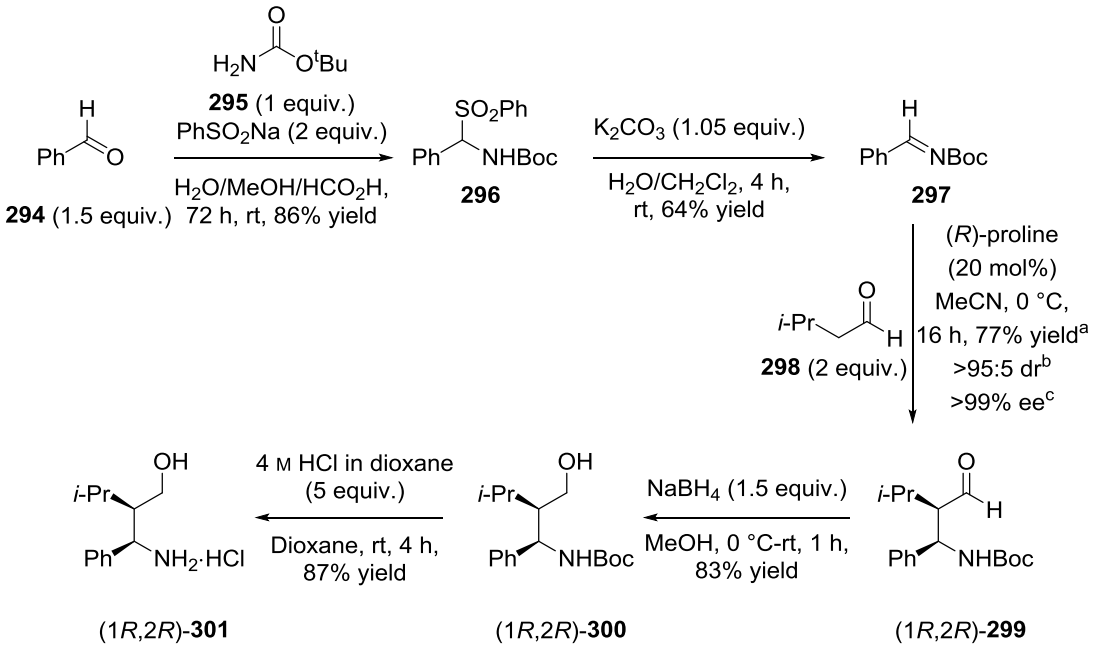

Figure 156: Synthesis of enantiopure amino alcohol (1*R*,2*R*)-301. [a]Isolated yield of major diastereoisomer of **298** (>95:5 dr). [b]Determined by ^{1}H NMR spectroscopy analysis of the crude reaction mixture. [c]Determined by chiral HPLC analysis

A stereochemical model explaining the diastero- and enantioselectivity of the proline-catalysed Mannich reaction has been proposed by Córdova *et al.* (Figure 157),[274] The model shows the enamine, formed upon reaction of (*R*)-proline with isovaleraldehyde **298**, reacting with the *Si* face of the *N*-Boc imine **297** that is stabilised by hydrogen boding with the catalyst. This arrangement directs the facial selectivity of the enamine. The *N*-Boc orients itself away from the pyrrolidine ring to minimise the energy of the pre-TS assembly, which results in a highly diasteroselectivity reaction.

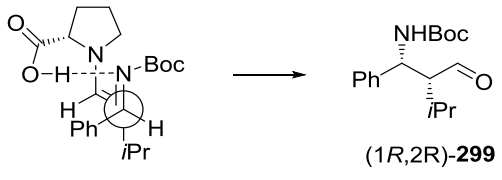

Figure 157: Pre-transition state assembly for the (*R*)-proline catalysed Mannich reaction.

Amino alcohol (1*R*,2*R*)-**301** was then subjected to the same reaction sequence as propargyl derivative (*R*)-BTM **284** (Section 4.4.4). Reaction with 2-chloro-6-methoxybenzo[*d*]thiazole **290** gave amino alcohol (1*R*,2*R*)-**302** which was isolated and used without further purification. Treatment with methane sulfonyl chloride in the presence of *i*Pr$_2$NEt at 40 °C afforded cyclised (2*R*,3*S*)-**303** in good yield. Demethylation of the methoxy group was achieved by treatment with BBr_3 to give the HBr salt (2*R*,3*S*)-**304** in excellent yield. Using previously optimised conditions (Entry 11, Table 20), (2*R*,3*S*)-**304** was successfully alkylated to give the desired propargyl derivative (2*R*,3*S*)-**306** in good yield (Figure 158).

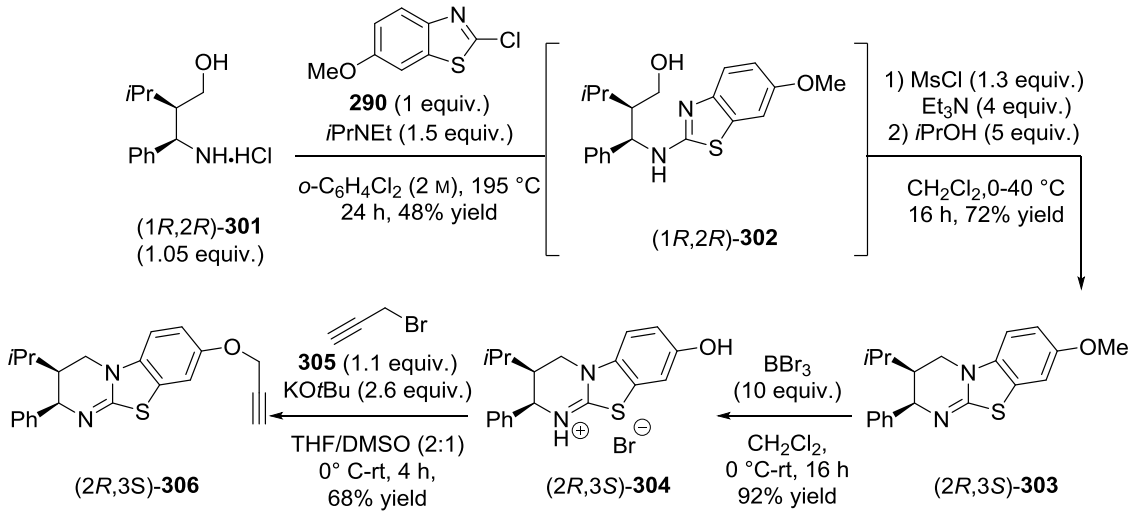

Figure 158: Synthesis of propargyl derivative (2*R*,3*S*)-306.

Propargyl derivative (2*R*,3*S*)-**306** was attached to the polymer-support using the same click methodology as before. In the presence of catalytic CuI and excess *i*Pr$_2$NEt, (2*R*,3*S*)-**306** was attached to azide PS-**293** and the progress of the reaction was conveniently monitored by disappearance of the azide band in the IR spectrum. A final loading of 0.97 mmol/g was calculated by nitrogen elemental analysis (Figure 159).

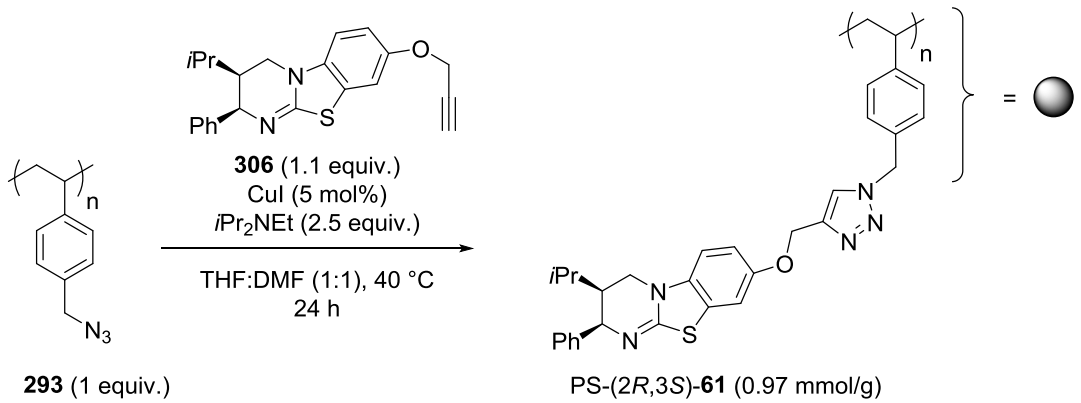

Figure 159: Attachment of propargyl derivative (2*R*,3*S*)-61 to azidomethyl(polystyrene) 293 using click methodology.

4.6 Initial investigation into heterogeneous Michael addition-lactonisation

With both PS-(*R*)-BTM **191** and PS-(2*R*,3*S*)-HyperBTM **60** in hand, their use in a Michael addition-lactonisation model reaction using phenylacetic acid **307** and trifluoromethylenone **308** could be investigated. Reaction conditions for the heterogeneous Michael addition-lactonisation were chosen based on the corresponding homogeneous Michael addition-lactonisation reaction developed within the Smith group. Using pivaloyl chloride as an activating agent and *i*Pr_2NEt as a base, PS-(*R*)-BTM **191** gave *anti*-dihydropyranone **309** with reasonable diastereoselectivity (81:19 dr) 2 h at 0 °C (entry 1 Table 22). Switching to PS-HyperBTM-(2*R*,3*S*) **61** gave *anti*-dihydropyranone **309** with reasonable diastereoselectivity (82:18 dr) after 2 h at 0 °C (Table 21, entry 1). Decreasing the temperature over an extended reaction period (2 h) gave full consumption of the starting material and a crude dr of 81:19 with the major diastereoisomers formed in an excellent 97% ee (Table 21, entry 2). Encouraged by this result, the reaction temperature was further decreased in order to improve the dr. Performing the reaction at −78 °C for 2 and 4 h did not give full consumption of the starting material however the isolated DHP **309** did have excellent ee's in both cases (Table 21, entries 3,4). Extending the reaction time to 6 h at −78 °C gave full consumption of the starting material (entry 5, Table 21) affording DHP **309** in 64% yield with high diastereo-and enantioselectivity. The catalyst loading was then decreased to 15 mol%, which gave an increase in yield and crude dr (88:12) while still maintaining a high level of enantioselectivity (98% ee). Attempts to lower the catalyst loading further were unsuccessful as 10 mol% of PS-HyperBTM-(2*R*,3*S*) **61** gave only a 40% conversion of the enone and a decreased crude dr (80:20). While both PS-(*R*)-BTM **191** and PS-HyperBTM-(2*R*,3*S*) **61** gave good results, only PS-(2*R*,3*S*)-(HyperBTM)-**61** was taken forward as the supported catalyst to evaluate in a recyclability study and several different reaction classes.

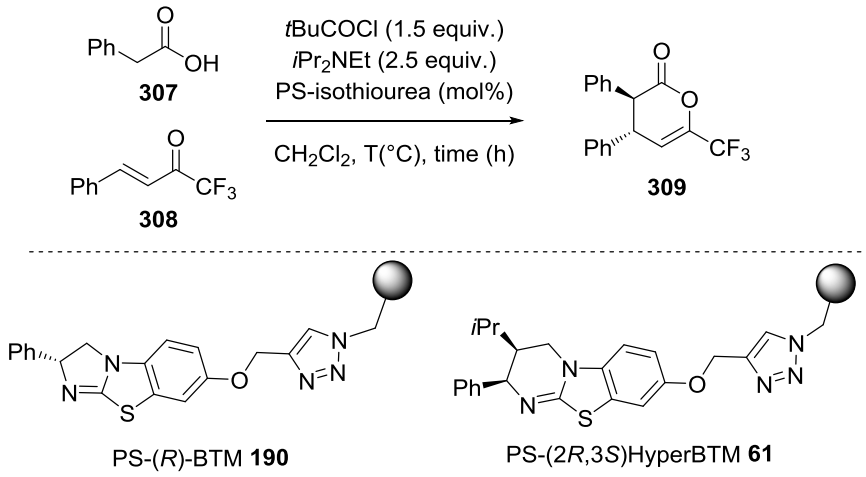

Entry	Isothiourea (mol%)	T (°C)	Time (h)	Conversion (%)[a]	Yield[b]	dr[a]	*ee* (%)[c]
1	PS-**191** (20)	0	2	100	56	81:19	72
2	PS-**61** (20)	0	2	100	72	82:18	97
3	PS-**61** (20)	−78	2	57	28	81:19	98
4	PS-**61** (20)	−78	4	70	35	85:15	99
5	PS-**61** (20)	−78	6	100	64	88:12	98
6	PS-**61** (15)	−78	6	100	66	89:11	99
7	PS-**61** (10)	−78	6	40	-[d]	80:20	-[d]

Table 21: Optimisation studies for heterogeneous Michael addition-lactonisation protocol. [a] Determined by ^{1}H NMR spectroscopic analysis of the crude reaction mixture. [b] Isolated yield of major diastereoisomer (>95:5 dr). [c] Determined by chiral HPLC analysis of major diastereoisomer. [d] Product not isolated from crude reaction mixture.

4.7 Kinetic resolution of secondary alcohols

Previous work within the Smith group has shown that HyperBTM **61** catalyses the acylative kinetic resolution (KR) of a range of secondary alcohols using propionic anhydrides, giving high levels of enantiodiscrimination between the two enantiomers of substrate (Figure 160). [275] The efficiency of a KR is characterised by the selectivity factor (s), which is defined as the ratio of the rate constants for the fast and slow reacting enantiomers of substrate. In practice the s-factor can be calculated using equations developed by Kagan (Equation 4),[276] which relate s to the reaction conversion (*c*) and the enantiomeric excess of the recovered alcohol (ee_{alc}). To be synthetically useful, the selectivity factor of a KR needs to be greater than $S = 10$.[277-278]

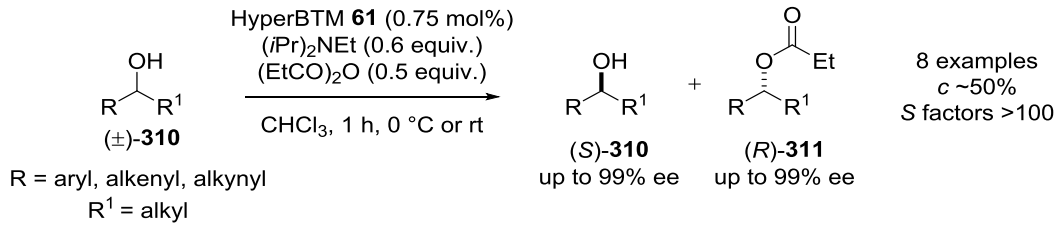

Figure 160: Kinetic resolution of secondary alcohols *via* enantioselective acylation.

$$s = \frac{\ln\left[(1-c)(1-ee_{SM})\right]}{\ln\left[(1-c)(1+ee_{SM})\right]} \qquad ee = \frac{[R]-[S]}{[R]+[S]}$$

ee = enantiomeric excess
c = conversion

$$c = \frac{ee_{SM}}{ee_P + ee_{SM}}$$

Equation 4: Derivation of selectivity factor, enantiomeric excess and conversion.

To evaluate the KR of secondary alcohols using PS-(2*R*,3*S*)-HyperBTM **61**, 1-(naphthalen-2-yl)ethan-1-ol **313** was chosen as a model substrate. Alcohol **313** was synthesised in one step from 2-naphthaldehyde **312** by reaction with methylmagnesium bromide to give **313** in 86% yield.

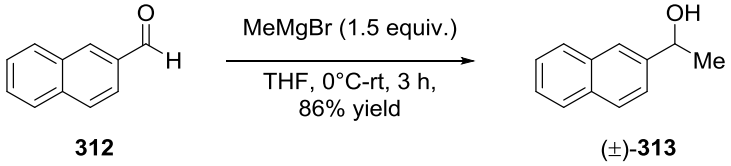

Figure 161: Synthesis of model substrate 1-(naphthalene-2-yl)prop-2-en-1-ol 313.

Under homogeneous conditions using HyperBTM **61**, alcohol **313** is resolved with s = 65. Reacting alcohol (±)-**313** with propionic anhydride (0.6 equiv.) in the presence of 5 mol% PS-(2*R*,3*S*)-HyperBTM **61** and *i*Pr$_2$NEt (0.6 equiv.) at 0 °C gave 56% conversion to ester (*R*)-**314** after 24 h. This allowed (*S*)-**313** to be recovered in >99% ee and (*R*)-**314** to be isolated in 78% ee, giving a calculated selectivity of *S* = 95 (Figure 162). The absolute configuration of the products were confirmed by specific rotation calculation and comparison with the literature in each case.

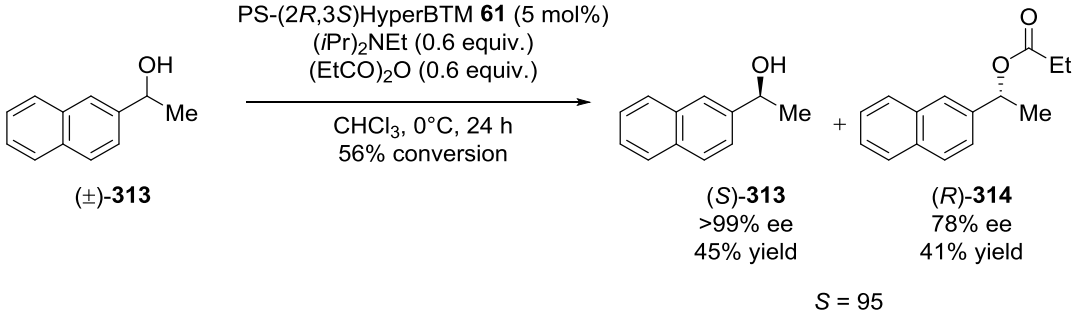

Figure 162: Acylative KR of secondary alcohols using PS-(2*R*,3*S*)-HyperBTM 61.

The high levels of selectivity observed is consistent with a preference for the (*R*)-enantiomer of the racemate to undergo esterification, which results in the isolation of the unreacted enantioenriched (*S*)-alcohol. This high selectivity can be rationalised by the stereochemical model proposed in Figure 163. The conformation of the key *N*-acyl ammonium is thought to be locked by a favourable n_o to $\sigma^*_{C\text{-}S}$ interaction between the carbonyl and the isothiourea sulfur atom (discussed in chapter 1). The pseudoaxial phenyl substituent on the catalyst blocks the *Re* face of the *N*-propionyl group. The enantiodiscrimination is proposed to be achieved through favourable interactions of the fast reacting enantiomer with *N*-acyl ammonium **315**. For example, there may be a favourable π-cation interaction between the aryl substituent on the alcohol and the catalyst, while π-π interactions between the extended napthyl ring and the benzenoid ring of the catalyst may provide additional stabilisation (Figure 163). While this stereochemical rationale was originally proposed for the homogeneous system, a similar sense of selectivity is observed in this

case therefore it can be postulated that a similar mechanism of ennantioenduction occurs. Pleasingly, this represents the first highly selective KR of secondary alcohols catalysed by a polymer-support isothiourea. Previous studies by Pericas and co-workers has shown that their version of PS-(*R*)-BTM **229** was unable to selectively catalyse this type of resolution (secondary benzylic alcohols), giving an s factor of 3.[249]

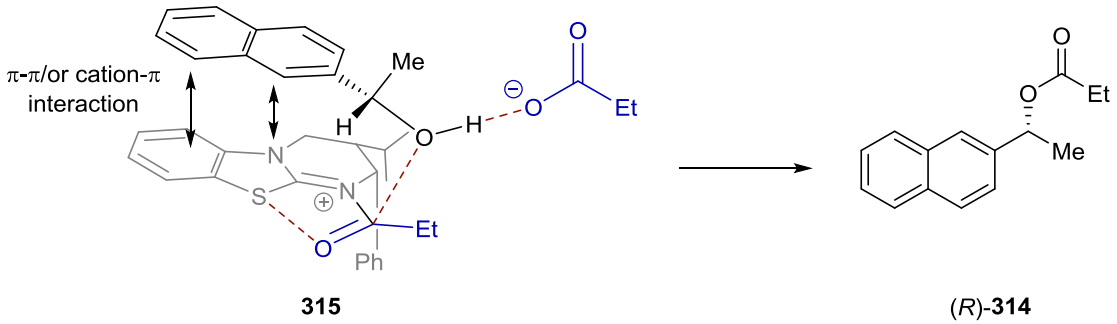

Figure 163: Proposed pre-transition state assembly accounting for the enantioselectivity of the kinetic resolution.

4.8 Kinetic resolution of tertiary alcohols

Work within the Smith group has shown that HyperBTM **61** can catalyse the efficient acylative kinetic resolution of tertiary heterocyclic alcohols under mild conditions using cheap and commercially available starting materials (Figure 164). Therefore, PS-(2*R*,3*S*)-HyperBTM **61** was also trialled in this process.

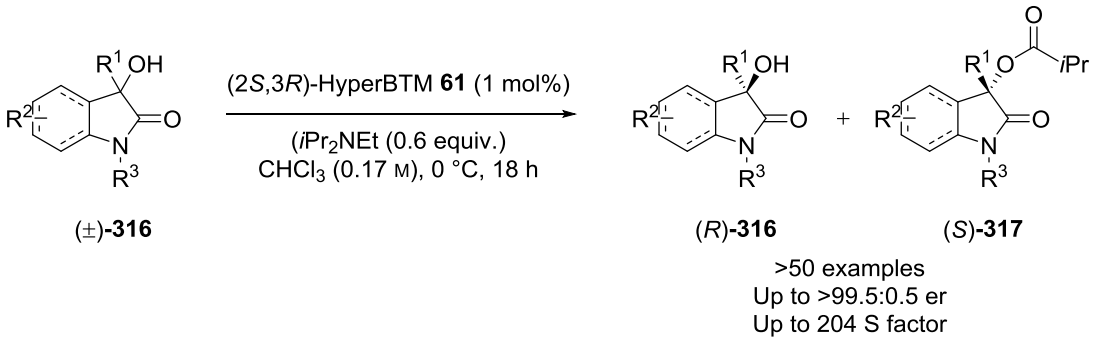

Figure 164: Acylative kinetic resolution of heterocyclic tertiary alcohols by HyperBTM 61.

Benzylphenyl indolinone **319** was used as the model substrate and was synthesised in a one-step procedure by addition of phenylmagnesium bromide to benzylindoline dione **318** affording **319** in 89% yield (Figure 165).†

†Synthesised and characterised by PDRA Dr Mark Greenhalgh.

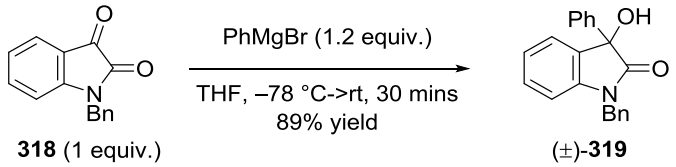

Figure 165: Synthesis of benzylphenyl indolinone 319 used in the kinetic resolution protocol.

Reaction conditions for the heterogeneous kinetic resolution of tertiary alcohols were chosen based on the already optimised corresponding homogeneous kinetic resolution within the Smith group. Using isobutyric anhydride and *i*Pr$_2$NEt as a base in $CHCl_3$ at 0 °C, PS-(2*R*,3*S*)-HyperBTM **61** (5 mol%) gave a s = 145 at 46% conversion after 24 h reaction time. The selectivity is higher and comparable to that obtained with the homogeneous system (s = 131) and this represents the first example of a KR of tertiary alcohols using a polymer-supported catalyst.

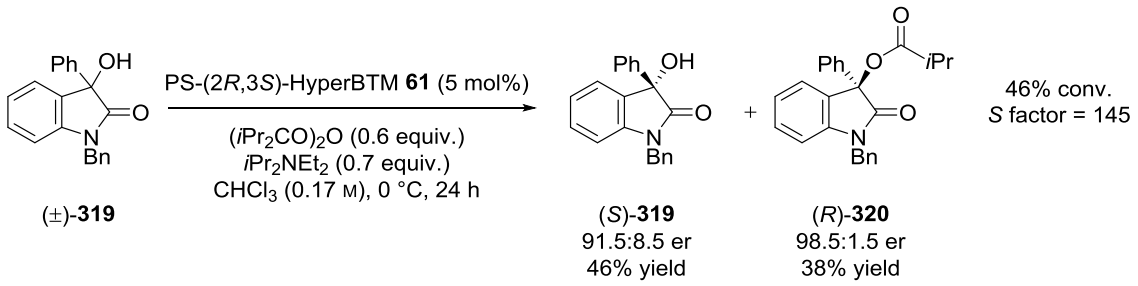

Figure 166: Kinetic resolution of tertiary heteroarmatic alcohols using PS-(2*R*,3*S*) HyperBTM-61.

In collaboration with Professor Paul Ha-Yeon Cheong at Oregon State University, a computational study for the stereochemical rationale was conducted for the homogeneous system.[†] The pre-transition state assembly for the fast reacting enantiomer of alcohol (*S*) of the ester was calculated to be 3.5 kcal/mol lower in energy than slow reacting enantiomer, which is in line with experimental observations. The pre-transition state assembly in Figure 167 shows the preference for the acylated intermediate to adopt a half-chair type conformation. Non-classical hydrogen bonding between the pseudo-equatorial hydrogen on the acylated catalyst and the carboxylate aids in the organisation of the pre-transition state assembly which further favours the conformation shown in Figure 167.

[†] Computational studies performed on (2*S*,3*R*)-HyperBTM **61**.

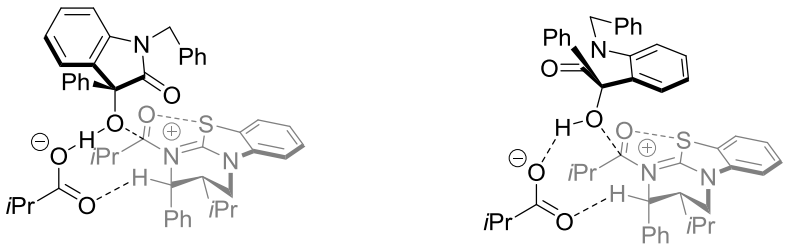

TS-*Major*-Acylation
321

TS-*Minor*-Acylation
322

Figure 167: Computationally calculated pre-transition state assembies for the kinetic resolution of tertiary alcohols.

4.9 Recyclability studies

Once high catalytic activity and versatility of PS-(2*R*,3*S*)-HyperBTM **61** in the KR of tertiary alcohols had been established, the robustness of the polymer-supported catalyst was tested. To this end, a recyclability study was performed on the KR of tertiary alcohols using optimised conditions (entry 8, Table 21). The experiments were carried out by fresh addition of reagents to PS-(2*R*,3*S*)-HyperBTM **61** and after 24 h at 0 °C the catalytic resin was filtered off from the reaction mixture and washed with EtOAc, before reuse. Pleasingly PS-(2*R*,3*S*)-HyperBTM **61** can be recycled up to 8 times without significant loss in selectivity. Throughout the recyclability study the er of the enantioenriched ester stayed high (entries 1-8, Table 22) while the er of the alcohol diminishes slightly as the conversion decreases. A noticeable result was run 6 (Table 22) where the conversion dropped significantly (23%). This results seems anomalous given the subsequent experiments (runs 7,8 Table 22) gave conversions similar to that obtained in previous runs (1-5, Table 22). Given the time constraints of this project there was no time to repeat the recyclability study.

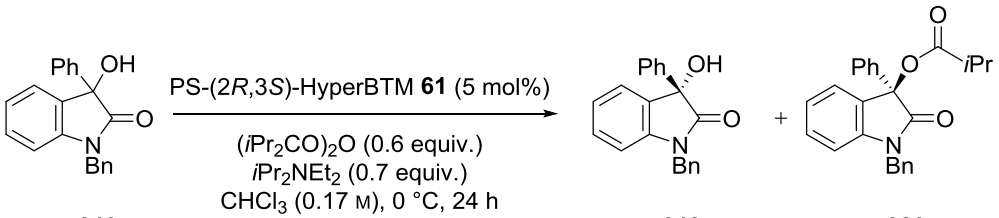

(±)-**319** (*S*)-**319** (*R*)-**320**

Run	Conversion (%)[a]	Alc. er[b] (% yield)[c]	Est. er[b] (% yield)[c]	*S*[d]
1	46	91.5:8.5 (46)	98:2 (38)	145
2	48	95:5 (36)	98:2 (34)	237
3	42	85.5:14.5 (43)	98:2 (37)	141
4	39	81:19 (42)	98:2 (33)	92

5	40	82:18 (42)	98.5:1.5 (35)	126
6	23	62:38 (45)	89:10 (17)	11
7	38	80:20 (42)	98:2 (34)	102
8	42	85:15 (43)	98:2 (38)	106

Table 22: Recyclability of PS-(2*R*,3*S*)-HyperBTM 61 in the kinetic resolution of tertiary alcohols. [a] Determined by ^{1}H NMR spectroscopy of the crude reaction mixture and chiral HPLC analysis. [b] Determined by chiral HPLC analysis. [c] Isolated yield after column chromatography. [d] Calculated using equations developed by Kagan (reference 280).

4.10 Catalytic enantioselective annulation of α,β-unsaturated acyl ammonium precursors

Previous work in the Smith group has shown that (*2S*,3*R*)-HyperBTM **61** can catalyse the enantioselective annulation of α,β-unsaturated acyl ammonium intermediates with 1,3-dicarbonyls, azaaryl ketones or β-ketoesters affording functionalised esters (upon ring-opening), dihydropyranones or dihydropyridones in good yield and selectivities (Figure 168).[279]

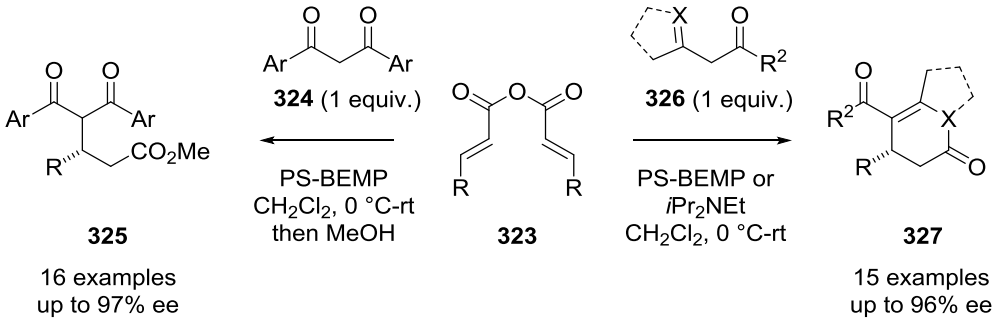

Figure 168: Enantioselective annulation of α,β-unsaturated acyl ammonium precursors.

The acyl ammonium intermediates can be generated from readily available α,β-unsaturated anhydrides. Based on this work, it was expected that PS-HyperBTM (2*R*,3*S*) **61** could act as a catalyst for the reaction of α,β-unsaturated acyl ammonium intermediates with 1,3-dicarbonyls giving a functionalised ester as the product. The desired homoanhydride can be generated from the appropriate α,β-unsaturated carboxylic acid by reaction with EDCI in CH_2Cl_2 at rt giving **329** in 65% yield (Figure 169).

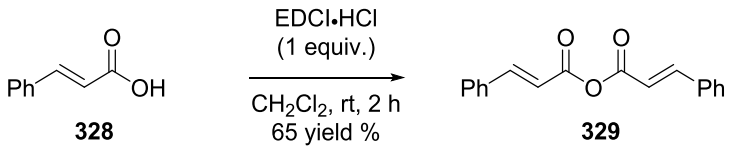

Figure 169: Synthesis of homoanhydride used as α,β-unsaturated acyl ammonium precursor.

Reaction conditions for the heterogeneous process were chosen based on the already optimised corresponding homogeneous system within the Smith group.[283] Homoanhydride **329** was reacted with PS-(2*R*,3*S*)-HyperBTM **61** (5 mol%) in the presence of 1,3-diphenyl-1,3-propanedione **330** and *i*Pr_2NEt as a base in CH_2Cl_2 at 0 °C and gradually warmed to rt over 5 h followed by ring-

opening *in situ* with MeOH. Pleasingly this protocol afforded the desired ring-opened functionalised ester **331** in 94% ee and 75 % yield, which is comparable with the homogeneous system (96% ee) (Figure 170).

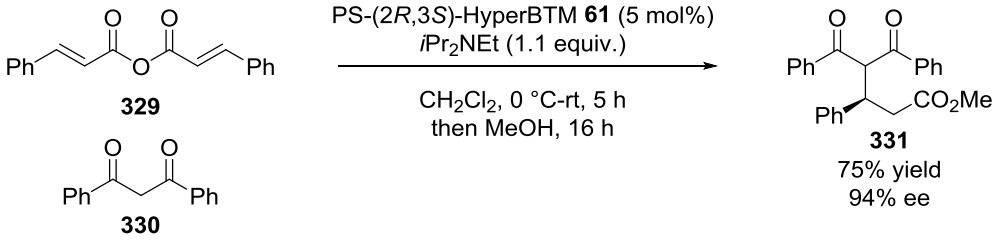

Figure 170: Use of PS-HyperBTM (2*S*,3*R*)-61 in the asymmetric annulation of α,β-unsaturated acyl ammonium precursors.

The catalytic cycle involve initial *N*-acylation of (2*R*,3*S*)-HyperBTM **61** with homoanhydride **329** generating the corresponding α,β-unsaturated acyl ammonium intermediate **334**. The *s-cis* conformation of ammonium **334** is favoured with the carbonyl oxygen atom adopting a *syn*-conformation with respect to the thiourea sulfur atom based on a non-bonding O-S interaction (n_o to $\sigma^*_{C\text{-}S}$) discussed previously. In the Michael addition pathway (Figure 171) addition of diketone enolate **330** to the *Re* face of ammonium **334** gives intermediate **335** with subsequent proton transfer followed by lactonisation generating dihydropyranone **336** or ester **331** by addition of MeOH. This work represents the first example of the use of a polymer-supported catalyst in the annulation of α,β-unsaturated acyl ammonium intermediates.

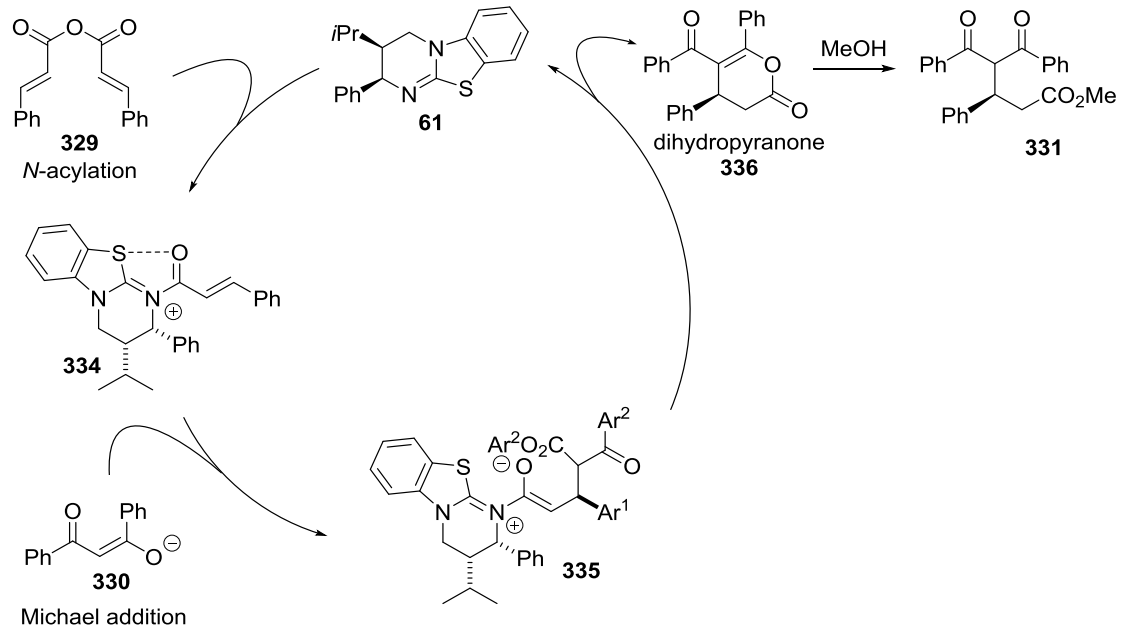

Figure 171: Proposed mechanisms of asymmetric dihydropyranone formation *via* Michael addition-lactonisation.

4.11 Conclusions and future outlook

Two isothiourea-based organocatalysts, PS-(2*R*,3*S*)-HyperBTM **61** and (*R*)-BTM **191**, were synthesised and attached to a polymer-support. PS-(2*R*,3*S*)-HyperBTM **61** was taken and evaluated in a variety of different reaction classes previously developed within the Smith group. PS-(2*R*,3*S*)-HyperBTM **61** shows promise in several model studies including a Michael addition-lactonisation procedure giving consistently high ee values (>97% ee) over an optimisation study.

Furthermore PS-(2*R*,3*S*)-HyperBTM **61** was evaluated in a model study for the KR of secondary alcohols, where its performance was comparable with the homogeneous counterpart affording both enantioenriched alcohol **313** (>99% ee) and ester **314** (78% ee) with an *S* factor of 95 at 56% conversion. Following on, PS-(2*R*,3*S*)-HyperBTM **61** also able catalyses the KR of heteroaromatic tertiary alcohols, a reaction which has not yet been performed in the literature using a polymer-supported catalyst. The resulting alcohol and ester were both highly enantioenriched with the process affording an excellent S factor of 172 at 46% conversion. These two examples show that PS-(2*R*,3*S*)-HyperBTM **61** can compete with the homogeneous system in terms of selectivity, yield and overall efficiency. PS-(2*R*,3*S*)-HyperBTM **61** can also be recycled up to 8 times without a major loss in conversion or selectivity. Further recyclability studies are need to fully validate the potential for PS-(2*R*,3*S*)-HyperBTM **61** to act as a catalyst in the KR of tertiary alcohols.

Finally PS-(2*R*,3*S*)-HyperBTM **61** was evaluated in a catalytic enantioselective annulation of α,β-unsaturated acyl ammonium precursors with 1,3-dicarbonyls. Results from the model study shown very similar levels of enantioselectivity (96% vs 94% ee) comparable with the homogeneous system. Again this work represents the first example of the use of a polymer-supported catalyst in the annulation of α,β-unsaturated acyl ammonium intermediates.

Future work in this area would be examination of the scope of all of the reaction classes discussed to assess the generality of the processes. More work is needed to examine the possible recyclability of the PS-(2*R*,3*S*)-HyperBTM **61** in the aforementioned catalytic processes. While PS-(2*R*,3*S*)-HyperBTM **61** was chosen as the optimal catalyst for these specific classes of reaction, (*S*)-BTM **191** is an efficient organocatalysts in the [2,3]-rearrangement of quaternary ammonium ylides[280] and as such PS-(*R*)-BTM may be applied to this methodology as a recyclable catalyst.

4.12 References and Notes

[220] R. B. Merrifield, *J. Am. Chem. Soc.* **1963**, *85*, 2149-2154.
[221] T. E. Kristensen, T. Hansen, *Eur. J. Org. Chem.* **2010**, *2010*, 3179-3204.

[222] S. V. Ley, I. R. Baxendale, R. N. Bream, P. S. Jackson, A. G. Leach, D. A. Longbottom, M. Nesi, J. S. Scott, R. I. Storer, S. J. Taylor, *J. Chem. Soc., Perkin Trans. 1* **2000**, 3815-4195.
[223] P. Hodge, *Ind. Eng. Chem. Res.* **2005**, *44*, 8542-8553.
[224] D. J. C. Constable, A. D. Curzons, V. L. Cunningham, *Green Chem.* **2002**, *4*, 521-527.
[225] P. H. Toy, K. D. Janda, *Tetrahedron Lett.* **1999**, *40*, 6329-6332.
[226] A. R. Vaino, D. B. Goodin, K. D. Janda, *J. Comb. Chem.* **2000**, *2*, 330-336.
[227] J. Lu, P. H. Toy, *Chem. Rev.* **2009**, *109*, 815-838.
[228] S. Zalipsky, J. L. Chang, F. Albericio, G. Barany, *React. Polym* **1994**, *22*, 243-258.
[229] T. Yamashita, H. Yasueda, N. Nakamura, *Chem. Lett.* **1974**, *3*, 585-588.
[230] H. Pracejus, G. Kohl, *Liebegs. Ann. Chem.* **1969**, *722*, 1-11.
[229] T. Yamashita, H. Yasueda, Y. Miyauchi, N. Nakamura, *Bull. Chem. Soc. Jpn.* **1977**, *50*, 1532-1534.
[230] K. Hermann, H. Wynberg, *Helv. Chim. Acta* **1977**, *60*, 2208-2212.
[231] P. Hedge, E. Khoshdel, J. Waterhouse, J. M. J. Frechet, *J. Chem. Soc., Perkin Trans. 1* **1985**, 2327-2331.
[232] M. H. Inagaki, J.; Yamamoto, Y.; Oda, **1987**, *60*, 4121-4126.
[233] R. Alvarez, M.-A. Hourdin, C. Cavé, J. d'Angelo, P. Chaminade, *Tetrahedron Lett.* **1999**, *40*, 7091-7094.
[234] A. M. Hafez, A. E. Taggi, T. Dudding, T. Lectka, *J. Am. Chem. Soc.* **2001**, *123*, 10853-10859.
[235] D. Nagai, T. Endo, *J. Polym. Sci. Pol. Chem.* **2009**, *47*, 653-657.
[236] M. Shekouhy, A. Khalafi-Nezhad, *Green Chem.* **2015**, *17*, 4815-4829.
[237] S. Matsukawa, T. Harada, S. Yasuda, *Org. Biomol. Chem.* **2012**, *10*, 4886-4890.
[238] F. Fringuelli, F. Pizzo, C. Vittoriani, L. Vaccaro, *Chem. Comm.* **2004**, 2756-2757.
[239] F. Fringuelli, F. Pizzo, C. Vittoriani, L. Vaccaro, *Eur. J. Org. Chem.* **2006**, *2006*, 1231-1236.
[240] T. Ishikawa, T. Heima, M. Yoshida, T. Kumamoto, *Helv. Chim. Acta* **2014**, *97*, 307-314.
[241] T. Ishikawa, Y. Araki, T. Kumamoto, H. Seki, K. Fukuda, T. Isobe, *Chem. Comm.* **2001**, 245-246.
[242] E. J. Delaney, L. E. Wood, I. M. Klotz, *J. Am. Chem. Soc.* **1982**, *104*, 799-807.
[243] A. Deratani, G. D. Darling, D. Horak, J. M. J. Frechet, *Macromolecules* **1987**, *20*, 767-772.
[244] F. Guendouz, R. Jacquier, J. Verducci, *Tetrahedron* **1988**, *44*, 7095-7108.
[245] A. Corma, H. Garcia, A. Leyva, *Chem. Comm.* **2003**, 2806-2807.
[246] J.-W. Huang, M. Shi, *Adv. Synth. Catal.* **2003**, *345*, 953-958.
[247] C. K.-W. Kwong, R. Huang, M. Zhang, M. Shi, P. H. Toy, *Chem. Eur. J.* **2007**, *13*, 2369-2376.
[248] G. P. Béatrice Pelotiera, Ian B. Campbell, Simon J. F. Macdonaldb, Mike S. Anson, *Synlett* **2003**, *5*, 679-683.
[249] J. Izquierdo, M. A. Pericàs, *ACS Catalysis* **2016**, *6*, 348-356.
[250] G. Chen, L. Tao, G. Mantovani, V. Ladmiral, D. P. Burt, J. V. Macpherson and D. M. Haddleton, *Soft Matter*, **2007**,*3*, 732-739.
[251] D. Font, S. Sayalero, A. Bastero, C. Jimeno, M. A. Pericàs, *Org. Lett.* **2008**, *10*, 337-340.
[252] D. Font, C. Jimeno, M. A. Pericàs, *Org. Lett.* **2006**, *8*, 4653-4655.
[253] P. Riente, J. Yadav, M. A. Pericàs, *Org. Lett.* **2012**, *14*, 3668-3671.
[254] B. Le Droumaguet, K. Velonia, *Macromol. Rapid Commun.* **2008**, *29*, 1073-1089.
[255] J. A. J. K. Mills, *Heterocyclic Chemistry*, 5th ed., Wiley-Blackwell, **2010**.
[256] A. Hugershoff, *Ber. Deut. Chem. Ges.* **1901**, *34*, 3130-3135.
[257] A. Hugershoff, *Ber. Deut. Chem. Ges.* **1903**, *36*, 3121-3134.
[258] A. Banerjee, S. K. Santra, S. K. Rout, B. K. Patel, *Tetrahedron* **2013**, *69*, 9096-9104.
[259] U. Heinelt, D. Schultheis, S. Jäger, M. Lindenmaier, A. Pollex, H. S. Beckmann, *Tetrahedron* **2004**, *60*, 9883-9888.
[260] K. Sonogashira, Y. Tohda, N. Hagihara, *Tetrahedron Lett.* **1975**, *16*, 4467-4470

[261] R. J. DeOrazio, J.-H. Maeng, D. D. Manning, B. A. Sherer, I. L. Scott, S. S. Nikam, *Synth. Commun.* **2011**, *41*, 3551-3555.
[262] E. J. Corey, P. L. Fuchs, *Tetrahedron Lett.* **1972**, *13*, 3769-3772.
[263] K. J. Schwarz, J. L. Amos, J. C. Klein, D. T. Do, T. N. Snaddon, *J. Am. Chem. Soc.* **2016**, *138*, 5214-5217.
[264] Personal communication with PhD colleague Stephanie Spoehrle.
[265] X. Jiang, J. J. Beiger, J. F. Hartwig, *J. Am. Chem. Soc.*, **2017**, *139*, 87–90.
[266] N. Miyaura, A. Suzuki, *J. Chem. Soc., Chem. Commun.* **1979**, 866-867.
[267] F. Izquierdo, M. Corpet, S. P. Nolan, *Eur. J. Org. Chem.* **2015**, *2015*, 1920-1924.
[268] T. Kurahashi, T. Hata, H. Masai, H. Kitagawa, M. Shimizu, T. Hiyama, *Tetrahedron* **2002**, *58*, 6381-6395.
[269] G. Hilt, K. I. Smolko, *Angew. Chem. Int. Ed.* **2003**, *42*, 2795-2797.
[270] T. Sandmeyer, *Ber. Deut. Chem. Ges.* **1884**, *17*, 1633-1635.
[271] G. Balz, G. Schiemann, *Ber. Dtsch.H. Chem. Ges.* **1927**, *60*, 1186-1190.
[272] N. Yoneda, T. Fukuhara, *Tetrahedron* **1996**, *52*, 23-36.
[273] A. Bastero, D. Font, M. A. Pericàs, *J. Org. Chem.* **2007**, *72*, 2460-2468.
[274] J. Vesely, R. Rios, I. Ibrahem, A. Córdova, *Tetrahedron Lett.* **2007**, *48*, 421-425.
[275] D. Belmessieri, C. Joannesse, P. A. Woods, C. MacGregor, C. Jones, C. D. Campbell, C. P. Johnston, N. Duguet, C. Concellon, R. A. Bragg, A. D. Smith, *Org. Biomol. Chem.* **2011**, *9*, 559-570.
[276] G. Balavoine, A. Moradpour, H. B. Kagan, *J. Am. Chem. Soc.* **1974**, *96*, 5152-5158.
[277] J. F. L. J. M. Keith, E. N. Jacobsen, *Adv. Synth. Catal.* **2001**, *343*, 5-26.
[278] H. B. Kagan, J. C. Fiaud, in *Topics in Stereochemistry*, John Wiley & Sons, Inc., **2007**, pp. 249-330.
[279] E. R. T. Robinson, C. Fallan, C. Simal, A. M. Z. Slawin, A. D. Smith, *Chem. Sci.* **2013**, *4*, 2193-2200.
[280] T. H. West, D. S. B. Daniels, A. M. Z. Slawin, A. D. Smith, *J. Am. Chem. Soc.* **2014**, *136*, 4476-4479.

Chapter 5 : Conclusions and Outlook

This thesis has described investigations into applications of isothioureas in surface chemistry. State-of-the-art methodology has been developed for the chiral discrimination of enantioenriched surfaces as well as the synthesis of novel polystyrene-supported recyclable organocatalysts.

Firstly, the DHBP catalysed synthesis of a small library of racemic dihydropyranones on a SAM has been achieved through a Michael addition-lactonisation procedure using a range of arylacetic acids (Figure 172). The conversions in this process range from 40-70% and as such this methodology offers an effective route to build a variety of complex surfaces containing these functionalities. The consistency of this methodology suggests that a wide range of phenylacetic derivatives could be applied providing a flexible methodology for facile surface functionalisation.

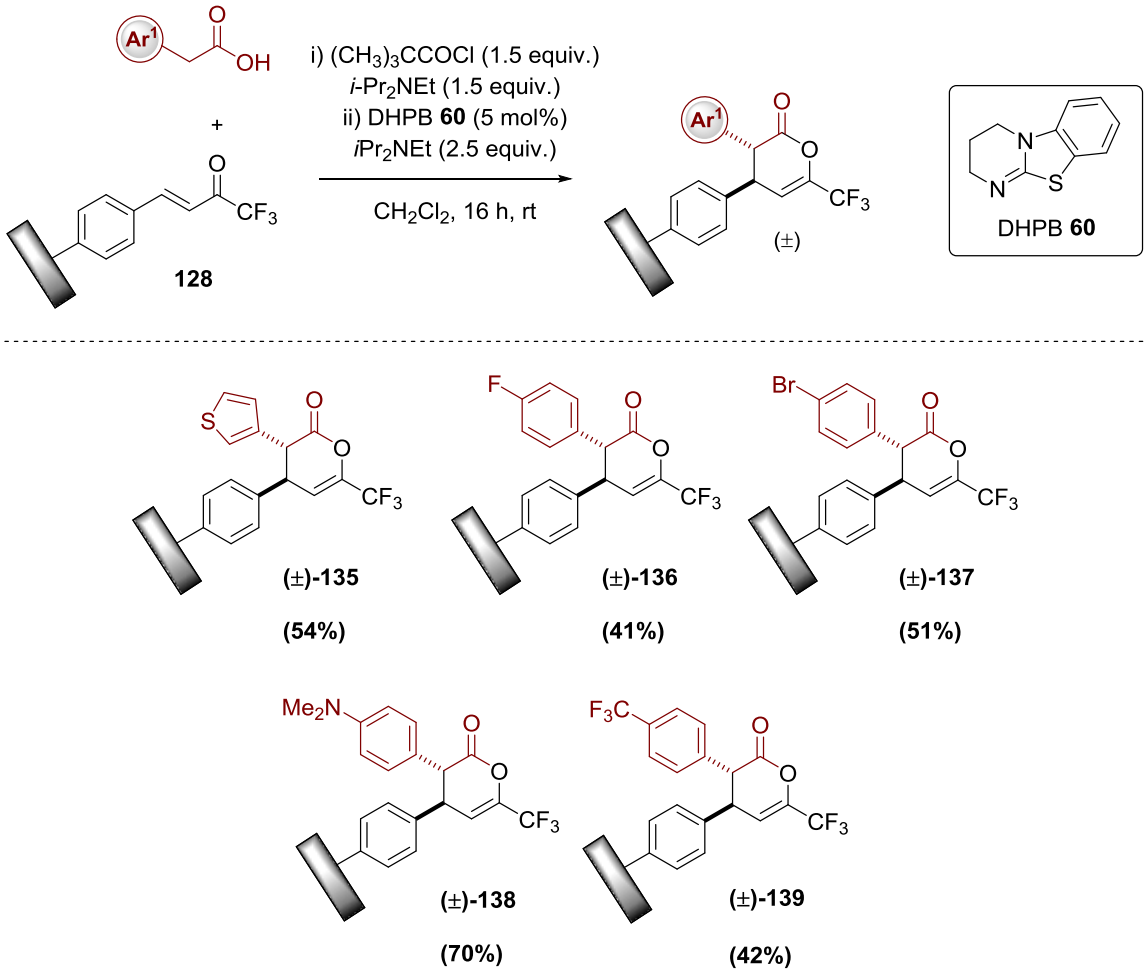

Figure 172: Michael addition-lactonisation of trifluoromethylenones on a surface using DHPB.

Following the initial report on the synthesis of racemic dihydropyranones on a surface, attention was focused towards the development of an asymmetric protocol. Both enantiomers of

HyperBTM **61** were used to synthesis surfaces that consisted of an enantiomeric excess of one particular enantiomer ((3*R*,4*R*), (3*S*,4*S*)) of DHP (Figure 173) A novel chiral AFM probe tip **179** was also developed and tested in the system against the enantioenriched surfaces giving a reasonable level of discrimination in the majority of cases. Both enantiomers of the enantioenriched DHP were also synthesised in solution then attached to the surface using click chemistry methodology. The results from this show that regardless of fabrication method, both types of surfaces give similar adhesion values, within error of each other, suggesting that similar chiral discrimination events are happening on the surfaces as well as comparable molecular packing of the surfaces. While the current methodology does not allow for the quantification of the level of enantioinduction imparted on the surfaces there is some evidence that the same sense of enantioenduction is occurring, that is, the same enantiomer is being formed in the solution phase homogeneous system as the heterogeneous, however contradictory results demand further investigation. Evidence for this hypothesis comes from the results obtained in the experiments conducted using the pre-synthesis enantioenriched DHPs. They show very similar results to those obtained in the heterogeneous system, suggesting similar molecular packing and possibly implying a significant enantiomeric excess. Further experiments using surfaces and probe tips of varying ee to test possible non-linear effects are needed to confirm this theory. Subsequent endeavours within the area of surface functionalisation of the discussed SAMs will aim to attach desired functional groups in a selective manner and possibly use as model systems for chiral selectors in enantioselective reactions.

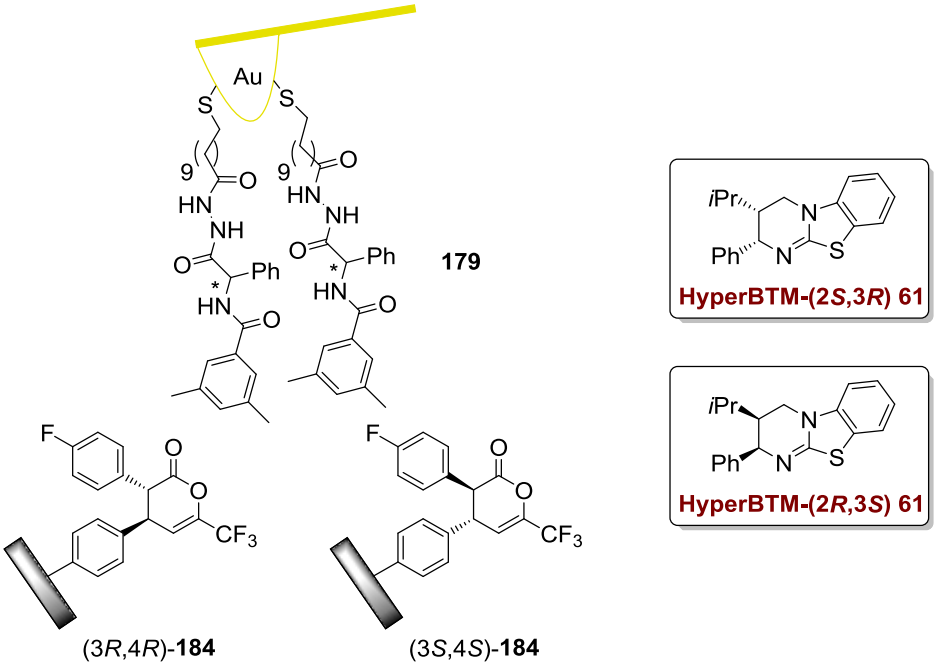

Figure 173: Chiral AFM probe evaluated in the chemical force microscopy of enantioenriched dihydrpyranones.

Two novel polymer-supported isothiourea organocatalysts were synthesised and evaluated in several different reaction classes previously developed within the Smith group. The supported catalyst PS-(2*R*,3*S*)-HyperBTM **61** showed promise in a optimisation study for a Michael addition-lactonisation process giving consistently high ee values (≥97% ee) (Figure 174). Furthermore, PS-(2*R*,3*S*)-HyperBTM **61** was evaluated in the KR of both secondary aryl and tertiary heteroaromatic alcohols giving high selectivity in both cases (up to *S* of 171). PS-(2*R*,3*S*)-HyperBTM **61** was also shown to be recyclable in the KR of tertiary heteroaromatic alcohols over at least 8 runs with no major loss in selectivity. Finally, PS-(2*R*,3*S*)-HyperBTM **61** was shown to be an effective catalyst in the enantioselective annulation of α,β-unsaturated acyl ammonium precursors with 1,3-dicarbonyls. Results show very similar levels of enatioselectivity (96% vs 94%) to those previously reported. This work represents the first example of KR of tertiary heteroaromatic alcohols and also annulation of α,β-unsaturated acyl ammonium intermediates using a polymer-supported catalyst. While PS-(2*R*,3*S*)-HyperBTM **61** was shown to work in a variety of processes using model substrates (Figure 174), more work is need to evaluate recyclability of the catalyst in different reaction processes as well as optimisation studies to lower catalyst loadings to assess the true robustness of this particular isothiourea catalyst.

While PS-(2*R*,3*S*)-HyperBTM **61** was chosen as the optimal catalyst for these specific classes of reaction, PS-(*R*)-BTM **191** was also synthesied and is known to catalyse a series of reaction classes. For example, PS-(*R*)-BTM **191** is an efficient organocatalysts in the [2,3]-rearrangement of quaternary ammonium ylides[284] and as such PS-(*R*)-BTM may be applied to this methodology as a recyclable catalyst however due to time constraints this could not be fully evaluated.

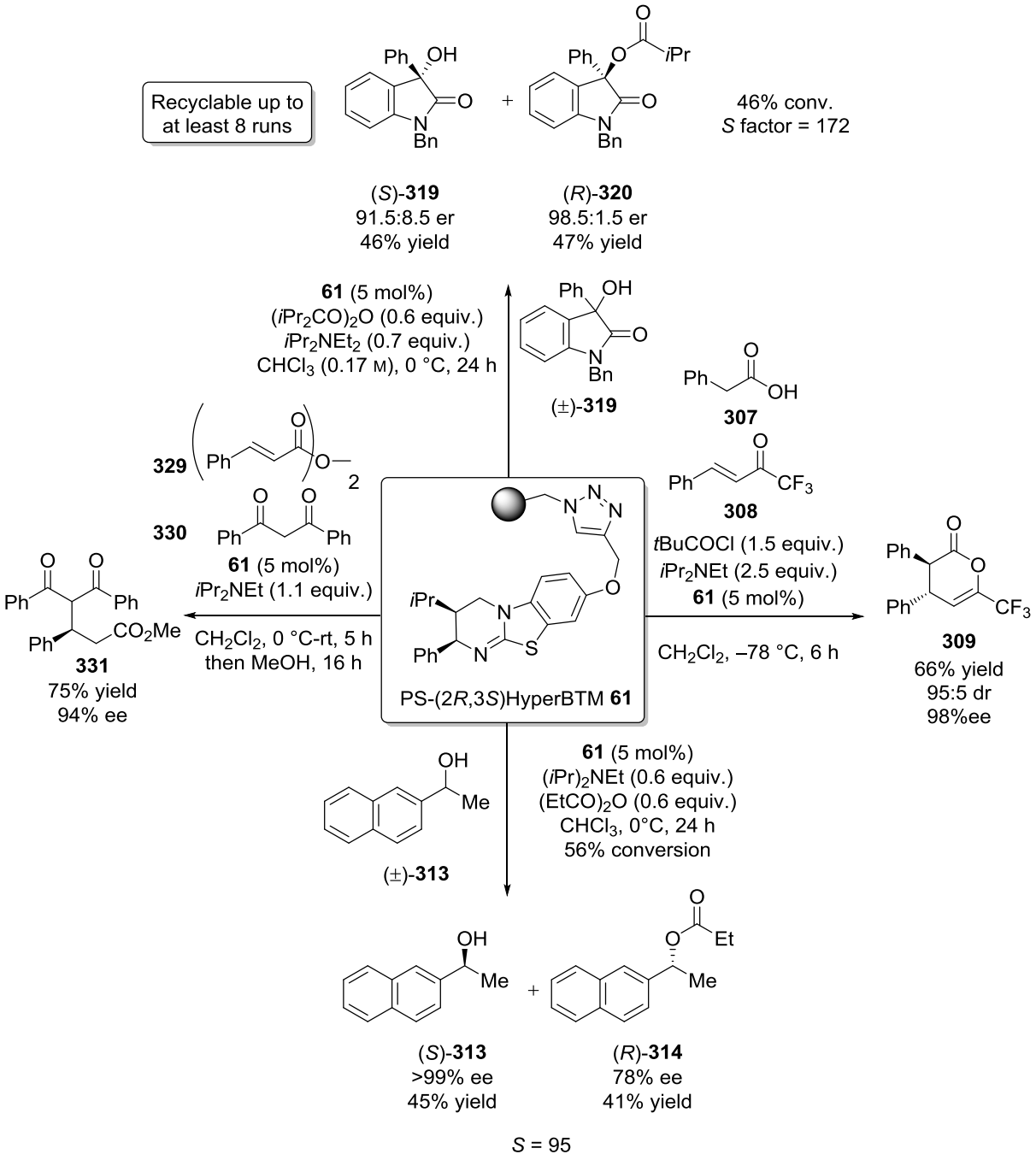

Figure 174: Summary of processes catalysed by PS-(2*R*,3*S*)-HyperBTM 61.

Chapter 6 Experimental

6.1 General Information

Reactions involving moisture sensitive reagents were carried out under a nitrogen atmosphere using standard vacuum line techniques in addition to dry solvents. All glassware used was flame dried and cooled under vacuum. For moisture sensitive reactions, solvents (THF, CH_2Cl_2, toluene, and Et_2O) were obtained anhydrous and purified by an alumina column (Mbraun SPS-800). Pet. ether is defined as petroleum ether 40-60 °C. All other solvents and commercial reagents were used as supplied without further purification unless stated otherwise. Room temperature (rt) refers to 20-25 °C. Temperatures of 0 °C and −78 °C were obtained using ice/water and CO_2(s)/acetone baths respectively. Reflux conditions were obtained using an oil bath or DrySyn® equipped with a contact thermometer. *In vacuo* refers to the use of a Büchi Rotavapor R-2000 rotary evaporator with a Vacubrand CVC2 vacuum controller or a Heidolph Laborota 4001 rotary evaporator with a vacuum controller.

Analytical thin layer chromatography was performed on pre-coated aluminium plates (Kieselgel 60 F254 silica). Plates were visualised under UV light (254 nm) or by staining with either phosphomolybdic acid or $KMnO_4$ followed by heating. Flash column chromatography was performed on Kieselgel 60 silica or Biotage® IsoleraTM 4, using Biotage® Snap Ultra or Biotage® KP Sil columns (CV = column volume) under the solvent system stated.

Melting points were recorded on an Electrothermal 9100 melting point apparatus, dec refers to decomposition.

HPLC analyses were obtained on a Shimadzu HPLC consisting of a DGU-20A5 degasser, LC-20AT liquid chromatography SIL-20AHT autosampler, CMB-20A communications bus module, SPDM20A diode array detector and a CTO-20A column oven that allows the temperature to be set from 25-40 °C. Separation was achieved using a Chiralcel OJ-H or Chiralpak AD-H column.

GC analyses were obtained on a Shimadzu GC-2025 consisting of an AOC-20i auto injector, SPL1 injection port, column oven and flame ionisation detector (FID). Helium (He) was used as the carrier gas in split injection mode at constant linear velocity. An Agilent DB-5 analytical column was used for analyses (30 m, 0.25 mm ID, 0.5 μm film thickness).

Infrared spectra (ν_{max}) were recorded on a Shimadzu IRAffinity-1 Fourier transform IR spectrophotometer using either thin film or solid using Pike MIRacle ATR accessory. Analysis was carried out using Shimadzu IRsolution v1.50 and only characteristic peaks are reported.

^{1}H, ^{13}C{^{1}H}, ^{19}F{^{1}H} ^{11}B and ^{29}Si NMR spectra were acquired on either a Bruker Avance 300 {δ_H (300 MHz), δ_C (75 MHz), δ_F (282 MHz), δ_{Si} (60 MHz)}, a Bruker Avance II 400 {δ_H (400 MHz), δ_C (100 MHz), δ_F (376 MHz), δ_B (128 MHz), δ_{Si} (60 MHz)}, Bruker Ultrashield 500 {δ_H (500 MHz), δ_C (126 MHz), δ_F (471 MHz), δ_{Si} (79 MHz)} or a Bruker AVIII-HD 700 {δ_H (700 MHz), δ_C (175 MHz)} spectrometer at ambient temperature (unless otherwise stated) in the deuterated solvent stated. Chemical shifts, δ, are quoted in parts per million (ppm) and are referenced to the residual solvent peak. Coupling constants, *J*, are quoted in Hertz (Hz) to the nearest 0.1 Hz. The following abbreviations are used: s, singlet; d, doublet; t, triplet; q, quartet; dd, doublet of doublets; ddd, doublet of doublet of doublets; dt, doublet of triplets; ddt, doublet of doublets of triplets; dtt, doublet of triplets of triplets; dq, doublet of quartets; td, triplet of doublets; ttd, triplet of triplets of doublets; tt, triplet of triplets; m, multiplet; and br, broad.

Mass spectrometry (HRMS)

Mass spectrometric (*m/z*) data was acquired by electrospray ionisation (ESI), electron impact (EI) or chemical ionisation (CI), either at the University of St Andrews Mass Spectrometry facility (quoted [M+H]) or from the EPSRC National Mass Spectrometry Service Centre, Swansea (quoted $[M+H]^+$).

Elemental analysis was carried out by the analytical services at London Metropolitan University and obtained for the determination of carbon, hydrogen and nitrogen analysis (%CHN). All values are quoted in mass percentage (%).

X-Ray photoelectron spectroscopy analysis was performed either at the University of Newcastle (NEXUS at nanoLAB) or at the University of St Andrews. St Andrews X-ray photoelectron spectroscopy spectra were obtained on a Scienta ESCA 300 instrument; all spectra were obtained using monochromated Al Ka radiation at 1486.6 eV. Survey scans were obtained using a pass energy of 300eV and the detailed scans at 150 eV, giving a resolution of approximately 0.8 eV on the detailed scans. All spectra were collected at normal emission, the operating pressure of the instrument is below $5x10^{-9}$ mbar. The XPS spectra were corrected for charging by referencing the aliphatic C 1s peak of hydrocarbons to 284.6 eV. Elemental compositions of the various surfaces were determined from the area under individual elemental peaks using sensitivity factors provided with the software as well as taking the transmission

function of the analyser into account. CasaXPS (Casa Software Ltd., UK) was used for the analysis. The spectra were fitted using Gaussian/Lorentzian peak shapes with a ratio of 70%/30%. A Shirley background was subtracted for the quantitative analysis.

Water contact angles (DI water) were measured with a G10 goniometer microscope (KRÜSS GmbH, Hamburg, Germany) under ambient conditions at room temperature. Droplets of ~3 µL were dispensed from a microburette. All reported values are the average of three measurements taken from different places of the surface.

Ellipsometry analysis was measured with an M-2000DI™ spectroscopic ellipsometer (J. A. Woollam Co., Inc., USA). Thickness values were extracted from fits to the data taken from 45 to 70° in steps of 5° over wavelengths from 200 to 1000 nm. The sample surface was modelled as a Si substrate with an oxide layer and a Cauchy layer. The thickness of the silicon oxide after the oxidative cleaning treatment was 16 ± 1 Å (average of three samples). The thickness of the monolayer films was calculated with a refractive index of 1.45. The error based on the observed variation of the thickness of the organic films prepared under identical conditions was ~2 Å.

Atomic Force Microscopy (AFM) images were obtained using Bruker Dimension Icon AFM system. AFM images were collected in the PeakForce Tapping™ mode using V-shaped cantilevers of nominal spring constant 0.58 N/m (Veeco SNL-A) with a peak force set point of around 1-4 nN and scan rate of 1 Hz. The RMS roughness of the surfaces was characterized from 1×1 µm^2 images of 512×512 pixels after appropriate image levelling. Quoted roughness values were calculated from an average of at least two samples and three images of each sample.

AFM force curve collection. A Bruker Dimension Icon AFM system was used to collect force curves between the thiol SAM coated AFM tip (Au coated Veeco SNL-B or SNL-D) and a modified surface in Millipore filtered deionized water. Force curves were collected at a ramp rate of ~1 Hz with 0.5 s of surface dwell time, with a ramp size of 200-500 nm, and with the maximum deflection minimized on a cantilever by cantilever basis to be as small as possible (typically ~0.5-8.0 nm). For each tip – sample system 25 force curves were collected in 5×5 grids in each of four different 500×500 nm^2 areas resulting in 100 force curves per surface. The same tip was used to interrogate multiple samples sequentially without alteration of optical readout positioning. Repeat measurements of samples were executed to check for tip changes. The modified tips were not used for imaging to preserve the thiol coating.

Section 6.2 contains the synthetic and experimental procedures for bulk reagents and catalysts that were used on multiple occasions throughout this work. *Section 6.3* describes all other compounds in the order in which they appear in the text.

6.2 Synthesis of Bulk reagents and Catalysts

1-Hydroxy-1-oxo-1λ^5-benzo[*d*][1,2]iodaoxol-3(1*H*)-one (IBX) 337

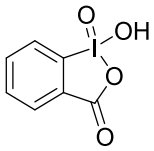

Following a procedure outlined by Santagostino *et al*.[281] iodobenzoic acid (75.0 g, 0.30 mol, 1 equiv.) was added to a solution of Oxone (241.7 g, 0.39 mol, 1.3 equiv.) in deionised H_2O (975 mL, 0.31 M) in a 2 L round bottomed flask. The reaction mixture was heated at 70 °C for 3 h then cooled to 0 °C in an ice bath and stirred for 1.5 h. The mixture was filtered through a sintered funnel and rinsed with H_2O (3 × 100 mL) and acetone (3 × 100 mL) and dried for 16 h at rt to afford a colourless solid (67.8 g, 81% yield) **mp** 230 °C (dec.) {lit.[281]233 °C dec.}; **^{1}H NMR** (500 MHz, d_6-DMSO) δ_H: 7.84 (1H, t, *J* 7.3, Ar*H*), 7.98-8.02 (2H, m, Ar*H*), 8.14 (1H, d, *J* 7.0, Ar*H*). All data in accordance with the literature.[281]

3-oxo-1λ^5-benzo[*d*][1,2]iodaoxole-1,1,1(3*H*)-triyl triacetate (Dess-Martin Periodinane) 338

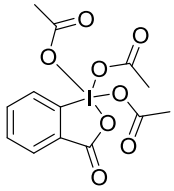

Following a procedure outlined by Ireland,[282] IBX **337** (68.7 g, 0.245 mol, 1 equiv.), acetic anhydride (300 mL) and AcOH (150 mL) were added to a 3-neck round bottomed flask under Ar. The mixture was heated to 85 °C (internal temperature) over 30 mins. The mixture was kept at 85 °C for 20 mins until all solids were dissolved affording a clear yellow solution. The solution was cooled to rt slowly over 24 h. The resulting reaction mixture was filtered under vacuum under a blanket of Ar. The filtered solid was washed with anhydrous Et_2O (200 mL) to afford the pure product as a colourless solid (52.1 g, 50% yield), **mp** 123-126 °C. {lit.[283]133-134 °C dec.}; **^{1}H NMR** (500 MHz, d6-DMSO) δ_H: 1.91 (6H, s, 2 × C*H*$_3$), 2.20 (3H, s, C*H*$_3$), 7.93 (1H, td, *J* 7.4,1.0, ArC(4)*H*), 8.10 (2H, m, ArC(5,6)*H*), 8.37 (1H, dd, *J* 8.3,1.0, ArC(7)*H*). All data in accordance with the literature.[283]

3-(Benzo[*d*]thiazol-2-ylamino)propan-1-ol 118

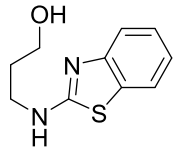

To a round bottomed flask containing 3-amino-1-propanol **117** (4.93 mL, 64.5 mmol, 1.05 equiv.), 2-chlorobenzothiazole **116** (8 mL, 61.5 mmol, 1 equiv.) and *o*-dichlorobenzene (30 mL, 2 M) was added *i*Pr_2NEt (26.5 mL, 153 mmol, 2.5 equiv.) with stirring. The resulting yellow solution was stirred vigorously and heated at reflux (195 °C DrySyn® temperature) until completion as judged by GC conversion (>95%, *ca.* 24 h). The resulting mixture was cooled to rt, H_2O (100 mL) was added and the aqueous phase was extracted with CH_2Cl_2 (3 × 100 mL). The organic layers were combined, washed with brine, dried ($MgSO_4$) and concentrated *in vacuo* to afford the crude product which was recrystallised from toluene to afford the pure product as a colourless solid (11.93 g, 93% yield); **mp** 119-121 °C. {Lit.[107] 123-123.5 °C}; **GC** [Agilent DB-5, 40 cm/s (He), inj. temp 250 °C, FID temp 325 °C; temp profile: initial 120 °C (2 min), then ramp to 320 °C (20 °C/min, hold 5 min), total run = 17 min]: t_R *i*Pr_2NEt, 1.84 min; *o*-dichlorobenzene, 3.15 min; 3-amino-1-propanol **118**, 5.62 min; 2-chlorobenzothiazole **117**, 5.74 min; 10.30 min; **^{1}H NMR** (500 MHz, CD_3OD) δ_H: 1.85 (1H, q, *J* 6.6, C(2)CH_2), 3.49 (1H, t, *J* 6.9, C(3)CH_2), 3.64 (1H, t, *J* 6.2, C(1)CH_2), 7.01 (1H, td, *J* 7.6, 1.2, ArC(5)*H*), 7.21 (1H, ddd, *J* 8.2, 7.6, 1.2, ArC(6)*H*), 7.37 (1H, *J* 7.6, ArC(4)*H*), 7.52 (1H, *J* 7.6, ArC(7)*H*). All data in accordance with the literature.[107]

3,4-Dihydro-2*H*-pyrimido[2,1-*b*]benzothiazole (DHPB) 60

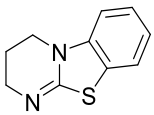

To a round bottomed flask was containing anhydrous CH_2Cl_2 (250 mL, 0.2 M) was added alcohol **118** (11.93 g, 57.3 mmol, 1 equiv.) with stirring under Ar. Et_3N (30.7 mL, 229.2 mmol, 4 equiv.) was added *via* syringe and the suspension was cooled to 0 °C. After 10 mins, methanesulfonyl chloride (5.76 mL, 74.5 mmol, 1.3 equiv.) was added dropwise, during which time the suspension dissolved to give a pale yellow solution. The ice/water bath was removed and the reaction was stirred for 30 mins. Once complete consumption of alcohol **118** was observed, as judged by TLC, *i*PrOH (11 mL) was added and the reaction was heated at reflux (50 °C DrySyn® temperature) for 16 h. The reaction was quenched with aq. 1 M NaOH (150 mL) and stirred for 30 mins. The aqueous phase was extracted with CH_2Cl_2 (3 × 100 mL). The organic layers were combined,

washed with brine, dried ($MgSO_4$) and concentrated *in vacuo* to afford the crude product. Et_2O (50 mL) was added to the crude solid and the mixture was heated at reflux with stirring for 30 mins. An equal volume of pet. ether (50 mL) was added and the mixture was cooled to rt then filtered. The filter cake was washed with pet. ether (3 × 50 mL) and dried to afford the pure product as a pale yellow solid (7.56 g, 70% yield); **mp** 120-122 °C; {Lit. [107]122-123 °C}; **^{1}H NMR** (400 MHz, $CDCl_3$) δ_H: 1.96 (2H, q, *J* 6.0, C(3)C*H*$_2$), 3.51 (2H, t, *J* 6.0, C*H*$_2$), 3.71 (2H, t, *J* 6.3, C*H*$_2$), 6.67 (1H, dd, *J* 8.1, 0.8, Ar*H*), 6.92, (1H, td, *J* 7.7, 1.1, Ar*H*), 7.12 (1H, td, *J* 7.7, 1.1, Ar*H*), 7.20-7.22 (1H, m, Ar*H*). All data in accordance with the literature. [107]

4-Methylbenzenesulfonyl azide 339

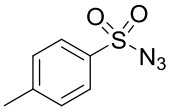

To a round bottomed flask containing acetone (85 mL) and H_2O (85 mL) was added *p*-toluenesulfonyl chloride (5.72 g, 30 mmol, 1 equiv.) and sodium azide (1.95 g, 30 mmol, 1 equiv.) at 0 °C with stirring. The mixture was stirred at 0 °C for 2 h and then warmed to rt. The solvent was concentrated *in vacuo*. The aqueous layer was extracted with EtOAc (3 × 30 mL), washed with brine, dried ($MgSO_4$) and concentrated *in vacuo* to afford the pure product as a colourless oil (3.96 g, 67% yield); **^{1}H NMR** (500 MHz, $CDCl_3$) δ_H: 2.51 (3H, s, ArC*H*$_3$), 7.42 (2H, app. dd, *J* 7.9, ArC(3,5)*H*), 7.85 (2H, app. dt, *J* 8.4, ArC(2,6)*H*); ν_{max} (thin film, cm^{-1}) 2130 (N_3). All data in accordance with the literature.[284]

Dimethyl (1-diazo-2-oxopropyl)phosphonate (Ohira-Bestmann reagent) 340

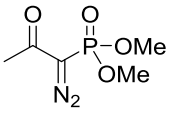

To round bottomed flask containing anhydrous toluene (45 mL) and THF (15 mL) was added NaH (0.86 g, 21.5 mmol, 1.1 equiv, *60% in mineral oil*) at 0 °C with stirring. A solution of dimethyl acetylmethylphosphonate (3.15 mL, 19.6 mmol, 1 equiv.) in toluene (15 mL) was added and a white precipitate formed. The reaction was stirred for 1 h at rt and tosylazide **339** (3.2 g, 20.8 mmol, 1.05 equiv.) was added in toluene (7.5 mL) resulting in an orange solution that was stirred for 16 h. The reaction mixture was diluted with pet. ether, filtered through celite and washed with Et_2O (100 mL). The resulting solution was concentrated *in vacuo* to afford the crude product. Flash chromatography on silica gel (1:1 hexane:EtOAc) afforded the pure product as a colourless oil (2.29 g, 61% yield); **^{1}H NMR** (500 MHz, $CDCl_3$) δ_H: 2.23 (3H, s, C*H*$_3$), 3.81 (6H,

d, $^{3}J_{H\text{-}P}$ 12.0, 2 × OCH_3); ν_{max} (thin film, cm^{-1}) 2135 (N_3). All data in accordance with the literature.[285]

2-Chloro-6-methoxybenzo[*d*]thiazole 290

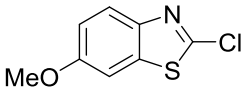

To a round bottomed flask was added $CuCl_2$ (13.56 g, 100.1 mmol, 1.2 equiv.) and dried for 1 h under vacuum at 110 °C. Anhydrous MeCN (500 mL) was added to the flask with stirring under Ar. To the reaction mixture was added *tert*-butyl nitrite (15 mL, 126.1 mmol, 1.5 equiv.) with stirring followed by dropwise addition of 6-methoxybenzo[*d*]thiazole-2-amine **287** (15.15 g, 84.1 mmol, 1 equiv.) in MeCN (50 mL). The reaction mixture was stirred at 65 °C for 3 h and allowed to cool to rt. 4 M HCl (200 mL) was added and the aqueous phase was extracted with Et_2O (3 × 100 mL). The organic layers were combined, washed with brine, dried ($MgSO_4$) and concentrated *in vacuo* to afford the crude product as a dark brown solid. Flash chromatography on silica gel (hexane: EtOAc 0→10%) afforded the pure product as a colourless solid (11.74 g, 71% yield); **mp** 51-52 °C {lit.[286] 52-53 °C}; **^{1}H NMR** (400 MHz, $CDCl_3$) δ_H: 3.87 (3H, s, OCH_3), 7.07 (1H, dd, *J* 9.0, 2.6, ArC(5)*H*), 7.23 (1H, d, *J* 2.6, ArC(7)*H*), 7.82 (1H, d, *J* 9.0, ArC(4)*H*). All data in accordance with the literature.[286]

(*E*)-2,2,2-Trifluoro-*N*-phenylacetimidoyl chloride 102

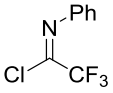

Following a procedure outlined by Uneyama.[148] to a round bottomed flask containing freshly distilled CCl_4 (90 mL, 1 M) was added TFA **103** (6.8 mL, 88 mmol, 1 equiv.), Et_3N (14.6 mL, 106 mmol, 1.2 equiv.) and triphenylphosphine (69.0 g, 264 mmol, 3 equiv.) with stirring. The reaction mixture was stirred at rt for 10 mins then aniline **104** (9.66 mL, 106 mmol, 1.2 equiv.) was added and the mixture was heated at reflux for 3 h and allowed to cool to rt. The mixture was concentrated *in vacuo* and hexane (300 mL) was added and the crude residue was stirred for 1 h and filtered to afford the crude product. Purification by Kugelrohr distillation afforded the pure product as a pale yellow oil (11.3 g, 62%); **bp** 120-122 °C (5 mbar); {lit.[148]**bp** 55-56 °C (14.6 mbar)}; **^{1}H NMR** (500 MHz, $CDCl_3$) δ_H: 7.08-7.12 (2H, m, ArC(2,6)*H*), 7.29-7.31 (1H, m, ArC(4)*H*), 7.35-7.51 (2H, m, ArC(3,5)*H*). All data in accordance with the literature. [148]

6.3 Experimental for Chapter 2

General Procedure A: *Formation of trichlorosilanes from alkyl bromides*

To a flame dried round bottomed flask containing magnesium turnings (1 equiv.) in anhydrous Et_2O (15 mL) was added a crystal of iodine at rt. The reaction was stirred until the brown colour disappeared. The appropriate bromide (1 equiv.) in anhydrous Et_2O (15 mL) was added dropwise with gentle heating until initiation occurred. The reaction mixture was stirred for 30 mins at rt. Silicon tetrachloride (1.2 equiv.) in anhydrous Et_2O (15 mL) was added *via* syringe over 1 h and the subsequent mixture stirred at rt for 16h. Upon completion anhydrous hexane was added *via* cannula to the 2 necked flask and the product was filtered under nitrogen using a fritted filter to remove any inorganic material. The solution was concentrated under reduced pressure to afford an oil that was purified by Kugelrohr distillation to afford the pure product as a colourless oil.

General procedure B: *Preparation of vinyl terminated surfaces on SiO_2*

Freshly cleaned silicon wafers were placed in a vial containing a freshly prepared 1 mM solution of the appropriate trichlorosilane in toluene for 16 h. The wafer was removed and rinsed with toluene and sequentially sonicated in toluene, CH_2Cl_2, and $CHCl_3$ for 5 min each. The vinyl terminated wafers were dried under a stream of Ar.

General procedure C: *Ozonolysis of vinyl terminated surfaces on SiO_2*

To a 250 mL round bottomed flask containing CH_2Cl_2 (200 mL) was added the appropriate vinyl terminated wafer at −78 °C. The mixture was subjected to ozonolysis until the reaction mixture turned blue (*ca*. 1 min) and the solution was quenched with dimethylsulfide (~2 mL) at −78 ° C. The mixture was allowed to warm to rt and the wafer was removed from the solution, sonicated in CH_2Cl_2, toluene and H_2O for 5 mins each then dried in a stream of Ar.

General procedure D: *Michael addition lactonisation on a surface using DHPB **60***

To a round-bottomed flask containing a stirrer bar and a solution of acid (1 equiv.) in CH_2Cl_2 (3 mL) was added *i*Pr_2NEt (1.5 equiv) and pivaloyl chloride (1.5 equiv.) at 0 °C. The reaction mixture was allowed to stir at 0 °C for 20 min. DHPB **60** (5 mol %), the Michael acceptor terminated surface and *i*Pr_2NEt (2.5 equiv) were added. The reaction was stirred at rt for 24 h. Upon completion, the DHP terminated surface was removed and rinsed with CH_2Cl_2 and sonicated in CH_2Cl_2 and $CHCl_3$ for 5 mins each. DHP terminated surfaces were dried under a stream of Ar.

Trichloro(undec-10-en-1-yl)silane 86

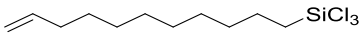

Following general procedure **A**, magnesium turnings (1.67 g, 68.7 mmol, 1 equiv), 11-bromo-undecene (5.00 mL, 22.9 mmol, 1 equiv), silicon tetrachloride (8.30 mL, 80.0 mmol, 1.1 equiv) were reacted to afford the crude product. Purification by Kugelrohr distillation (105 °C, 1 mbar) afforded the pure product as a colourless oil (1.64 g, 26% yield); ν_{max} (thin film, cm^{-1}) 2924 (C-H), 1641 (C=C), 1193 (Si-C); **^{1}H NMR** (400 MHz, C_6D_6) δ_H: 0.98 (2H, m, CH_2SiCl$_3$), 1.07-1.26 (8H, bs, 4 × CH_2), 1.30-1.35 (4H, m, 2 × CH_2), 2.00 (2H, app. q, *J* 7.1, CH_2), 4.98 (1H, dd, *J* 10.1, 1.9, =C*H*), 5.03 (1H, app. dq, *J* 17.1, 1.9, =C*H*^{A}H^{B}) 5.79 (1H, ddt, *J* 17.1, 10.1, 6.7=CH^{A}*H*^{B}); **^{13}C{^{1}H} NMR** (75 MHz, C_6D_6) δ_C: 22.5 (*C*H$_2$), 24.3 (*C*H$_2$), 29.3 (*C*H$_2$), 29.4 (*C*H$_2$), 29.5 (*C*H$_2$), 29.7 (*C*H$_2$), 29.8 (*C*H$_2$), 32.0 (*C*H$_2$), 34.3 (*C*H$_2$), 114.6 (=*C*H$_2$), 139.1 (*C*H); **^{29}Si NMR** (79 MHz, C_6D_6) δ_{Si}: 13.1 (*Si*Cl$_3$); **HRMS** (APCI) $C_{11}H_{21}SiCl_3$ $[M+H]^+$, found 286.7251, requires 286.0673 (+3.8 ppm).

Methyl 15-hydroxypentadecanoate 90

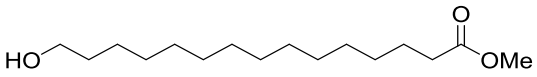

To a round bottomed flask containing methanol (81 mL) was added concentrated H_2SO_4 (9 mL) and *ω*-pentadecalactone **89** (10.0 g, 41 mmol, 1 equiv) with stirring. The solution was stirred at reflux for 3 h and cooled to rt. Brine (100 mL) was added to the reaction mixture and the aqueous layer was extracted with Et_2O (3 × 30 mL). The organic layers were combined, washed with brine, dried ($MgSO_4$) and concentrated *in vacuo* to afford the pure product as a colourless solid (10.1g, 90% yield); **mp** 50-51.5 °C. {Lit.[287] 47-48 °C}; **^{1}H NMR** (300 MHz, $CDCl_3$) δ_H: 1.23-1.36 (20H, bs, 10 × CH_2), 1.51-1.63 (4H, m, 2 × CH_2), 2.30 (2H, t, *J* 8.2, C(O)CH_2), 3.63 (2H, t, *J* 6.7, CH_2OH), 3.65 (3H, s, OCH_3). All data in accordance with the literature.[287]

Methyl 15-bromopentadecanoate 91

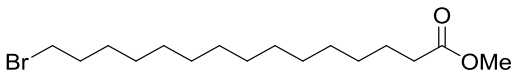

Following a procedure outlined by Katzenellenbogen,[287] to a round bottomed flask containing DMF (30 mL) was added triphenylphosphine (2.53g, 9.66 mmol, 1.1 equiv) and alcohol **90** (2.39 g, 8.8 mmol, 1 equiv) with stirring under Ar. *N*-Bromosuccnimide (1.71g, 9.66 mmol, 1.1 equiv) was added in portions until fully dissolved. The reaction mixture was heated at 55 °C for 30 mins and allowed to cool to rt. Methanol (15 mL), followed by aq. HCl (1 M, 60 mL) was added to the

solution. The aqueous layer was extracted with Et_2O (3 × 20 mL). The organic layers were combined, washed with brine, dried ($MgSO_4$) and concentrated *in vacuo* to afford the crude product. Flash chromatography on silica gel (20:1 Hexane:EtOAc) afforded the pure product as a colourless solid (2.27 g, 77% yield); **mp** 37-38.5 °C {Lit.[287] 38-39 °C }; **^{1}H NMR** (400 MHz, $CDCl_3$) δ_H: 1.22-1.35 (18H, bs, 9 × C*H*$_2$), 1.41 (2H, m, C*H*$_2$), 1.61 (2H, m, C*H*$_2$), 1.85 (2H, m, C*H*$_2$), 2.30 (2H, t, *J* 7.6, C(O)C*H*$_2$), 3.40 (2H, t, *J* 6.9, C*H*$_2$Br), 3.66 (3H, s, C*H*$_3$). All data in accordance with the literature.[287]

tert-Butyl pentadec-14-enoate 92

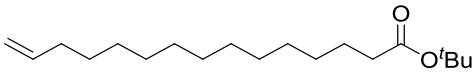

Following a procedure outlined by Katzenellenbogen,[287] to a round bottomed flask containing bromide **91** (4.43g, 13.2 mmol) was added to a solution of potassium *tert*-butoxide (2.96 g, 26.4 mmol, 2 equiv.) in THF (20 mL) under Ar. The mixture was stirred at room temperature for 1 h and quenched with aq. HCl (1 M, 20 mL) and the aqueous layer extracted with Et_2O (3 × 10 mL). The organic layers were combined, washed with brine, dried ($MgSO_4$) and concentrated *in vacuo* to afford the crude product. Flash chromatography on silica gel (98:2 pet. ether:Et_2O) afforded the pure product as a colourless oil (1.6 g, 41% yield); **^{1}H NMR** (400 MHz, $CDCl_3$) δ_H: 1.18-1.26 (14H, bs, 7 × C*H*$_2$), 1.32 (2H, m, C*H*$_2$), 1.38 (9H, s, C(C*H*$_3$)$_3$), 1.52 (2H, m, C*H*$_2$), 1.82 (2H, m, C*H*$_2$), 1.97 (2H, m, C*H*$_2$CHCH$_2$), 2.16 (2H, t, *J* 8.0, C*H*$_2$, C(O)C*H*$_2$), 4.86 (1H, app. dq, *J* 10.1, 1.8, =C*H*^{A}H^B), 4.93 (1H, app. dq, *J* 17.0, 1.8, =CH^A*H*^{B}), 5.75 (1H, ddt, *J* 17.0, 10.1, 6.6, =C*H*). All data in accordance with the literature.[287]

Pentadec-14-en-1-ol 93

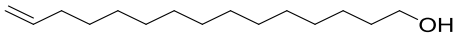

To a round bottomed flask containing anhydrous THF (5 mL) was added alkene **92** (490mg, 1.65 mmol, 1 equiv) and $LiAlH_4$ (1.81 mL, 4.5 mmol, 2.5 M in hexanes, 2.7 equiv.) was added at 0 °C with stirring. The reaction mixture was stirred for 1 h and quenched with a saturated solution of potassium sodium tartrate (10 mL). The mixture was filtered through celite, washed with CH_2Cl_2 (3 × 20 mL) and the filtrate concentrated *in vacuo* to yield the crude product as an off white solid. Flash chromatography on silica gel (CH_2Cl_2) afforded the pure alcohol as a colourless solid (289 mg, 77% yield); **mp** 38-39°C{Lit.[288] 38-39°C}; **^{1}H NMR** (400 MHz, $CDCl_3$) δ_H: 1.23-1.38 (20H, bs, 10 × C*H*$_2$), 1.56 (2H, t, *J* 6.7, C*H*$_2$), 2.04 (2H, m, C*H*$_2$), 3.64 (2H, t, *J* 6.6 Hz, C*H*$_2$OH), 4.92 (1H, app. ddt, *J* 10.2, 2.3, =C*H*^{A}H^B), 4.99 (1H, app. d, *J* 17.0, =CH^A*H*^{B}) 5.81 (1H, ddt, *J* 17.0, 10.2, 6.7, =C*H*). All data in accordance with the literature.[288]

15-Bromopentadec-1-ene 94

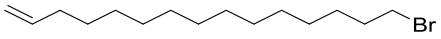

Following a procedure outlined by Katzenellenbogen,[287] to a round bottomed flask containing DMF (15 mL) was added triphenylphosphine (577 mg, 2.20 mmol, 1.1 equiv.) and alcohol **93** (2.39 g, 8.8 mmol, 1 equiv) with stirring under Ar. *N*-bromosuccnimide (392 mg, 2.20 mmol, 1.1 equiv.) was added in portions until fully dissolved. The reaction mixture was heated at 55 °C for 30 mins and allowed to cooled to rt. Methanol (10 mL), followed by aq. HCl (1 M, 20 mL) was added to the solution. The aqueous layer was extracted with Et_2O (3 × 20 mL). The organic layers were combined, washed with brine, dried ($MgSO_4$) and concentrated *in vacuo* to afford the crude product. Flash chromatography on silica gel (20:1 hexane:EtOAc) afforded the pure product as a brown oil (461 mg, 80% yield); **^{1}H NMR** (400 MHz, $CDCl_3$) δ_H: 1.19-1.33 (16H, bs, 8 × C*H*$_2$), 1.34-1.46 (4H, m, 2 × C*H*$_2$), 1.85 (2H, m, C*H*$_2$CH$_2$Br), 2.03 (2H, m, C*H*$_2$CH), 3.39 (2H, t, *J* 6.9, C*H*$_2$Br), 4.92 (1H, app. ddt, *J* 10.2, 2.3, =C*H*^{A}H^B), 4.98 (1H, app. d, *J* 17.0, 1=CH^A*H*^{B}) 5.81 (1H, ddt, *J* 17.0, 10.2, 6.7, =C*H*). All data in accordance with the literature[289]

Trichloro(pentadec-14-en-1-yl)silane 76

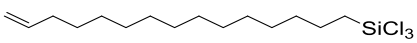

Following general procedure **A**, magnesium turnings (190 mg, 7.92 mmol, 1 equiv.), 15-bromopentadec-1-ene **94** (2.30 g, 7.92 mmol, 1 equiv.), silicon tetrachloride (1 mL, 8.71 mmol, 1.1 equiv.) were reacted to afford the crude product. Purification by Kugelrohr distillation afforded the pure product as a colourless oil (560 mg, 20% yield); **bp** 115 °C, 1 mbar; {Lit.[114] 145-150 °C, 4 mbar} **^{1}H NMR** (400 MHz, C_6D_6) δ_H: 0.98 (2H, m, C*H*$_2$SiCl$_3$), 1.11-1.30 (18H, bs, 9 × C*H*$_2$), 1.32-1.36 (4H, m, 2 × C*H*$_2$), 2.02 (2H, app. q, *J* 7.1, C*H*$_2$), 4.98 (1H, app. dd, *J* 10.1, 1.9, =C*H*^{A}H^B), 5.01 (1H, app. dq, *J* 17.1, 1.9, =CH^A*H*^{B}) 5.78 (1H, ddt, *J* 17.1, 10.1, 6.7, =C*H*); All data in accordance with the literature. [114]

C_{11}-vinyl-terminated SAM on SiO_2 96

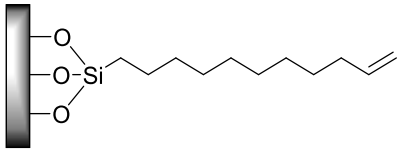

Freshly cleaned silicon wafers (as per the cleaning procedure outlined in chapter 2) were placed in a vial containing a 5 mL of freshly prepared 1mM solution of trichloro(undec-10-en-1-yl)silane **86** (5.70 mg, 0.02 mmol, in 20 mL toluene) for 16 h. Once deposition was complete the wafer

was removed and rinsed with toluene and subsequently sonicated in toluene, CH_2Cl_2 and $CHCl_3$ for 5 mins each. The vinyl terminated wafers were dried under a stream of Ar.

C_{15}-vinyl-terminated SAM on SiO_2 97

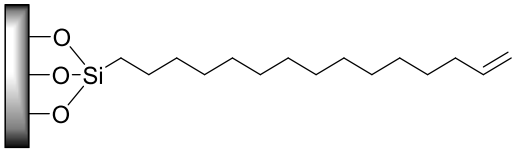

Freshly cleaned silicon wafers (as per the cleaning procedure outlined in chapter 2) were placed in a vial containing a 5 mL of freshly prepared 1mM solution of trichloro(pentadec-14-en-1-yl)silane **76** (6.90 mg, 0.02 mmol, in 20 mL toluene) for 16 h. Once deposition was complete the wafer was removed and rinsed with toluene and subsequently sonicated in toluene, CH_2Cl_2 and $CHCl_3$ for 5 mins each. The vinyl terminated wafers were dried under a stream of Ar.

Phenylacetic acid terminated surface 99

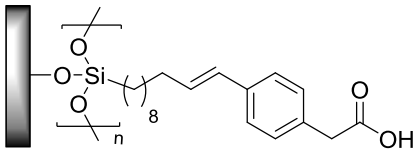

To a round bottomed flask containing DMF (2 mL) was added $Pd(OAc)_2$ (16 mg, 0.069 mmol, 10 mol%), P(*o*-tol)$_3$ (21 mg, 0.069 mmol, 10 mol%), *p*-bromophenylacetic acid **98** (150 mg, 0.69 mmol, 1 equiv.) and Et_3N (0.49 mL, 3.48 mmol, 5 equiv.) with stirring. C_{11}-vinyl terminated surface **96** was immersed in the reaction mixture and heated at 125 °C for 2 h then cooled to rt. The wafer was removed and rinsed with Et_2O (20 mL) and further sonicated in Et_2O for 5 mins then rinsed with EtOH (20 mL) and dried under a stream of argon to afford the phenylacetic acid terminated surface.

C_{10}-aldehyde terminated surface on SiO_2 96a

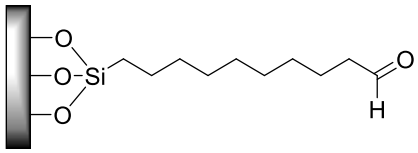

Following general procedure **C**, C_{11}-vinyl terminated SAM **96** was reacted with ozone at −78 °C to afford aldehyde terminated surface **96a** after rinsing and sonication.

C_{14}-aldehyde terminated surface on SiO_2 97a

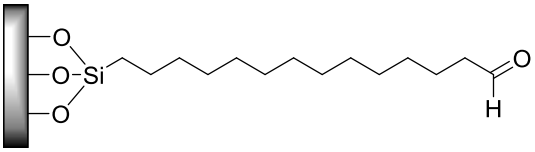

Following general procedure **C**, C_{15}-vinyl terminated SAM **97** was reacted with ozone at −78 °C to afford aldehyde terminated surface **97a** after rinsing and sonication.

(3,4-Dinitrophenyl)hydrazine 100

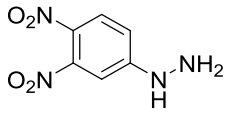

To a round bottomed flask containing EtOH (100 mL) was added 2,4-dinitrochlorobenzene (5.0 g, 24.6 mmol, 1 equiv) with stirring. Hydrazine monohydrate (12 mL, 256 mmol, 10 equiv.) in EtOH (50 mL) was added dropwise over 30 mins. The reaction mixture was heated at reflux for 3 h, cooled to rt and brine was added to the mixture. The resulting solid was filtered to afford the pure product as a bright orange solid (4.09 g, 84% yield); **mp** 205 dec. °C {Lit. [290] 202-203 °C}; **^{1}H NMR** (500 MHz, CD_3OD) δ_H: 7.83 (1H, d, *J* 9.7, ArC(5)*H*), 8.27 (1H, dd, *J* 9.7, 2.6, ArC(6)*H*), 8.99 (1H, d, *J* 2.6, ArC(2)*H*). All data in accordance with the literature.[290]

Dinitrophenylhydrazine (DNPH) terminated surface 101

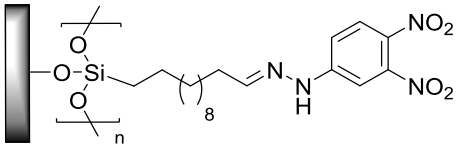

To a round bottomed flask containing DMSO (20 mL) was added 3,4-dinitrophenylhydrazine **100** (50 mg, 0.254 mmol) and aldehyde terminated wafer **96a**. The reaction was stirred for 72 h and the wafer was removed and rinsed with EtOH (20 mL) and dried under a stream of Ar.

Bromine terminated SAM on Si/SiO_2 115 (solution deposition)

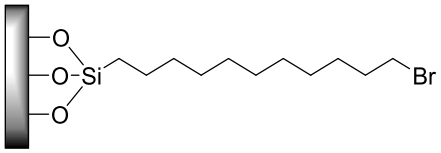

Freshly cleaned silicon wafers (as per the cleaning procedure outlined in chapter 2) were placed in a vial containing a 5 mL of freshly prepared 1 mM solution of 11-bromoundecyltrichlorosilane

114 (5.80 µL, 0.0198 mmol, in 20 mL toluene) for 16 h. Once deposition was complete the wafer was removed and rinsed with toluene and subsequently sonicated in toluene, CH_2Cl_2 and $CHCl_3$ for 5 mins each. The bromine terminated wafers were dried under a stream of Ar.

Bromine terminated SAM on Si/SiO_2 114 (vapour deposition)

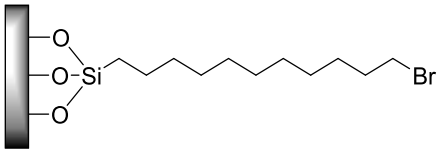

A freshly cleaned silicon wafer (as per the cleaning procedure outlined in chapter 2) was placed in the centre of a 100 mL Schott Duran bottle with a sidearm modification (for vacuum use). Next, 11-bromoundecyltrichlorosilane **114** (50 µL, 172 mmol) was added to a standard grade HPLC vial and placed inside the 100 mL Schott Duran bottle. The lid was placed on the bottle and the internal atmosphere was removed under reduced pressure. The bottle was clamped and placed in a preheated oil bath at 60° C, paying careful attention to ensure the external level of the oil bath was above the top of the HPLC vial. Once deposition was complete (*ca*. 36 h) the wafer was removed and rinsed with toluene and subsequently sonicated in toluene, CH_2Cl_2 and $CHCl_3$ for 5 mins each. The bromine terminated wafers were dried under a stream of Ar.

Azide terminated surface 112

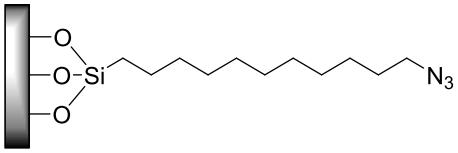

Bromine terminated SAM **114** was immersed in a saturated solution of sodium azide in DMF (10 mL) and the reaction was stirred for 24 h. Upon completion the azide terminated wafer was removed and rinsed with DMF. The wafer was sonicated in EtOH and H_2O for 5 mins each, and dried under a stream of Ar.

5-(Trimethylsilyl)pent-4-yn-1-ol 121

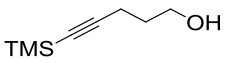

To a round bottomed flask containing anhydrous THF (45 mL, 0.5 M) at −78 °C was added pent-4-yn-ol **120** (2 mL, 26.3 mmol, 1 equiv.) and *n*BuLi (21.0 mL, 52.6 mmol, 2.5 M in hexanes, 2 equiv.) and the resulting solution was stirred at −78°C for 30 mins under Ar. Trimethylchlorosilane (8 mL, 63.1 mmol, 2.4 equiv.) was added to the yellow solution and the

reaction was stirred for a further 30 mins at −78 °C then allowed to warm to rt over 30 mins. The reaction was quenched with aq. 2 M HCl (40 mL) and the aqueous phase was extracted with Et_2O (3 × 50 mL). The organic layers were combined, dried ($MgSO_4$) and concentrated *in vacuo* to afford the crude product as a light yellow oil. Purification by Kugelrohr distillation afforded the pure product as a colourless oil (2.50 g, 61% yield); **bp** 100-104 °C (2 mbar) {Lit.[291] 118-120 °C (29 Torr)}; **^{1}H NMR** (400 MHz, $CDCl_3$) δ_H: 0.13 (9H, s, Si(CH_3)$_3$), 1.71–1.79 (2H, m, CH_2), 2.33 (2H, t, *J* 6.9, CH_2), 3.73 (2H, t, *J* 6.1, C(1)H_2). All data in accordance with the literature[292]

5-(Trimethylsilyl)pent-4-ynal 122

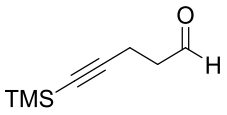

To a round bottomed flask containing anhydrous CH_2Cl_2 (40 mL, 0.4 M) at −78 °C was added oxalyl chloride (1.62 mL, 18.8 mmol, 1.2 equiv.) with stirring under Ar. Dimethylsulfoxide (2.44 mL, 31.4 mmol, 2 equiv.) in anhydrous CH_2Cl_2 (10 mL) was added dropwise to the solution over 10 mins and allowed to stir for 20 mins. Alcohol **121** (2.45 g, 15.7 mmol, 1 equiv.) in anhydrous CH_2Cl_2 (20 mL) was added to the reaction mixture and the resulting solution was stirred at −78 °C for 1 h. Et_3N (8.41 mL, 62.7 mmol, 4 equiv.) was added dropwise to the solution at −78 °C and the reaction was stirred for 30 mins then warmed to rt and stirred for a further 30 mins at this temperature. The reaction was quenched with aq. 1 M HCl (30 mL) and the aqueous phase was extracted with CH_2Cl_2 (3 × 40 mL). The organic layers were combined, dried ($MgSO_4$) and concentrated *in vacuo* to afford the crude product which was purified by Kugelrohr distillation to afford the pure product as a colourless oil (1.06 g, 44% yield); **bp** 170-172 °C (atm pressure) {Lit.[293] 125 °C (35 Torr)}; **^{1}H NMR** (300 MHz, $CDCl_3$) δ_H: 0.13 (9H, s, Si(CH_3)$_3$), 2.53 (1H, app. dd, *J* 7.7, 6.7, C(3)H_2), 2.67 (2H, app. ddt, *J* 7.7, 6.7, 1.3, C(2)H_2), 9.78 (1H, t, *J* 1.3, C*H*O). All data in accordance with the literature.{Lit.[293]

4-((Trimethylsilyl)ethynyl)benzaldehyde 125

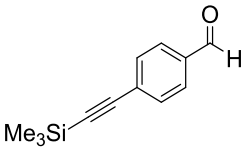

To a round bottomed flask containing THF (135 mL, 0.2 M degassed with Ar) was added copper (I) iodide (52 mg, 0.27 mmol, 1 mol%), triethylamine (18.10 mL, 13.5 mmol, 5 equiv.) and $Pd(PPh_3)_2Cl_2$ (190 mg, 0.27 mmol, 1 mol%) with stirring. 4-Bromobenzaldehyde (5.00 g, 27 mmol, 1 equiv.) was added with stirring followed by dropwise addition of trimethylsilylacetylene (3.82 mL, 27 mmol, 1 equiv.). The reaction mixture was stirred for 16 h at rt then concentration

in vacuo, water (50 mL) was added to the crude reaction mixture and t**he** aqueous phase was extracted with Et_2O (3 × 50 mL). The organic layers were combined, dried ($MgSO_4$) and concentrated *in vacuo* to afford the crude product. Flash chromatography on silica gel (9:1 pet ether:Et_2O) afforded the pure product as a tan solid (4.09 g, 75%); **mp** 60-62 °C {Lit.[294] 65-66 °C}; **^{1}H NMR** (400 MHz, $CDCl_3$) δ_H: 0.27 (9H, s, Si(C*H*$_3$)$_3$), 7.59 (2H, d, *J* 8.5, Ar*H*), 7.82 (2H, d, *J* 8.5, Ar*H*), 10.0 (1H, s, C*H*O). All data in accordance with the literature.[294]

(*E*)-1,1,1-Trifluoro-4-(4'-((trimethylsilyl)ethynyl)phenyl)but-3-en-2-one 126

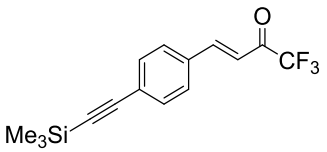

Following a procedure outlined by Smith[101]; to a round bottomed flask containing anhydrous THF (25 mL, 0.2 M) was added diisopropylamine (1.35 mL, 9.66 mmol, 2 equiv.) and *n*BuLi (4.60 mL, 9.66 mmol, 1.92 M in hexanes, 2 equiv.) at −78 °C and the solution was allowed to stir for 20 minutes. Diethyl methylphosphonate (0.71 mL, 4.83 mmol, 1 equiv.) was added at −78 °C followed by a further 30 minutes of stirring. (*Z*)-2,2,2-trifluoro-*N*-phenylacetimidoyl chloride **102** (1.00 g, 4.83 mmol, 1 equiv.) was then added slowly followed by stirring at −78 °C for 1 h. A solution of aldehyde **125** (0.976 g, 4.83 mmol, 1 equiv.) in anhydrous THF (10 mL) was added dropwise at −78 °C. The reaction mixture was then warmed over 2 h and stirred at rt for 16 h. Aq. 2 M HCl (12 mL, 4 equiv.) was added and the reaction mixture was stirred for a further 4 h before being extracted with Et_2O (3 × 50 mL). The combined organic extracts were washed with sat. aq. $NaHCO_3$ (50 mL), brine (50 mL), dried ($MgSO_4$) and concentrated *in vacuo* to give the crude reaction mixture. Flash chromatography on silica gel (9:1 Pet:Et_2O) afforded the pure product as a colourless solid (675 mg, 47%); **mp** 40-42 °C; ν_{max} (thin film, cm^{-1}) 2158 (C≡C), 1608 (C=O), 1595 (C=C); **^{1}H NMR** (400 MHz, $CDCl_3$) δ_H: 0.27 (9H, s, Si(C*H*$_3$)$_3$), 7.00 (1H, d, *J* 16.0, C(3)*H*), 7.52 (2H, d, *J* 8.3, ArC(3,5)*H*), 7.58 (2H, d, *J* 8.1, ArC(2,6)*H*), 7.92 (1H, d, *J* 16.0, C(4)*H*); **^{13}C{^{1}H} NMR** (100 MHz, $CDCl_3$) δ_C: −0.04 (Si(*C*H$_3$)$_3$), 98.6 (C≡*C*-Si(CH$_3$)), 104.2 (*C*≡C-Si(CH$_3$)), 117.2 (*C*(3)), 117.6 (q, ^1J 290, *C*F$_3$), 127.3 (Ar*C*(1)), 129.1 (Ar*C*(2,6)H), 132.7 (Ar*C*(3,5)H), 133.2 (*C*(4)H), 149. 1 (Ar*C*(4)), 179.9 (q, ^2J 35.3, *C*=O); **^{19}F {^{1}H} NMR** (376 MHz, $CDCl_3$) δ_F: −78.1 (C*F*$_3$); **HRMS** (ESI$^+$) $C_{15}H_{15}OF_3Si$ [M]$^+$, found 296.0848, requires 296.0839 (−1.4 ppm).

(*E*)-4-(4'-Ethynylphenyl)-1,1,1-trifluorobut-3-en-2-one 127

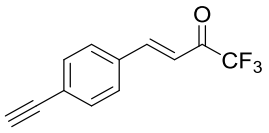

To a round bottomed flask containing MeOH (20 mL) was added **126** (675 mg, 2.28 mmol, 1 equiv.). K_2CO_3 (724 mg, 5.24 mmol, 2.3 equiv.) was added and the resulting mixture was stirred at rt for 2 h. The reaction mixture was concentrated *in vacuo*, H_2O (20 mL) was added and the crude product was extracted using EtOAc (3 × 30 mL). The combined organic extracts were washed sequentially with sat. aq. $NaHCO_3$ (30 mL) and brine (30 mL), dried ($MgSO_4$), and concentrated *in vacuo* to afford the crude reaction mixture. Flash chromatography on silica gel (9:1 pet. ether:Et_2O) afforded the pure product as a colourless solid (228 mg, 45%); **mp** 50-52 °C; ν_{max} (thin film, cm^{-1}) 3253 (≡C-H), 2104 (C≡C), 1681 (C=O), 1620 (C=C); **^{1}H NMR** (400 MHz, $CDCl_3$) δ_H: 3.27 (1H, s, C≡*H*), 7.01 (1H, d, *J* 16.0, C(3)*H*), 7.56 (2H, d, *J* 8.4, ArC(3,5)*H*), 7.60 (2H, d, *J* 8.4, ArC(2,6)*H*), 7.93 (1H, d, *J* 16.0, C(4)*H*); **^{13}C{^{1}H} NMR** (100 MHz, $CDCl_3$) δ_C: 80.7 (*C*≡CH), 82.9 (C≡*C*H), 117.5 (q, *J* 290, *C*F_3), 126.2 (Ar*C*(1)), 129.2 (Ar*C*(2,6)H), 130.0 (Ar*C*(3,5)H), 133.6 (Ar*C*(4)), 148.9 (*C*(4)), 180.2 (q, ^2J 35.8, *C*=O); **^{19}F{^{1}H} NMR** (376 MHz, $CDCl_3$) δ_F: −78.1 (C*F*$_3$); **HRMS** (CI^+) $C_{12}H_8OF_3$ $[M+H]^+$ found 225.0527, requires 225.0522 (+0.0 ppm).

CF_3 enone terminated surface 128

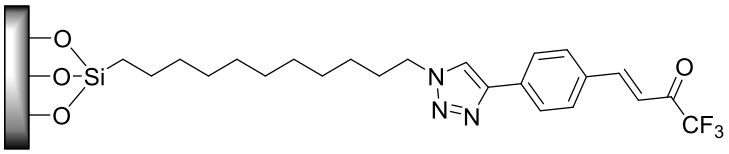

To a solution of enone **127** (7 mg, 0.03 mmol, 1 equiv.) in EtOH (8 mL) was added 1 mL of a 25 mL solution of $CuSO_4.5H_2O$ (7.5 mg, 0.03 mmol, 1 equiv.) and 1 mL of a 25 mL solution of sodium ascorbate (8.9 mg, 0.045 mmol, 1.5 equiv.) with stirring. The azide terminated wafer **112** was immersed in the reaction mixture for 24 h. Upon completion the enone terminated wafer was removed and rinsed with EtOH. The wafer was sonicated in EtOH and H_2O for 5 mins each, and dried under a stream of Ar.

1-azidooctane 130

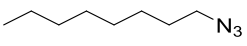

To a round bottomed flask containing DMF (20 mL) was added 1-bromooctane **129** (2.00 mL, 11.5 mmol, 1 equiv.) and sodium azide (900 mg, 13.5 mmol, 1.2 equiv.) with stirring at 100 °C for 2 h. The reaction was quenched using sat. aq. $NaNO_2$ (30 mL) and diluted with H_2O (10 mL). The aqueous phase was extracted with hexane (3 × 20 mL) and organic layers were combined, dried ($MgSO_4$) and concentrated *in vacuo* to afford the pure product as a colourless oil (1.60 g, 90% yield); **^{1}H NMR** (400 MHz, $CDCl_3$) δ_H: 0.88 (3H, t, *J* 6.9, C*H*$_3$), 1.23-1.31 (8H, m, 4 × C*H*$_2$), 1.32-1.38 (2H, m, C*H*$_2$), 1.96 (2H, app. quintet, *J* 6.5, $N_3CH_2CH_2$), 3.24 (2H, t, *J* 7.0, N_3CH_2). All data in accordance with the literature[295]

(*E*)-1,1,1-Trifluoro-4-(4'-(1-octyl-1H-1,2,3-triazol-4-yl)phenyl)but-3-en-2-one 131

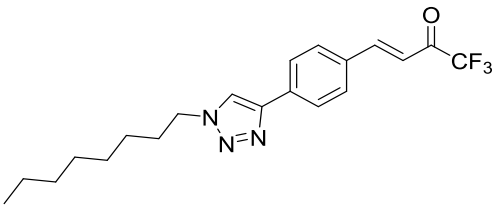

To a round bottomed flask containing EtOH (8 mL) was added enone **127** (50 mg, 0.23 mmol, 1 equiv.) and azide **130** (76 mg, 0.46 mmol, 2 equiv.) with stirring. $CuSO_4{\cdot}5H_2O$ (6 mg, 0.023 mmol, 10 mol%) in 1 mL H_2O and sodium ascorbate (7.5 mg, 15 mol%) in 1 mL H_2O were then added and the reaction was stirred overnight at rt then concentrated *in vacuo*. CH_2Cl_2 (10 mL) and water (10 mL) were added and the crude product extracted using CH_2Cl_2 (3 × 10 mL). The organic layers were combined, washed with brine, dried ($MgSO_4$), and concentrated *in vacuo* to give the crude reaction mixture which was purified by Biotage® Isolera™ 4 [SNAP Ultra 25 g, 75 mL min^{-1}, CH_2Cl_2 :EtOAc (97 : 3 5CV, 97 : 3 to 90 : 10 10CV, 90 : 10 5CV)] to afford the pure product as a colourless solid (74 mg, 47% yield); **mp** 60-62 °C; ν_{max} (thin film, cm^{-1}); 2924 (C-H), 1712 (C=O), 1602 (C=C); **^{1}H NMR** (500 MHz, $CDCl_3$) δ_H: 0.88 (3H, t, *J* 6.6, C*H*$_3$), 1.23-1.30 (6H, m, 3 × C*H*$_2$), 1.33-1.39 (4H, m, 2 × C*H*$_2$), 1.96 (2H, quintet, *J* 7.2, $ArNCH_2CH_2$), 4.42 (2H, t, *J* 7.2, $ArNCH_2$), 7.04 (1H, d, *J* 16.0, C(3)*H*), 7.71 (2H, d, *J* 8.3, (ArC(2,6)*H*), 7.83 (1H, s, N(1)C*H*), 7.93 (2H, d, *J* 8.3, (ArC(3,5)*H*), 7.98 (1H, d, *J* 16.0, C(4)*H*); **^{13}C{^{1}H} NMR** (100 MHz) δ_C: 14.2 (*C*H$_3$), 22.8 (*C*H$_2$), 26.6 (*C*H$_2$), 29.1 (*C*H$_2$), 29.2 (*C*H$_2$), 30.5 ($ArN(1)CH_2CH_2$), 30.9 (*C*H$_2$), 50.8 ($ArN(1)CH_2$), 116.5 (*C*(3)*H*)), 117.7 (q, *J* 289, *C*F$_3$) 120.3 (N(1)*C*H), 126.3 (Ar*C*(3,5)H), 130.1 (Ar*C*(2,6)H), 132.9 (Ar*C*(1)), 134.7 (Ar*C*(4)), 146.7 (N(3)*C*=C), 149.6 (*C*(4)), 179.9 (q, ^2J 34.8, *C*=O); **^{19}F {^{1}H} NMR** (470 MHz) δ_F: −78.6 (C*F*$_3$); **HRMS** (ESI$^+$) $C_{20}H_{25}F_3N_3O$ $[M+H]^+$, found 380.1940, requires 380.1944 (−1.1 ppm).

Methyl (2*R*,3*R*)-2-(4-bromophenyl)-6,6,6-trifluoro-3-(4'-(1-octyl-1H-1,2,3-triazol-4-yl)phenyl)-5-oxohexanoate (*anti* 132) and methyl (2*S*,3*R*)-2-(4-bromophenyl)-6,6,6-trifluoro-3-(4'-(1-octyl-1H-1,2,3-triazol-4-yl)phenyl)-5-oxohexanoate (*syn* 132)

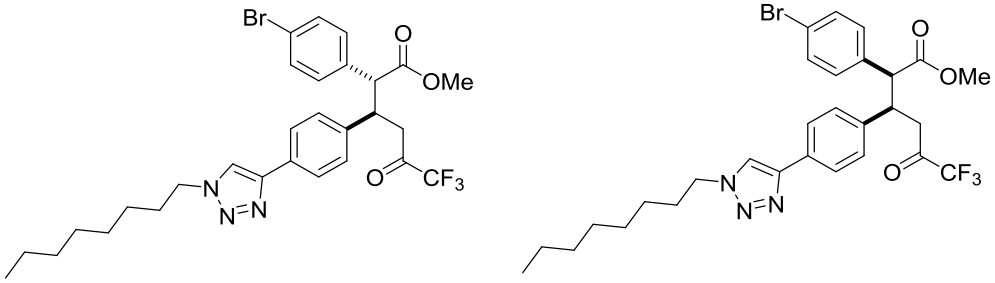

To a round bottomed flask containing CH_2Cl_2 (5 mL) was added 4-bromophenylacetic acid **98** (45mg, 0.21 mmol, 1 equiv.), *i*Pr_2NEt (55 µL, 0.32 mmol, 1.5 equiv.) and pivaloyl chloride (39 µL, 0.32 mmol, 1.5 equiv.) at 0 °C. The reaction mixture was allowed to stir at 0 °C for 20 mins. DHPB (3 mg, 0.0143 mmol, 5 mol%), enone **127** (74 mg, 0.21 mmol, 1 equiv.) and *i*Pr_2NEt (91 µL, 0.53 mmol, 2.5 equiv.) were then added and the resulting mixture was stirred at rt for 1 h. MeOH (5 mL) was added and stirring was continued for a further 16 h. The reaction was quenched by addition of aq. 1M HCl (5 mL), poured into water and extracted with CH_2Cl_2 (2 × 10 mL). The combined organic extracts were washed with brine (10 mL), dried ($MgSO_4$), and concentrated *in vacuo* to give an 80:20 mixture (*anti*:*syn*) of **132**. The crude mixture was purified by Biotage® Isolera™ 4 [SNAP Ultra 25 g, 75 mL min^{-1}, CH_2Cl_2 :EtOAc (97 : 3 5CV, 97 : 3 to 90 : 10 10CV, 90 : 10 5CV)] to afford an 80:20 mixture of *anti* and *syn* diastereoisomers as a colourless solid (89 mg, 70% yield); **mp** 110-117 °C; ν_{max} (thin film, cm^{-1}) 2972 (C-H), 1757 (C=O), 1728 (C=O); *Data for major diastereomer anti **132***:**^{1}H NMR** (500 MHz) δ_H: 0.86 (3H, m, CH_3), 1.23-1.30 (6H, m, 3 × CH_2), 1.33-1.39 (4H, m, 2 × CH_2), 1.96 (2H, m, ArN(1)CH_2CH_2), 3.14 (1H, dd, *J* 18.4, 3.8, C(4)*H*), 3.32 (1H, dd, *J* 18.4, 9.8, C(4)*H*), 3.70 (3H, s, CO_2CH_3), 3.85 (1H, d, *J* 10.9, C(2)*H*), 3.95 (1H, app. td, *J* 10.3, 3.8, C(3)*H*), 4.36 (2H, t, *J* 7.2, ArN(1)CH_2), 7.00 (2H, d, *J* 8.4, (C(3)ArC(2,6)*H*)), 7.05 (2H, d, *J* 8.4, (C(3)ArC(3,5)*H*), 7.28 (2H, d, *J* 8.5, (C(2)ArC(2',6')*H*), 7.61 (2H, d, *J* 8.5, (C(2)ArC(3',5')*H*), 7.65 (1H, s, N(1)C*H*); **^{13}C{^{1}H} NMR** (126 MHz) δ_C: 14.2 (*C*H_3), 22.7 (*C*H_2), 26.6 (*C*H_2), 29.1 (*C*H_2), 29.2 (*C*H_2), 30.5 (ArN(1)CH_2*C*H_2), 31.9 (*C*H_2), 41.2 (*C*(4)H_2), 43.2 (*C*(3)), 50.6 (ArN(1)*C*H_2), 52.7 (O*C*H_3), 56.4 (*C*(2)), 118.6 (q, ^{2}*J* 288, *C*F_3), 119.5 (N(3)*C*=C), 121.9 (N(1)*C*H), 126.0 (C(2)Ar*C*(3,5)), 128.6 (C(3)Ar*C*(3',5')), 130.2 (C(3)Ar*C*(2',6')), 131.8 (C(2)Ar*C*(2,6)), 132.5 (C(3)Ar*C*(1'), 135.2 (C(2)Ar*C*(1'), 139.0 (C(2)Ar*C*(4)), 147.3 (C(3)Ar*C*(4'), 172.8 (*C*(1)), 188.9 (q, *J* 35.1, *C*(5)); **^{19}F {^{1}H} NMR** (470 MHz) δ_F: −79.5 (CF_3).

*Data for minor diastereomer syn **132***: **^{1}H NMR** (500 MHz) (*selected*) δ_H: 2.71 (1H, dd, *J* 18.3, 3.5, C(4)*H*), 2.99 (1H, dd, *J* 18.3, 10.3, C(4)*H*), 3.41 (3H, s, CO_2CH_3), 3.89 (1H, d, *J* 11.4, C(2)*H*),

4.00 (1H, app. td, *J* 10.5, 3.5, C(3)*H*), 7.33 (2H, m, C(3)ArC(2',6')*H*), 7.34 (2H, m, C(2)ArC(2,6)*H*), 7.72 (1H, s, N(1)C*H*), 7.78 (2H, m, C(2)ArC(3,5)*H*); **^{13}C{^{1}H} NMR** (126 MHz) δ_C: 40.3 (*C*(4)H_2), 43.0 (*C*(3)H), 52.3 (O*C*H_3), 56.7 (*C*(2)H), 119.6 (N(1)C=*C*), 126.2 (C(2)Ar*C*(3,5)H), 129.9 (C(3)Ar*C*(3',5')H), 130.3 (*C*(3)Ar*C*(2',6')), 134.9 (C(2)Ar*C*(1), 171.9 (C(1)); **^{19}F {^{1}H} NMR** (470 MHz) δ_F: −79.7 (C*F*$_3$); **HRMS** (ESI$^+$) $C_{29}H_{34}F_3N_3O$ $[M+H]^+$, found 608.1714, requires 608.1730 (−2.67 ppm).

(±)-3-thiophene dihydropyranone terminated surface 135

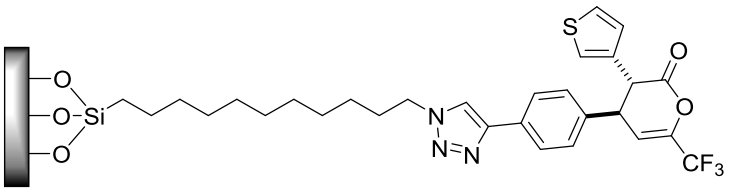

Following General Procedure **D**, 3-thiophenylacetic acid **134** (28 mg, 0.2 mmol), *i*Pr_2NEt (51 μL, 0.30 mmol), pivaloyl chloride (36.0 μL, 0.29 mmol) in CH_2Cl_2 (3 mL), DHPB **60** (3.0 mg, 0.001 mmol, 5 mol%), enone terminated wafer **128** and *i*Pr_2NEt (85 μL, 0.5 mmol) were stirred for 24 h at rt affording lactone terminated surface **135.**

(±)-4-FC_6H_4 dihydropyranone terminated surface 136

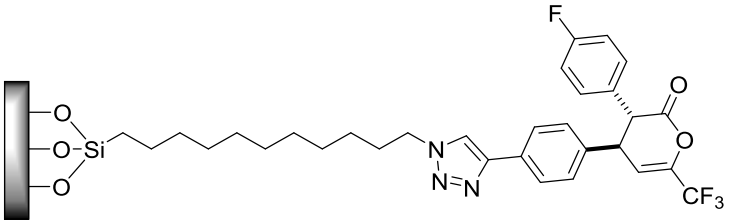

Following General Procedure **D**, 4-fluorophenylacetic acid (30 mg, 0.2 mmol), *i*Pr_2NEt (51 μL, 0.30 mmol), pivaloyl chloride (33.0 μL, 0.27 mmol) in CH_2Cl_2 (3 mL), DHPB **60** (3.0 mg, 0.001 mmol, 5 mol%), enone terminated wafer **128** and *i*Pr_2NEt (85 μL, 0.5 mmol) were stirred for 24 h at rt affording lactone terminated surface **136.**

(±)-4-BrC_6H_4 dihydropyranone terminated surface 137

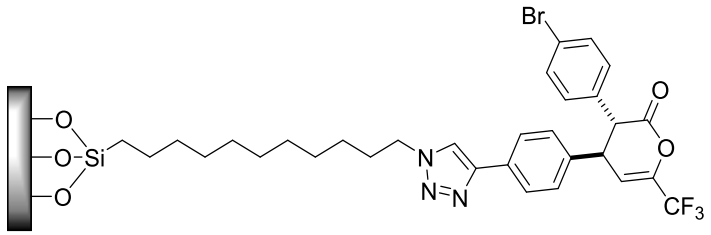

Following General Procedure **D**, 4-bromophenylacetic acid **98** (28 mg, 0.2 mmol), *i*Pr_2NEt (51 μL, 0.30 mmol), pivaloyl chloride (36.0 μL, 0.29 mmol) in CH_2Cl_2 (3 mL), DHPB **60** (3.0 mg, 0.001 mmol, 5 mol%), enone terminated wafer **128** and *i*Pr_2NEt (85 μL, 0.5 mmol) were stirred for 24 h at rt affording lactone terminated surface **137**.

(±)-4-N$Me_2C_6H_4$ dihydropyranone terminated surface 138

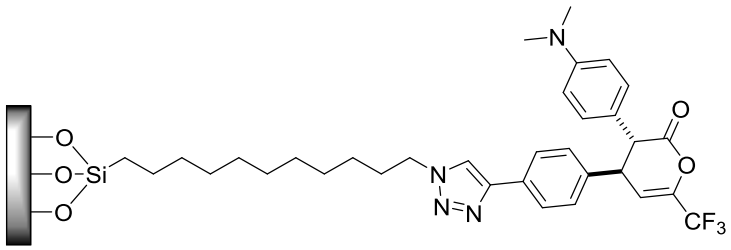

Following General Procedure **D**, 4-(dimethylamino)phenylacetic acid (35 mg, 0.196 mmol), *i*Pr_2NEt (51 μL, 0.30 mmol), pivaloyl chloride (36.0 μL, 0.29 mmol) in CH_2Cl_2 (3 mL), DHPB **60** (3.0 mg, 0.001 mmol, 5 mol%), enone terminated wafer **128** and *i*Pr_2NEt (85 μL, 0.5 mmol were stirred for 24 h at rt affording lactone terminated surface **138**.

(±)-4-$CF_3C_6H_4$ dihydropyranone terminated surface 139

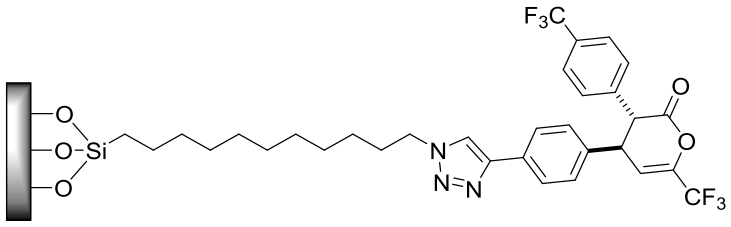

Following General Procedure **D**, 4-(Trifluoromethyl)phenylacetic acid (40 mg, 0.196 mmol), *i*Pr_2NEt (51 μL, 0.30 mmol), pivaloyl chloride (36.0 μL, 0.29 mmol) in CH_2Cl_2 (3 mL), DHPB **60** (3.0 mg, 0.001 mmol, 5 mol%), enone terminated wafer **128** and *i*Pr_2NEt (85 μL, 0.5 mmol) were stirred for 24 h at rt affording lactone terminated surface **139**.

6.4 Experimental for Chapter 3

General Procedure E: *Generation of carboxylic acids from phenylglycines*

To a round bottomed flask containing aq. 2 M NaOH (50 mL) at 0 °C was added the appropriate amino-2-phenylacetic acid (1 equiv.) with stirring. Acid chloride **170** (1.1 equiv.) was added dropwise over 10 mins. The solution was allowed to warm to rt and stir for 2 h. The reaction mixture was acidified with 2 M HCl (50 mL) and adjusted to between pH 3-4. The mixture was filtered and washed with ice cold water (3 × 50 mL) to afford the pure product as a colourless solid.

General Procedure F: *Generation of methyl esters from carboxylic acids*

To a round bottomed flask containing MeOH (15 mL) was added the appropriate phenylacetic acid (1 equiv.) with stirring. H_2SO_4 (2 mL) was added and the reaction was stirred at reflux for 16 h. The reaction was cooled to rt and concentrated *in vacuo* then dissolved in CH_2Cl_2 and washed with sat. aq. $NaHCO_3$ and brine to afford the crude product. Recrystallisation from EtOH/H_2O afforded the pure ester.

General Procedure G: *Generation of hydrazines from methyl esters*

To a round bottomed flask containing MeOH (0.4 M) the appropriate methyl ester (1 equiv.) was added hydrazine monohydrate (20 equiv.) and the reaction as stirred at reflux for 16 h. The reaction was cooled to rt and concentrated *in vacuo* to afford the crude hydrazine which was recrystallised from EtOH to afford the pure product.

General Procedure H: *Amino acid coupling of hydrazines with carboxylic acids*
To a round bottomed flask containing DMF:CH_2Cl_2 (10:10 mL) was added the appropriate acid (1.5 equiv.), EDCI (1.8 equiv.), HOBt (1.8 equiv.) and the resulting yellow solution was stirred at rt for 30 mins. To the reaction mixture was added hydrazide (1 equiv.) and *N*-methyl morpholine (2.5 equiv.) and the solution was stirred for 16 h. The resulting mixture was quenched with H_2O (30 mL) and the aqueous phase was extracted with EtOAc (3 × 30 mL), washed with $NaHCO_3$ (30 mL), citric acid (30 mL) and H_2O (30 mL) and the combined organic extracts were washed with brine, dried ($MgSO_4$), filtered and concentrated *in vacuo* to afford the crude product. Recrystallisation from EtOH afforded the pure product as a colourless solid.

General Procedure I: *Deposition of cysteine on Au coated SiO_2 and Au coated AFM tips*
The tip side of an AFM cantilever was coated with ~5 nm of Ti as an adhesion promotor followed by ~50 nm of Au using a thermal evaporator which afforded Au coated AFM tips. The Au coated AFM tip or wafer was rinsed with EtOH and immersed in a 2 mM solution of the appropriate

cysteine in H_2O. After 24 h the AFM tip or wafer was removed from the solution and rinsed with H_2O, EtOH and dried under a stream of Ar to afford the appropriate cysteine terminated surface.

General Procedure J: *Deposition of chiral benzamide on Au coated SiO_2 and Au coated AFM tips*

The Au coated AFM tip or wafer was rinsed with EtOH and immersed in a 0.5 mM solution of the appropriate benzamide in EtOH. After 24 h the AFM tip or wafer was removed from the solution and rinsed with H_2O, EtOH and dried under a stream of Ar to afford the appropriate benzamide terminated surface.

General procedure K: *Michael addition lactonisation using HyperBTM **61***

To a round-bottomed flask containing a stirrer bar and a solution of acid (1 equiv.) in CH_2Cl_2 (3 mL) was added *i*Pr_2NEt (1.5 equiv) and pivaloyl chloride (1.5 equiv.) at 0 °C. The reaction mixture was allowed to stir at 0 °C for 20 min. The solution was cooled to −78 °C and the appropriate enantiomer of HyperBTM **61** (5 mol %) was added. A pre-cooled (−78 °C) solution of enone **127** in CH_2Cl_2 (2 mL) added followed by *i*Pr_2NEt (2.5 equiv). The reaction was stirred at −78 °C for 16 h and quenched with aq. 1 M HCl. The aqueous phase was extracted using CH_2Cl_2 (2 × 10 mL) and the combined organic extracts were washed with brine, dried ($MgSO_4$), filtered and concentrated *in vacuo* to afford the crude product which was purified by flash chromatography (pet. ether: Et_2O) to afford the pure product.

Bromine terminated SAM on Si/SiO_2 using 11-bromoundecyltrimethoxysilane (solution deposition) 115

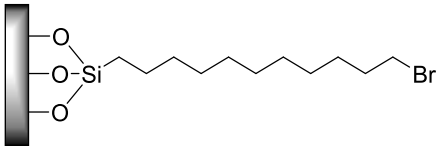

Freshly cleaned silicon wafers (as per the cleaning procedure outlined in chapter 2) were placed in an oven at 130 °C for 30 mins prior to being immersed in a freshly prepared solution of 11-bromoundecyltrimethoxysilane **165** (64 µL, 10 mmol, 1 equiv.) and NEt_3 (42 µL, 15 mmol, 1.5 equiv.) in toluene (20 mL) for 24 h. Once deposition was complete the wafer was removed and rinsed with copious amounts of toluene, EtOH and H_2O and dried under a stream of Ar.

3,5-Dimethylbenzoyl chloride 170

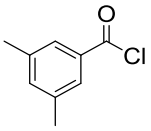

To a round bottomed flask containing thionyl chloride (20.0 mL, 266.0 mmol, 8 equiv.) was added 3,5-dimethylbenzoic acid **171** (5.0 g, 33.3 mmol, 1 equiv.) with stirring and the mixture was heated at reflux for 16 h. Excess thionyl chloride was removed by azeotrope with toluene (2 × 10 mL) under reduced pressure. The crude product was purified by Kugelrohr distillation to afford the pure product as a colourless oil (4.75 g, 85% yield); **bp** 140 °C, (5 mbar) {Lit.[296] **bp** 85-86 °C, (1.2 mbar)}; **^{1}H NMR** (400 MHz, $CDCl_3$) δ_H: 2.37 (6H, s, 2 × ArC*H*$_3$), 7.31 (1H, s, ArC(4)*H*), 7.73 (2H, s, ArC(2,6)*H*). All data in accordance with the literature.[296]

(±)-2-[(3,5-Dimethylphenyl)formamido]-2-phenylacetic acid 172

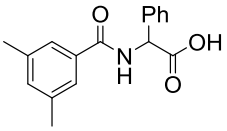

Following general procedure **E**, (±)-2-amino-2-phenylacetic acid **169** (3.0 g, 19.9 mmol, 1 equiv.), acid chloride **170** (3.66 g, 21.8 mmol, 1.1 equiv.) afforded the pure product as a colourless solid after recrystallisation (2.16 g, 83% yield); **mp** 176-179 °C; ν_{max} (thin film, cm^{-1}) 3307 (N-H), 2912 (C-H), 1705 (N-*C*=O), 1635 (C=O); **^{1}H NMR** (400 MHz, d_6-DMSO) δ_H: 2.31 (6H, s, 2 × ArC*H*$_3$), 5.58 (1H, d, *J* 7.5, C(2)*H*), 7.16 (1H, s, ArC(4)*H*), 7.29-7.36 (1H, m, PhC(4)*H*), 7.38 (2H, m, PhC(3,5)*H*), 7.49 (2H, d, *J* 7.3, PhC(2,6)*H*), 7.53 (2H, s, ArC(2,6)*H*), 8.91 (1H, d, *J* 7.5, N*H*), 12.8 (1H, bs, COO*H*); **^{13}C{^{1}H} NMR** (100 MHz, , d_6-DMSO) δ_C: 20.8 (2 × Ar*C*H$_3$), 56.8 (*C*(2)H), 125.4 (Ar*C*(2,6)H), 127.9 (Ph*C*(2,6)H), 128.1 (Ph*C*(4)H), 128.4 (Ph*C*(3,5)H), 132.7 (Ar*C*(4)H), 133.7(Ar*C*(3,5)), 137.2 (Ph*C*(1)), 137.3 (Ar*C*(1)), 166.4 (N*C*=O), 171.9 (*C*=O); **HRMS** (NSI$^-$) $C_{17}H_{17}NO_3$ $[M-H]^-$, found 282.1136, requires 282.1136 (+0.0 ppm).

(2*S*)-2-[(3,5-dimethylphenyl)formamido]-2-phenylacetic acid 172

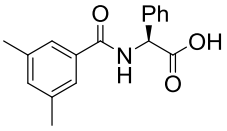

Following general procedure **E**, (*S*)-2-amino-2-phenylacetic acid **169** (1.40 g, 9.22 mmol, 1 equiv.), acid chloride **170** (1.7 g, 10.14 mmol, 1.1 equiv.) afforded the pure product as a colourless solid after recrystallisation (2.11 g, 81% yield) $[\alpha]_D^{20} = -74.9$ (*c* 1.0 MeOH), **mp** 170-172 °C; All spectroscopic data were identical to those of (±)-**172**.

(2*R*)-2-[(3,5-dimethylphenyl)formamido]-2-phenylacetic acid 172

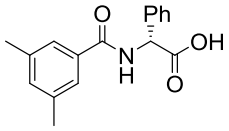

Following general procedure **E**, (*R*)-2-amino-2-phenylacetic acid **169** (1.40 g, 9.22 mmol, 1 equiv.) and acid chloride **170** (1.7 g, 10.14 mmol, 1.1 equiv.) afforded the pure product as a colourless solid after recrystallisation (2.23 g, 82% yield); $[\alpha]_D^{20} = +65.6$ (*c* 1.0 MeOH), **mp** 176-178 °C; All spectroscopic data were identical to those of (±)-**172**.

2-(undec-10-en-1-yl)isoindoline-1,3-dione 175

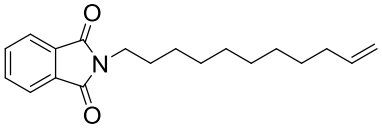

To a round bottomed flask containing 11-bromo-1-undecene **174** (10.9 g, 47 mmol, 1 equiv.) in DMF (100 mL) was added potassium phthalimide **173** (8.70 g, 47 mmol, 1 equiv.) under Ar. The reaction mixture was stirred for 16 h, poured into a 1:1 mix of H_2O:brine and extracted with Et_2O (3 × 50 mL). The combined organic extracts were washed with brine, dried ($MgSO_4$), filtered and concentrated *in vacuo* to afford the pure product as a colourless solid (8.09 g, 75 % yield); **mp** 37-40 °C {Lit.[297] 42-45 °C}; **^{1}H NMR** (400 MHz, $CDCl_3$) 1.26-1.36 (12H, bs, 6 × CH_2), 1.66 (2H, m, CH_2), 2.02 (2H, tdd, *J* 6.6, 5.4, 1.4, CH_2), 3.67 (2H, t, *J* 7.6, NCH_2), 4.93 (1H, dq, *J* 10.2, 1.2, =CH^AH^B), 4.98 (1H, dq, *J* 17.0, 1.8, =CH^AH^B), 5.81 (1H, ddt, *J* 17.0, 10.2, 6.7, =C*H*), 7.70 (2H, dd, *J* 5.5, 3.0, Ar*H*), 7.84 (2H, dd, *J* 5.5, 3.0, Ar*H*). All data in accordance with the literature.[298]

Undec-10-en-1-amine 168

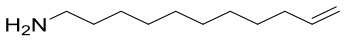

To a round bottomed flask was containing EtOH (30 mL) was added phthalimide **175** (2.42 g, 6.44 mmol, 1 equiv.) with stirring. Hydrazine monohydrate (0.345 mL, 7.1 mmol, 1.1 equiv.) was added and the suspension was heated at reflux for 16 h. The reaction was cooled to rt, quenched with 2 M HCl (30 mL) and the aqueous layer washed with Et_2O (3 × 30 mL). The organic layers were discarded and the aqueous layer was basified to pH 8 with aq. 2 M NaOH. The aqueous layer was extracted with CH_2Cl_2 (3 × 50 mL). The combined organic extracts were washed with brine, dried ($MgSO_4$), filtered and concentrated *in vacuo* to afford the crude product as a colourless oil which was used without further purification or if desired purified using flash chromatography on silica gel (89:10:1 $CHCl_3$:MeOH:NH_4OH) (801 mg, 75% yield); **^{1}H NMR** (400 MHz, $CDCl_3$) 1.25-1.33 (12H, bs, 6 × CH_2), 1.36 (2H, m, CH_2), 1.44 (4H, m, 2 × CH_2), 2.03 (2H, m, CH_2), 2.67

(2H, t, *J* 7.0, NCH_2), 4.92 (1H, dd, *J* 10.2, 1.9, =CH^AH^B), 4.98 (1H, app. dq, *J* 17.0, 1.8, =CH^AH^B), 5.80 (1H, ddt, *J* 17.0, 10.2, 6.7, =C*H*). All data in accordance with the literature.[298]

(*R*)-3,5-Dimethyl-N-(2-oxo-1-phenyl-2-(undec-10-en-1-ylamino)ethyl)benzamide 176

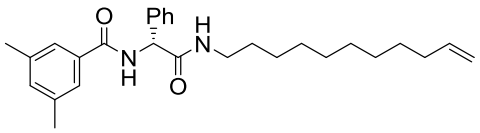

To a round bottomed flask containing CH_2Cl_2 (40 mL) was added EDCI (2.28 g, 11.9 mmol, 1.8 equiv.), HOBt (1.61 g, 11.9 mmol, 1.8 equiv.) and acid (*S*)-**172** (2.81 g, 9.93 mmol, 1.5 equiv.) and the resulting mixture was stirred for 30 mins. Amine **168** (1.12 g, 6.62 mmol, 1 equiv.), was added to the bright yellow reaction mixture as a solution in CH_2Cl_2 (10 mL). *N*-Methyl morpholine (1.82 mL, 16.5 mmol, 2.5 equiv.) was added and the reaction was stirred for 16 h. The reaction was quenched with H_2O (40 mL), and the aqueous phase was extracted with EtOAc (3 × 50 mL) and washing of the organic phase with sat. aq. $NaHCO_3$ (40 mL), citric acid (40 mL, 10 %) and brine afforded the crude product. Flash chromatography on silica gel (8:2 Hex:EtOAc) afforded the pure product as an off white solid (3.27 g, 66% yield); $[\alpha]_D^{20} = -1.1$ (*c* 1.0 MeOH), **mp** 108-111 °C; ν_{max} (thin film, cm^{-1}) 3282 (N-H), 2922 (C-H), 2852 (C-H), 1629 (NC=O), 1539 (C=O); **^{1}H NMR** (400 MHz, $CDCl_3$) 1.21-1.29 (10H, bs, 5 × CH_2), 1.37 (2H, m, CH_2), 1.44 (2H, m, CH_2), 2.02 (2H, ddt, *J* 8.1, 6.7, 1.4, CH_2), 2.34 (6H, s, 2 × ArCH_3), 3.23 (2H, tdd, *J* 7.1, 5.8, 1.2, NCH_2), 4.93 (1H, dd, *J* 10.2, 2.3, CH^AH^B), 4.99 (1H, dq, *J* 17.0, 1.8, CH^AH^B), 5.67 (1H, d, *J* 6.6, C*H*), 5.80 (1H, ddt, *J* 17.0, 10.1, 6.7, =C*H*), 6.09 (1H, t, *J* 5.8, N*H*), 7.13 (1H, s, ArC(4)*H*), 7.28-7.36 (2H, m, PhC(2,6)*H*), 7.43-7.38 (3H, m, Ph(3,5)*H* and PhC(4)*H*)), 7.63 (1H, d, *J* 6.6, Ar*H*); **^{13}C{^{1}H} NMR** (125 MHz, $CDCl_3$) 21.4 (ArCH_3), 26.8 (*C*H$_2$), 29.0 (*C*H$_2$), 29.2 (*C*H$_2$), 29.3 (*C*H$_2$), 29.4 (*C*H$_2$), 29.5 (*C*H$_2$), 29.6 (*C*H$_2$), 33.94 (*C*H$_2$), 40.1 (N*C*H$_2$), 57.5 (*C*H), 114.2 (=*C*HH), 125.05 (Ar*C*(3,5)H), 127.4 (Ph*C*(2,6)H), 128.4 (Ar*C*(4)H), 129.1 (Ph*C*(3,5)H), 133.5 (Ar*C*(4)H), 133.8 (Ph*C*(1)H), 138.3 (Ar*C*(2,6)H), 138.6 (Ph*C*(1)), 139.3 (=*C*H), 167.1 (*C*=O), 170.1 (*C*=O); **HRMS** (NSI$^+$) $C_{28}H_{39}N_2O_2$ $[M+H]^+$, found 435.3006, requires 435.2993 (+3.0 ppm).

(*R*)-S-(11-(2-(3,5-Dimethylbenzamido)-2-phenylacetamido)undecyl) ethanethioate 177

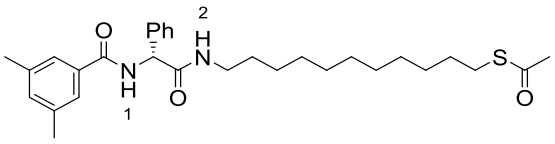

To a round bottomed flask containing carbon tetrachloride (30 mL) was added alkene **176** (1.2 g, 2.76 mmol, 1 equiv.) with stirring under Ar. Benzoyl peroxide, Luperox® A75 (80 mg, 0.276

mmol, 10 mol%) and thioacetic acid (1.0 mL, 13.8 mmol, 5 equiv.) were added and irradiated at 365 nm in a photochemical reactor (made in house) for 16 h under Ar. The reaction was quenched with cyclohexene (1 mL) and the solvent removed *in vacuo* to afford the crude product. The residue was dissolved in CH_2Cl_2 and aq. 1 M NaOH was used to adjust to pH 7. The aqueous phase was extracted with CH_2Cl_2 (3 × 30 mL) and the combined organic extracts were washed with brine, dried ($MgSO_4$), filtered and concentrated *in vacuo* to afford the crude product. The crude residue was purified by Biotage® Isolera™ 4 [SNAP Ultra 25 g, 75 mL min−1, hexane : EtOAc (95 : 5 2CV, 95 : 5 to 70 : 30 10 CV, 60 : 40 3 CV)] to give the title compound as a colurless solid (370 mg, 10% yield); $[\alpha]_D^{20}$ = +0.4 (*c* 1.0 $CHCl_3$); **mp** 88-91 °C; ν_{max} (thin film, cm^{-1}) 3323 (N-H), 2914 (C-H), 2848 (C-H), 1687 (NC=O), 1629 (C=O); **^{1}H NMR** (400 MHz, $CDCl_3$) δ_H: 1.20-1.30 (12H, bs, 6CH_2), 1.34 (2H, m, CH_2), 1.43 (2H, m, CH_2), 2.32 (3H, s, C=OCH_3), 2.34 (6H, s, ArCH_3), 2.86 (2H, t, *J* 7.4, SCH_2), 3.25 (2H, td, *J* 7.1, 5.9, NCH_2), 5.57 (1H, d, *J* 6.8, C*H*), 5.71 (1H, t, *J* 5.9, N*H*), 7.12 (1H, s, ArC(4)*H*), 7.31 (1H, dd, Ph(4)*H*), 7.34 (2H, t, Ph(3,5)*H*), 7.43 (2H, s, Ar(2,6)*H*), 7.46 (2H, d, *J* 6.3, Ph(2,6)*H*), 7.36 (1H, d, *J* 6.8, N(1)*H*); **^{13}C{^{1}H} NMR** (126 MHz) δ_C: 21.4 (2 × Ar*C*H_3), 26.8 (*C*H_2), 28.9 (*C*H_2), 29.1 (2 × *C*H_2), 29.2 (S*C*H_2), 29.3 (2 × *C*H_2), 29.4 (2 × *C*H_2), 29.5 (NCH_2*C*H_2), 29.6 (*C*H_2), 30.8 (C=O*C*H_3), 40.1 (N*C*H_2), 57.5 (*C*(2)H), 125.1 (Ar*C*(2,6)H), 127.5 (Ph*C*(2,6)H), 128.4 (Ph*C*(4)H), 129.1 (Ph*C*(3,5)H), 133.5 (Ar*C*(4)H), 133.9 (Ar*C*(1)), 138.4 (Ar*C*(2,6)H), 138.6 (Ph*C*(1)), 167.1 (O=*C*N(1)H), 170.1 (O=*C*N(2)H), 196.3 (S*C*=O); **HRMS** (NSI^+) $C_{30}H_{43}N_2O_3$ $[M+H]^+$, found 511.2989, requires 511.2916 (+1.4 ppm).

(±)-Methyl 2-(3,5-dimethylbenzamido)-2-phenylacetate 182

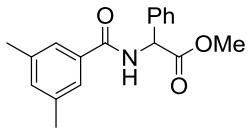

Following general procedure **F**, **(±)**-2-[(3,5-dimethylphenyl)formamido]-2-phenylacetic acid **172** (500 mg, 1.76 mmol, 1 equiv.) in MeOH and H_2SO_4 afforded pure methyl ester as a colourless solid after recrystallisation (346 mg, 62% yield), **mp** 128-129 °C; ν_{max} (thin film, cm^{-1}) 3454 (C-H), 1743 (C=O), 1635 (C=O), 1602 (N-C=O), 1525 (N-C=O); **^{1}H NMR** (500 MHz, $CDCl_3$) δ_H: 2.35 (6H, s, 2ArCH_3), 3.78 (1H, s, OCH_3), 5.78 (1H, d, *J* 7.1, C(2)*H*), 7.09 (1H, d, *J* 7.1, N*H*), 7.14 (1H, s, ArC(4)*H*), 7.32-7.40 (3H, m, PhC(3,5)*H* and PhC(4)*H*), 7.42 (2H, s, ArC(2,6)*H*), 7.45 (2H, d, *J* 7.3, PhC(2,6)*H*); **^{13}C{^{1}H} NMR** (126 MHz, $CDCl_3$) δ_C: 21.4 (2 × Ar*C*H_3), 53.1 (O*C*H_3), 58.9 (*C*(2)H), 125.0 (Ar*C*(2,6)H), 127.5 (Ph*C*(2,6)H), 128.7 (Ph*C*(4)H), 129.2 (Ph*C*(3,5)H), 133.6 (Ar*C*(4)H), 133.7 (Ar*C*(3,5)), 136.8 (Ph*C*(1)), 138.5 (Ar*C*(1)), 167.0

(N*C*=O), 171.7 (*C*=O); **HRMS** (NSI$^+$) $C_{18}H_{20}O_3N$ $[M+H]^+$, found 298.1438, requires 298.1455 (+2.5 ppm).

Methyl (*R*)-2-(3,5-dimethylbenzamido)-2-phenylacetate 182

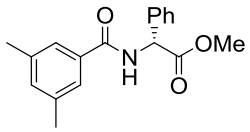

Following general procedure **F**, (2*R*)-2-[(3,5-dimethylphenyl)formamido]-2-phenylacetic acid **172** (500 mg, 1.76 mmol, 1 equiv.) in MeOH and H_2SO_4 afforded pure methyl ester as a colourless solid after recrystallisation (221 mg, 42 %yield); $[\alpha]_D^{20}$ = +72.0 (*c* 1.0 MeOH), **mp** 148-150 °C. All spectroscopic data were identical to those of (±)-**182**

Methyl (*S*)-2-(3,5-dimethylbenzamido)-2-phenylacetate 182

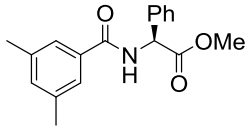

Following general procedure **F**, (2*S*)-2-[(3,5-dimethylphenyl)formamido]-2-phenylacetic acid **172** (450 mg, 1.51 mmol, 1 equiv.) in MeOH and H_2SO_4 afforded pure methyl ester as a colourless solid after recrystallisation (310 mg, 55% yield); $[\alpha]_D^{20}$ = −65.3 (*c* 1.0 MeOH), **mp** 150-152 °C. All spectroscopic data were identical to those of (±)-**182**

(±)-*N*-(2-hydrazinyl-2-oxo-1-phenylethyl)-3,5-dimethylbenzamide 180

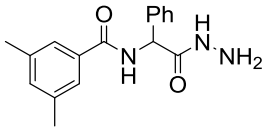

Following general procedure **G**, **(±)-**methyl-2-(3,5-dimethylbenzamido)-2-phenylacetate **182** (243 mg, 0.817 mmol, 1 equiv.) and $N_2H_4{\cdot}H_2O$ (0.8 mL, 16.3 mmol, 20 equiv.) in MeOH afforded pure hydrazine as a colourless solid after recrystallisation (134 mg, 55% yield); **mp** 186-188 °C; ν_{max} (thin film, cm^{-1}) 3340 (N-H), 1635 (C=O), 1600 (C=O), 1510 (N-C=O); **^{1}H NMR** (700 MHz, d_6-DMSO) δ_H: 2.31 (6H, s, 2 × C*H*$_3$), 4.31 (2H, d, *J* 3.7, N*H*$_2$), 5.66 (1H, d, *J* 8.1, C(1)*H*), 7.16 (1H, s, ArC(4)*H*), 7.28 (1H, t, *J* 7.3, ArC(2)*H*), 7.34 (1H, t, *J* 7.5, ArC(6)*H*), 7.48–7.55 (3H, m, PhC(2,6)*H*) and PhC(4)*H*), 8.67 (1H, d, *J* 8.1, N*H*), 9.50 (1H, t, *J* 3.7, N*H*NH$_2$); **^{13}C{^{1}H} NMR** (126 MHz, d_6-DMSO) δ_C: 20.8 (2 × Ar*C*H$_3$), 55.4 (*C*H), 125.4 (Ar*C*(2,6)H), 127.4 (Ph*C*(2,6)H), 127.5 (Ph*C*(4)H), 128.2 (Ph*C*(3,5)H), 132.6 (Ar*C*(4)H), 133.8 (Ar*C*(3,5)), 137.2 (Ph*C*(1)), 138.7

(Ar*C*(1)), 166.2 (N*C*=O), 169.2 (NH_2NHC=O); **HRMS** (NSI^+) $C_{17}H_{19}O_2N_3$ $[M+H]^+$, found 298.1552, requires 298.1550 (+0.7 ppm).

(*R*)-*N*-(2-Hydrazinyl-2-oxo-1-phenylethyl)-3,5-dimethylbenzamide 180

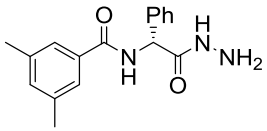

Following general procedure **G**, methyl (*R*)-2-(3,5-dimethylbenzamido)-2-phenylacetate **182** (221 mg, 0.743 mmol, 1 equiv.) and $N_2H_4{\cdot}H_2O$ (0.72 mL, 14.9 mmol, 20 equiv.) in MeOH afforded pure hydrazine as a colourless solid after recrystallisation (117 mg, 53% yield); $[\alpha]_D^{20}$ = +9.0 (*c* 1.0 MeOH), **mp** 196-198 °C; **Chiral HPLC analysis:** Chiralcel AD-H (10% *i*PrOH:hexane, flow rate 1 mL min^{-1}, 211 nm) t_R (1*R*): 16.0 min, >99% ee. All spectroscopic data were identical to those of (±)-**180**.

(*S*)-*N*-(2-Hydrazinyl-2-oxo-1-phenylethyl)-3,5-dimethylbenzamide 180

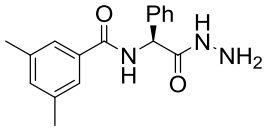

Following general procedure C, methyl (*S*)-2-(3,5-dimethylbenzamido)-2-phenylacetate **182** (273 mg, 0.92 mmol, 1 equiv.) and $N_2H_4{\cdot}H_2O$ (0.9 mL, 18.3 mmol, 20 equiv.) in MeOH afforded pure hydrazine as a colourless solid after recrystallisation (104 mg, 39% yield) $[\alpha]_D^{20}$ = −8.8 (*c* 0.5 MeOH),), **mp** 198-200 °C; **Chiral HPLC analysis:** Chiralcel AD-H (10% *i*PrOH:hexane, flow rate 1 mL min^{-1}, 211 nm) t_R (1*S*): 26.7 min, >99% ee. All spectroscopic data were identical to those of (±)-**180**.

11-Mercaptoundecanoic acid 181

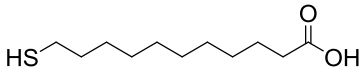

To a round bottomed flask containing H_2O (25 mL) was added 11-bromoundecanoic acid **183** (4.0 g, 15.1 mmol, 1 equiv.) and thiourea (1.51 g, 19.8 mmol, 1.3 equiv.). The mixture was stirred at reflux for 3 h, aq. 2 M NaOH (16 mL, 2 equiv.) was added and the reaction stirred at reflux for one additional hour. The reaction was cooled in an ice bath and aq. 1 M HCl was added until the solution reached pH 2. The aqueous phase was extracted using Et_2O (2 × 30 mL) and the combined

organic extracts were washed with brine, dried ($MgSO_4$), filtered and concentrated *in vacuo* to afford the pure product as a colourless solid (3.1 g, 94% yield); **mp** 40-42 °C {Lit.[299] 43.5-45 °C}; **^{1}H NMR** (400 MHz, d_6-DMSO) δ_H: 1.24 (10H, bs, 5 × C*H*$_2$), 1.28–1.37 (4H, m, 2 × C*H*$_2$), 1.44–1.57 (2H, m, C*H*$_2$), 2.16-2.20 (3H, m, SC*H*$_2$ and S*H*), 2.45 (2H, q, *J* 7.3, C=OC*H*$_2$), 11.97 (1H, s, COO*H*). All data in accordance with the literature.[299]

(±)-*N*-(2-(2-(11-mercaptoundecanoyl)hydrazinyl)-2-oxo-1-phenylethyl)-3,5-dimethylbenzamide 179

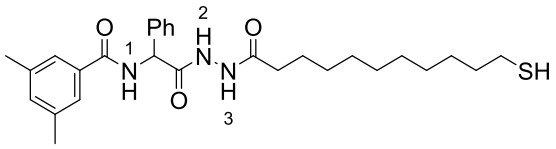

Following general procedure **H**, acid **181** (77 mg, 0.35 mmol, 1.5 equiv.), EDCI (81 mg, 0.42 mmol, 1.8 equiv.), HOBt (57 mg, 0.42 mmol, 1.8 equiv.), (±)-hydrazide **180** (70 mg, 0.24 mmol, 1 equiv.) and *N*-methyl morpholine (65 µL, 0.59 mmol, 2.5 equiv.) afforded the pure product as a colourless solid after recrystallisation (15 mg, 13% yield); ν_{max} (thin film, cm^{-1}); 3203 (N-H), 2922 (C-H), 1640 (C=O), 1600 (C=O); **mp** 172-174 °C; **^{1}H NMR** (400 MHz, d_6-DMSO) δ_H: 1.24 (12H, bs, 6× C*H*$_2$), 1.32-1.36 (2H, m, SCH$_2$C*H*$_2$), 1.50-1.57 (4H, m, 2 × C*H*$_2$),1.59 (2H, app. q, *J* 7.0, SC*H*$_2$), 2.09 (2H, t, *J* 7.0, C=OC*H*$_2$), 2.31 (6H, s, 2 × ArC*H*$_3$), 2.68 (1H, t, *J* 7.2, S*H*), 5.81 (1H, d, *J* 8.6, C*H*), 7.16 (1H, s, ArC(4)*H*), 7.31 (1H, d, *J* 7.0, PhC(4)*H*), 7.35 (2H, t, *J* 7.0, PhC(2,6)*H*), 7.54 (2H, s, ArC(2,6)*H*), 7.57 (2H, d, *J* 7.4, PhC(3,5)*H*), 8.75 (1H, d, *J* 8.6, N(1)*H*), 9.82 (1H, d, *J* 1.4, N(3)*H*), 10.30 (1H, d, *J* 1.4, N(2)*H*); **^{13}C{^{1}H} NMR** (125 MHz, d_6-DMSO) δ_H: 20.7 (2 × Ar*C*H$_3$), 25.0 (2*C*H$_2$), 28.2 (*C*H$_2$), 28.4 (SCH$_2$*C*H$_2$), 28.5 (*C*H$_2$), 28.6 (*C*H$_2$), 28.7 (*C*H$_2$), 28.8 (*C*H$_2$), 28.9 (*C*H$_2$), 33.1 (C=O*C*H$_2$), 55.1 (*C*H), 125.4 (Ar*C*(2,6)H), 127.6 (Ph*C*(3,5)H and Ph*C*(4)H), 128.2 (Ph*C*(2,6)H), 132.7 (Ar*C*(4)H), 133.7 (ArC(3,5)), 137.3 (Ar*C*(1)), 138.2 (Ph*C*(1)), 166.7 (N(1)*C*=O), 169.2 (N(2)*C*=O), 171.5 (N(3)*C*=O); **HRMS** (ESI$^-$) $C_{28}H_{39}N_3O_3S$ [M−H]$^-$, found 497.2645, requires 497.2631 (+2.8 ppm).

(*S*)-*N*-(2-(2-(11-Mercaptoundecanoyl)hydrazinyl)-2-oxo-1-phenylethyl)-3,5-dimethylbenzamide 179

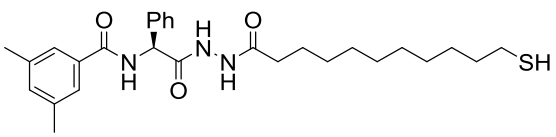

Following general procedure **H**, acid **181** (115 mg, 0.53 mmol, 1.5 equiv.), EDCI (120 mg, 0.63 mmol, 1.8 equiv.), HOBt (85 mg, 0.63 mmol, 1.8 equiv.), (*S*)-hydrazide **180** (104 mg, 0.43 mmol, 1 equiv.) and *N*-methyl morpholine (96 mL, 1.93 mmol, 2.5 equiv.) afforded the pure product as a colourless solid after recrystallisation (29 mg, 17% yield); $[\alpha]_D^{20}$ = −5.3 (*c* 0.25 MeOH), **mp** 173-175 °C; All spectroscopic data were identical to those of (±)-**179**

(*R*)-*N*-(2-(2-(11-Mercaptoundecanoyl)hydrazinyl)-2-oxo-1-phenylethyl)-3,5-dimethylbenzamide 179

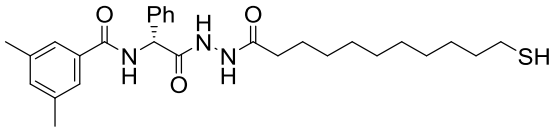

Following general procedure **H**, acid **181** (130 mg, 0.59 mmol, 1.5 equiv.), EDCI (136 mg, 0.70 mmol, 1.8 equiv.), HOBt (95 mg, 0.70 mmol, 1.8 equiv.), (*R*)-hydrazide **180** (117 mg, 0.39 mmol, 1 equiv.) and *N*-methyl morpholine (0.11 mL, 98 mmol, 2.5 equiv.) in DMF:CH_2Cl_2 (10:10 mL) afforded the pure product as a colourless solid after recrystallisation (35 mg, 18% yield); $[\alpha]_D^{20}$ = +5.8 (*c* 0.25 MeOH), **mp** 172-176 °C; All spectroscopic data were identical to those of (±)-**179**.

Generation of (*R*), (*S*) and (±)-cysteine terminated surfaces 184

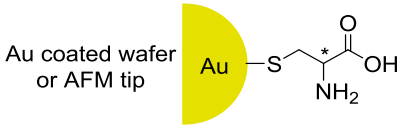

Following general procedure **I**, the Au coated AFM tip or wafer was rinsed with EtOH (10 mL) and immersed in a 2 mM solution (2.5 mg, 2 mmol) of the appropriate cysteine H_2O (10 mL). After 24 h the AFM tip or wafer was removed from the solution and rinsed with H_2O (10 mL), EtOH (10 mL) and dried under a stream of Ar to afford the appropriate cysteine terminated surface.

Generation of (*R*), (*S*) and (±)-benzamide terminated surfaces 186

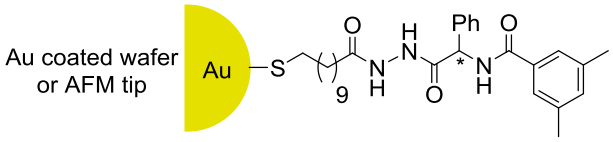

Following general procedure **J**, the Au coated AFM tip or wafer was rinsed with EtOH (10 mL) and immersed in a 0.5 mM solution (2.5 mg, 0.5 mmol) of the appropriate benzamide ((*R*), (*S*) or (±)) in EtOH (10 mL). After 24 h the AFM tip or wafer was removed from the solution and rinsed with H_2O (10 mL), EtOH (10 mL) and dried under a stream of Ar to afford the appropriate benzamide terminated surface.

(±)-4-(4-ethynylphenyl)-3-(4-fluorophenyl)-6-(trifluoromethyl)-3,4-dihydro-2H-pyran-2-one 183

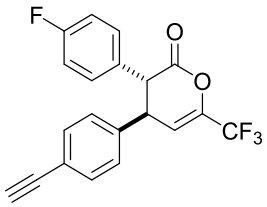

Following general procedure **K** 4-fluorophenylacetic acid **182** (138 mg, 0.892 mmol, 1 equiv.), pivaloyl chloride (165 µL, 1.34 mmol, 1.5 equiv.) and *i*Pr_2NEt (232 µL, 1.34 mmol, 1.5 equiv.) were stirred at 0 °C followed by addition of (±)-HyperBTM-**61** (14 mg, 0.045 mmol, 5 mol%) and enone **127** (200 mg. 0.982 mmol. 1 equiv.) and *i*Pr_2NEt (386 µL, 2.23 mmol, 2.5 equiv.) at −78 °C gave crude (±)-**188** (85:15 dr). The crude mixture was purified by Biotage® Isolera™ 4 [SNAP Ultra 10 g, 75 mL min^{-1}, pet. ether :Et_2O (100 : 0 3CV, 100 : 0 to 90 : 0 10 CV] afforded (±)-**188** as a colourless oil (155 mg, 48% yield, >95:5 dr); ν_{max} (thin film, cm^{-1}) 3311 (C-H), 1786 (C=O), 1726 (C=C); **^{1}H NMR** (500 MHz, $CDCl_3$) δ_H: 3.09 (1H, s, C≡*H*), 3.87 (1H, d, *J* 10.7, C(3)*H*), 3.99 (1H, dd, *J* 10.7, 2.8, C(4)*H*), 6.11 (1H, d, *J* 2.8, C(5)*H*), 6.94 (2H, d, *J* 8.2, ArC(3,5)*H*), 6.98 (4H, m, ArC(2,6)*H* and ArC(2',6')*H*), 7.39 (2H, d, *J* 8.2, ArC(3,5)*H*); **^{13}C{^{1}H} NMR** (126 MHz, $CDCl_3$) δ_C: 44.9 (*C*(4)H), 52.1 (*C*(5)H), 78.3 (C≡*C*H), 82.8 (*C*≡CH), 110.7 (d, $^3J_{C\text{-}F}$ 3.1, *C*(5)H), 116.1 (d, $^2J_{C\text{-}F}$ 21.8, C(3)Ar*C*(3,5)H), 119.5 (q, $^2J_{C\text{-}F}$ 273.0, *C*F_3), 122.2 (C(4)Ar*C*(4)), 127.6 (C(3)Ar*C*(3,5)H), 130.3 (C(4)Ar*C*(2,6)H), 133.0 (C(3)Ar*C*(2,6)H), 139.3 (C(4)Ar*C*(1)), 141.3 (q, $^2J_{C\text{-}F}$ 38.3, *C*(6)), 162.5 (d, $^1J_{C\text{-}F}$ 247.8, C(3)Ar*C*(4)), 165.6 (*C*=O); **^{19}F {^{1}H} NMR** (470 MHz, $CDCl_3$) δ_F: −72.2 (C*F*$_3$), −113.3 (ArC*F*); **HRMS** (ESI$^-$) $C_{20}H_{11}O_2F_4$ [M-H]$^-$, found 359.0703, requires 359.0701 (+0.6 ppm).

(3*R*,4*R*)-4-(4-Ethynylphenyl)-3-(4-fluorophenyl)-6-(trifluoromethyl)-3,4-dihydro-2*H*-pyran-2-one 183

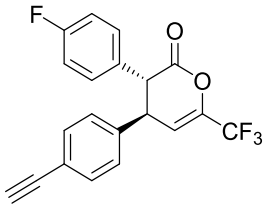

Following general procedure **K**, 4-fluorophenylacetic acid **182** (138 mg, 0.892 mmol, 1 equiv.), pivaloyl chloride (165 µL, 1.34 mmol, 1.5 equiv.) and *i*Pr$_2$NEt (232 µL, 1.34 mmol, 1.5 equiv.) were stirred at 0 °C followed by addition of (2*S*,3*R*)-HyperBTM **61** (14 mg, 0.045 mmol, 5 mol%) and enone **127** (200 mg. 0.982 mmol. 1 equiv.) and *i*Pr$_2$NEt (386 µL, 2.23 mmol, 2.5 equiv.) at −78 °C affording crude (3*R*,4*R*)-**188** (85:15 dr). The crude mixture was purified by Biotage® Isolera™ 4 [SNAP Ultra 10 g, 75 mL min^{-1}, pet. ether :Et$_2$O (100 : 0 3CV, 100 : 0 to 90 : 0 10 CV] afforded **183** as a colourless oil (155 mg, 48% yield, >95:5 dr); $[\alpha]_D^{20}$ = −105.3 (*c* 1.0 $CHCl_3$); **Chiral HPLC analysis:** Chiralcel OD-H (10% *i*PrOH:hexane, flow rate 1 mL min^{-1}, 211 nm) t_R (3*S*,4*S*): 19.6 min, (3*R*,4*R*): 11.8 min, 87% ee. All spectroscopic data were identical to those of (±)-**188**

(3*S*,4*S*)-4-(4-Ethynylphenyl)-3-(4-fluorophenyl)-6-(trifluoromethyl)-3,4-dihydro-2*H*-pyran-2-one 183

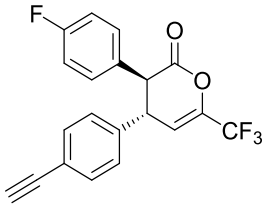

Following general procedure **K**, 4-fluorophenylacetic acid (138 mg, 0.892 mmol, 1 equiv.), pivaloyl chloride (165 µL, 1.34 mmol, 1.5 equiv.) and *i*Pr$_2$NEt (232 µL, 1.34 mmol, 1.5 equiv.) were stirred at 0 °C followed by addition of HyperBTM (2*R*,3*S*)-**61** (14 mg, 0.045 mmol, 5 mol%) and enone **127** (200 mg. 0.982 mmol. 1 equiv.) and *i*Pr$_2$NEt (386 µL, 2.23 mmol, 2.5 equiv.) at −78 °C affording crude (3*S*,4*S*)-**183** (90:10 dr). The crude mixture was purified by Biotage® Isolera™ 4 [SNAP Ultra 10 g, 75 mL min^{-1}, Pet. ether:Et$_2$O (100 : 0 3CV, 100 : 0 to 90 : 0 10 CV] afforded **183** as a colourless oil (133 mg, 42% yield, >95:5 dr); $[\alpha]_D^{20}$ = +71.6 (*c* 1.0 $CHCl_3$); **Chiral HPLC analysis:** Chiralcel OD-H (10% *i*PrOH:hexane, flow rate 1 mL min^{-1}, 211 nm) t_R (3*S*,4*S*): 19.6 min, (3*R*,4*R*): 11.8 min, 90% ee. All spectroscopic data were identical to those of (±)-**183**.

Generation of (3*R*,4*R*)-terminated surface from DHP (3*R*,4*R*)-183

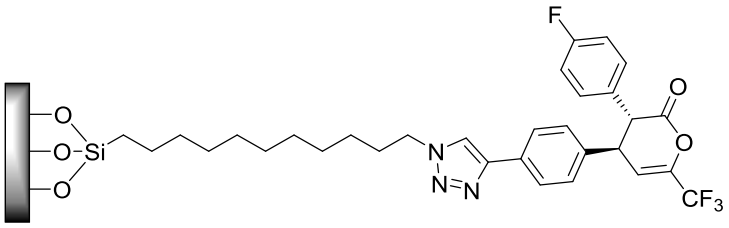

To a solution of (3*R*,4*R*)-**188** (10 mg, 0.027 mmol, 1 equiv.) in EtOH (8 mL) was added 1 mL of a 25 mL solution of $CuSO_4.5H_2O$ (7.5 mg, 0.03 mmol, 1 equiv.) and 1 mL of a 25 mL solution of sodium ascorbate (8.9 mg, 0.045 mmol, 1.5 equiv.) with stirring. The azide terminated wafer **112** was immersed in the reaction mixture for 24 h. Upon completion the enone terminated wafer was removed and rinsed with EtOH. The wafer was sonicated in EtOH and H_2O for 5 mins each, and dried under a stream of Ar.

Generation of (3S,4*S*)-terminated surface from DHP (3*S*,4*S*)-183

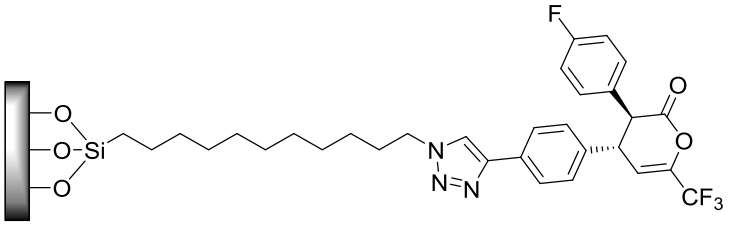

To a solution of (3*S*,4*S*)-**188** (10 mg, 0.027 mmol, 1 equiv.) in EtOH (8 mL) was added 1 mL of a 25 mL solution of $CuSO_4.5H_2O$ (7.5 mg, 0.03 mmol, 1 equiv.) and 1 mL of a 25 mL solution of sodium ascorbate (8.9 mg, 0.045 mmol, 1.5 equiv.) with stirring. The azide terminated wafer **112** was immersed in the reaction mixture for 24 h. Upon completion the enone terminated wafer was removed and rinsed with EtOH. The wafer was sonicated in EtOH and H_2O for 5 mins each, and dried under a stream of Ar.

6.5 Experimental for Chapter 4

General procedure L: *Generation of thioureas from isothiocyanates*

Isothiocyanate (1 equiv.) and the appropriate amino alcohol (1.1 equiv.) were added (neat) to a round bottomed flask and stirred for 10 mins. Toluene (5 mL) was added and the resulting solution was stirred for 20 mins. The reaction mixture was washed with H_2O (5 mL), 0.1 M HCl (5 mL) and the aqueous phase was extracted with CH_2Cl_2 (3 × 10 mL). The organic phases were combined, dried ($MgSO_4$) and concentrated *in vacuo* to afford the pure product. If necessary the products were purified using flash chromatography.

General procedure M: *Kinetic resolution of secondary and tertiary alcohols using PS-(2R,3S)-HyperBTM.*

To a round bottomed flask containing $CHCl_3$ (0.17 M) was added the appropriate alcohol with stirring at 0 °C. The appropriate anhydride and *i*Pr_2NEt were subsequently added followed by the addition of PS-(2*R*,3*S*)-HyperBTM (5 mol%) and the reaction was allowed to stir (200 rpm) at 0 °C for 24 h. Upon completion the reaction mixture was filtered using a sintered funnel and the filtrate was washed with aq. 1M HCl, sat. aq. $NaHCO_3$ and brine. The organic layer was dried (MgSO4) and concentrated *in vacuo* to afford the crude products which were purified using flash chromatography to afford the enantioenriched alcohol and ester.

***tert*-Butyl 6-bromo-2-oxobenzo[d]thiazole-3(2*H*)-carboxylate 260**

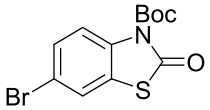

To a round bottomed flask containing anhydrous CH_2Cl_2 (10 mL) was added 6-bromo-2-benzothiazolinone **259** (500 mg, 2.2 mmol, 1 equiv.) under Ar with stirring. Boc_2O (524 mg, 2.4 mmol, 1.1 equiv.), DMAP (44 mg, 0.36 mmol, 15 mol%) and NEt_3 (0.321 mL, 2.4 mmol, 1.1 equiv.) were added and the reaction mixture was stirred for 16 h and then quenched with sat. aq. NH_4Cl (10 mL). The aqueous phase was extracted with CH_2Cl_2 (3 × 10 mL). The organic layers were combined, dried ($MgSO_4$) and concentrated *in vacuo* to afford the pure product as a light purple solid (546 mg, 76% yield); **mp** 211-213 °C; ν_{max} (thin film, cm^{-1}) 2980 (C-H), 1675 (C=O), 1645 (N-C=O); **^{1}H NMR** (500 MHz, $CDCl_3$) δ_H: 1.64 (9H, s, C(C*H*$_3$)$_3$), 7.41 (dd, *J* 8.9, 2.1, C(5)*H*), 7.48 (d, *J* 2.1, C(7)*H*), 7.77 (d, *J* 8.9, C(4)*H*); **^{13}C{^{1}H} NMR** (126 MHz, $CDCl_3$) δ_C: 27.6 (C(*C*H$_3$)$_3$), 29.1 (*C*(CH$_3$)$_3$), 114.1 (*C*(7)H), 125.1 (*C*(4)H), 126.3 (*C*(3a)), 129.4 (*C*(5)H), 136.3 (*C*(7a)), 147.7 (*C*(6)), 170.2 (*C*=O), 171.4 (Boc*C*=O); **HRMS** $(CI)^+$ $C_{12}H_{13}BrNO_3S$ $[M+H]^+$, found 329.9786, requires 329.9800 (−4.2 ppm).

2-oxo-2,3-Dihydrobenzo[*d*]thiazole-6-carbaldehyde 262

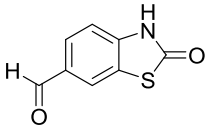

Following a procedure outlined by DeOrazio[300], to a three-necked round bottomed flask containing anhydrous THF (50 mL) was added 6-bromo-2-benzothiazolinone **259** (1.0 g, 4.37

mmol, 1 equiv.) at −78 °C with stirring under Ar. MeMgBr (1.92 mL, 4.8 mmol, 2.5 M, 1.1 equiv.) was added and the mixture was stirred at −78 °C for 45 mins. The reaction mixture was diluted with anhydrous THF (100 mL) while the internal temperature was kept below −50 °C. Once the solution was at −78 °C *t*-BuLi (4.60 mL, 8.74 mmol, 1.9 M in pentane, 2 equiv.) was added dropwise and stirred for 15 mins. DMF (2.1 mL, 26.2 mmol, 6 equiv.) was added to the yellow reaction mixture and the solution was warmed to rt. The reaction was stirred for 2 h, quenched with H_2O (100 mL) and the aqueous phase was extracted with EtOAc (3 × 70 mL). The organic layers were combined, dried ($MgSO_4$) and concentrated *in vacuo* to afford the crude product. Flash chromatography on silica gel (9:1 CH_2Cl_2:MeOH) afforded the pure product as an off white solid (595 mg, 76% yield); **mp** 229–231 °C {lit.[300] 227–228 °C};

^{1}H NMR (400 MHz, d_6-DMSO) δ_H: 7.28 (1H, d, *J* 8.2, C(4)*H*), 7.83 (1H, dd, *J* 8.2, 1.7, C(5)*H*), 8.16 (1H, d, *J* 1.7, C(7)*H*), 9.89 (1H, s, C*H*O), 12.38 (1H, bs, N*H*). All data in accordance with the literature.[300]

6-Bromo-2-chlorobenzo[*d*]thiazole 266

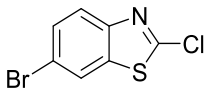

To a round bottomed flask containing DMF (1.21 mL, 15.7 mmol, 1.2 equiv.) was added phosphoryl chloride (12.2 mL, 131 mmol, 10 equiv.) and the mixture was stirred for 15 mins. 6-bromo-2-benzothiazolinone **259** was added and the reaction mixture was heated to 100 °C for 16 h. Upon cooling to rt the reaction mixture was slowly poured into a saturated solution of K_2CO_3 (75 g) in water (200 mL). The resulting mixture was stirred for 1 h at rt, filtered and washed with water to afford the pure product as a brown solid (3.00 g, 93%); **mp** 80-83 °C; **^{1}H NMR** (400 MHz, $CDCl_3$) δ_H: 7.59 (1H, dd, *J* 8.7, 2.0, ArC(5)*H*), 7.80 (1H, dd, *J* 8.7, ArC(4)*H*), 7.92 (1H, d, *J* 1.9, ArC(7)*H*). All data in accordance with the literature.[301]

(*S*)-2-((6-Bromobenzo[d]thiazol-2-yl)amino)-2-phenylethan-1-ol 267

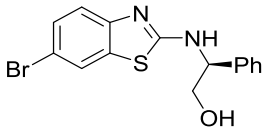

Following the procedure outline by Smith[164], to a round bottomed containing *o*-dichlorobenzene (2.1 mL, 2.0 M) was added (*S*)-phenylglycinol **257** (583 mg, 4.25 mmol, 1.05 equiv.), *i*Pr_2NEt (2.9 mL, 28.3 mmol, 2.5 equiv.), 6-bromo-2-chlorobenzothiazole **266** (1.0 g, 4.05 mmol, 1 equiv.) and the resulting pale yellow suspension was heated at reflux (195 °C DrySyn® temperature) for

24 h. After 24 h the orange mixture was allowed to cool to rt. The solvent was removed *in vacuo* and the resulting crude mixture purified using flash chromatography on silica gel (95:5 CH_2Cl_2:*i*PrOH) to afford the crude product which was recrystallised from toluene to afford the pure product as a colourless solid (1.0 g, 71% yield); $[\alpha]_D^{20}$ = −72.0 (*c* 0.5 MeOH), **mp** 157-160 °C ν_{max} (thin film, cm^{-1}); 3224 (C-H), 1541 (C=N), 1060 (CH_2OH); **^{1}H NMR** (400 MHz, d_6-DMSO) δ_H: 3.67 (2H, m, C(1)*H*$_2$), 4.99 (1H, app. q, *J* 6.8, C(2)*H*), 5.05 (1H, t, *J* 5.5, C*H*), 7.22-7.27 (2H, m, Ph(2,6)*H*), 7.30 (1H, d, *J* 2.1, ArC(7)*H*), 7.33 (2H, d, *J* 7.5, PhC(3,5)*H*), 7.35 (d, *J* 8.2, C(4)*H*), 7.37-7.42 (1H, m, PhC(4)*H*), 7.89 (1H, dd, *J* 8.2, 2.1, ArC(5)*H*), 8.69 (1H, d, *J* 7.9, N*H*); **^{13}C{^{1}H} NMR** (126 MHz, d_6-DMSO) δ_C: 60.4 (*C*(1)H_2), 64.9 (*C*(2)H), 112.2 (Ar*C*(5)H), 119.4 (Ar*C*(7)H), 123.3 (Ar*C*(7a)), 126.9 (Ph*C*(2,6)H), 127.1 (Ph*C*(4)H), 128.2 (Ph*C*(3,5)H), 128.4 (Ar*C*(4)), 132.6 (Ar*C*(3a)), 140.7 (Ph*C*(1)), 151.6 (Ar*C*(6)), 166.5(*C*=N); **HRMS** $C_{15}H_{14}N_2BrOS^+$ $[M+H]^+$, found 330.9894, requires 330.9899 (−1.5 ppm).

(*S*)-7-Bromo-2-phenyl-2,3-dihydrobenzo[d]imidazo[2,1-b]thiazole 268

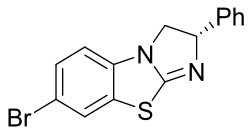

Following the procedure outlined by Smith *et al.* [164] to a round bottomed flask containing CH_2Cl_2 (20 mL) was added amino alcohol **267** (500 mg, 1.43 mmol, 1 equiv.), Et_3N (0.77 mL, 5.72 mmol, 4 equiv.) and the reaction mixture was stirred at 0 °C. After 10 mins methanesulfonyl chloride (144 μL, 1.87 mmol, 1.3 equiv.) was added with stirring. The ice/water bath was removed and the reaction stirred for 15 mins. The reaction was checked by TLC (CH_2Cl_2 / Et_2O 1:1, UV_{254} / $KMnO_4$, R_f **(*S*)-267** ~0.3, and a further portion of MsCl (0.1 equiv.) added if **(*S*)-267** remaineS. Once complete consumption of **(*S*)-267** was observed, *i*PrOH (0.5 mL) was added and the reaction was heated to reflux for 16 h. The reaction was quenched with aq. 1 M NaOH (20 mL) and the biphasic mixture stirred vigorously for 30 mins. The aqueous layer was extracted with CH_2Cl_2 (3 x 20 mL) and the combined organic washed with brine (50 mL), dried ($MgSO_4$) and concentrated *in vacuo* to afford the crude product which was purified by flash chromatography (8:2 hex: EtOAc) to afford the pure product as a white crystalline solid (274 mg, 58% yield); $[\alpha]_D^{20}$ = +67.5 (*c* 1.0 $CHCl_3$); **mp** 122-126 °C; ν_{max} (thin film) 2912 (C-H), 1687 (C=N); **^{1}H NMR** (400 MHz, $CDCl_3$) δ_H: 3.70 (1H, dd, *J* 8.9, 8.1, C(1)*H*^{A}H^B), 4.26 (1H, dd, *J* 10.2, 8.9, C(1)H^A*H*^{B}), 5.68 (1H, dd, *J* 10.2, 8.1, C(2)*H*), 6.53 (1H, d, 8.3, ArC(5)*H*), 7.28-7.31 (2H, m, ArC(6)*H* and ArC(8)*H*), 7.35-7.38 (4H, m, Ph*H*), 7.42 (1H, d, *J* 1.9, PhC(4)*H*); **^{13}C{^{1}H} NMR** (126 MHz, $CDCl_3$) δ_C: 52.9 (*C*(3)H_2), 75.9 (*C*(3)H), 109.9 (Ar*C*(5)H), 113. 6 (Ar*C*(8)H), 126.07 (Ar*C*(6)H), 126.8 (Ph*C*(2,6)H), 128.1 (Ar*C*(8a)), 129.2 (Ph*C*(3,5)H), 129.6 (Ph*C*(4)H), 129.9 (Ar*C*(4a)), 136.5

(Ar*C*(3)), 142.9 (Ph*C*(1)), 158.4 (Ar*C*(7)), 166.3 (*C*=N) **HRMS** $C_{15}H_{12}N_2BrS^+$ $[M+H]^+$, found 330.9891, requires 330.9899 (−2.4 ppm).

((4-Bromophenyl)ethynyl)triisopropylsilane 276

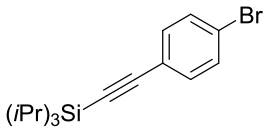

To a round bottomed flask containing 1-bromo-4-iodobenzene **274** (5.0 g, 17.6 mmol, 1 equiv.) in bench grade THF (90 mL, 0.2 M) (degassed for 10 mins) was added $Pd(PPh_3)_2Cl_2$ (246 mg, 0.352 mmol, 2 mol%) and NEt_3 (13 mL, 88 mmol, 5 equiv.) with stirring at rt. CuI (67 mg, 0.352 mmol, 2 mol%) was added to the reaction mixture followed by the dropwise addition of ethynyltriisopropylsilane **275** (4.15 mL, 19.4 mmol, 1.05 equiv.). The reaction was stirred at rt for 16 h followed and subsequently quenched with aq. 0.1 M HCl (100 mL). The aqueous layer was extracted with Et_2O (3 × 50 mL) and the combined organic washed with brine, dried ($MgSO_4$) and concentrated *in vacuo* to afford the crude product which was purified by flash chromatography (95:5 hex: tOAc) to afford the pure product as a brown oil (3.82 g, 68% yield); **^{1}H NMR** (300 MHz, $CDCl_3$) δ_H: 1.13 (21H, s, Si((C*H*(C*H*$_2$)$_3$), 7.33 (2H, d, *J* 8.6, ArC(3,5)*H*), 7.43 (2H, d, *J* 8.7, ArC(2,6)*H*). All data in accordance with the literature.[302]

(4-((Triisopropylsilyl)ethynyl)phenyl)boronic acid 277

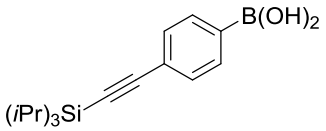

To a round bottomed flask containing bromide **276** (3.81 g, 11.3 mmol, 1 equiv.) in anhydrous THF (60 mL, 0.2 M) at −78 °C was added *n*-BuLi (5.63 mL, 12.4 mmol, 2.2 M in hexanes, 1.1 equiv.) with stirring under Ar. The reaction mixture was stirred for 30 mins at −78 °C then triisopropylborate (2.9 mL, 12.4 mmol, 1.1 equiv.) was added. The reaction was allowed to warm to rt over 16 h then 1 M HCl (35 mL, 3 equiv.) was subsequently added and the reaction was stirred for 2 h. The aqueous layer was extracted with Et_2O (3 × 50 mL) and the combined organic layers washed with brine, dried ($MgSO_4$) and concentrated *in vacuo* to afford the crude product which was purified by flash chromatography (1:1 hex:Et_2O) to afford the pure product as a colourless solid (1.36 g, 43% yield); **mp** 196-198 °C; **^{1}H NMR** δ_H (400 MHz, $CDCl_3$) 1.16 (21H, s, Si((C*H*(C*H*$_2$)$_3$), 7.59 (2H, d, *J* 8.3, ArC(3,5)*H*), 7.43 (2H, d, *J* 8.3, ArC(2,6)*H*). All data in accordance with the literature.[302]

Iodoethynyltrimethylsilane 282

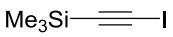

To a round bottomed flask containing trimethylsilyl acetylene **281** (1.0 mL, 14.3 mmol, 1 equiv.) in anhydrous THF (25 mL, 0.5 M) at −78 °C was added *n*BuLi (6.6 mL, 14.3 mmol, 2.17 M in hexanes, 1 equiv.) with stirring under Ar. The reaction mixture was stirred for 15 mins at −78 °C then iodine (3.6 g, 14.3 mmol, 1 equiv.) was added. The reaction flask was covered in aluminium foil and allowed to warm to rt over 16 h.[†] The reaction mixture was diluted with CH_2Cl_2 (20 mL), and washed with $Na_2S_2O_3$ (30 mL) and H_2O (30 mL). The organic phase was washed with brine, dried ($MgSO_4$) and concentrated *in vacuo* to afford the crude product which was purified by distillation to afford the pure product as a colourless oil (2.62 g, 82% yield); **bp** 70-72 °C, (20 mbar) {Lit.[303] **bp** 61-63 °C, 26 mbar}; **^{1}H NMR** (400 MHz, $CDCl_3$) δ_H: 0.18 (Si(C*H*$_3$)$_3$). All data in accordance with the literature.[304]

4-((Trimethylsilyl)ethynyl)aniline 247

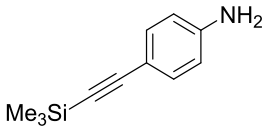

To a round bottomed flask containing THF (115 mL, 0.2 M) was added iodoaniline **246** (5.0 g, 22.8 mmol, 1 equiv.), NEt_3 (15.3 mL, 114 mmol, 5 equiv.), $Pd(PPh_3)_2Cl_2$ (160 mg, 0.23 mmol, 1 mol %), CuI (88 mg, 0.46 mmol, 2 mol%) was added with stirring and the solution was degassed for 10 mins. Trimethylsilylacetylene (3.55 mL, 25 mmol, 1.1 equiv.) was added dropwise and the reaction mixture was stirred for 16 h.[††] The reaction was quenched with 0.1 M HCl and the aqueous phase was extracted with Et_2O (3 × 50 mL). The organic layers were combined, dried ($MgSO_4$) and concentrated *in vacuo* to afford the crude product which was purified by flash chromatography (9:1 pet ether:Et_2O) to afford the pure product as a brown solid (3.27 g, 76% yield); **mp** 72-74 °C {Lit.[305] 93-95 °C}; **^{1}H NMR** (400 MHz, $CDCl_3$) δ_H: 0.22 (9H, s, SiC(C*H*$_3$)$_3$), 3.79 (2H, bs, N*H*$_2$), 6.57 (2H, d, *J* 8.5, ArC(2,6)*H*), 7.27 (2H, d, *J* 8.5, ArC(3,5)*H*). All data in accordance with the literature.[305]

((4-Isothiocyanatophenyl)ethynyl)trimethylsilane 249

[†] Work up was performed in the dark inside the fume hood.

[††] If the reaction conversion was not satisfactory then the crude material was subjected to the same reaction conditions again.

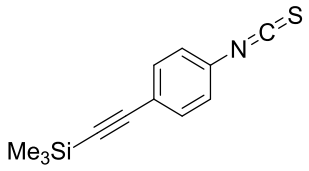

To a solution of 1,1'-thiocarbonyldiimidazole **248** (1.90 g, 10.6 mmol, 1 equiv.) in $CHCl_3$ (50 mL, 0.2 M) was added amine **247** (2.0 g, 10.6 mmol, 1 equiv.) in one portion and the resulting solution was stirred for 16 h. The mixture was concentrated *in vacuo* and re-dissolved in CH_2Cl_2 and washed with H_2O (30 mL) and brine (30 mL). The organic layers were combined, dried ($MgSO_4$) and concentrated *in vacuo* to afford the crude product. Flash chromatography on silica gel (9:1 pet ether:Et_2O) afforded the pure product as an orange oil (2.25 g, 92% yield); ν_{max} (thin film, cm^{-1}) 2156 (C≡C), 2021 (N=C=S), 1498 (C=C); **^{1}H NMR** (500 MHz, $CDCl_3$) δ_H: 0.25 (9H, s, Si(C*H*$_3$)$_3$), 7.14 (2H, d, *J* 8.8, ArC(3,5)*H*), 7.43 (2H, d, *J* 8.8, ArC(2,6)*H*); **^{13}C{^{1}H} NMR** (126 MHz, $CDCl_3$) δ_C: 0.0 (Si(*C*H$_3$)$_3$), 96.7 (C≡*C*-Si(CH$_3$)), 103.9 (*C*≡C-Si(CH$_3$)), 122.3 (Ar*C*(4)), 125.8 (Ar*C*(3,5)H), 131.2 (Ar*C*(1)), 133.2(Ar*C*(2,6)H), 138.8 (N*C*S); **HRMS** (CI^+) C_7H_4BrNOS $[M+H]^+$, found 232.2290, requires 232.2281 (+3.9 ppm).

(*R*,*Z*)-2-((4-Methoxybenzylidene)amino)-2-phenylethan-1-ol 341

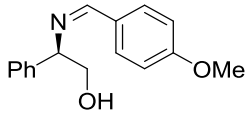

To a round bottomed flask containing anhydrous CH_2Cl_2 (40 mL) and $MgSO_4$ (5 g) was added (*R*)-phenylglycinol **257** (2.5 g, 17.86 mmol, 1 equiv.) with stirring under Ar. 4-Methoxybenzaldehyde (2.67 g, 19.7 mmol, 1.1 equiv.) was added and the reaction was stirred for 16 h at rt. The reaction mixture was filtered and washed with CH_2Cl_2 (30 mL), and the filtrate was dried ($MgSO_4$) and concentrated *in vacuo* to afford the crude product which was recrystallised from EtOH to afford the pure product as a colourless solid (3.27 g, 72%); $[\alpha]_D^{20}$ = +97.6 (*c* 1.0 $CHCl_3$) {Lit.[306] $[\alpha]_D^{20}$ = +110.7 (*c* 1.0 $CHCl_3$)}; **mp** 78-80 °C, {Lit.[306] 62 °C.}; **^{1}H NMR** (400 MHz, $CDCl_3$) δ_H: 3.85 (3H, s, OC*H*$_3$), 3.87–4.00 (2H, m, OCH$_2$), 4.46 (1H, dd, *J* 8.3, 4.5, C(2)*H*), 6.93 (2H, d, *J* 8.7, ArC(3,5)*H*), 7.27 (1H, d, *J* 6.9, PhC(4)*H*), 7.35 (2H, ddd, *J* 8.1, 7.1, 0.8, PhC(3,5)*H*), 7.43 (2H, d, *J* 7.6, PhC(2,6)*H*), 7.74 (2H, d, *J* 8.7, ArC(2,6)*H*), 8.33 (1H, s, N=C*H*). All data in accordance with the literature. [306]

(*R*)-2-((4-Methoxybenzyl)amino)-2-phenylethan-1-ol 342

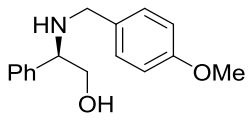

To a round bottomed flask containing CH_2Cl_2:EtOH (5:5 mL) at 0 °C was added imine **341** (500 mg, 1.96 mmol, 1 equiv.) with stirring. $NaBH_4$ (119 mg, 3.13 mmol, 1.6 equiv.) was added portionwise and the solution was warmed to rt and stirred for 16 h. The reaction mixture was poured into ice water and conc. HCl was added until the pH was ~1. The biphasic mixture was then basified with aq. 5 M NaOH (30 mL) and the aqueous phase was extracted with CH_2Cl_2 (3 × 50 mL). The organic layers were combined, washed with brine, dried ($MgSO_4$) and concentrated *in vacuo* to afford the pure product as a pale yellow oil (346 mg, 69% yield); $[\alpha]_D^{20}$ = −149.2 (*c* 0.5 $CHCl_3$), ν_{max} (thin film, cm^{-1}) 3307 (N-H), 2954 (C-H), 1508 (C=C); **^{1}H NMR** δ_H (700 MHz, $CDCl_3$) δ_H: 3.51–3.58 (2H, m, NC*H*^{A} and OC*H*^{B}), 3.67–3.72 (2H, m, NC*H*^{A} and OC*H*^{B}), 3.79-3.93 (4H, m, C(2)*H* and OC*H*$_3$), 6.86 (2H, d, *J* 8.0, ArC(3,5)*H*), 7.20 (2H, d, *J* 8.6, ArC(2,6)*H*), 7.32 (3H, m, PhC(3,5)*H* and PhC(4)*H*), 7.38 (2H, d, *J* 7.1, PhC(2,6)*H*); **^{13}C{^{1}H} NMR** δ_C (176 MHz, $CDCl_3$) δ_C: 50.7 (O*C*H$_2$), 55.4 (O*C*H$_3$), 63.7 (NC*H*$_2$), 66.8 (*C*(2)H), 113.9 (Ar*C*(3,5)H), 127.4 (Ph*C*(3,5)H), 127.8 (Ph*C*(4)H), 128.8 (Ph*C*(2,6)H), 129.5 (Ar*C*(2,6)H), 132.2 (Ar*C*(1)), 140.6 (Ph*C*(1)), 158.8 (Ar*C*(4)); **HRMS** (ESI$^+$) $C_{16}H_{20}NO_2$ $[M+H]^+$, found 258.1484, requires 258.1489 (−1.9 ppm).

(*R*)-2-((*tert*-Butyldimethylsilyl)oxy)-*N*-(4-methoxybenzyl)-1-phenylethan-1-amine 343

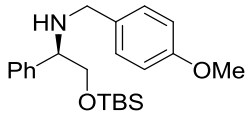

To a round bottomed flask containing CH_2Cl_2 (95 mL, 0.2 M) at 0 °C was added alcohol **342** (4.95 g, 19.3 mmol, 1 equiv.) with stirring under Ar. Imidazole (1.44 g, 21.1 mmol, 1.1 equiv.) and DMAP (1 crystal) were added followed by portionwise addition of *tert*-butyldimethylsilyl chloride (3.18 g, 21.1 mmol, 1.1 equiv.). The reaction mixture was stirred at rt for 1 h and quenched with sat. aq. $NaHCO_3$ (50 mL) and the aqueous phase was extracted with CH_2Cl_2 (3 × 50 mL). The organic layers were combined, washed with brine, dried ($MgSO_4$) and concentrated *in vacuo* to afford the pure product as a colourless oil (4.63 g, 65% yield); $[\alpha]_D^{20}$ = +56.6 (*c* 1.0 $CHCl_3$); ν_{max} (thin film, cm^{-1}) 2953 (N-H), 2854 (C-H), 1462 (C=C); **^{1}H NMR** (700 MHz, $CDCl_3$) δ_H: 0.04 (6H, s, 2SiC*H*$_3$), 0.88–0.95 (9H, s, SiC(C*H*$_3$)$_3$), 3.51 (1H, m, OC*H*^{A}), 3.60 (1H, m, NC*H*^{A}), 3.65-3.75 (2H, m, NC*H*^{B} and OC*H*^{B}), 3.80-3.86 (4H, m, C(2)*H* and OC*H*$_3$), 6.88 (2H, d, *J* 8.4, ArC(3,5)*H*), 7.19-7.24 (2H, m, ArC(2,6)*H*), 7.31 (1H, m, PhC(4)*H*), 7.34-7.40 (2H, m, PhC(3,5)*H*), 7.43 (2H, d, *J* 6.8, PhC(2,6)*H*); **^{13}C{^{1}H} NMR** (175 MHz) δ_C: −5.29 (2 × Si*C*H$_3$)

18.4 (Si*C*(CH$_3$)$_3$), 26.0 (SiC(*C*H$_3$)$_3$), 50.8 (O*C*H$_2$), 55.4 (O*C*H$_3$), 64.1 (*C*(2)H), 68.5 (NC*H*$_2$), 113.9 (Ar*C*(3,5)H), 127.5 (Ph*C*(3,5)H), 128.0 (Ph*C*(4)H), 128.5 (Ph*C*(2,6)H), 129.3 (Ar*C*(2,6)H), 133.0 (Ar*C*(1)), 140.9 (Ph*C*(1)), 158.6 (Ar*C*(4)); **HRMS** (ESI$^+$) $C_{22}H_{34}NO_2Si$ $[M+H]^+$, found 372.2353, requires 372.2361 (−2.1 ppm).

(*R*)-1-(2-Hydroxy-1-phenylethyl)-3-(4-((trimethylsilyl)ethynyl)phenyl)thiourea 251

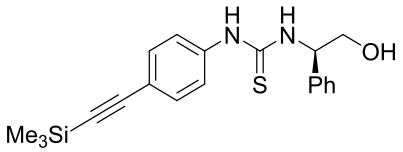

Following general procedure **L**, isothiocyanate **249** (530 mg, 2.3 mmol, 1 equiv.), (*R*)-phenylglycinol **257** (346 mg, 2.52 mmol, 1.1 equiv.) were reacted to afford the crude product. Flash chromatography on silica gel (hex:CH_2Cl_2, 100:0→80:20) afforded the pure product as a crunchy orange solid (715 mg, 85% yield); $[\alpha]_D^{20}$ = +133.4 (*c* 1.0 $CHCl_3$), **mp** 59-62 °C; ν_{max} (thin film, cm^{-1}) 3252 (C-H), 2154 (C≡C), 1506 (C=NH), 1246 (C=S); **^{1}H NMR** (400 MHz, $CDCl_3$) δ_H: 0.25 (9H, s, SiC(C*H*$_3$)$_3$), 3.85–4.07 (2H, m, C(2)*H*$_2$), 5.68 (1H, bs, O*H*), 7.01 (1H, d, *J* 7.8, C(1)*H*), 7.18 (2H, d, *J* 8.6, ArC(2,6)*H*), 7.24 (2H, d, *J* 8.5, Ph(2,6)*H*), 7.30 (1H, d, *J* 7.0, PhC(4)*H*), 7.35 (2H, d, *J* 7.7, PhC(3,5)*H*), 7.48 (2H, d, *J* 8.8, ArC(3,5)*H*); **^{13}C{^{1}H} NMR** (126 MHz, $CDCl_3$) δ_C: 0.04 (Si(*C*H$_3$)$_3$), 60.3 (*C*(1)H), 66.2 (*C*(2)H), 95.7 (C≡*C*-Si(CH$_3$), 104.0 (*C*≡C-Si(CH$_3$), 124.1 (Ar*C*(2,6)H), 126.8 (Ph*C*(2,6)H), 128.2 (Ph*C*(4)H), 129.1 (Ph*C*(3,5)H), 133.7 (Ar*C*(4)), 136.4 (Ar*C*(1)), 138.1 (Ph*C*(1)), 180.4 (*C*=S); **HRMS** (ESI)$^+$ $C_{20}H_{24}N_2NaOSSi$ $[M+Na]^+$, found 391.1266, requires 391.1271 (−1.3 ppm).

(*R*)-1-(2-hydroxy-1-phenylethyl)-1-(4-methoxybenzyl)-3-(4-((trimethylsilyl)ethynyl)phenyl) thiourea 252

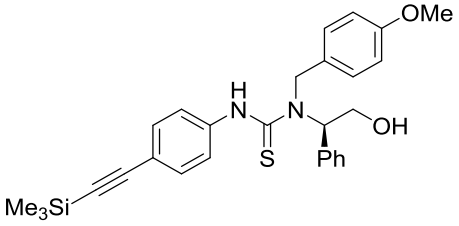

Following general procedure **L**, isothiocyanate **249** (2.95 g, 12.7 mmol, 1 equiv.) and amino alcohol **342** (3.27 g, 13.9 mmol, 1.1 equiv.) were reacted to afford the pure product as a dark orange solid (5.77 g, 94% yield); $[\alpha]_D^{20}$ = +63.2 (*c* 1.0 $CHCl_3$); **mp** 76-79 °C; ν_{max} (thin film, cm^{-1}) 2963 (C-H), 2154 (C≡C), 1508 (C=N-H), 1244 (C=S); **^{1}H NMR** (500 MHz, $CDCl_3$) δ_H: 0.25 (9H, s, Si(C*H*$_3$)$_3$), 3.77 (2H, m, C(2)*H*$_2$), 3.82 (3H, s, OC*H*$_3$), 4.24 (1H, dd, *J* 11.3, 9.5, NC*H*^{A}),

4.35 (1H, dd, *J* 11.3, 4.3, NC*H*^{B}), 4.52 (1H, m, C(1)*H*), 4.81 (1H, bs, O*H*), 6.88 (2H, d, *J* 8.6, C(1)ArC(3,5)*H*), 7.11 (2H, d, *J* 8.5, C(1)ArC(2,6)*H*), 7.26 (3H, m, ArC(2,6)*H* and PhC(4)H), 7.33–7.43 (6H, m, 4Ph*H* and ArC(3,5)*H*); **^{13}C{^{1}H} NMR** (126 MHz, $CDCl_3$) δ_C: δ 0.1 (Si(*C*H_3)$_3$), 52.2 (O*C*H_2), 55.5 (O*C*H_3), 63.5 (*C*(2)H), 64.3 (NC*H*$_2$), 94.2 (Si*C*≡C), 104.9 (SiC≡*C*), 114.3 (C(1)Ar*C*(3,5)H) 114.7 (Ar*C*(4), 124.3 (Ar*C*(2,6)H) , 125.8 (Ar*C*(1)), 128.0 (Ph*C*(3,5)H), 128.2 (Ph*C*(4)H), 129.1 (Ph*C*(2,6)H), 132.3 (C(1)Ar*C*(2,6)H), 136.4 (C(1)Ar*C*(1)), 139.7 (Ph*C*(1)), 159.5 (C(1)Ar*C*(4)), 183.9 (*C*=S); **HRMS** (ESI)$^{+}$ $C_{28}H_{33}N_2O_2SSi$ $[M+H]^+$, found 489.2013, requires 489.2027 (−2.9 ppm).

(*R*)-1-(2-Hydroxy-1-phenylethyl)-1-(4-methoxybenzyl)-3-(4((trimethylsilyl)ethynyl)phenyl)thiourea 253

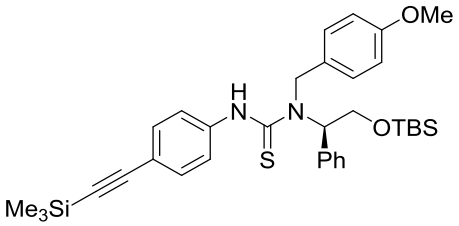

Following general procedure **L**, isothiocyanate **249** (887 mg, 3.8 mmol, 1 equiv.) and amine **343** (1.41 g, 3.8 mmol, 1.1 equiv.) were reacted and purified by Biotage® Isolera™ 4 [SNAP Ultra 25 g, 75 mL min^{-1}, Hexane :Et_2O (95 : 5 5CV, 95 : 5 to 75 : 25 10 CV, 75 : 25 3 CV)] to afford the pure product as a dark orange solid (540 mg, 24% yield); $[\alpha]_D^{20}$ = +89.2 (*c* 1.0 $CHCl_3$); **mp** 58-60 °C; ν_{max} (thin film, cm^{-1}) 2953 (C-H), 2154 (C≡C), 1508 (C=N-H), 1246 (C=S); **^{1}H NMR** (500 MHz, $CDCl_3$) δ_H: 0.05 (3H, s, SiC*H*$_3$), 0.08 (3H, s, SiC*H*$_3$), 0.22 (9H, s, Si(C*H*$_3$)$_3$), 0.85 (9H, s, SiC(C*H*$_3$)$_3$), 3.80 (1H, s, OC*H*$_3$), 4.17 (1H, dd, *J* 10.9, 3.7, C(2) *H*^{A}H^{B}), 4.23 (1H, dd, *J* 10.9, 6.3, C(2) H^{A}*H*^{B}), 4.36 (1H, m, NC*H*^{A}), 4.45 (1H, m, NC*H*^{B}), 4.71 (1H, m, C(1)*H*), 6.85 (2H, d, *J* 8.7, C(1)ArC(3,5)*H*), 7.09 (2H, d, *J* 8.5, ArC(3',5')*H*), 7.27-7.30 (2H, m, C(1)ArC(2,6)*H*), **^{13}C{^{1}H} NMR** (126 MHz) −5.4 (Si*C*H$_3$) δ_C: 0.1 (2 × Si(*C*H$_3$)$_3$), 18.5 (Si*C*(CH$_3$)$_3$), 26.0 (SiC(*C*H$_3$)$_3$), 51.4 (O*C*H^{AB}), 55.4 (O*C*H$_3$), 63.5 (*C*(2)H), 64.3 (NC*H*^{AB}), 93.9 (Si*C*≡C), 105.1 (SiC≡*C*), 114.3 (Ar*C*(3,5)H), 119.8 (Ar*C*(4')), 122.5 (Ar*C*(3',5')H), 124.4 (Ar*C*(2',6')H), 125.8 (Ar*C*(1')), 127.8 (Ph*C*(3,5)H), 128.2 (Ph*C*(4)H), 128.9 (Ph*C*(2,6)H), 129.5 (Ar*C*(2,6)H), 136.9 (Ar*C*(1)), 140.1 (Ph*C*(1)), 159.3 (Ar*C*(4)); 183.8 (*C*=S); **HRMS** (ESI^{+}) $C_{34}H_{47}N_2O_2SSi_2$ $[M+H]^+$, found 603.2891, requires 603.2897 (−0.9 ppm).

(*R*,*Z*)-3-(4-Methoxybenzyl)-4-phenyl-*N*-(4-((trimethylsilyl)ethynyl)phenyl)oxazolidin-2-imine 254 and (*R*,*Z*)-3-(4-Methoxybenzyl)-4-phenyl-*N*-(4-((trimethylsilyl)ethynyl)phenyl)thiazolidin-2-imine 255

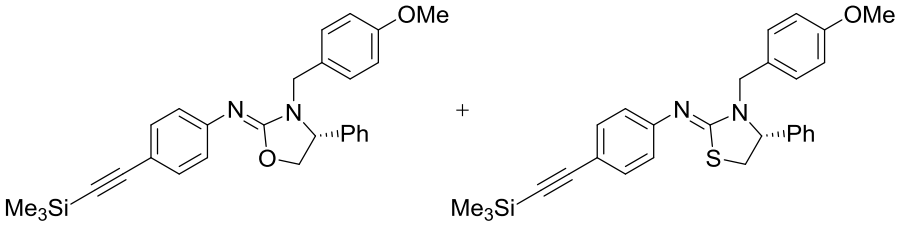

A solution of thiourea **252** (1.0 g, 2.05 mmol, 1 equiv.) in PhMe (20 mL) was purged with O_2 (1 balloon) and $Cu(OTf)_2$ (74 mg, 0.205 mmol, 10 mol%) was added with stirring. The reaction mixture was heated to reflux for 12 h under an O_2 atmosphere (1 atm) then H_2O (20 mL) was added and the aqueous phase was extracted with EtOAc (3 × 20 mL). The organic layers were combined, washed with brine, dried ($MgSO_4$) and concentrated *in vacuo* to afford the crude product. Flash chromatography (7:3 Hexane: Et_2O) afforded the pure products as a colourless oils:

Data for 254: (418 mg, 45% yield); ν_{max} (thin film) 2954 (C-H), 2150 (C≡C), 1660 (C=N); **^{1}H NMR** (500 MHz, $CDCl_3$) δ_H: 0.26 (9H, s, SiCH_3), 3.67 (1H, d, *J* 14.7, NCH^AH^B), 3.81 (3H, s, OCH_3), 4.11 (1H, dd, *J* 8.2, 7.2, C(4)*H*), 4.49 (1H, dd, *J* 8.3, 7.1, C(5)H^AH^B), 4.55 (1H, t, *J* 8.3, C(5)H^AH^B), 5.07 (1H, d, *J* 14.7, NCH^AH^B), 6.84 (2H, d, *J* 8.6, ArC(3,5)*H*), 7.13 (2H, d, *J* 8.5, PhC(3,5)*H*), 7.16 (2H, d, *J* 8.6, ArC(2,6)*H*), 7.28 (1H, d, *J* 6.9, PhC(4)*H*) 7.40 (5H, m, PhC(2,6)*H*) and ArC(2',6')*H*); **^{13}C{^{1}H} NMR** (126 MHz, $CDCl_3$) δ_C: 0.18 (Si(*C*H_3)$_3$), 45.6 (N*C*H_2), 55.3 (O*C*H_3), 59.5 (*C*(5)H_2), 72.5 (*C*(4)H) 92.3 (Si*C*≡C), 106.2 (SiC≡*C*), 113.8 (Ar*C*(3,5)H), 116.2 (Ar*C*(4')), 123.6 (Ar*C*(3,5)H), 127.4(Ph*C*(4)H), 128.1 (Ar*C*(1)), 128.90 (Ar*C*(3',5')H), 129.23 (Ph*C*(2,6)H), 130.3 (Ar*C*(2,6)H), 132.5 (Ar*C*(2',6')H), 137.5 (Ph*C*(1)), 148.2 (Ar*C*(1')), 153.4 (*C*=N), 159.1 (Ar*C*(4)); **HRMS** (ESI$^+$) $C_{28}H_{30}N_2O_2Si$ $[M+H]^+$, found 455.2139, requires 455.2077 (+1.4 ppm).

Data for 255: (212 mg, 22% yield); ν_{max} (thin film, cm^{-1}) 2955 (C-H), 2150 (C≡C), 1581 (C=N);**^{1}H NMR** (500 MHz, $CDCl_3$) δ_H: 0.25 (9H, s, SiCH_3), 3.03 (1H, dd, *J* 11.0, 7.0, C(5)H^AH^B), 3.40 (1H, dd, *J* 11.0, 7.4, C(5)H^AH^B), 3.67 (1H, d, *J* 14.7, NCH^AH^B), 4.61 (1H, t, *J* 7.1, C(4)*H*), 5.35 (1H, d, *J* 14.7, NCH^AH^B), 6.83 (2H, d, *J* 8.6, ArC(3,5)*H*), 6.99 (2H, d, *J* 8.4, ArC(2',6')*H*), 7.11 (2H, d, *J* 8.5, ArC(2',6')*H*), 7.29 (2H, d, *J* 6.8, PhC(2,6)*H*), 7.38 (1H, d, *J* 6.9, PhC(4)*H*), 7.41 (2H, d, *J* 7.1, PhC(3,5)*H*), 7.44 (2H, d, *J* 8.4, ArC(3',5')*H*); **^{13}C{^{1}H} NMR** (126 MHz, $CDCl_3$) δ_C: 0.11 (Si(*C*H_3)$_3$), 35.2 (*C*(5)H_2), 47.4 (N*C*H_2), 64.2 (*C*(4)H), 92.9 (Si*C*≡C), 105.8

(SiC≡*C*), 113.8 (Ar*C*(3,5)H), 117.3 (Ar*C*(4)), 122.1 (ArC(2',6')*H*), 127.2 (Ph*C*(2,6)H), 128.6 (Ph*C*(4)H), 128.7 129.0 (Ar*C*(1)), 130.0 (Ar*C*(2,6)H), 132.9 (Ph*C*(3,5)H), 139.2 (Ar*C*(1')), 152.3 (Ar*C*(1')), 158.9 (Ar*C*(4)), 159.5 (*C*=N); **HRMS** (ESI^+) $C_{28}H_{30}N_2OSSi$ $[M+H]^+$, found 471.1913, requires 471.1898 (+3.2 ppm).

(*R*)-2-((6-Methoxybenzo[d]thiazol-2-yl)amino)-2-phenylethan-1-ol 285

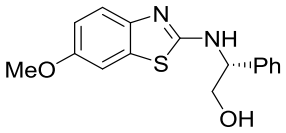

Following a procedure outline by Smith[164] to a round bottomed containing *o*-dichlorobenzene (5 mL, 2.0 M) was added (*R*)-phenylglycinol **257** (1.51 g, 11 mmol, 1.05 equiv), *i*Pr_2NEt (4.35 mL, 25 mmol, 2.5 equiv.), 2-chloro-6-methoxybenzothiazole **290** (2.0 g, 10 mmol, 1 equiv.) and the resulting pale yellow suspension was heated at reflux (195 °C DrySyn®) until completion as judged by GC conversion (>95%, *ca.* 48 h). The orange mixture was allowed to cool to rt. H_2O (15 mL) was added and the aqueous phase was extracted with CH_2Cl_2 (3 × 20 mL). The organic layers were combined, washed with brine, dried ($MgSO_4$) and concentrated *in vacuo*. The resulting residue was triturated with hexane to afford the crude product as an off-white solid that was recrystallised from toluene to give the pure product as fluffy colourless crystals (1.43 g, 48% yield), $[\alpha]_D^{20}$ = −36.5 (*c* 1.0 $CHCl_3$); **mp** 130-133 °C; ν_{max} (thin film, cm^{-1}) 1604 (C=C), 1548 (C=N); **GC** [Agilent DB-5, 40 cm/s (He), inj. temp 250 °C, FID temp 325 °C; temp profile: initial 120 °C (2 min), then ramp to 320 °C (20 °C/min, hold 5 min), total run = 17 min]: t_R *i*Pr_2NEt, 1.87 min; *o*-dichlorobenzene, 3.20 min; (*R*)-phenylglycinol **257**, 5.30 min; 2-chloro-6-methoxybenzothiazole **290**, 7.65 min; **^{1}H NMR** (400 MHz, $CDCl_3$) δ_H: 3.80 (3H, s, OC*H*$_3$), 3.98 (2H, m, C(1)$_2$), 4.88 (1H, dd, *J* 6.3, 4.0, C(2)*H*), 5.98 (1H, bs, N*H*), 6.88 (1H, dd, *J* 8.8, 2.6, C(5)Ar*H*), 7.07 (1H, d, *J* 2.6, C(7)Ar*H*), 7.32 (1H, m, PhC(4)*H*), 7.39 (4H, m, PhC(2,6)*H* and PhC(3,5)*H*), 7.43 (1H, d, *J* 8.8, C(4)Ar*H*); **^{13}C{^{1}H} NMR** (125 MHz, $CDCl_3$) δ_C: 56.0 (OC*H*$_3$), 62.1 (*C*(1)H_2), 67.5 (*C*(2)H), 105.4 (Ar*C*(5)H), 113.6 (Ar*C*), 119.6 (Ar*C*), 127.0 (2 × Ph*C*H), 128.4 (Ph*C*H), 129.1 (2 × Ph*C*H), 131.7 (Ph*C*), 138.9 (Ar*C*(a7)), 145.7 (Ar*C*(3a)), 155.5 (Ar*C*(6)), 165.8 Ar*C*=N), **HRMS** (ESI^+) $C_{16}H_{17}N_2O_2S$ $[M+H]^+$, found 301.1005, requires 301.1011 (−1.9 ppm).

(*R*)-7-methoxy-2-phenyl-2,3-dihydrobenzo[d]imidazo[2,1-b]thiazole 291

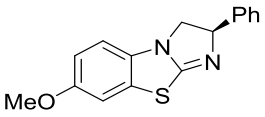

Following a procedure outlined by Smith *et al.*,[164] to a round bottomed flask containing anhydrous CH_2Cl_2 (20 mL) was added **285** (500 mg, 1.66 mmol, 1 equiv.), Et_3N (0.9 mL, 6.64 mmol, 4 equiv.) and the reaction mixture was stirred at 0 °C. After 10 mins methanesulfonyl chloride (167 μL, 2.17 mmol, 1.3 equiv.) was added with stirring. The ice/water bath was removed and the reaction stirred for 15 mins. Once complete consumption of (*R*)-**285** was observed, *i*PrOH (0.3 mL) was added and the reaction was heated at reflux for 16 h. The reaction was quenched with 1 M NaOH (20 mL) and the biphasic mixture stirred vigorously for 30 mins. The aqueous layer was extracted with CH_2Cl_2 (3 × 20 mL) and the combined organic washed with brine (50 mL), dried (MgSO4) and concentrated *in vacuo* to afford the crude product which was purified by Biotage® Isolera™ 4 [SNAP Ultra 25 g, 75 mL min^{-1}, CH_2Cl_2 :EtOAc (95 : 5 5CV, 95 : 5 to 80 : 20 10 CV, 80 : 20 3 CV)] to afford the pure product as a colourless crystalline solid (374 mg, 80% yield); $[\alpha]_D^{20}$ = +58.2 (*c* 0.5 $CHCl_3$); **mp** 106-108 °C; ν_{max} (thin film) 1597 (C=C), 1573 (C=N); **^{1}H NMR** (500 MHz, $CDCl_3$) δ_H: 3.67 (1H, t, *J* 8.6, C(3)H^AH^B), 4.25 (1H, dd, *J* 10.1, 8.6, C(3)H^AH^B), 5.64 (1H, dd, *J* 10.1, 8.6, C(2)*H*), 6.59 (1H, d, *J* 8.5, C(5)*H*), 6.74 (1H, dd, *J* 8.6, 2.5, C(6)Ar*H*), 6.93 (1H, d, *J* 2.6, C(8)Ar*H*), 7.29 (1H, m, Ph*H*), 7.38 (4H, m, Ph*H*); **^{13}C{^{1}H} NMR** (125 MHz, $CDCl_3$) δ_C: 53.2 (OCH_3), 56.1 (*C*(1)H_2), 75.4 (*C*(2)H), 108.9 (Ar*C*(5)H), 109.8 (Ar*C*(6)H), 112.3 (Ar*C*(8)H), 126.7 (2 × Ph*C*H), 127.7 (Ph*C*H), 128.6 (Ph*C*(2)), 128.9 (Ph*C*H), 131.5 (Ar*C*), 143.0 (Ar*C*(3a)), 155.2 (Ar*C*(6)), 167.4 (Ar*C*=N); **HRMS** (ESI^+) $C_{16}H_{15}N_2OS$ $[M+H]^+$, found 283.0900, requires 283. 0905 (−1.7 ppm).

(*R*)-7-hydroxy-2-phenyl-2,3-dihydrobenzo[*d*]imidazo[2,1-*b*]thiazol-1-ium bromide 292

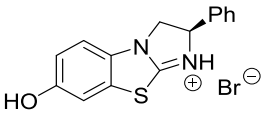

To a solution of (*R*)-**291** (900 mg, 3.19 mmol, 1 equiv.) in CH_2Cl_2 (10 mL) at 0 °C was added BBr_3 (32 mL, 32 mmol, 1 M in CH_2Cl_2, 10 equiv.) dropwise. The solution was stirred at 0°C for 2 h then warmed to rt and stirred for 16 h. The reaction was carefully quenched with MeOH (10 mL) at and warmed to rt. CH_2Cl_2 (10 mL) was added and the aqueous phase was extracted with CH_2Cl_2 (3 × 20 mL). The organic layers were combined, dried ($MgSO_4$) and concentrated *in vacuo* to afford the pure product as a colourless solid (932 mg, 84 % yield); $[\alpha]_D^{20}$ = +93.6 (*c* 1.0 MeOH), **mp** 182-185 °C; ν_{max} (thin film, cm^{-1}) 3026 (C-H), 1558 (C=N), 1550 (N-C); **^{1}H NMR** (500 MHz, d6-DMSO) 4.34 (1H, dd, *J* 10.7, 8.4, C(1)H^AH^B), 4.92 (1H, app. t, *J* 10.7, C(1)H^AH^B), 5.91 (1H, dd, *J* 10.7, 8.4, C(2)*H*), 6.98 (1H, dd, *J* 8.7, 2.4, ArC(6)*H*), 7.34 (1H, d, *J* 8.7, ArC(5)*H*), 7.43 (1H, d, *J* 7.7, PhC(4)*H*), 7.46 (2H, d, *J* 8.2, PhC(3,5)*H*), 7.50 (1H, s, ArC(8)*H*), 7.54 (2H, d, *J* 7.7, PhC(2,6)*H*), 10.09 (1H, s, N*H*), 11.1 (1H, s, O*H*); **^{13}C{^{1}H} NMR** (125 MHz, d_6-DMSO)

53.7 (*C*(1)H_2), 66.5 (*C*(2)H), 111.0 (Ar*C*(8)H), 113.4 (Ar*C*(5)H), 115.7 (Ar*C*(6)H), 127.1 (Ph*C*(2,6)H), 127.3 (Ar*C*(8a)), 128.7 (Ar*C*(4a)), 128.9 (Ph*C*(4)H), 129.0 (Ph*C*(3,5)H), 138.8 (Ph*C*(1)), 155.0 (Ar*C*(7)), 168.7 (*C*=N); **HRMS** (ESI^+) $C_{15}H_{13}N_2OS$ $[M+H]^+$, found 269.0736, requires 269. 0743 (−2.6 ppm).

(*R*)-2-phenyl-7-(prop-2-yn-1-yloxy)-2,3-dihydrobenzo[d]imidazo[2,1-*b*]thiazole 284

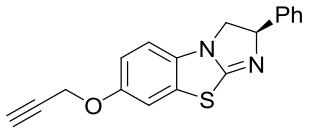

To a solution of salt **292** (52 mg, 0.15 mmol, 1 equiv.) in THF/DMSO (1:1 mL) was added KO*t*Bu (44 mg, 0.39 mmol, 2.6 equiv.) and the reaction mixture was stirred at 0 °C for 2 h. Propargyl bromide (25 µL, 0.23 mmol, 80% in toluene, 1.5 equiv.) was then added and the reaction mixture was allowed to warm to rt (*ca*. 2 h) and quenched with brine (10 mL). The aqueous phase was extracted with EtOAc (3 × 10 mL). The organic layers were combined, washed with brine, dried (MgSO4) and concentrated *in vacuo* to afford the crude product was purified by Biotage® Isolera™ 4 [SNAP Ultra 25 g, 75 mL min^{-1}, CH_2Cl_2:EtOAc (95 : 5 5CV, 95 : 5 to 60 : 40 10 CV, 60 : 40 5 CV)] to afford the pure product as a colourless semi-solid (32 mg, 70% yield); $[\alpha]_D^{20}$ = +26.4 (*c* 1.0 $CHCl_3$); ν_{max} (thin film, cm^{-1}) 1591 (C=C), 1575 (C=N); **^{1}H NMR** (500 MHz, $CDCl_3$) δ_H: 2.53 (1H, t, *J* 2.4, C≡*H*), 3.68 (1H, app. t, *J* 8.5, C(1)*H*^{A}H^B), 4.25 (1H, dd, *J* 10.2, 8.7, C(1)*H*^{A}H^B), 4.66 (2H, d, *J* 2.4, OCH_2), 5.64 (1H, dd, *J* 10.2, 8.2, C(2)*H*), 6.60 (1H, d, *J* 8.5, ArC(5)*H*), 6.83 (1H, dd, *J* 8.5, 2.5, ArC(6)*H*), 7.02 (1H, d, *J* 2.5, ArC(8)*H*), 7.29 (1H, m, Ph*H*), 7.37 (4H, m, PhC(2,6)*H* and PhC(3,5)*H*); **^{13}C{^{1}H} NMR** (126 MHz, $CDCl_3$) 53.1 (*C*(1)H_2), 57.0 (OCH_2), 75.5 (*C*(2)H), 75.9 (C≡*C*H), 78.5 (*C*≡CH), 108.8 (Ar*C*(5)H), 111.4 (Ar*C*(6)H), 113.8 (Ar*C*(8)H), 126.6 (2 × Ph*C*H), 127.7 (Ph*C*(4)H), 128.5 (Ph*C*), 128.9 (2 × Ph*C*H), 132.3 (Ar*C*(8a)), 143.0 (Ar*C*(4a)), 152.9 (Ar*C*(7)), 167.2 (*C*=N); **HRMS** (ESI^+) $C_{18}H_{15}N_2OS$ $[M+H]^+$, found 307.0895, requires 307.0900 (−1.6 ppm).

(Azidomethyl)polystyrene 293

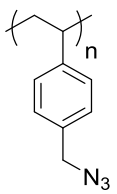

Following a procedure outlined by Pericàs *et al.* [253] to a round bottomed flask containing NaN_3 (780 mg, 51 mmol) was added (chloromethyl)polystyrene resin **191** (3.0 g, *f* = 1.23 mmol/g) in

DMSO (30 mL). The mixture was heated at 60 °C (without stirring) for 16 h and then cooled to rt. The suspension was filtered and washed sequentially with H_2O (500 mL), THF-MeOH 1:1 (250 mL), MeOH (250 mL) and THF (250 mL). The resulting solid was dried *in vacuo* for 24 h at 40 °C.

ν_{max} (thin film, cm^{-1}) 2094 (N_3)

Elemental analysis (%) C 85.61, H 6.75, N 5.48

f = 1.20 mmol/g

(*R*)- 2-Phenyl-7-(prop-2-yn-1-yloxy)-2,3-dihydrobenzo[*d*]imidazo[2,1-*b*]thiazole on polymer support 191s

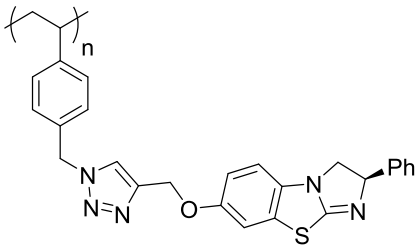

To a round bottomed flask containing (azidomethyl)polystyrene (156 mg, 0.188 mmol, *f* = 1.20 mmol/g, 1 equiv.) suspended in THF:DMF 1:1 (6 mL) was added alkyne **284** (75 mg, 0.207 mmol, 1.1 equiv.), *i*Pr_2NEt (94 µL, 0.724 mmol, 3.5 equiv.) and CuI (18 mg, 0.094 mmol, 5 mol%) with slow stirring. The reaction mixture was stirred until disappearance of the azide band (~2094 cm^{-1}) was confirmed by IR (*ca.* 21 h). The suspension was filtered and washed sequentially with THF (130 mL), H_2O (130 mL), H_2O-MeOH (1:1, 130 mL), MeOH (130 mL), MeOH-THF (1:1, 130 mL), THF (130 mL) and CH_2Cl_2 (130 mL) and the resin was dried *in vacuo* at 40 °C for 24 h to afford a dark brown resin (188 mg);

Elemental analysis (%) C 71.53, H 5.25, N 6.49

f = 0.927 mmol/g

tert-Butyl (phenyl(phenylsulfonyl)methyl)carbamate 295

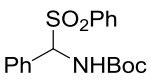

Following a literature procedure[101] to a round bottomed flask was added benzaldehyde **294** (20 mL, 164 mmol, 1.5 equiv.) in 2:1:0.7 H_2O/MeOH/HCO_2H (4 mL/mmol) with stirring. Sodium benzenesulfinate (35.7 g, 220 mmol, 2 equiv.) and *tert*-butyl carbamate (12.83 g, 110 mmol, 1

equiv.) were added and the reaction was stirred at rt for 72 h. The resulting solids were collected by filtration and triturated with H_2O for 1 h followed by a second trituration with hexane:Et_2O (4:1) for 1 h. The resulting solids were collected by filtration and washed with hexane:Et_2O (4:1) (200 mL) which afforded the pure product as a colourless solid (32.83 g, 86%); **mp** 162-164 °C {Lit.[101] 164-165 °C}; **^{1}H NMR** δ_H (500 MHz, d_6-DMSO) 1.17 (9H, s, C(C*H*$_3$)$_3$), 5.94 (1H, d, *J* 10.6, C*H*), 7.37-7.44 (3H, m, ArC(3,5)*H* and ArC(4)*H*), 7.55-7.80 (5H, 5 × PhC*H*), 7.81-7.93 (2H, m, SO_2ArC(2,6)*H*), (2H, t, *J* 7.8, PhC(2,)*H*), 7.71 (1H, d, *J* 7.6, C(4)*H*), 7.84 (2H, dd, *J* 8.3, 1.3, ArC(2,6)*H*), 8.8.74 (1H, d, *J* 10.6, N*H*). All data in accordance with the literature.[101]

***tert*-Butyl (*E*)-benzylidenecarbamate 297**

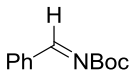

Following a modified literature procedure,[101] to a stirred slurry of *tert*-butyl (phenyl(phenylsulfonyl)methyl)carbamate **295** (10.0 g, 28.8 mmol, 1 equiv.) in bench grade CH_2Cl_2 (120 mL) was added a solution of K_2CO_3 (39.8 g, 288 mmol, 10 equiv.) in water (200 mL) and the reaction mixture was stirred at rt for 2 h. The layers were separated and the aqueous layer was extracted with CH_2Cl_2 (3 × 100 mL). The combined organic fractions were washed with brine, dried ($MgSO_4$), filtered and concentrated under reduced pressure to give the title compound as a colourless oil (5.55 g, 94% yield); **^{1}H NMR** (500 MHz, d_6-DMSO) δ_H: 1.50 (9H, s, C(C*H*$_3$)$_3$), 7.09 (2H, d, *J* 8.8, ArC(2,6)*H*), 7.90-7.95 (3H, m, ArC(2,6)*H* and ArC(4)*H*), 8.79 (1H, s, NC=*H*). All data in accordance with the literature.[101]

***tert*-Butyl ((1*R*,2*R*)-2-formyl-3-methyl-1-phenylbutyl)carbamate 299**

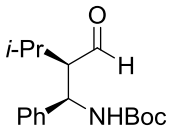

Following a literature procedure,[101] to a stirred solution of *tert*-butyl (*E*)-benzylidenecarbamate **297** (5.0 g, 24.3 mmol, 1 equiv.) in dry HPLC grade CH_3CN (100 mL) was added freshly distilled isovaleraldehyde **298** (5.35 mL, 48.7 mmol, 2 equiv.) at 0 °C. (*R*)-Proline (140 mg, 1.22 mmol, 20 mol%) was added and the reaction mixture was stirred for 16 h at 0 °C before warming to rt. Water (100 mL), Et_2O (80 mL) and brine (20 mL) were added and the organic layer separated. The aqueous layer was extracted with Et_2O (3 × 100 mL). The combined organic layers were washed with brine, dried ($MgSO_4$), filtered and concentrated *in vacuo* to afford the crude product. The crude product was triturated with hexane (200 mL) and filtered to give the title compound (1*R*,2*R*)-**299** as a colourless solid (10.5 g, 77% yield, >95:5 dr isolated); $[\alpha]_D^{20}$ = +60.4 (*c* 1.0

$CHCl_3$) {Lit.[101] $[\alpha]_D^{20}$ = −66.7 (*c* 1.0 $CHCl_3$) *ent* >99%ee}; **mp** 139-140 °C {Lit.[101] 141-142 °C}; **Chiral HPLC analysis**: Chiralcel OD-H (98:2 hexane:*i*PrOH, flow rate 1 mL/min^{-1}, 210 nm, 30 °C) t_R(1*S*,2*S*): 11.4 min, t_R(1*R*,2*R*): 12.3 min, >99% ee; **^{1}H NMR** (400 MHz, $CDCl_3$) δ_H: 1.02 (1H, d, *J* 6.9, C*H*$_3$), 1.12 (3H, d, *J* 6.9, C*H*$_3$), 1.40 (9H, s, C(C*H*$_3$)$_3$), 2.04-2.12 (1H, m, C(3)*H*), 2.46 (1H, td, *J* 7.1, 4.2, C(2)*H*), 5.10 (2H, bs, C(1)*H* and N*H*), 7.14-7.38 (5H, m, Ph*H*), 9.48 (1H, d, *J* 4.2, C*H*O). All data in accordance with the literature.[101]

tert-Butyl ((1*R*,2*R*)-2-(hydroxymethyl)-3-methyl-1-phenylbutyl)carbamate 300

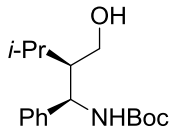

Following a literature procedure,[101] to a slurry of *tert*-butyl ((1*R*,2*R*)-2-formyl-3-methyl-1-phenylbutyl)carbamate **299** (10.0 g, 31.1 mmol, 1 equiv.) in bench grade MeOH (200 mL) at 0 °C was added $NaBH_4$ (1.76 g, 46.7 mmol, 1.5 equiv.) portion wise over 10 minutes and the reaction mixture was left to stir at rt for 1 h. Sat. aq. $NaHCO_3$ (30 mL) was added drop wise over 10 minutes forming a white precipitate. The methanol was removed under reduced pressure after which water (50 mL) and CH_2Cl_2 (250 mL) were added. The layers were separated and the aqueous layer was extracted with CH_2Cl_2 (3 × 100 mL). The combined organic layers were combined and washed with brine, dried ($MgSO_4$), filtered and concentrated under reduced pressure to give the title compound as a colourless solid (8.35 g, 83% yield, >95:5 dr isolated); $[\alpha]_D^{20}$ = +22.4 (*c* 1.0 $CHCl_3$) {Lit.[101] $[\alpha]_D^{20}$ = −26.7 (*c* 1.0 $CHCl_3$) *ent* >99%ee }; **mp** 90-91 °C {Lit.[101] 92-94 °C}; **^{1}H NMR** (400 MHz, $CDCl_3$) δ_H: 0.85 (3H, d, *J* 6.9, C*H*$_3$), 1.00 (1H, d, *J* 6.9, C*H*$_3$), 1.42 (9H, s, C(C*H*$_3$)$_3$), 1.73 (1H, m, *i*PrC*H*), 1.87 (1H, m, C(2)*H*), 2.09 (1H, m, O*H*), 3.49 (1H, ddd, *J* 11.4, 8.8, 4.4, C(3)*H*^{A}H^B), 3.67 (1H, m, C(3)H^A*H*^{B}), 5.03 (1H, m, C(1)*H*), 5.49 (1H, d, *J* 9.3, N*H*), 7.23-7.36 (5H, m, Ph*H*). All data in accordance with the literature [101]

(1*R*,2*R*)-2-(Hydroxymethyl)-3-methyl-1-phenylbutan-1-aminium chloride 301

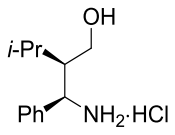

Following a literature procedure,[101] to a slurry of *tert*-butyl ((1*R*,2*R*)-2-(hydroxymethyl)-3-methyl-1-phenylbutyl)carbamate **299** (2.37 g, 8.1 mmol, 1 equiv.) in bench grade 1,4-dioxane (20 mL) at rt was added 4 M HCl in 1,4-dioxane (11.0 mL, 41 mmol, 5 equiv.) drop wise over 30 minutes and the reaction mixture was left to stir at rt for 4 h before being concentrated under

reduced pressure. The resulting solid was triturated with Et_2O (500 mL) and filtered to give the title compound as a white solid (1.67 g, 90% yield, >95:5 dr); $[\alpha]_D^{20}$ = −17.4 (*c* 1.0 MeOH); {Lit.[101] $[\alpha]_D^{20}$ = +25.0 (*c* 1.0 MeOH) *ent* >99%ee }; **mp** 138-140 °C {Lit.[101] 142-144 °C}; **^{1}H NMR** (500 MHz, $CDCl_3$) δ_H: 0.84 (3H, d, *J* 6.8, CH_3), 1.14 (1H, d, *J* 6.8, CH_3), 1.54 (1H, dq, *J* 13.7, 6.8, *i*PrC*H*), 2.02 (1H, ddt, *J* 9.2, 7.2, 4.4, C(2)*H*), 3.48 (1H, dd, *J* 10.7, 9.2, C(1)H^AH^B), 3.75 (1H, ddd, *J* 10.7, 4.6, 0.9, C(1)H^A*H*^{B}), 4.57 (1H, d, *J* 4.3, C(3)*H*), 7.47-7.51 (3H, m, C(3,5)*H* and C(4)*H*), 7.51-7.55 (2H, m, C(2,6)*H*). All data in accordance with the literature.[101]

(2*R*,3*S*)-3-isopropyl-8-methoxy-2-phenyl-3,4-dihydro-2*H*-benzo[4,5]thiazolo[3,2-*a*]pyrimidine 303

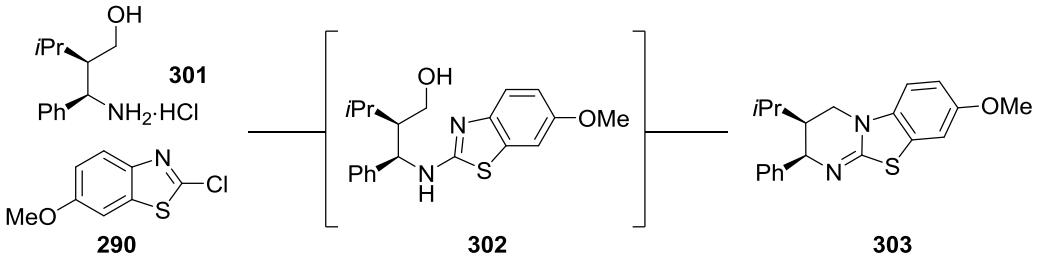

Following a procedure outline by Smith [101] to a round bottomed flask containing was added (1*R*,2*R*)-**301** (4.81 g, 21.0 mmol, 1.05 equiv.), *o*-dichlorobenzene (7.5 mL, 2.0 M), *i*Pr_2NEt (10.45 mL, 60.0 mmol, 4 equiv.) was added 2-chloro-6-methoxybenzo[*d*]thiazole **290** (4.0 g, 20 mmol, 1 equiv.) and the resulting pale yellow suspension was heated at reflux (195 °C DrySyn® temperature) until completion as judged by GC conversion (>95%, *ca.* 48 h). The resulting mixture was cooled to rt, H_2O (15 mL) was added and the aqueous phase was extracted with CH_2Cl_2 (3 × 20 mL). The organic layers were combined, washed with brine, dried ($MgSO_4$) and concentrated *in vacuo* to afford the crude product which was triturated with hexane to afford a brown solid which was used in the next step without further purification (5.43 g, 76% yield); **GC** [Agilent DB-5, 40 cm/s (He), inj. temp 250 °C, FID temp 325 °C; temp profile: initial 120 °C (2 min), then ramp to 320 °C (20 °C/min, hold 5 min), total run = 17 min]: t_R *i*Pr_2NEt, 1.87 min; *o*-dichlorobenzene, 3.20 min; (1*R*, 2*R*)-**301**, 7.56 min; 2-chloro-6-methoxybenzo[*d*]thiazole **290**, 7.65 min; **^{1}H NMR** for **302** (500 MHz, $CDCl_3$) δ_H: 0.81 (3H, d, *J* 6.8, CH_3), 1.09 (3H, d, *J* 6.8, CH_3), 1.69 (1H, m, *i*PrC*H*), 2.10 (1H, app. ddt, *J* 10.2, 6.3, 4.2, C(2)*H*), 3.66 (1H, dd, *J* 11.0, 9.8, C(1)H^AH^B), 3.78 (3H, s, OCH_3), 3.85 (1H, dd, *J* 11.0, 4.0, C(1)H^A*H*^{B}), 4.94 (1H, d, *J* 4.3, C(2)*H*), 6.84 (1H, d, *J* 8.8, 2.6, ArC(4)*H*), 7.08 (1H, d, *J* 2.6, ArC(7)*H*), 7.25 (1H, d, *J* 7.2, ArC(4)*H*), 7.31-7.35 (3H, m, PhC(3,5)*H* and PhC(4)*H*), 7.46 (2H, d, *J* 7.9, PhC(2,6)*H*);

To a slurry of crude (1*R*, 2*R*)-amino alcohol **302** (5.43 g, 15.2 mmol, 1 equiv.) in anhydrous CH_2Cl_2 (80 mL, 0.2 M) was added Et_3N (8.47 mL, 60.8 mmol, 4 equiv.) and the reaction mixture was cooled to 0 °C. Methanesulfonyl chloride (1.53 mL, 19.8 mmol, 1.3 equiv.) was added and the reaction mixture was stirred at rt for 30 mins. Once complete consumption of (1*R*, 2*R*)-**302** was observed, *i*PrOH (1 mL) was added and the reaction was heated at reflux for 16 h. The reaction was quenched with aq. 1 M NaOH (20 mL) and the biphasic mixture stirred vigorously for 30 mins. The aqueous layer was extracted with CH_2Cl_2 (3 × 20 mL) and the combined organic layers were washed with brine (50 mL), dried ($MgSO_4$) and concentrated *in vacuo* to afford the crude product which was purified by Biotage® Isolera™ 4 [SNAP Ultra 25 g, 75 mL min^{-1}, CH_2Cl_2 :EtOAc (95 : 5 5CV, 95 : 5 to 60 : 40 10 CV, 60 : 40 5 CV)] to afford an off white solid that was recrystallised from EtOAc to give a **303** as a colourless solid (2.05 g, 40% yield, >95:5 dr); $[\alpha]_D^{20}$ = −249.1 (*c* 1.0 $CHCl_3$), **mp** 139-141 °C; ν_{max} (thin film, cm^{-1}) 1614 (C=N), 1487 (C=C); **^{1}H NMR** (500 MHz, $CDCl_3$) δ_H: 0.84 (1H, d, *J* 6.7, CH_3), 1.13 (1H, d, *J* 6.5, CH_3), 1.30 (1H, m, *i*PrC*H*), 1.95 (1H, ddt, *J* 11.4, 9.4, 4.4, C(3)*H*), 3.33 (1H, app. t, *J* 11.4, C(4)H^AH^B), 3.83 (1H, s, OCH_3), 3.86 (1H, m, C(4)H^AH^B), 4.91 (1H, dd, *J* 4.4, 1.8, C(2)*H*), 6.72 (1H, d, *J* 8.6, ArC(6)*H*), 6.79 (1H, dd, *J* 8.7, 2.5 ArC(7)*H*), 6.95 (1H, d, *J* 2.5, ArC(9)*H*), 7.20 (2H, d, *J* 6.6, PhC(3,5)*H*), 7.25 (1H, m, PhC(4)*H*), 7.30 (2H, t, *J* 7.0 PhC(2,6)*H*); **^{13}C{^{1}H} NMR** (125 MHz, $CDCl_3$) δ_C: 20.2 (*C*H_3), 22.2 (*C*H_3), 27.1 (*i*Pr*C*H), 41.0 (*C*(3)H), 42.1 (*C*(4)H_2), 56.1 (O*C*H_3), 61.1 (*C*(2)H), 108.1 (Ar*C*(6)H), 108.3 (Ar*C*(9)H), 111.8 (Ar*C*(7)H), 124.3 (Ar*C*(5a)), 127.3 (Ph*C*(4)H), 128.2 (Ph*C*(3,5)H), 128.5 (Ph*C*(2,6)H), 134.9 ((Ar*C*(9a)), 140.7 (Ph*C*(1)), 155.5 (Ar*C*(8)), 158.8 (*C*=N); **HRMS** (ESI$^+$) $C_{20}H_{23}N_2OS$ $[M+H]^+$, found 339.1516, requires 339.1526 (−2.8 ppm).

(2*R*,3*S*)-8-Hydroxy-3-isopropyl-2-phenyl-3,4-dihydro-2*H*-benzo[4,5]thiazolo[3,2-*a*]pyrimidin-1-ium bromide 304

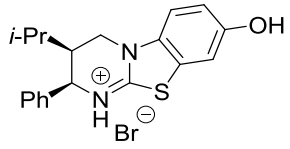

To a solution of (2*S*,3*R*)-**303** (500 mg, 1.48 mmol, 1 equiv.) in CH_2Cl_2 (10 mL) at 0 °C was added BBr_3 (15 mL, 8.86 mmol, 1 M in CH_2Cl_2, 10 equiv.) dropwise. The solution was stirred at 0°C for 2 h then warmed to rt and stirred for 16 h. The reaction was carefully quenched with MeOH (10 mL) at rt and warmed to rt. CH_2Cl_2 (10 mL) was added and the aqueous phase was extracted with CH_2Cl_2 (3 × 20 mL). The organic layers were combined, dried ($MgSO_4$) and concentrated *in vacuo* to afford the pure product as a colourless solid (566 mg, 95% yield, >95:5 dr); $[\alpha]_D^{20}$ =

−174.7 (*c* 1.0 MeOH), **mp** 194-196 °C; ν_{max} (thin film, cm^{-1}) 3140 (O-H), 2920 (C-H), 1597 (C=N), 1450 (C=C); **^{1}H NMR** (500 MHz, d_6-DMSO) δ_H: 0.79 (3H, d, *J* 6.7, CH_3), 1.07 (3H, d, *J* 6.5, CH_3), 1.21 (1H, app. td, *J* 13.2, 6.0, 3.2), 2.32 (1H, ddt, *J* 11.6, 9.4, 4.8, C(3)*H*), 3.68 (1H, dd, *J* 13.3, 11.6, C(4)H^AH^B), 4.40 (1H, m, C(4)H^AH^B), 5.17 (1H, d, *J* 4.8, C(2)*H*), 6.99 (1H, dd, *J* 8.8, 2.4, C(7)*H*), 7.30 (2H, d, *J* 7.4, PhC(2,6)*H*), 7.36-7.43 (3H, m, PhC(3,5)*H* and PhC(4)*H*), 7.46 (1H, d, *J* 2.4, ArC(9)*H*), 7.64 (1H, d, *J* 8.9, ArC(6)*H*), 9.98 (1H, s, O*H*), 11.14 (1H, s, N*H*); **^{13}C{^{1}H} NMR** (125 MHz, d_6-DMSO) δ_C: 19.2 (*C*H_3), 21.5 (*C*H_3), 26.3 (*i*Pr*C*H), 39.8 (*C*(3)H), 42.1 (*C*(4)H_2), 55.4 (*C*(2)H), 109.7 (Ar*C*(9)H), 114.0 (Ar*C*(6)H), 115.2 (Ar*C*(7)H), 123.4 (Ar*C*(5a)), 127.8 (Ph*C*(2,6)H), 128.4 (Ph*C*(4)H), 128.9 (Ph*C*(3,5)H), 131.2 ((Ar*C*(9a)), 137.6 (Ph*C*(1)), 155.4 (Ar*C*(8)), 162.3 (*C*=N); **HRMS** (ESI^+) $C_{19}H_{20}N_2OS$ $[M+H]^+$ found 324.1361, requires 324.1296 (−2.5 ppm).

(2*R*,3*S*)-3-Isopropyl-2-phenyl-8-(prop-2-yn-1-yloxy)-3,4-dihydro-2*H*-benzo[4,5]thiazolo[3,2-a]pyrimidine 306

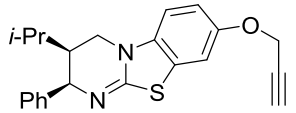

To a solution of salt **305** (1.00 g, 2.47 mmol, 1 equiv.) in THF/DMSO (1:1, 10mL) was added KO*t*Bu (722 mg, 6.43 mmol, 2.6 equiv.) and the reaction mixture was stirred at 0 °C for 2 h. Propargyl bromide (413 µL, 3.71 mmol, 80% in toluene, 1.5 equiv.) was then added and the reaction mixture was allowed to warm to rt (*ca*. 2 h) and quenched with brine (10 mL). The aqueous phase was extracted with EtOAc (3 × 10 mL). The organic layers were combined, washed with brine, dried (MgSO4) and concentrated *in vacuo* to afford the crude product was purified by Biotage® Isolera™ 4 [SNAP Ultra 25 g, 75 mL min^{-1}, CH_2Cl_2:EtOAc (95 : 5 5CV, 95 : 5 to 60 : 40 10 CV, 60 : 40 5 CV)] to afford the pure product as a colourless fluffy solid (495 mg, 68% yield, >95:5 dr); $[\alpha]_D^{20}$ = −201.4 (*c* 1.0 $CHCl_3$), **mp** 60-63 °C; ν_{max} (thin film, cm^{-1}) 2956 (C-H), 1616 (C=N), 1487 (C=C); **^{1}H NMR** (500 MHz, $CDCl_3$) δ_H: 0.84 (1H, d, *J* 6.7, CH_3), 1.13 (1H, d, *J* 6.5, CH_3), 1.28–1.32 (1H, m, *i*PrC*H*), 1.94 (1H, ddt, *J* 11.4, 9.4, 4.8, C(3)*H*) 2.54 (1H, t, *J* 2.4, C≡*H*), 3.33 (1H, t, *J* 11.5, C(4)H^AH^B), 3.83 (1H, ddd, *J* 11.5, 5.3, 1.8, C(4)H^AH^B), 4.68 (1H, d, *J* 2.4, CH_2O), 4.90 (1H, dd, *J* 4.5, 1.7, C(2)*H*), 6.72 (1H, d, *J* 8.7, ArC(6)*H*), 6.87 (2H, dd, *J* 8.7, 2.5, ArC(7)*H*), 7.04 (1H, d, *J* 2.5, ArC(9)*H*), 7.20 (2H, d, *J* 7.2, PhC(3,5)*H*), 7.23–7.25 (1H, m, PhC(4)*H*), 7.30 (2H, d, *J* 6.8, PhC(2,6)*H*); **^{13}C{^{1}H} NMR** (126 MHz, $CDCl_3$) δ_C: 20.2 (*C*H_3), 22.1 (*C*H_3), 27.1 (*i*Pr*C*H), 41.0 (*C*(3)H), 42.5 (*C*(4)H_2), 57.0 (*C*H_2O), 61.1 (*C*(2)H), 75.9 (C≡*C*H), 78.6 (*C*≡CH), 108.0 (Ar*C*(9)H), 110.0 (Ar*C*(6)H), 113.2 (Ar*C*(7)H), 124.4 (Ar*C*(5)), 127.4 (Ph*C*(4)H),

128.1 (Ph*C*(2,6)H), 128.5 (Ph*C*(3,5)H), 135.8 ((Ar*C*(9a)), 140.6 (Ph*C*(1)), 153.3 (Ar*C*(8)), 158.7 (*C*=N); **HRMS** (ESI$^+$) $C_{22}H_{23}N_2OS^+$ $[M+H]^+$ found 363.1517, requires 363.1526 (−2.4 ppm).

(2*R*,3*S*)-3-isopropyl-2-phenyl-8-(prop-2-yn-1-yloxy)-3,4-dihydro-2*H*-benzo[4,5]thiazolo[3,2-*a*]pyrimidine on polymer support 61

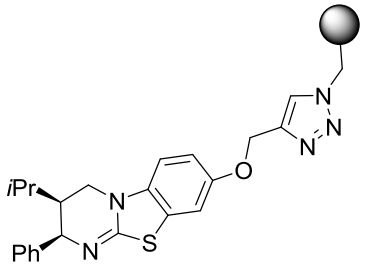

To a round bottomed flask containing azidomethyl polystyrene **293** (1.04 g, 1.25 mmol, *f* = 1.20 mmol/g, 1 equiv.) suspended in THF:DMF 1:1 (14 mL) was added alkyne **306** (495 mg, 1.37 mmol, 1.1 equiv.), *i*Pr$_2$NEt (762 µL, 0.546 mmol, 3.5 equiv.) and CuI (12 mg, 0.625 mmol, 5 mol%) with slow stirring (100 rpm). The reaction mixture was stirred until disappearance of the azide band (~2094 cm^{-1}) was confirmed by IR (*ca.* 17 h). The suspension was filtered and washed sequentially with THF (1:1, 130 mL), H_2O (130 mL), H_2O-MeOH (1:1, 130 mL), MeOH (130 mL), MeOH-THF (1:1, 130 mL), THF (130 mL) and CH_2Cl_2 (130 mL) and the resin was dried *in vacuo* at 40 °C for 24 h to afford a brown resin (1.22 g) with a loading of *f* = 0.972 mmol/g.

Elemental analysis (%) C 78.66, H 6.20, N 6.81

f = 0.972 mmol/g

(*E*)-1,1,1-Trifluoro-4-phenylbut-3-en-2-one 308

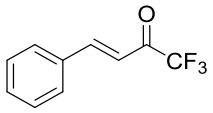

Following a procedure outlined by Smith[101] to a round bottomed flask containing anhydrous THF (25 mL, 0.2 M) was added *i*Pr$_2$NEt (3.32 mL, 24.0 mmol, 2 equiv.) and *n*BuLi (13.7 mL, 24.0 mmol, 1.75 M in hexanes, 2 equiv.) at −78 °C and the solution was allowed to stir for 20 minutes. Diethyl methylphosphonate (1.75 mL, 12.0 mmol, 1 equiv.) was added at −78 °C followed by a further 30 minutes of stirring. (*Z*)-2,2,2-Trifluoro-*N*-phenylacetimidoyl chloride **102** (2.50 g, 12.0 mmol, 1 equiv.) was then added slowly followed by stirring at −78 °C for 1 h. A solution of benzaldehyde (1.28 mL, 12.0 mmol, 1 equiv.) in anhydrous THF (10 mL) was added dropwise at −78 °C. The reaction mixture was then warmed over 2 h and stirred at rt for 16 h. Aq. 2 M HCl (24 mL, 4 equiv.) was added and the reaction mixture was stirred for a further 4 h before

being extracted with Et_2O (3 × 50 mL). The combined organic extracts were washed with sat. aq. $NaHCO_3$ (50 mL), brine (50 mL), dried ($MgSO_4$) and concentrated *in vacuo* to give the crude reaction mixture. Flash chromatography on silica gel (9:1 Pet:Et_2O) afforded the pure product as a yellow oil (950 mg, 40% yield); **^{1}H NMR** (700 MHz, $CDCl_3$) δ_H: 7.02 (1H, d, *J* 16.0, C(3)*H*), 7.43 (2H, t, *J* 7.3, ArC(2,6)*H*), 7.50 (1H, d, *J* 8.1, ArC(4)*H*), 7.61–7.66 (2H, t, *J* 7.3, ArC(3,5)*H*), 7.97 (1H, d, *J* 16.0, C(3)*H*). All data in accordance with the literature.[101]

(3*R*,4*R*)-3,4-diphenyl-6-(trifluoromethyl)-3,4-dihydro-2H-pyran-2-one 309

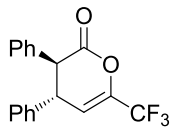

To a Schlenk flask containing CH_2Cl_2 (2 mL) was added phenylacetic acid **307** (27 mg, 0.2 mmol, 1 equiv.), pivaloyl chloride (37 µL, 0.3 mmol, 1.5 equiv.) and *i*Pr_2NEt (52 µL, 0.3 mmol, 1.5 equiv.) and the resulting solution was allowed to stirred for 5 mins at rt. The solution was then cooled to −78 °C and PS-(2*R*,3*S*)-HyperBTM **61** (31 mg, 0.03 mmol, *f* = 0.972 mmol/g, 15 mol%) was added with slow stirring (200 rpm) followed by enone **308** (40 mg, 0.2 mmol, 1 equiv.) and and *i*Pr_2NEt (35 µL, 0.2 mmol, 1 equiv.). The reaction mixture was stirred (200 rpm) at −78 °C for 16 h and allowed to warm to rt. The reaction was filtered using a sintered funnel to remove the polymer-supported catalyst. The filtrate was washed with aq. 1 M HCl (5 mL) and brine (10 mL). The organic layers were combined, dried ($MgSO_4$) and concentrated *in vacuo* to afford the crude product (89:11 dr) which was purified by by Biotage® Isolera™ 4 [SNAP Ultra 10 g, 75 mL min^{-1}, pet. ether:Et_2O (100 : 0 5CV, 100 : 5 to : 90 : 10 CV, 90 : 10 5 CV)] to afford the pure product as a colourless solid with spectroscopic data in accordance with the literature.[101] (42 mg, 66% yield, 95:5 dr); $[\alpha]_D^{20}$ = +171.6 (*c* 0.5 CH_2Cl_2) {Lit. [101] −227.2 (*c* 0.25 CH_2Cl_2) *ent* >99%ee}; **mp** 42-44 °C {Lit. [101] 90-92 °C}; **Chiral HPLC**: Chiralcel OD-H (98:2 hexane:, flow rate 1 mL/min^{-1}, 210 nm, 30 °C) t_R(3*S*,4*S*): 8.7 min, t_R(3*R*,4*R*): 9.4 min, 98% ee; **^{1}H NMR** (500 MHz, $CDCl_3$) δ_H: 4.00 (1H, d, *J* 8.9, C(3)*H*), 4.05 (1H, m, C(4)*H*), 6.17 (1H, d, *J* 3.8, C(5)*H*), 7.03-7.08 (2H, m, 2 × PhC*H*), 7.09–7.15 (2H, m, 2 × PhC*H*), 7.31 (6H, m, 6 × PhC*H*). **^{19}F{^{1}H} NMR** (376 MHz, $CDCl_3$) δ_F: −72.2 (CF_3).

1-(naphthalen-2-yl)prop-2-en-1-ol 313

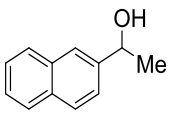

To a round bottomed flask containing anhydrous THF (40 mL, 0.3 M) was added 2-naphthaldehyde **312** (2.0 g, 12.8 mmol, 1 equiv.) followed by MeMgBr (4.3 mL, 12.8 mmol, 3.0 M in THF, 1 equiv.) at −78 °C with stirring under Ar. The solution was stirred at −78 °C °C for 16 h and allowed to warm to rt. The reaction was quenched with NH_4Cl (15 mL) and the aqueous phase was extracted with EtOAc (3 × 30 mL). The organic layers were combined, washed with brine, dried (MgSO4) and concentrated *in vacuo* to afford the pure product as an off-white solid (1.89 g, 86 % yield); **mp** 60-63 °C {Lit[307] 56-58 °C}; **^{1}H NMR** (400 MHz, $CDCl_3$) δ_H: 5.08 (1H, q, *J* 6.5, C(1)*H*), 7.49 (3H, 3 × Ar*H*), 7.80–7.88 (4H, m, Ar*H*). All data in accordance with the literature.[307]

1-(naphthalen-2-yl)ethyl propionate 314

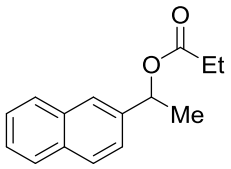

To a round bottomed flask containing CH_2Cl_2 (2 mL) was added alcohol **313** (71 mg. 0.39 mmol, 1 equiv.), isobutyric anhydride (63 µL, 0.39 mmol, 1 equiv.), DMAP (1 crystal, ~10 mol%) and *i*Pr_2NEt (68 µL, 0.39 mmol, 1 equiv.). The reaction was stirred at rt for 16 h and diluted with CH_2Cl_2 (10 mL). The organic phase was washed with aq. 1M HCl (5 mL), $NaHCO_3$ (5 mL) and brine. The organic layer was dried (MgSO4) and concentrated *in vacuo* to afford the pure product as a colourless oil (85 mg, 86% yield); **^{1}H NMR** δ_H: (400 MHz, $CDCl_3$) 1.16 (3H, t, *J* 7.6, CH_2CH_3), 1.61 (3H, d, *J*, 6.6, CH_3), 2.39 (2H, app. qd, *J* 7.6, 1.8, CH_2CH_3), 6.08 (1H, q, *J* 6.6, C(1)*H*), 7.44–7.52 (3H, m, Ar*H*), 7.78–7.88 (4H, m, Ar*H*). data in accordance with the literature.[275]

(*R*)-1-(naphthalen-2-yl)prop-2-en-1-ol 313 and (*S*)-1-(naphthalen-2-yl)ethyl propionate 314

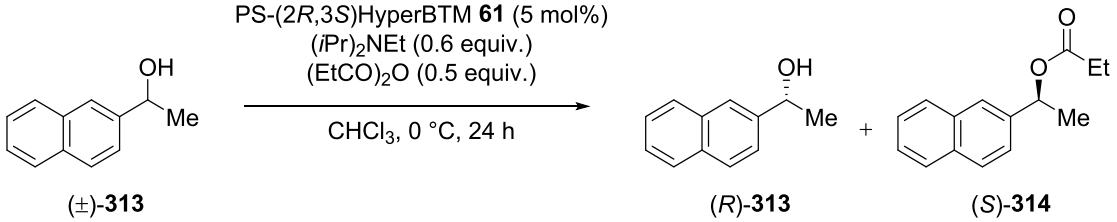

(±)-**313** (*R*)-**313** (*S*)-**314**

Following general procedure **M**, (±)-1-(naphthalen-2-yl)ethan-1-ol **313** (50 mg, 0.291 mmol, 1 equiv.), propionic anhydride (19 µL, 0.145 mmol, 0.6 equiv.), PS-(2*S*,3*R*)-HyperBTM **61** (15 mg, 0.014 mmol, *f* = 0.972 mmol/g, 5 mol%) and *i*Pr_2NEt (30 µL, 0.174 mmol, 0.5equiv.) were reacted in $CHCl_3$ (2 mL) at 0 °C for 24 h to give the crude products, which were purified by Biotage®

Isolera 4 chromatography (eluent: 0%→30% EtOAc in pet.ether) to give (*S*)-1-(naphthalen-2-yl)ethyl propionate **314** (47 mg, 48% yield) and (*R*)-1-(naphthalen-2-yl)ethan-1-ol **313** (46 mg, 41%).

(*R*)-1-(naphthalen-2-yl)ethan-1-ol 313: $[\alpha]_D^{20}$ = +35.6 (*c* 0.5 $CHCl_3$) {Lit.[275] −53.0 (*c* 0.4 $CHCl_3$) *ent* >99%ee; **Chiral HPLC analysis:** Chiralpak OJ-H (95:5 hexane:*i*PrOH, flow rate 1 mL min^{-1}, 254 nm, 30 °C) t_R (*S*): 14.9 min, t_R (*R*): 19.2 min, >99% ee

(*S*)-1-(naphthalen-2-yl)ethyl propionate 314: $[\alpha]_D^{20}$ = −80.6 (*c* 0.5 $CHCl_3$) {Lit.[275] +71.2 (*c* 0.6 $CHCl_3$), 67% ee); **Chiral HPLC analysis:** Chiralpak AD-H (90:10 hexane:*i*PrOH, flow rate 0.5 mL min^{-1}, 254 nm, 30 °C) t_R (*R*): 21.4 min, t_R (*S*): 24.1 min, 79% ee.

S factor = 95

1-Benzyl-3-hydroxy-3-phenylindolin-2-one 319

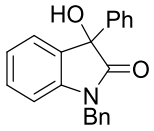

To a round bottomed flask containing anhydrous THF (140 mL, 0.1 M) at −78 °C was added 1-benzylindoline-2,3-dione **318** (3.33 g, 14 mmol) with stirring. Phenylmagnesium bromide (3.0 M, 5.6 mL, 16.8 mmol) was added and the reaction mixture was stirred for 30 at −78 °C then warmed to rt over 30 mins. The reaction was quenched with sat. aq. NH_4Cl (50 mL) and the aqueous phase was extracted with EtOAc (3 × 30 mL). The organic layers were combined, washed with brine, dried ($MgSO_4$) and concentrated *in vacuo* to afford the crude product that was purified by Biotage® Isolera 4 chromatography (eluent: 0%→30% EtOAc in hexanes) to give a yellow solid. The product was further purified by recrystallisation by dissolving in a minimal amount of CH_2Cl_2 (~30 mL), layering with hexane (~150 mL), and cooling at −10 °C overnight to give 1-benzyl-3-hydroxy-3-phenylindolin-2-one as a colourless solid (3.94 g, 89% yield); **mp** 140-142 °C {Lit.[275] **mp** 139-141 °C}; **^{1}H NMR** (400 MHz, $CDCl_3$) δ_H: 3.39 (1H, br, s, O*H*), 4.84 (1H, d, *J* 15.7, C$H_A$$H_B$Ph), 5.05 (1H, d, *J* 15.7, C$H_A$$H_B$Ph), 6.79 (1H, app. d, *J* 7.9, C(7)*H*), 7.05 (1H, app. td, *J* 7.6, 1.0, C(5)*H*), 7.23 (1H, td, *J* 7.8, 1.3, C(6)*H*), 7.27-7.38 (9H, m, Ar*H*), 7.39-7.44 (2H, m, Ar*H*). All data in accordance with the literature.[275]

1-benzyl-2-oxo-3-phenylindolin-3-yl isobutyrate 320

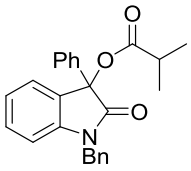

To a Schenk flask containing $CHCl_3$ (2 mL) was added alcohol **319** (50 mg, 0.158 mmol, 1 equiv.), isobutyric anhydride (29 µL, 0.174 mmol, 1.1 equiv.), *i*Pr_2NEt (29 µL, 0.158 mmol, 1 equiv.) and DMAP (10 mol%, 1 crystal) at rt with stirring. The reaction was stirred at rt for 16 h and diluted with EtOAc (10 mL). The organic phase was washed with 1M HCl (5 mL), sat. aq. $NaHCO_3$ (5 mL) and brine. The organic layer was dried (MgSO4) and concentrated *in vacuo* to afford the pure product as a colourless oil (51 mg, 83% yield); ν_{max} (thin film, cm^{-1}) 2974 (C-H), 1728(C=O), 1614 (C=C); **^{1}H NMR** (400 MHz, $CDCl_3$) δ_H: 1.23 (3H, d, *J* 7.0, CH(CH_3)$_A$(CH_3)$_B$), 1.27 (3H, d, *J* 7.0, CH(CH_3)$_A$(CH_3)$_B$), 2.74 (1H, sept, *J* 7.0, *i*PrC*H*), 4.86 (1H, d, *J* 15.9, C$H_A$$H_B$Ph), 5.01 (1H, d, *J* 15.9, CH_AH_BPh), 6.72 (1H, d, *J* 7.8, C(7)*H*), 7.05 (1H, app td, *J* 7.5, 1.0, C(5)*H*), 7.18-7.39 (12H, m, C(3)Ar*H* and CH_2Ar*H* and ArC(4,6)*H*); **^{13}C NMR** (101 MHz, $CDCl_3$) δ_C: 18.8 (*C*H_3), 19.0 (*C*H_3), 34.0 (*C*H(CH_3)$_2$), 44.4 (N*C*H_2Ph), 81.1 (*C*(3)), 109.9 (Ar*C*(7)H), 123.2 (Ar*C*(5)H), 123.9 (Ar*C*(4)H), 126.4 (C(3)Ph*C*(2,6)H), 127.3 (CH_2Ph*C*(2,6)H), 127.7 (CH_2Ph*C*(4)H), 128.6 (*C*(3a)), 128.8 (CH_2Ph*C*(3,5)H), 128.9 (C(3)Ph*C*(3,5)H), 129.0 (C(3)Ph*C*(4)H), 130.1 (Ar*C*(6)H), 135.8 (CH_2Ph*C*(1)), 137.0 (C(3)Ph*C*(1)), 143.8 (*C*(7a)), 174.3 (*C*(2)=O), 175.2 (*C*O_2R); **HRMS** (NSI^+) calculated for $C_{25}H_{27}N_2O_3^+$ ($[M+NH_4]^+$) requires 403.2016; found 403.2012 (−1.0 ppm).

(*R*)-1-benzyl-2-oxo-3-phenylindolin-3-yl isobutyrate 320 and (*S*)-1-benzyl-3-hydroxy-3-phenylindolin-2-one 319

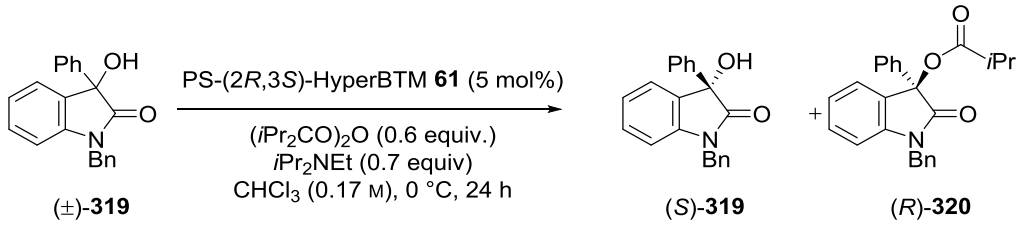

Following general procedure **M**, 1-benzyl-3-hydroxy-3-phenylindolin-2-one **319** (100 mg, 0.317 mmol, 1 equiv.), isobutyric anhydride (37 µL, 0.22 mmol, 0.7 equiv.), PS-(2*S*,3*R*)-HyperBTM **61** (16.4 mg, 0.016 mmol, *f* = 0.972 mmol/g, 5 mol%) and *i*Pr_2NEt (33 µL, 0.19 mmol, 0.6 equiv.) were reacted in $CHCl_3$ (2 mL, 0.17 M) at 0 °C for 24 h to give the crude products, which were purified by Biotage® Isolera 4 chromatography (eluent: 0%→30% EtOAc in pet.ether) to give (*R*)-1-benzyl-2-oxo-3-phenylindolin-3-yl isobutyrate **320** (47 mg, 46% yield) and (*S*)-1-benzyl-3-hydroxy-3-phenylindolin-2-one **319** (46 mg, 38%);

(*R*)-1-Benzyl-2-oxo-3-phenylindolin-3-yl isobutyrate 320: $[\alpha]_D^{20}$ = −83.6 (*c* 1.0, $CHCl_3$); **Chiral HPLC analysis**: Chiralpak AD-H (90:10 hexane:*i*PrOH, flow rate 1.25 mL min^{-1}, 211 nm, 40 °C) t_R (*S*): 12.7 min, t_R (*R*): 25.7 min, 98.5:1.5 (*S*:*R*) er;

(*S*)-1-Benzyl-3-hydroxy-3-phenylindolin-2-one 319: $[\alpha]_D^{20}$ = −39.4 (*c* 1.0, $CHCl_3$) {Lit.[275] −35.4 (*c* 1.0, $CHCl_3$) 98% ee}; **Chiral HPLC analysis**: Chiralpak AD-H (90:10 hexane: *i*PrOH, flow rate 1.25 mL min^{-1}, 211 nm, 40 °C) t_R (*S*): 21.4 min, t_R (*R*): 27.1 min, 91.5:8.5 (*R*:*S*) er.

S factor = 145.

***trans*-Cinnamic anhydride 329**

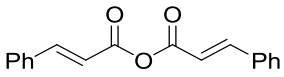

To a round bottomed flask containing CH_2Cl_2 (6 mL) was added *trans*-cinnamic acid **328** (741 mg, 5 mmol, 1 equiv.) and EDCI (959 mg, 5 mmol, 1 equiv.) with stirring. The reaction was stirred at rt for 2 h and diluted with CH_2Cl_2. $NaHCO_3$ (40 mL) was added and the aqueous phase was extracted. The organic layers were combined, washed with brine, dried ($MgSO_4$) and concentrated *in vacuo* to afford the pure product as a colourless solid (450 mg, 65% yield); **mp** 116-119 °C {Lit.[279] 118-120 °C}; **^{1}H NMR** δ_H (400 MHz, $CDCl_3$) 6.53 (1H, d, *J* 15.9, ArCH=C*H*), 7.36–7.47 (6H, m, ArC*H*), 7.55–7.60 (4H, m, ArC*H*), 7.86 (1H, d, *J* 15.9, ArC*H*=CH). All data in accordance with the literature.[279]

(3*R*)-methyl 4-benzoyl-5-oxo-3,5-diphenylpentanoate 331

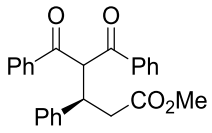

To a Schlenk flask containing anhydrous CH_2Cl_2 (250 µL, 0.75 M) was added PS-(2*R*,3*S*)-HyperBTM **61** (19 mg, 0.018 mmol, *f* = 0.972 mmol/g, 5 mol%) under argon with stirring (200 rpm). Anhydride **329** (100 mg, 0.36 mmol, 2 equiv.), 1,3-diphenylpropane-1,3-dione **330** (40 mg, 0.18 mmol, 1 equiv.) and *i*Pr_2NEt (78 µL, 0.45 mmol, 1 equiv.) were added to the reaction mixture. The reaction was stirred at 0 °C and allowed to warm to rt over 5 h then MeOH (2 mL) was added and the reaction was stirred for a further 16 h at rt. The reaction mixture was filtered to remove the polymer supported catalyst and the catalyst was washed with CH_2Cl_2 (10 mL). The filtrate was concentrated *in vacuo* and the residue was purified by flash chromatography (CH_2Cl_2→2% EtOAc: CH_2Cl_2) to afford the pure product as a colourless solid (52 mg, 75%

yield); $[\alpha]_D^{20}$ = −17.2 (*c* 0.5, $CHCl_3$) {Lit.[279] +9.6 (*c* 0.25, $CHCl_3$) *ent* 96% ee}; **mp** 100-101 °C {Lit.[279]104-107 °C}; **Chiral HPLC analysis** Chiralpak AD-H (80:20 hexane:*i*PrOH, flow rate 1 mL min^{-1}, 211 nm, 30 °C) t_R (*S*) 11.3 min, t_R (*R*) 16.1 min, 94 % ee; **^{1}H NMR** δ_H (500 MHz, $CDCl_3$) 2.76–2.94 (2H, m, C(2)*H*), 3.49 (3H, s, OCH_3), 4.40 (1H, app. td, *J* 9.5, 4.7, C(3)*H*), 5.84 (1H, d, *J* 9.5, C(4)*H*), 7.06–7.10 (1H, m, Ar*H*), 7.15 (2H, dd, *J* 8.4, 6.9, 2Ar*H*), 7.24-7.34 (4H, m, 4 × Ar*H*), 7.39–7.47 (3H, m, 3 × Ar*H*), 7.54 (1H, t, *J* 7.4, Ar*H*), 7.75 (2H, d, *J* 7.2, 2 × Ar*H*), 7.98 (2H, d, *J* 6.8, 2 × Ar*H*). All data in accordance with the literature.[279]

6.6 References and Notes

[281] M. Frigerio, M. Santagostino, S. Sputore, *J. Org. Chem.* **1999**, *64*, 4537-4538.
[282] R. E. Ireland, L. Liu, *J. Org. Chem.* **1993**, *58*, 2899-2899.
[283] D. B. Dess, J. C. Martin, *J. Am. Chem. Soc.* **1991**, *113*, 7277-7287.
[284] O. A. Davis, R. A. Croft, J. A. Bull, *Chem. Comm.* **2015**, *51*, 15446-15449.
[285] J. C. Slootweg, N. Peters, H. C. Quarles van Ufford, E. Breukink, R. M. J. Liskamp, D. T. S. Rijkers, *Biorg. Med. Chem.* **2014**, *22*, 5345-5353.
[286] N. Suzuki, T. Nomoto, Y. Toya, N. Kanamori, B. Yoda, A. Saeki, *Bioscience, Biotechnology, and Biochemistry* **1993**, *57*, 1561-1562.
[287] S. F. E. D. Hostetler, T. J. McCarthy, Michael J. Welch, J. A. Katzenellenbogen, *J. Org. Chem.* **1998**, *63*, 1348-1351.
[288] A. N. Rai, A. Basu, *Org. Lett.* **2004**, *6*, 2861-2863.
[289] C. V. Ramana, B. Induvadana, *Tetrahedron Lett.* **2009**, *50*, 271-273.
[290] Y.-S. Feng, L. Mao, X.-S. Bu, J.-J. Dai, H.-J. Xu, *Tetrahedron* **2015**, *71*, 3827-3832.
[291] E. C. Davison, I. T. Forbes, A. B. Holmes, J. A. Warner, *Tetrahedron* **1996**, *52*, 11601-11624.
[292] J. E. Baldwin, R. M. Adlington, R. Singh, *Tetrahedron* **1992**, *48*, 3385-3412.
[293] W. S. Johnson, T. M. Yarnell, R. F. Myers, D. R. Morton, *Tetrahedron Lett.* **1978**, *19*, 2549-2552.
[294] Z. Li, F. W. Fowler, J. W. Lauher, *J. Am. Chem. Soc.* **2009**, *131*, 634-643.
[295] M. Kitamura, S. Kato, M. Yano, N. Tashiro, Y. Shiratake, M. Sando, T. Okauchi, *Org. Biomol. Chem.* **2014**, *12*, 4397-4406.
[296] Y. Tachibana, H. Kawasaki, N. Kihara, T. Takata, *J. Org. Chem.* **2006**, *71*, 5093-5104.
[297] A. B. Sieval, R. Linke, G. Heij, G. Meijer, H. Zuilhof, E. J. R. Sudhölter, *Langmuir* **2001**, *17*, 7554-7559.
[298] R. Cao, J. Zhou, W. Wang, W. Feng, X. Li, P. Zhang, P. Deng, L. Yuan, B. Gong, *Org. Lett.* **2010**, *12*, 2958-2961.
[299] E. B. Troughton, C. D. Bain, G. M. Whitesides, R. G. Nuzzo, D. L. Allara, M. D. Porter, *Langmuir* **1988**, *4*, 365-385.
[300] R. J. DeOrazio, J.-H. Maeng, D. D. Manning, B. A. Sherer, I. L. Scott, S. S. Nikam, *Synth. Commun.* **2011**, *41*, 3551-3555.
[301] L. Zhu, M. Zhang, M. Dai, *J. Heterocycl. Chem.* **2005**, *42*, 727-730.
[302] A. Godt, Ö. Ünsal, M. Roos, *J. Org. Chem.* **2000**, *65*, 2837-2842.
[303] A. Commerçon, J. F. Normant, J. Villieras, *Tetrahedron* **1980**, *36*, 1215-1221.
[304] S. López, F. Fernández-Trillo, P. Midón, L. Castedo, C. Saá, *J. Org. Chem.* **2005**, *70*, 6346-6352.
[305] S. M. Kelly, B. H. Lipshutz, *Org. Lett.* **2014**, *16*, 98-101.

[306] K. Higashiyama, H. Inoue, H. Takahashi, *Tetrahedron* **1994**, *50*, 1083-1092.
[307] E. Fernández-Mateos, B. Maciá, M. Yus, *Tetrahedron-Asymmetr*. **2012**, *23*, 789-794.